TITLE PAGE

Report Title:	**SECA Coal-Based Systems - FuelCell Energy, Inc.**
Type of Report:	Final Technical Report
Reporting Period Start Date:	February 27, 2004
Reporting Period End Date:	January 31, 2014
Principal Author:	Hossein Ghezel-Ayagh
Date Report Issued	September 2014
DOE Award No.:	DE-FC26-04NT41837
Name & Address of Submitter:	FuelCell Energy, Inc. 3 Great Pasture Road Danbury, CT 06813
Subcontractors:	Versa Power Systems, Inc. 10720 Bradford Road, Suite 110 Littleton, CO 80127-4298 USA Versa Power Systems, Ltd. 4852 – 52nd Street SE Calgary, Alberta, Canada T2B 3R2 WorleyParsons Group, Inc. 2675 Morgantown Road Reading, PA 19607 Nexant, Inc. 101 2nd St. San Francisco, CA 94105-3672 Gas Technology Institute 1700 South Mount Prospect Road Des Plaines, IL 60018-1804 Materials and Systems Research, Inc. 5395 West 700 South Salt Lake City, UT 84104 University of Utah 201 South Presidents Circle Salt Lake City, UT 84112-9008

DISCLAIMER

ABSTRACT

The overall goal of this U.S. Department of Energy (DOE) sponsored project is the development of solid oxide fuel cell (SOFC) cell and stack technology suitable for use in highly-efficient, economically-competitive central generation power plant facilities fueled by coal synthesis gas (syngas). This program incorporates the following supporting objectives:

- Reduce SOFC-based electrical power generation system cost to $700 or less (2007 dollars) for a greater than 100 MW Integrated Gasification Fuel Cell (IGFC) power plant, exclusive of coal gasification and CO_2 separation subsystem costs.
- Achieve an overall IGFC power plant efficiency of at least 50%, from coal (higher heating value or HHV) to AC power (exclusive of CO_2 compression power requirement).
- Reduce the release of CO_2 to the environment in an IGFC power plant to no more than 10% of the carbon in the syngas.
- Increase SOFC stack reliability to achieve a design life of greater than 40,000 hours.

At the inception of the project, the efforts were focused on research, design and testing of prototype planar SOFC power generators for stationary applications. FuelCell Energy, Inc. successfully completed the initial stage of the project by meeting the program metrics, culminating in delivery and testing of a 3 kW system at National Energy Technology Laboratory (NETL). Subsequently, the project was re-aligned into a three phase effort with the main goal to develop SOFC technology for application in coal-fueled power plants with >90% carbon capture. Phase I of the Coal-based efforts focused on cell and stack size scale-up with concurrent enhancement of performance, life, cost, and manufacturing characteristics. Also in Phase I, design and analysis of the baseline (greater than 100 MW) power plant system—including concept identification, system definition, and cost analysis—was conducted.

Phase II efforts focused on development of a ≥25 kW SOFC stack tower incorporating multiple stack building blocks of scaled-up cells, suitable for integration into a large-scale fuel cell power module. Activities in Phase II also included the development of the baseline system, factory cost estimate for the baseline plant's power block, and conceptual design of a natural gas fueled sub-MW system to be used for testing and verification of the fuel cell stacks in a system environment.

The specific objective for Phase III was the validation of the performance and robustness of stacks and scaled stack arrays suitable for use in large-scale power generation systems such as an IGFC with reliable, fail-safe operation being of paramount importance. The work culminated in the verification tests of a 60 kW SOFC stack module in a power plant facility.

This final technical report summarizes the progress made during the project period. Significant progress was made in the areas of cell and stack technology development, stack module design, sub-scale module tests, Baseline Power Plant system development and Proof-of-Concept Module unit design. The development of this technology will significantly advance the nation's energy security and independence interests while simultaneously addressing environmental concerns, including greenhouse gas emissions and water usage.

TABLE OF CONTENTS

LIST OF FIGURES V
LIST OF TABLES X
EXECUTIVE SUMMARY XI
INTRODUCTION AND OBJECTIVES 1
EXPERIMENTAL METHODS 2
RESULTS AND DISCUSSIONS 3
1.0 CELL TECHNOLOGY DEVELOPMENT 3
1.1 CELL (COMPONENT) MATERIAL DEVELOPMENT 3
1.2 CELL AREA SCALE-UP AND CELL TECHNOLOGY INTEGRATION 21
1.3 CELL MANUFACTURING PROCESS DEVELOPMENT 25
2.0 STACK TECHNOLOGY DEVELOPMENT 28
2.1 STACK DESIGN DEVELOPMENT AND TESTING 28
2.2 STACK COMPONENT DEVELOPMENT AND TESTING 51
2.3 IN-CELL MANIFOLDED (ICM) STACK DEVELOPMENT 72
3.0 STACK MODULE DEVELOPMENT AND TESTS 82
3.1 STACK MODULE DESIGN 82
3.2 SUB-SCALE MODULE TESTS 94
4.0 BASELINE POWER PLANT SYSTEM DEVELOPMENT 120
4.1 BASELINE SYSTEM CONCEPTUAL DESIGN AND PLANT LAYOUT 120
4.2 IGFC POWER ISLAND FACTORY COST ESTIMATE 125
5.0 PROOF-OF-CONCEPT MODULE (PCM) SYSTEM DESIGN 129
5.1 EARLY-STAGE 1-5 KW SYSTEM DEVELOPMENT 129
5.2 50 KW PCM SYSTEM PRELIMINARY DESIGN 132
5.3 BALANCE-OF-PLANT (BOP) COMPONENT DEVELOPMENT AND TESTING 139
CONCLUSION 142
REFERENCES 144
LIST OF ACRONYMS 145

LIST OF FIGURES

Figure 1-1 Solid Oxide Fuel Cell Electrochemical Performance Enhancement. 4
Figure 1-2 Long Term Steady-State Test of an Improved Cell (LTS-3 Cell) at 750°C. 5
Figure 1-3 Comparison of Performance Characteristics for Different Cell Types (81 cm^2 Active Area) at 650°C 6
Figure 1-4 Comparison of Voltage-Time Characteristics (at Constant Current) for Various Cell Types at 750°C 7
Figure 1-5 Voltage-Time Characteristic at Constant Current for LTS Cells (81 cm^2 Active Area) from 650 to 800°C 8
Figure 1-6 Hydrothermal Stability of Thin TSC-3 Cells in a 16-cell Stack Demonstrated in Fuel Utilization and Thermal Cycle Test 9
Figure 1-7 SOFC Cathode Degradation Mechanisms Related to Cr Species 10
Figure 1-8 Performance Degradation of a TSC-3 Cell Stack During Test with 3.5% Cathode Gas Humidity 10
Figure 1-9 Effect of Cathode Gas Humidity Level on Performance Degradation of TSC-3 Cell Glob 101792 Containing Coated Stainless Steel Hardware 11
Figure 1-10 SEM and EDX Analysis of Cell Glob101843 Containing Cr Getter Gb after Test at 10% Cathode Gas Humidity 12
Figure 1-11 SEM and EDX Analysis of Cell Glob101838 Containing Cr Getter Gc after Test at 10% Cathode Gas Humidity 12
Figure 1-12 Accelerated Single Cell Tests of Cathodes with Cr Getter Materials Using Coated Cathode Jigs 13
Figure 1-13 Stability and Thermal Cycling Capability of Cell Glob101859 Containing 30% Gb-70% Gc Blend of Cr Getter Materials and Co-coated Cathode Hardware 14
Figure 1-14 Stability of Cell Containing Cathode with 70% Gb - 30% Gc Blend of Cr Getter Materials and Co Coated Cathode Jig 15
Figure 1-15 Testing of Six-Cell Stack Containing Cathodes with Blended Cr Getters 16
Figure 1-16 Stability of Six-Cell Stack GT055296-0134 containing Blended Cr Getters Gb and Gc Compared with Baseline Stack GT055296-0111 17
Figure 1-17 Stability and Thermal Cycling Capability of Cell Glob 101875 Containing 30% Gb-70% Gc Cr Getter Blend and Coated Cathode Hardware 18
Figure 1-18 Performance Enhancement and Degradation Rate Reduction though Materials Development (Long-Term Single-Cell Testing) 19
Figure 1-19 Overview of Long-Term Single-Cell Test (Glob101749) at 650°C 20
Figure 1-20 Long-Term Single-Cell Test (Glob101837) at 750°C 21
Figure 1-21 Electrochemical Performance of the Scaled-Up Cells vs. the Baseline Cells 22
Figure 1-22 Cell Voltage vs Time Trend at 500 mA/cm^2 for 25 cm x 25 cm Advanced Cathode LTS Cell 23
Figure 1-23 Performance Characteristics of 33 cm x 33 cm Size Scaled-up Cell 24
Figure 1-24 1000 cm^2 Cell Area 10-cell Stack Peak Power Test Results 25
Figure 1-25 Performance Stability Comparison in 6-cell Stack for Cells Fired in Deltech and Lindberg Furnaces 27
Figure 1-26 In-Cell Manifolded (ICM) Stack Production Half Cell 27
Figure 2-1 10 kW Stack Building Block (64 cells, 550 cm^2 cell active area) 29
Figure 2-2 End-of-Phase I Metric Test (550 cm^2 cell area 64-cell stack block) - Average Cell Voltage and Stack Power Trends 30
Figure 2-3 Long Term Steady-State Test of a 16-cell, 2.5 kW Stack 30
Figure 2-4 Phase II Stack Development Focus and Current Status 31
Figure 2-5 92-cell SOFC Stack Building Block (550 cm^2 cell active area) 32
Figure 2-6 550 cm^2 Cell Area 16-cell Stack Test at Phase II Type Conditions 33

Figure 2-7 End-of-Phase II Metric Test (120-cell Stack) at VPS 34
Figure 2-8 Stack GT058116-0001 Performance over the Total Test Period 35
Figure 2-9 Stack GT057235-0083 Performance during Fuel Utilization Testing After Thermal Cycle (TC1) 36
Figure 2-10 Stack GT057235-0083 Steady-State Hold Average Cell Voltage 37
Figure 2-11 Stack GT057235-0089 – TC1 Steady-State Hold Performance 38
Figure 2-12 Stack GT057235-0089 TC1 Hold Individual Cell Degradation Rates Profile 39
Figure 2-13 Performance Degradation Trends for Different Cell Pedigrees in Stack GT057235-0093 40
Figure 2-14 Stack GT057235-0095 Performance during Fuel Utilization Testing 41
Figure 2-15 Performance of Stack GT057235-0095 at Phase I and Phase II System Conditions 42
Figure 2-16 Performance Stability of Stack GT057235-0097 at Phase II System Conditions 43
Figure 2-17 Individual Cell Performance Degradation Rates for Stack GT057235-0097 Operating at System Conditions 43
Figure 2-18 Stack GT057832-0003 Performance during Steady State Holds 45
Figure 2-19 Stack GT057832-0003 Individual Cell Voltage Trends during Steady-State Holds 46
Figure 2-20 Performance of 96-cell Stack GT058116-0003 During Long-term Steady-State Test 47
Figure 2-21 Stack GT058116-0003: Performance of Individual Cells 48
Figure 2-22 Stack GT058116-0002 Performance during Fuel Utilization Test 49
Figure 2-23 Performance Characterization of Stack GT058742-0001 before shipment 50
Figure 2-24 Performance Comparison of Stacks Fabricated for Quad Module Test 51
Figure 2-25 Pressure Mat Force Distribution Indicating Height Variation of ‘As-Received’ Anode Flow Field Sample (dark blue – low, red –high) 52
Figure 2-26 Anode Flow Field Fin with Fuel By-Pass Gap 53
Figure 2-27 Dimpled Flow Field Development 54
Figure 2-28 Dimpled Cathode Flow Field Finished Parts (Left: low pressure drop direction, Right: high pressure drop direction) 54
Figure 2-29 Six-Cell Stack Featuring Brazed (Joined) Interconnects 55
Figure 2-30 Braze Assembly Jig 55
Figure 2-31 Brazed IC from Vendor 56
Figure 2-32 Brazed IC after Annealing 56
Figure 2-33 Brazed IC after Modifying Braze Furnace Temperature-Time Profile 57
Figure 2-34 Performance Stability of 32-Cell Large-Area Stack Containing Sanergy and SS434 Cathode Flow Fields (TSC-3 Cells) 58
Figure 2-35 Interconnect Related Degradation during Long-Term Single Cell Test 101729 59
Figure 2-36 Long-term Performance of Stack GT056019-0132 Featuring Co-Coated Sanergy Interconnects 60
Figure 2-37 Oxide at Cathode Contact 61
Figure 2-38 Chrome Deposition Analysis 62
Figure 2-39 Cross Sections of Coated Coupons: (a) as Received and (b) After Testing in Air at 750°C for 1000 Hours 63
Figure 2-40 Performance Stability of Cell Containing a Nextech Coated Jig (Test Glob 101853) 64
Figure 2-41 Performance Stability of Cell (Test GT101863) Containing PNNL Coated Jig 65
Figure 2-42 Performance Stability of Cell Containing Co Coated ZMG232G10 Alloy Cathode Hardware (Jig) 65
Figure 2-43 SEM of Cathode Jig Showing Oxide Presence (Test Glob 101869) 66

Figure 2-44 SEM of Cell Cross Sections Corresponding to Cathode Jig Channel and Rib Areas (Test Glob 101869) 66
Figure 2-45 Evaluation of MCO Coated (by Nextech) Interconnects in Stack GT056019-0156 67
Figure 2-46 Steady-State Test Glob101851 of Coated Jig and Tubing with 10% Cathode Gas Humidity (2491 h with humid gas) 68
Figure 2-47 Cross Section of the Tested Coated Tubing 69
Figure 2-48 Cross Section of the Tested Cell 69
Figure 2-49 Cross Section of the Tested Co-Coated Cathode Jig 70
Figure 2-50 Long-Term Single-Cell Test (Glob101881) With Glass-Ceramic Seals 71
Figure 2-51 Nickel Mesh Endplate for Current Collection 72
Figure 2-52 20-Cell In-Cell Manifolded (ICM) Stack Rendering 73
Figure 2-53 8-cell In-Cell Manifolded (ICM) Mock Stack in Assembly 73
Figure 2-54 Baseline Flow Distribution in 80-cell ICM stack 74
Figure 2-55 Pressure Drop, Temperature and Fuel Flow Variations in 80-Cell ICM Stack 75
Figure 2-56 Sensitivity of Anode Side Flow Distribution to Stack End Heating Loads 75
Figure 2-57 Graded Anode Flow Field Contact Media in Hydraulic Flow Direction 76
Figure 2-58 Model Predicted Thermal Profile for 80-Cell ICM Stack Operating at Phase II System Conditions 77
Figure 2-59 Model Generated Static Pressure Profile for 80-Cell ICM Stack Operating at Phase II Conditions (pressure drop per Tested 19-cell Stack) 77
Figure 2-60 Performance of In-cell Manifolded (ICM) Stack GT059391-0004 during Fuel Utilization Testing before Thermal Cycle 78
Figure 2-61 Performance of In-cell Manifolded (ICM) Stack GT059391-0004 during Steady State Testing at Phase I and Phase II System Conditions 79
Figure 2-62 19-Cell In-cell Manifolded (ICM) Stack 79
Figure 2-63 Performance of In-cell Manifolding (ICM) Stack GT059328-0001 during Fuel Utilization Testing after Thermal Cycle 80
Figure 2-64 Thermal Profile of 19-cell ICM Stack GT059328-0001 during Steady State Testing 81
Figure 2-65 Performance Stability of 19-Cell In-Cell Manifolded (ICM) Stack GT059328-0001 at System Conditions 82
Figure 3-1 Cutaway Side View of 60 kW Module 83
Figure 3-2 CFD Flow Analysis of 60 kW Module 83
Figure 3-3 60 kW Mock Stack Quad Assembly Module Prior to Vessel Closure 84
Figure 3-4 Electrical System Configuration for Stack Quad Assembly 85
Figure 3-5 Stack Dielectric Isolation Components 86
Figure 3-6 Buss Bar System Resistance Change Over Time (During 60 kW Mock Stack Module Hot Test) 86
Figure 3-7 Anode Flow Path in Quad Base 87
Figure 3-8 Fuel HX Performance: Mock and Live Stack Module Cases 88
Figure 3-9 Potential Leak Sources Inside the Stack Module 89
Figure 3-10 60 kW Vessel Thermal Characterization 90
Figure 3-11 Thermally Integrated 50 kW SOFC Module 91
Figure 3-12 Catalytic Fuel Reformer and Radiative Heat Exchanger (Temperature Scale Shows Fluid Temperature in Kelvin) 91
Figure 3-13 3-5 kW Module (Containing 16-cell SOFC Stack) Integrated into the 30 kW Test Facility 92
Figure 3-14 Sub-Scale Stack Conductive Gasket Test Fixture 93
Figure 3-15 Comparison of Two Conductive Gasket Configurations Evaluated 94
Figure 3-16 Stack Tower Assembled at FCE Using Phase II Stack Blocks from VPS (Two 92-cell Blocks, 550 cm^2 Active Area Cells) 95

Figure 3-17 SO-30-5 Stack Tower (Two 96-cell Blocks, 550 cm^2 Active Area Cells) and Module Enclosure Assembly 96
Figure 3-18 30 kW SOFC Stack Tower Average Cell Voltage and Current over the Course of Testing 97
Figure 3-19 30 kW Stack Tower Individual Stack Average Cell Voltage and Current Over the Course of Testing 98
Figure 3-20 30 kW Stack Tower Individual Stack Average Cathode Outlet Temperature and In-cell dT over the Course of Testing 99
Figure 3-21 30 kW Stack Tower Individual Stack In-cell Temperatures of the Center Cell before and after Swapping the Stack Positions 100
Figure 3-22 Performance Degradation Rate Characterization during 30 kW Stack Tower Test 101
Figure 3-23 Four Stacks on a Quad Base in the 60 kW SOFC Module 102
Figure 3-24 60 kW Module Stack Electrical Configuration 103
Figure 3-25 60 kW Module Stack Performance at 75% Load Level 104
Figure 3-26 60 kW SOFC Module Average Cell Voltage and Current over the Course of Testing 105
Figure 3-27 Cell Voltages and Stack Current of Stack 1 during 60 kW Module Test 106
Figure 3-28 Cell Voltage Spread while Flowing Purge Gas during a System Trip of 60 kW Module 107
Figure 3-29 Cell Voltage Spread (During Purge Flows of a System Trip on 10/11/12) Indicating Oxidation of the Anode Active Layer at the Top of Each Stack in 60 kW Module 108
Figure 3-30 Cathode-out Temperature and Air Flow during 60 kW Module Thermal Cycles 109
Figure 3-31 Electrical Resistance of the Conductive Stack Gasket, Bus Bar, and Base Plate Components during 60 kW Module Test 110
Figure 3-32 Modified 30 kW Facility with a 16-cell Stack Module Installed for Testing 111
Figure 3-33 Power Output of the 16-cell Stack during Testing History 111
Figure 3-34 Anode Recycle Ratio Test Results 112
Figure 3-35 On-Cell Temperature Maps for 59% (Left) and 66% (Right) Anode Recycle Ratio Conditions 113
Figure 3-36 Fuel Utilization Test Results 114
Figure 3-37 On-Cell Temperature Maps for 62% (Left) and 75% (Right) Fuel Utilization Conditions 114
Figure 3-38 On-Cell Temperature Maps for 25% (Left) and 13.5% (Right) Air Utilization Conditions (Temperature Contours in °C) 115
Figure 3-39 Stack Performance Before and After System-style Heat-up (SO-3-03 Test) 116
Figure 3-40 16-Cell Stack Testing at Low and High DIR (In-stack Reforming) Conditions 117
Figure 3-41 Individual Cell Voltages and Degradation Rates at Low and High DIR Conditions During 16-cell Stack Test 118
Figure 3-42 Difference Between Individual Cell Voltages and Stack Average Cell Voltage 119
Figure 3-43 Effect of In-stack Reforming Level (DIR) on Center-Cell Temperature Profile (Anode Inlet Face is on left, Cathode Outlet Face is at Top) 120
Figure 4-1 Configuration B System Featuring Steam Turbine 121
Figure 4-2 Block Flow Diagram for Integrated Gasification Fuel Cell (IGFC) Baseline Power Plant 122
Figure 4-3 Baseline System Development Progress in Phase II 123
Figure 4-4 Power Island Layout for Coal-Based SOFC Baseline Power Plant 124
Figure 4-5 1 MW SOFC Stack Module 125
Figure 4-6 Compact MW-class SOFC Module 126
Figure 4-7 Contribution to Fuel Cell Stack Cost ($85/kW) by Functional Area 127
Figure 4-8 Contribution to Fuel Cell Stack Cost ($85/kW) by Cost Category 127

Figure 4-9 Contribution to Balance of Plant (BOP) Cost by Cost Category 128
Figure 4-10 SOFC Stack Cost Reduction Progress 129
Figure 5-1 RP-2 (Residential Prototype 2) System with Skins Attached (Left), CAD Representation of Hot Balance of Plant (Right). 130
Figure 5-2 Photo of Complete Aurora System with Skins (left) and 84-Cell Stack Tower and Integrated Module (Rad HX removed) (right) 130
Figure 5-3 Picture of 3-1 SOFC System Module 131
Figure 5-4 3-1 System Test Results: Stack Voltage (Tower) and Stack Current – Formal SECA Phase 1 Test 132
Figure 5-5 Block Flow Diagram of 50 kW PCM System 133
Figure 5-6 Electrical Balance-of-Plant Enclosure Showing DC/DC Converter and DC/AC Inverter 135
Figure 5-7 Central Control System Layout within EBOP 136
Figure 5-8 Schematic of Packaged 50 kW PCM Power Plant Showing Key System Equipment 138
Figure 5-9 Packaged Unit for Supplying Startup Gas for the 50 kW PCM System 139
Figure 5-10 Schematic of Catalytic Heat Exchanger 140
Figure 5-11 Cathode and Anode Exhaust Mixing in Catalytic Heat Exchanger – Computational Fluid Dynamic Modeling 140

LIST OF TABLES

Table I-1 SECA Cost Reduction Program (2005) Metric Test Results....1
Table 1-1 Summary of Major Cell Development Tests in Phase I Compared to Baseline Cell....5
Table 1-2 A Comparison of Cell Performance at Various Operating Temperatures (81 cm^2 Active Area)....6
Table 1-3 Performance Comparison of 16-cell Stacks (550 cm^2 cell area) Containing Baseline 1 mm Anode Substrate TSC-2 Cells and Thin TSC-3 Cells....23
Table 2-1 Summary of Results from 92-Cell Stack Block (550 cm^2 cell area) Performance Testing Conducted at VPS....32
Table 2-2 Main Additive Elements in Steel Compositions....58
Table 3-1 Beginning-of-Life (BOL) Performance and Operational Characteristics of the 60 kW Stack Module....104
Table 3-2 Effect of Cathode Airflow on the 60 kW Module Cool-down Parameters....109
Table 3-3 Fuel (Anode) Recycle Ratio Test Conditions....112
Table 4-1 Baseline Commercial Gasification / SOFC System Summary....121
Table 4-2 SOFC Power Plant Performance Summary – Normal Operating Conditions....124
Table 5-1 Summary of Phase I Metric Testing Results for 3-1 System....131
Table 5-2 Performance Summary of 50 kW PCM System....134
Table 5-3 Catalytic Heat Exchanger Performance for a Range of Normal Operating Flows....141

EXECUTIVE SUMMARY

FuelCell Energy, Inc. (FCE) has been engaged in DOE's Solid State Energy Conversion Alliance (SECA) program since February 2004. The initial objective of the program was to verify reduced-cost SOFC stack operation in a 3-10 kW power plant (Cost Reduction Program). The FCE team successfully completed the initial stage of the SOFC development program, surpassing all specified metrics for performance and cost. In 2006, the FCE team was selected through a competitive process by the DOE to participate in a new SECA multi-phase program for development of very efficient coal-to-electricity power plants. In September, 2006, the 3-10kW Cost Reduction program was merged with the coal-based multi-phase program for development of very efficient large scale (multi-MW) SOFC power plants with near zero-emissions. During the project period, significant progress was made in the areas of cell and stack technology development, stack module development, sub-scale module tests, Baseline Power Plant development and Proof-of-Concept Module unit design. A brief summary for each follows.

Cell Technology Development:

Cathode development including material improvements and microstructure optimization, and modified anodes led to cell performance enhancement of up to 18% (compared to baseline TSC-2 cell technology) at lower operating temperature (650°C) and reduction in performance degradation rate of more than 50% in 81-cm^2 (cell active area) single cells. Degradation rates of <0.7%/1000 h (at ~500 mA/cm^2) were achieved for the operating temperature range of 650°C to 800°C. The expansion of the operating temperature window facilitated stack implementation of the new improved cell technology. In particular, 0.32%/1000hours degradation was achieved by a single cell operating over 18,000 hours at laboratory conditions and 750°C.

Cell size was scaled up from 10 cm x 10 cm (81 cm^2 active area) to 33 cm x 33 cm (961 cm^2 active area) successfully, with no decrease in cell performance. Cell size of 25 cm x 25 cm (550 cm^2 active area) was selected for stack technology development. The cell technology improvements were implemented in the scaled up cell (550 cm^2 active area) and the TSC (tape casting, screen printing and co-firing) cell manufacturing process achieving production yield of 95% based on over 1000 cells fabricated. SOFC pilot production facility was upgraded to a annual production volume of 1 MW.

Thin anode substrate cells with improved mechanical strength, offering cost reductions of ~25%, were fabricated and validated through testing of scaled up (550 cm^2 active area) single cells and 16-cell stacks which demonstrated comparable performance level to the smaller cells (small performance improvement of ~2%).

Chromium-tolerant cells using Cr getter materials Gb and Gc were developed and tested under the cathode gas humidity level of 10%, as the presence of moisture in cathode gas is linked to the Cr poisoning of the cell. Both Cr getter materials worked effectively. An accelerated cell (81 cm^2 active area) test, evaluating a combination of Cr getters Gb and Gc (30% - 70% mix, Design 2) along with coated cathode side hardware, accumulated over 8,500 h of operation demonstrating a performance degradation rate less than 0.5%/1000 h. In a repeat test of Cr getter Design 2 cell, thermal cycling capability was evaluated after about 2000 h of exposure to 10% cathode gas humidity. The cell was subjected to 10 thermal cycles, showing a performance loss of only 0.8 mV/cycle. Design 2 Cr-getter materials set was selected and implemented in 16-cell (550 cm^2 cell active area) stacks.

Single cell tests of coated cathode side hardware to evaluate spinel Manganese–Cobalt Oxide (MCO) coatings developed by Nextech and PNNL (Pacific Northwest National Laboratory)

showed promising results. Nextech coated hardware was tested for over 10,000 h, showing a low performance degradation rate of 0.45%/1000 h (at 500 mA/cm^2). PNNL coated hardware was tested for over 8,400 h with 7,390 h at 10% cathode gas humidity condition. The cell performance degradation rate over the 7,390 h-period was estimated to be 0.45%/ 1000 h.

Stack Technology Development:

Many 550-cm^2 cell active area stacks ranging in size from 6 cells to 96 cells were built and tested during the project period. In Phase I, the stack building block was scaled up to a stack size of 64 cells (550 cm^2 cell active area). End-of-Phase I metric testing, based on the 64-cell stack block, was conducted successfully. During the initial peak power testing period, a power output of 11 kW and a power density of 314 mW/cm^2 were achieved. The stack completed the required 5000 h of steady state testing, demonstrating a performance degradation rate of 2.7%/1000 h, much lower than DOE SECA requirement of <4%/1000 h.

In Phase II, the stack building block was further scaled up from a stack size of 64 cells to 92 cells (550 cm^2 cell active area). Also, operation at more aggressive system-representative conditions (higher reactant utilizations and more in-stack reforming) was pursued. The stack block power output increased from 10 kW (at Phase I system conditions) to 18 kW (at Phase II system conditions). Thin TSC-3 (third generation TSC) cell technology was implemented in stacks. End-of-Phase II metric test was conducted by simultaneous testing of a stack tower containing two 92-cell building blocks (at FCE, Danbury) and of a 120-cell thin TSC-3 cell stack (also containing thin interconnects) at VPS. During initial peak power testing period, both tests met the requirement of ≥25 kW. The stack tower generated 30.2 kW DC, whereas the 120-cell stack achieved a power density of 381 mW/cm^2. Both tests were terminated after about 2000 h of testing because of low performance of some cells. The stack demonstrated a performance degradation rate of 0.9%/1000 h in first 1500 h of testing. This was well within Phase II target of ≤2%/1000 h. In Phase III, the stack building block was scaled up to a stack size of 96 cells (550 cm^2 cell active area), to serve as a representative of the manufactured building blocks for large-scale modules (>50 kW). Long-term steady state testing of 96-cell stack blocks was conducted for the 5000 h metric test completion. The first 96-cell stack block was tested for >5000 h and achieved 16 kW of DC power during steady state operation. The second block, which was tested for performance stability at system-representative conditions, exhibited a degradation rate of 1.4%/1000 h during ~3500 h of steady state testing.

The 16-cell (550 cm^2 cell active area) stack tests were continued to study the issues related to higher performance degradation rate and cell performance drop observed in 96-cell stack block tests. The stack builds were designed or configured to facilitate parametric studies. Sensitivity to more aggressive (Phase II) system operating conditions was evaluated. Based on results of one 16-cell stack test, a decision was made to use an improved cell manufacturing method, which entailed covered (with half-cell) cathode and barrier layer firing procedures, for all future cell production. Another 16-cell stack contained chromium getter materials in Cells 4, 6, 8, 10 and 12. The stack was assembled with contact paste layers screen-printed with more uniform print thickness. Starting with this stack, all new 550 cm^2 active area cell size stacks had anode flow field improvements (pinch rolled to a lower height target to ensure component expansion and height consistency) implemented. The stack underwent steady state testing at 68% Uf, 70% in-stack reforming (DIR), 15% air utilization and 387 mA/cm^2 conditions (Phase II system representative conditions). In ~1,100 h test period at these conditions, the stack demonstrated a very low performance degradation rate of 0.54%/1000 h. The impressive result was mostly attributed to anode flow field improvements.

An advanced In-Cell Manifolded (ICM) stack design was implemented in an 8-cell stack. The stack passed the factory test at high fuel utilizations. The design of ICM stack was subsequently

scaled up and implemented in a 19-cell stack. This stack was tested at Phase II system conditions for over 1,100 h showing a low performance degradation rate of 0.71%/1000 h.

A 10-cell stack containing 1000 cm^2 cell active area scaled up cells was designed and tested successfully, demonstrating a power output of 4 kW.

Stack Module Development and Sub-scale Module Tests:

A 60 kW-class SOFC stack module design was developed. The module accommodates four stacks supported on a quad base. The quad base design provides the support structure as well as facilitates the gas flow distribution to stacks located within the module. The stacks are electrically connected to form two parallel strings with a series-connected stack pair in each string. The module enclosure and base are internally insulated (thermal), as the enclosure void space serves as the oxidant-In manifold and provides hot process gas to the stacks. The 2^{nd} generation Proof-of-Concept Module design was also developed. Integration of some of the system balance-of-plant (BOP) components with the SOFC stack module was performed. The integrated module design offers overall system compactness (packaging), reduced piping (and related cost savings), reduced module enclosure penetrations (and heat losses) and better thermal integration.

The stack tower concept containing multiple stack building blocks was developed. A few stack towers were built and tested during the project. The first stack tower was assembled using three 64-cell stack building blocks and was used to test validate the tower concept successfully. Subsequently, stack towers containing two 92-cell stack blocks each were assembled and tested. One of these was a part of the End-of-Phase II metric test. As mentioned earlier, the stack tower generated 30.2 kW DC power. In Phase III, a stack tower assembled using two 96-cell stack blocks was tested. The test accumulated over 3300 h of on-load operations. To investigate the effects of block location (within the tower) on performance, the positions of the two stack blocks within the 30 kW tower were swapped. Cell voltages, performance degradation rates, cell temperature profiles and in-cell ΔTs for the two stack blocks before and after the position-swap were compared. It was observed that the position of stack in the tower did not have a significant effect on the stack performance or degradation rates. The results of the test and the analysis of data validated the feasibility and operability of the 30 kW stack tower configuration as an assembly of stack blocks in a vertical array arrangement.

The 60 kW quad-base module test was conducted using four 96-cell stack blocks. FCE's 400 kW-class (carbonate fuel cell) test facility was modified for this test. The 60 kW system achieved 1645 hours of hot operational time including 1130 hours on load. The module test endured multiple facility trips caused by the balance-of-plant equipment failure and anomalies in the control software. Considering that the facility was upgraded to an SOFC test station including implementations of new software and hardware, the forced shutdowns and involuntarily trips were expected. The module test data analysis showed that the top half of each stack experienced higher performance degradation rates. The cause-and-effect analysis showed that the issues were related to the operation of the facility and not to the module design. The analysis of data validated the module configuration robustness as a platform for future proof-of-concept systems.

Baseline Power Plant Development:

In Phase I, a utility-scale Baseline Power Plant was developed which utilized commercially-available equipment. The plant employed ConocoPhillips E-Gas coal gasifier, Selexol acid gas removal subsystem and a steam turbine bottoming cycle (in addition to SOFC modules). Illinois No. 6 coal was used as the feedstock for system analysis. The system generated 408 MW net

AC power (meeting >100 MW size requirement) with a 42% electrical efficiency (coal HHV basis), while capturing 90.2% carbon (as CO_2) from coal syngas.

An advanced Baseline Power Plant system configuration was developed in Phase II to achieve higher efficiency. The Baseline System employed catalytic gasification and warm gas cleanup technology (in conjunction with Flue Gas Desulfurization). The system further employed oxy-combustion of the anode exhaust for CO_2 capture using a portion of the oxygen from the air separation unit at the gasification site. After a comprehensive system optimization effort, the system efficiency of 58.7% was achieved (significantly exceeding >50% efficiency target). The Baseline Power Plant system produced 414.6 MW net AC power while capturing >99% carbon (as CO_2) from coal syngas (significantly exceeding 90% minimum removal requirement). The coal-based SOFC system consumes 75% less water compared to PC (pulverized coal boiler) plants using scrubbing technology for carbon capture.

A conceptual layout of the Baseline Power Plant (general arrangement of the power island) was developed. The layout included eight sections, each with 42 fuel cell modules. The MW-class module concept was developed with 16 stack towers arranged in a horizontal configuration to provide better thermal performance and a compact footprint. Each tower consists of four 96-cell (550 cm^2 cell active area) stack building blocks. The footprint of the IGFC (integrated gasification fuel cell) plant was found to be slightly smaller (5.5 acres or 22,407 m^2) than a comparable IGCC (integrated gasification combined cycle) plant (5.6 acres or 22,814 m^2).

Cost analysis for Phase II Factory Cost Estimate Report was performed near the end of Phase II. The SOFC stack cost was estimated to be $85/kW and the power island (IGFC plant) Factory Equipment Cost was estimated to be $371/kW. The cost estimates are in Y2000 USD (for consistency with DOE cost targets). The cost numbers were based on a peak power output of 671.8 MW net AC and assumed an annual production level of two Baseline Power Plants per year. This required the production of 43,008 stacks (stack building blocks) per year. The power island layout and the conceptual design of compact MW-class SOFC module (mentioned above) facilitated the cost estimation. The factory cost report was later revised to update the SOFC stack block, stack module and balance-of-plant factory equipment costs. The updated estimates (early in Phase III) were based on Year 2007 US dollars for easy comparison with DOE's updated cost targets. The revised stack block cost estimate was $147/kW and the power island Factory Equipment Cost was $635/kW. Both costs met the SECA Phase III requirements of $175/kW and $700/kW for stack cost and power island Factory Equipment Cost, respectively.

Proof-of-Concept Module (PCM) Unit Design:

A 50 kW (60 kW peak) proof-of-concept module (PCM) system was developed. The system was based on a module containing four 120-cell stacks. The system uses pipeline natural gas as the fuel. Process modeling of the system was performed for full power, rated power, and heat-up modes of operation. At full power operation, the system electrical efficiency was estimated at 62% (LHV natural gas) with the potential for nearly 84% overall efficiency for CHP (combined heat and power) applications.

The 50 kW PCM system engineering package was prepared. Equipment specification, vendor contacting and selection activities were performed. The PCM system control philosophy document was developed, covering 13 steps/operational modes including heat up, hot standby and power generation (electrical load ramp) steps. Trip – restart strategies were also developed. The plant piping pressure drop mapping was carried out.

The design and fabrication of a catalytic heat exchanger to oxidize unused fuel from SOFC and recover waste heat for preheating of cathode air were carried out. The catalytic air preheater design was validated through testing in FCE's 400 kW facility. Detailed design, fabrication, and

factory testing of the system's start-up assembly (for PCM plant heat-up) were completed. Packaging design of the PCM plant was conducted. The plant was designed as single-skid with removable façade for easy replacement of plant equipment or the SOFC module.

INTRODUCTION AND OBJECTIVES

FuelCell Energy, Inc. (FCE) initiated the work described in this report in February 2004 by participating in the U.S. Department of Energy (DOE) managed, Solid State Energy Conversion Alliance (SECA) program to develop a 3-10 kW solid oxide fuel cell (SOFC) power system. Development efforts in cell technology were focused on improved materials for anode and cathode as well as cell testing for internal reforming. Stack development efforts were focused on development of improved seals and delivering and testing of a 3kW SOFC power system. As shown in Table I-1, the FCE team successfully completed this initial stage of the SOFC development program, surpassing all specified metrics for performance, reliability, endurance and cost. Much progress was made on cell and stack scale-up. The SOFC cell active area was scaled-up from 81 cm^2 to 121 cm^2 [1]. The SOFC stack building block size was scaled-up from 16-cell to 28-cell size. The cell and stack block scale-up provided an approximate five-fold increase in stack power output (220 W gross to 1.152 kW gross). The 3 kW test demonstration (Table I-1) was based on a stack tower configuration containing four of the scaled-up SOFC stack building block units. The 112-cell (121cm^2 cell active area) stack and system was operated for over 2000 h. The milestone performance test included seven load transients, three thermal cycles and peak power demonstration. In September 2006, this program was merged with a multi-phase program for development of very efficient coal-to-electricity, large scale (multi-MW) SOFC power plants with near zero-emissions. The SOFC technology developed and verified in the SECA 3-10 kW development program served as the basis for further development and scale-up in this multi-MW, SECA Coal-Based Systems program.

Table I-1 SECA Cost Reduction Program (2005) Metric Test Results

	STEADY STATE OPERATION (BOT)	STEADY STATE OPERATION (EOT)	PEAK POWER OPERATION	SECA METRIC	
Net DC Electrical Power	3.39kW	3.13kW	5.26kW	3 to 10kW	✓
Net DC Electrical Efficiency	38.7%	36.4%	33.3%	>35% (Steady State)	✓
Stack Power Density	280mW/cm^2	260mW/cm^2	430mW/cm^2	N/A	
Steady State Degradation		1.2%/500hrs	N/A	<2%/500hours	✓
Transient Degradation (7 load interruptions, 3 thermal cycles)		0.7%	N/A	<1.0%	✓
Availability		98.6%	N/A	>80%	✓

✓ All SECA 3kW Phase I Cost Reduction Program performance metrics have been successfully demonstrated!

The overall goal of this three-phase DOE sponsored project is the development of SOFC cell and stack technology suitable for use in highly-efficient, economically-competitive central generation power plant facilities fueled by coal synthesis gas (syngas). The development of this technology will significantly advance the nation's energy security and independence interests

while simultaneously addressing environmental concerns, including greenhouse gas (GHG) emissions and water usage. This program incorporates the following supporting objectives:

- Reduce SOFC-based electrical power generation system cost to $700 or less (2007 dollars) for a greater than 100 MW Integrated Gasification Fuel Cell (IGFC) power plant, exclusive of coal gasification and CO_2 separation subsystem costs.
- Achieve an overall IGFC power plant efficiency of at least 50%, from coal (higher heating value or HHV) to AC power (exclusive of CO_2 compression power requirement).
- Reduce the release of CO_2 to the environment in an IGFC power plant to no more than 10% of the carbon in the syngas.
- Increase SOFC stack reliability to achieve a design life of greater than 40,000 hours.

FuelCell Energy has completed all three phases of the program. Phase I efforts focused on cell and stack size scale-up with concurrent enhancement of performance, life, cost, and manufacturing characteristics. Fabrication and verification testing of scaled-up cells and stacks was conducted. Also in Phase I, design and analysis of the baseline (more than 100 MW) power plant system—including concept identification, system definition, and cost analysis—was conducted.

Phase II efforts focused on development of an at least 25 kW SOFC stack (stack tower) incorporating multiple stack building blocks of scaled-up cells, with the stack deliverable to be suitable for integration into a large scale fuel cell power module. Activities in Phase II also included the development of the baseline system, factory cost estimate for the baseline plant power block, and conceptual design of Module Demonstration Unit (MDU).

The specific objective for Phase III was the validation of the performance and robustness of stacks and, subject to a decision point, of scaled stack arrays suitable for use in large-scale power generation systems such as an IGFC with reliable, fail-safe operation being of paramount importance. In support of the aforementioned goal and Phase III objective, activities during Phase III included:

- Continued development of cell and stack technology via design and materials development, focusing on performance, reliability, cost, and manufacturing enhancement.
- Fabrication, testing, and post-test analyses of the fuel cells and fuel cell stacks, culminating in the test of an at least 30 kW stack tower for 3,000 hours or more. The stack tower test was expected to meet DOE cost goals (no more than $175 per kW for the stack, in 2007 dollars) and endurance goals (no more than 1.5% per 1,000 hours of steady-state performance degradation).
- Design an SOFC-based Proof of Concept Module (PCM) system, including the SOFC stacks, mechanical balance-of-plant (BOP), and electrical BOP.

EXPERIMENTAL METHODS

The project involved cell component development and scale-up; manufacturing process improvements and scale-up; stack block, stack tower and multi-stack module design and testing; and balance-of-plant (BOP) system design and component testing. Various tests such as single cell, short stack, stack block, stack tower, four-stack module, and out-of-cell characterization tests were used to support these developments and activities. FuelCell Energy, Inc. (FCE) and Versa Power Systems (VPS), both, have test stands and test facilities including analytical equipment. These test tools were used routinely throughout the reporting period.

Additional experimental details and photographs are provided along with relevant test results under 'Results and Discussion' section of the report.

Significant effort was placed on test facility expansion to accommodate large area stack tests. The activities included modification of existing and acquisition of new single cell and stack test stands at VPS. This facilitated cell scale-up development to 33 cm x 33 cm cell size and large area (250 cm^2 active area) stack scale-up development to 10-25 kW size. Development of a 10-30 kW test facility at FCE's Danbury, CT location was also carried out to accommodate SOFC stack block and tower testing. FCE's 400 kW-class facility was modified for SOFC 60 kW quad module test. Additional information on test stand and test facility modifications is provided under 'Results and Discussion' section of the report.

At the cell level, a reliable electrochemical testing method for separating over-potential and resistance losses during steady state and transient operations was implemented to facilitate investigation of cell performance degradation mechanisms.

RESULTS AND DISCUSSIONS

1.0 CELL TECHNOLOGY DEVELOPMENT

(*VPS Technical Lead, support from FCE)*

Development work concentrated on key cell issues of materials stability, cell robustness, and degradation - specifically subject to the system operating conditions. Opportunities for efficiency improvement and cost reduction were also addressed as appropriate. Fundamental materials solutions are very effective for cost reduction, endurance enhancement, robustness improvements, and efficiency improvements (higher operating voltage). Investigations into the performance and endurance of the cathode and anode functional layers at various operating temperatures as well as with different fuel and oxidant gas compositions were carried out. Other major areas of cell technology development included scale-up of cell size and cell manufacturing process development.

1.1 Cell (Component) Material Development

Performance Enhancement and Degradation Rate Reduction: Electrochemical performance enhancement was critical to the overall project objectives (cost, life, and efficiency). During **Phase I**, materials development focused on improving baseline cell electrochemical performance via several parallel approaches of materials modifications and (electrode) microstructure optimizations. Major performance improvement breakthroughs were achieved as shown in Figure 1-1.

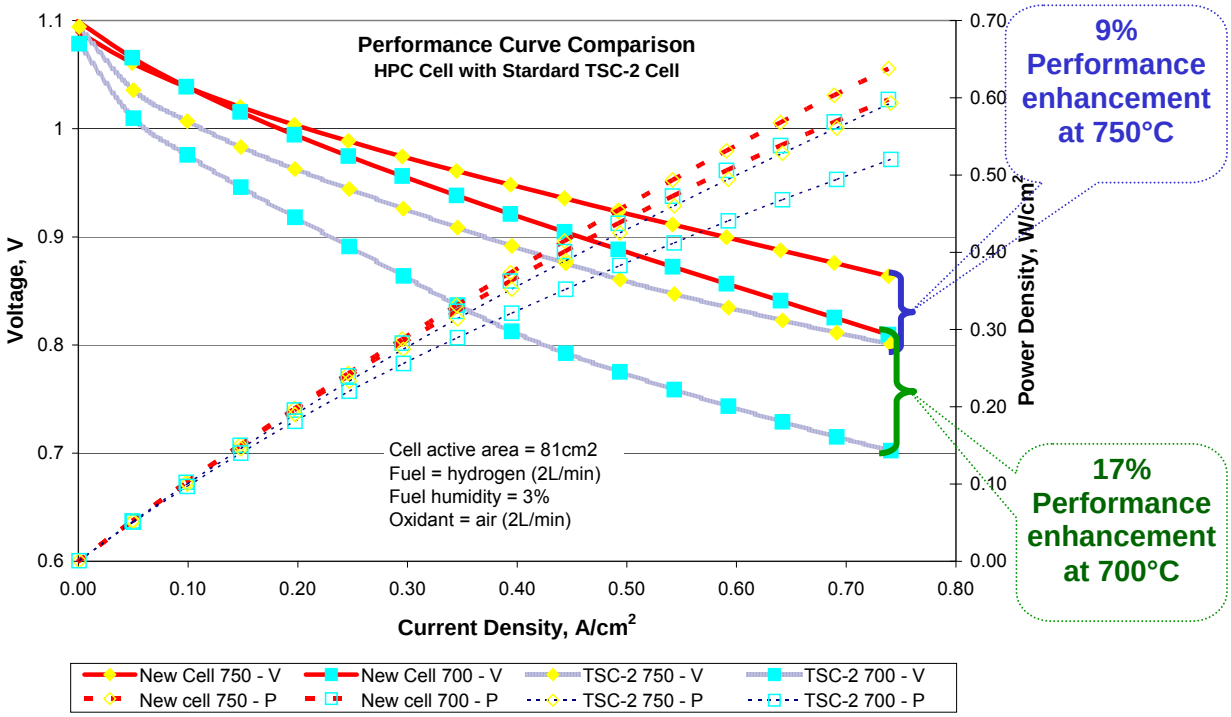

Figure 1-1 Solid Oxide Fuel Cell Electrochemical Performance Enhancement.

The figure compares the polarization curves of an improved cell (HPC-3) with a baseline TSC-2 (second generation tape casting, screen printing and co-firing manufacturing process) cell. Performance enhancements of 9% and 17% were achieved at operating temperatures of 750°C and 700°C, respectively. This improvement enabled cell operation at higher power density, lower temperature, higher operating voltage, or some combination of these.

Cell degradation is one of the major technical challenges in Solid Oxide Fuel Cell (SOFC) development. During Phase I, excellent progress was made in understanding cell degradation mechanisms over a range of operating conditions. A reliable electrochemical testing configuration was developed for single cells with metallic interconnects to independently measure over-potentials at various component interfaces. The test setup was stable and repeatable over the course of an entire endurance test of thousands of hours through various operating conditions. This enabled the team to focus development resources in the most critical areas, and contributed significantly to the degradation reduction breakthroughs in Phase I. The insights gained from this troubleshooting diagnostics yielded the development of an improved, LTS (low temperature super) cell, with significantly lower degradation rate. Figure 1-2 shows the long term steady-state results (from a single cell test) over 5000 hours, with a degradation rate of 6 mV per 1000 hours, or 0.7% per 1000 hours. This is more than a 50% reduction in the degradation rate of the baseline cell.

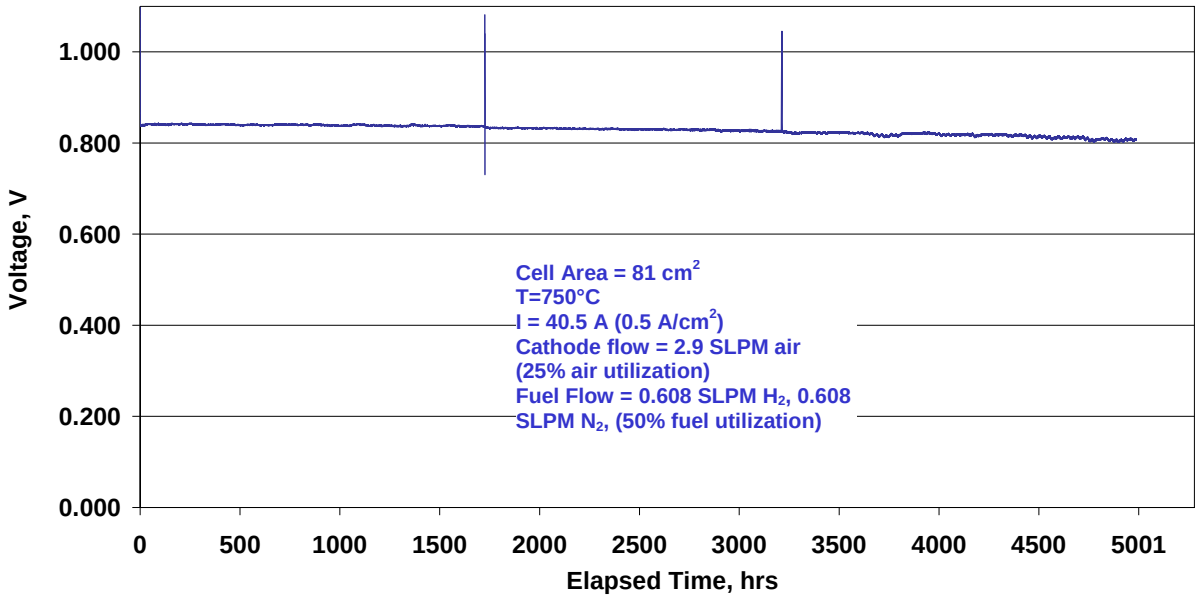

Figure 1-2 Long Term Steady-State Test of an Improved Cell (LTS-3 Cell) at 750°C.

Table 1-1 is a summary of the significant cell tests conducted in Phase I, including both performance data and long term endurance data (performance degradation rates at 750°C and 0.5 A/cm^2). Significant progress was made in both life and performance areas. Although performance improvements of the HPC (high performance cathode)-type cells were greater, especially at a lower operating temperature of 700°C, the newly developed "LTS-type" cells had a superior combination of both performance and longevity characteristics. The LTS (cathode) cell (LTS-3) was selected as the new cell materials platform (baseline) for further development in Phase II.

Table 1-1 Summary of Major Cell Development Tests in Phase I Compared to Baseline Cell

Cell Type	Performance at 700°C, 0.74 A/cm^2		Performance at 750°C, 0.74 A/cm^2		Degradation per1000 hrs		Testing Duration
	Peak V	Gain	Peak V	Gain	mV	%	
TSC II	730 mV	Baseline	812 mV	Baseline	14	1.7%	6500 hrs
HPC - 1	788 mV	8%	854 mV	5%	13	1.5%	8600 hrs
HPC - 2	783 mV	7%	864 mV	6%	14	1.6%	7100 hrs
HPC - 3	852 mV	17%	885 mV	9%	13	1.5%	4300 hrs
LTS - 3	794 mV	9%	847 mV	4%	6	0.7%	5000 hrs

In Phase II, the cell performance was further enhanced through anode development. Three anode variations (AC-5, AC-10 and AF-10) were developed with the LTS cathode. The performance of these cells (81 cm^2 active area) was better than the LTS (baseline) cells at all temperatures and most notably at 650°C. Figure 1-3 compares the performance characteristics of the different cell types at the operating temperature of 650°C. The newly developed AC-10 cell delivered a power density of 500 mW/cm^2 at an operating voltage of 0.8 V. This was more

than double the power density provided by TSC-2 (Phase I baseline) cells at the same operating conditions.

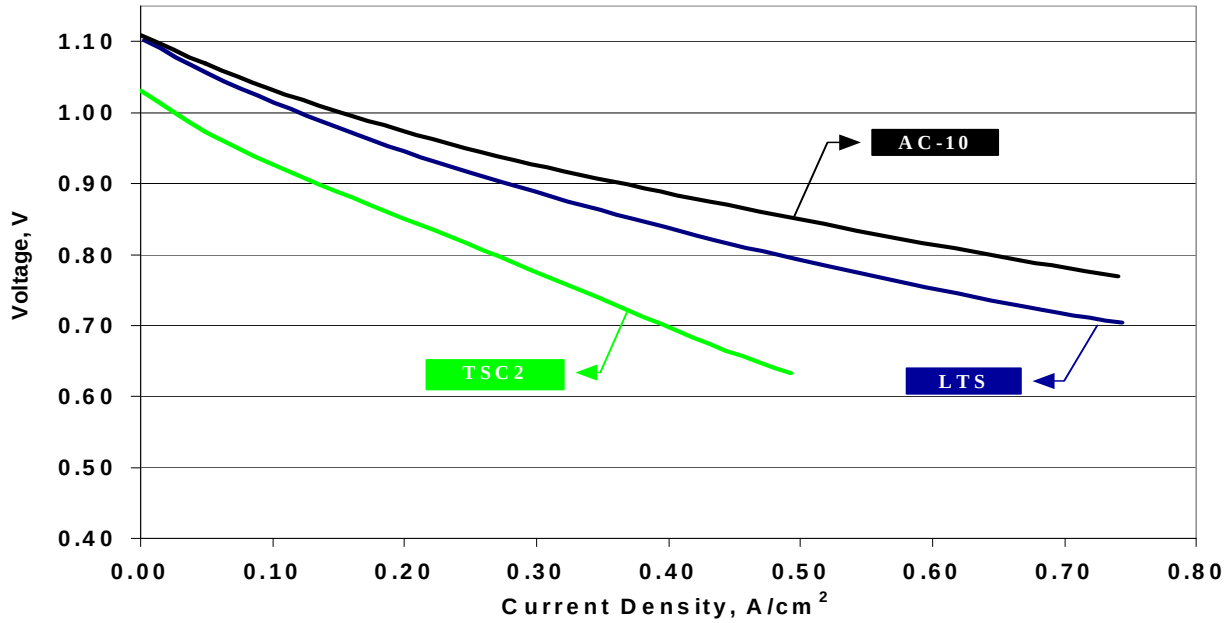

Figure 1-3 Comparison of Performance Characteristics for Different Cell Types (81 cm^2 Active Area) at 650°C

Table 1-2 compares the performance of the modified anode cells with other cell types, in the 650°C - 800°C operating temperature range. The cells with modified anodes increased the performance of the LTS-style cathode cells to that of the HPC-type cells while maintaining the lower degradation rates of the LTS-type cells. Figure 1-4 shows a comparison of cell voltage vs. time characteristics at 750°C for various cell types developed in the project. The performance and endurance improvements made with the AC-5 and AC-10 cells are evident. The long-term test of modified anode cell AC-5 accumulated over 10,700 h at 750°C. The degradation rate was 0.5%/1000 h.

Table 1-2 A Comparison of Cell Performance at Various Operating Temperatures (81 cm^2 Active Area)

Cell Type	Performance at 0.74 A/cm^2 (mV)			
	650°C	700°C	750°C	800°C
TSC-2		714	803	842
HPC	773	852	885	893
LTS	704	809	860	881
AC-5	730	829	871	888
AC-10	763	842	876	889
AF-10	734	829	872	891

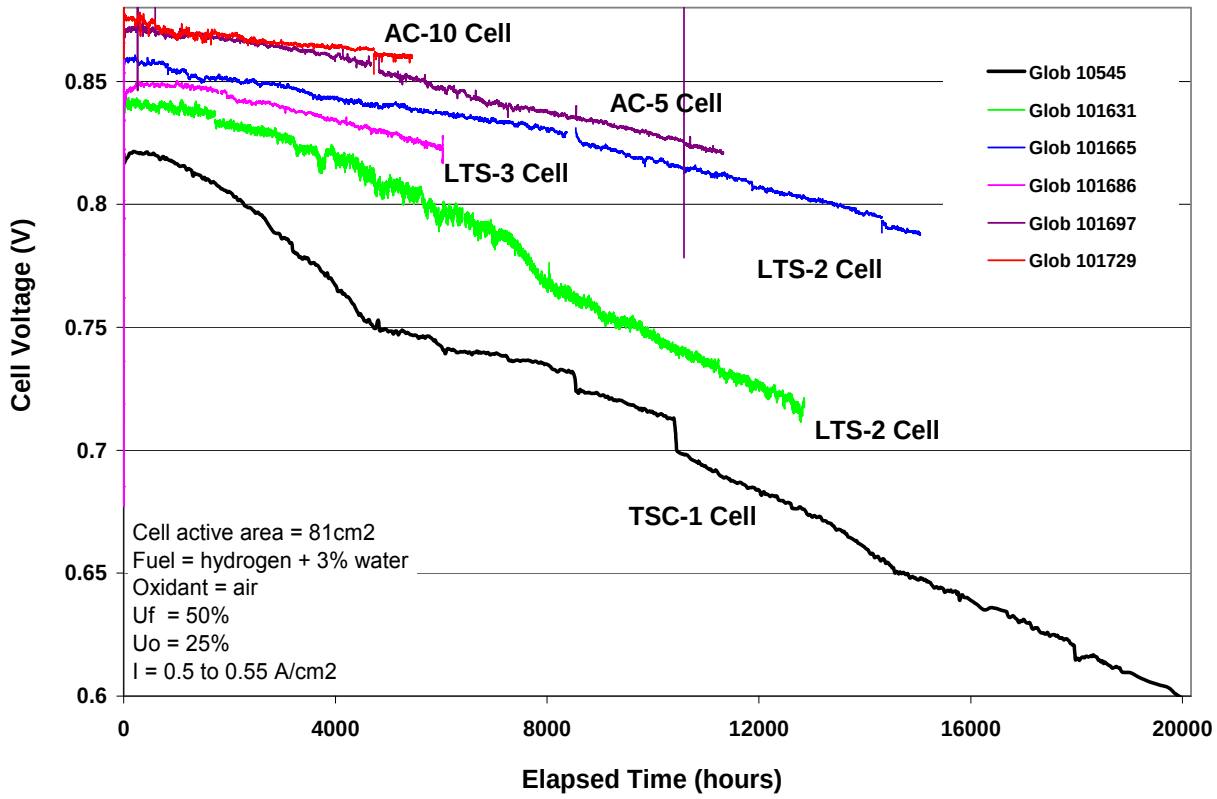

Figure 1-4 Comparison of Voltage-Time Characteristics (at Constant Current) for Various Cell Types at 750°C

The development efforts also focused on expanding the operating temperature window, to accommodate larger temperature gradients in stacks. Cell performance degradation rate was reduced significantly at high temperature of 800°C and at low temperature of 650°C. Figure 1-5 shows the effect of temperature on voltage-time characteristics for cells in the 650 to 800°C range. Degradation rates of <0.7%/1000 h (at ~500 mA/cm^2) were achieved for the temperature range of 650 to 800°C, in 81 cm^2 active area cells. This facilitated stack implementation of the new improved cell technology.

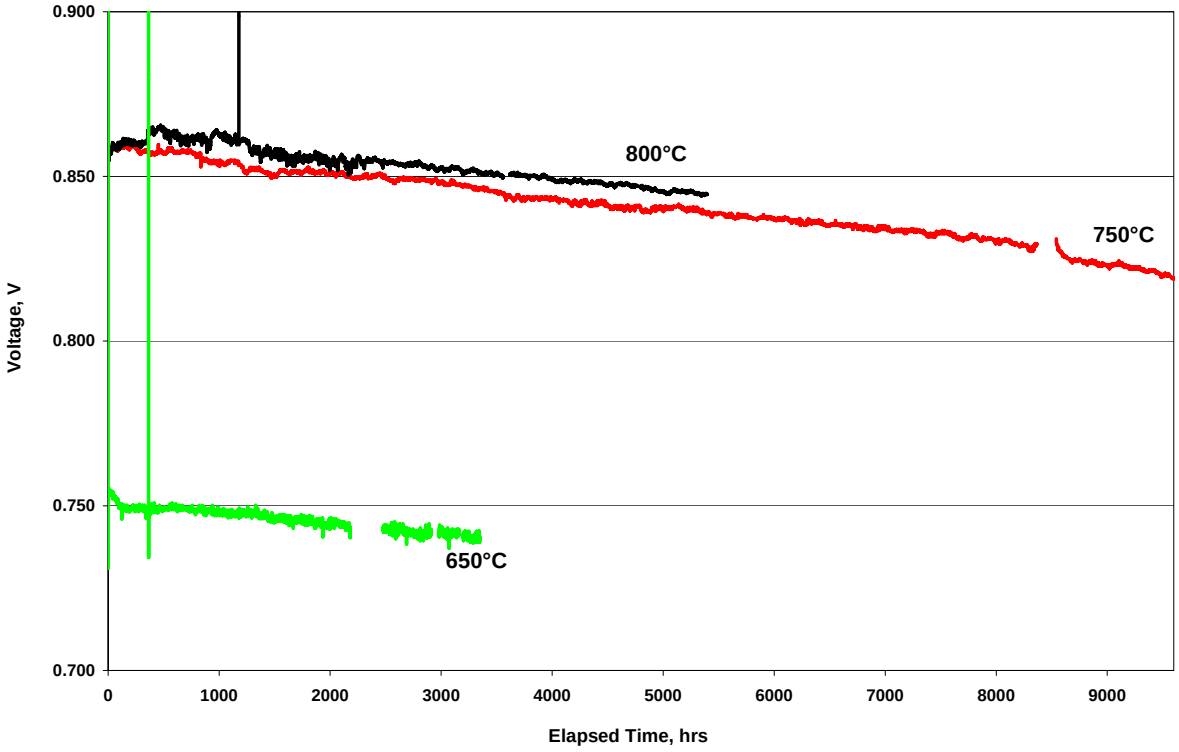

Figure 1-5 Voltage-Time Characteristic at Constant Current for LTS Cells (81 cm^2 Active Area) from 650 to 800°C

Thin Cell Development for Cost Reduction: Development of thin anode substrate cells was carried out for cost reduction. The anode substrate represented more than 65% of the cell's material cost. By reducing the anode substrate thickness from 1.0 mm to less than 0.6 mm, the cell material cost could be reduced by more than 25%. Potential challenges in utilizing thin cells in stacks were identified through testing and modeling. Improving intrinsic anode substrate strength was one of the key strategies for implementing thinner cells in a stack. Experiments with 3 mole% yttria-stabilized zirconia (3YSZ) in the anode substrate showed more than 50% improvement in biaxial strength compared to 8YSZ anode substrates. A cell with higher biaxial strength is expected to be stronger and less likely to fracture during fabrication and operation. Scaled-up thin cells with an anode substrate thickness of 0.57 mm and 25 cm x 25 cm cell size were produced using the TSC process and the 3YSZ material. The cells were tested in a 16-cell stack. Performance validation in fuel utilization tests (50-80% utilization range) indicated that the cells were structurally intact. Performance comparison of the thin cell stack with the stack containing baseline cells indicated that performance of the thin cell stack was slightly higher (up to 3% improvement at 80% utilization). Test results are presented in Section 1.2 (Cell Area Scale-up and Cell Technology Integration).

The standard (stack) heat-up procedure results in anode exposure to humidity. Thin anode TSC-3 (third generation TSC process) cells fabricated using partially stabilized zirconia containing 3 mole% yttria (3YSZ) possessed good mechanical strength. However, the 3YSZ material transforms from tetragonal phase to monoclinic phase in presence of steam (humidity) with increasing temperature or stress. The anode volume increase and corresponding mechanical stress on cell caused by this transformation are detrimental to cell performance.

Efforts were focused on improving hydrothermal stability of the anode. Effect of anode sintering temperature on hydrothermal stability was investigated in the temperature range from 1275°C to 1375°C. The out-of-cell tests involved exposing anode half-cells to 10% relative humidity environment at 150°C for 24 h. The investigation also included x-ray diffraction (XRD) examination of anode substrate surface after the humidity treatment to check for phase transformation. The increase in sintering temperature of a 3YSZ anode was found to increase the change to monoclinic phase from humidity treatment. Effect of 3YSZ anode doping with a number of additives on its behavior upon humidity treatment was also investigated. Al_2O_3 and MgO additives in combination with a lower sintering temperature of 1325°C showed promising results. The cells remained flat after the humidity treatment.

An improved, hydrothermally stable thin TSC-3 cell was developed. The design was validated in a 16-cell (550 cm^2 cell area) stack test by completing five thermal cycles, while progressively increasing anode gas humidity during heat up and cool down. Figure 1-6 shows the test results. The fuel utilization test performance after each thermal cycle and post-test examination showed that the newly developed cell met the hydrothermal stability requirements for the most stringent anode gas humidity conditions.

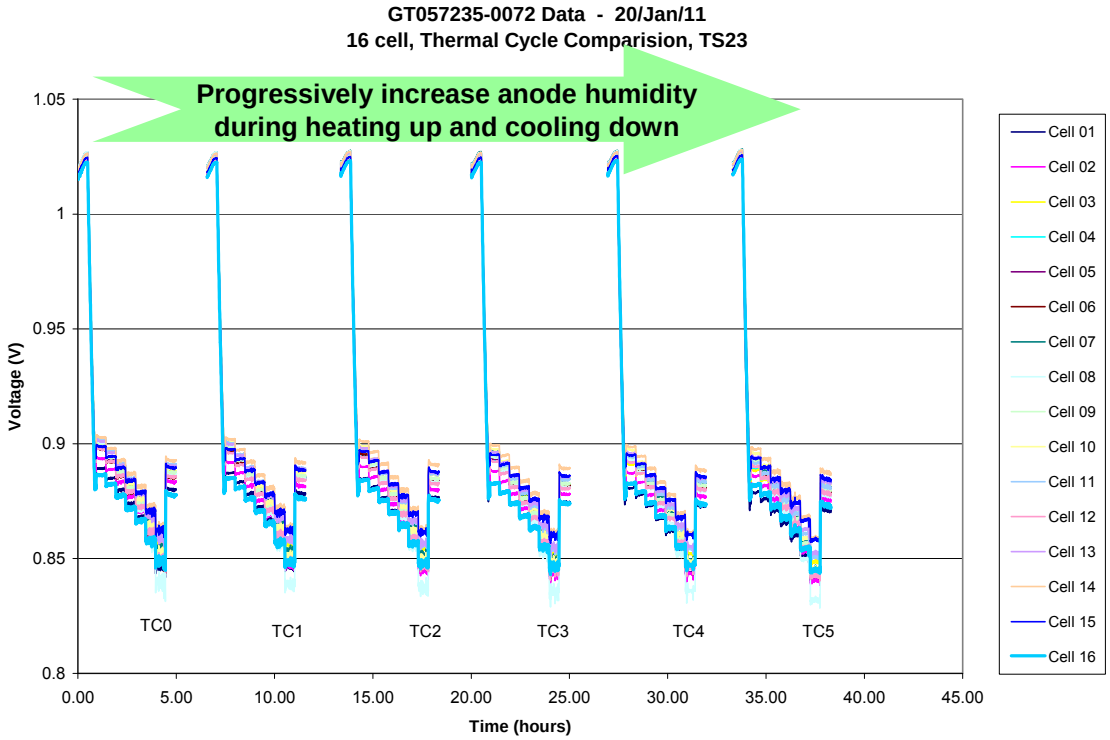

Figure 1-6 Hydrothermal Stability of Thin TSC-3 Cells in a 16-cell Stack Demonstrated in Fuel Utilization and Thermal Cycle Test

Chromium Tolerant Cell Development for System Compatibility: Cell performance degradation at different cathode gas humidity levels was studied through a number of cell tests. Higher degradation rates at higher humidity levels are largely due to higher Cr vapor pressures when steam is present at the cathode. When steam is present, $CrO_2(OH)_2$ is the dominant Cr specie. The key mechanisms through which Cr vapor species can cause degradation in the cathode are illustrated in Figure 1-7. Both, Cr oxide formation in cathode and Cr_2O_3 deposition at cathode/electrolyte interface significantly increase cathode overpotential.

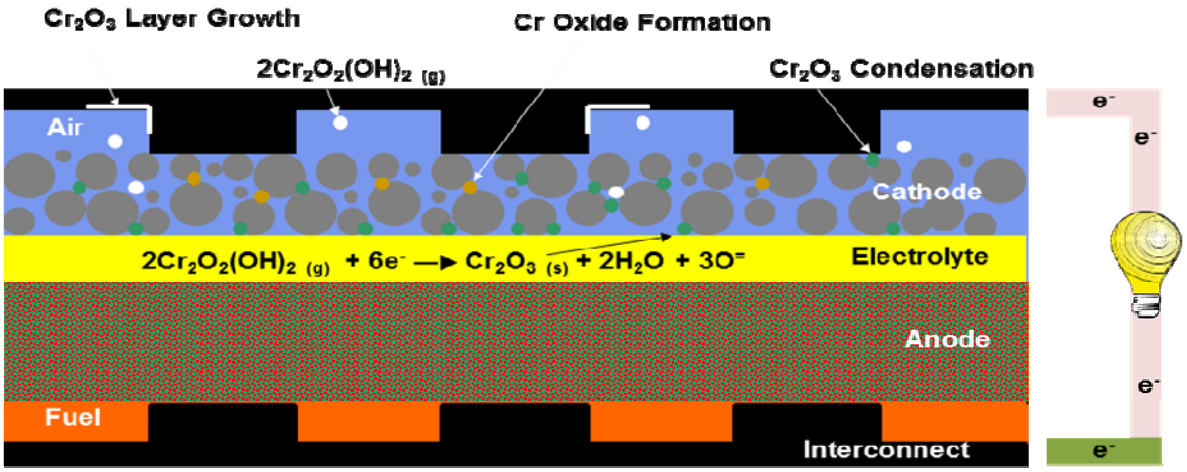

Figure 1-7 SOFC Cathode Degradation Mechanisms Related to Cr Species

The impact of Cr on cell degradation is dependent on cathode materials. Different cathodes will respond to similar cathode humidity levels (similar induced Cr concentration) differently. To study the new Cr poisoning baseline for TSC-3 cells, the degradation rate at humidified cathode gas conditions was evaluated in a 6-cell stack, as shown in Figure 1-8. Upon increasing cathode humidity from 0% (dry facility air) to 3.5% at the cathode, the cell degradation started to accelerate as indicated by the parabolic voltage response in the next 4,000 hours.

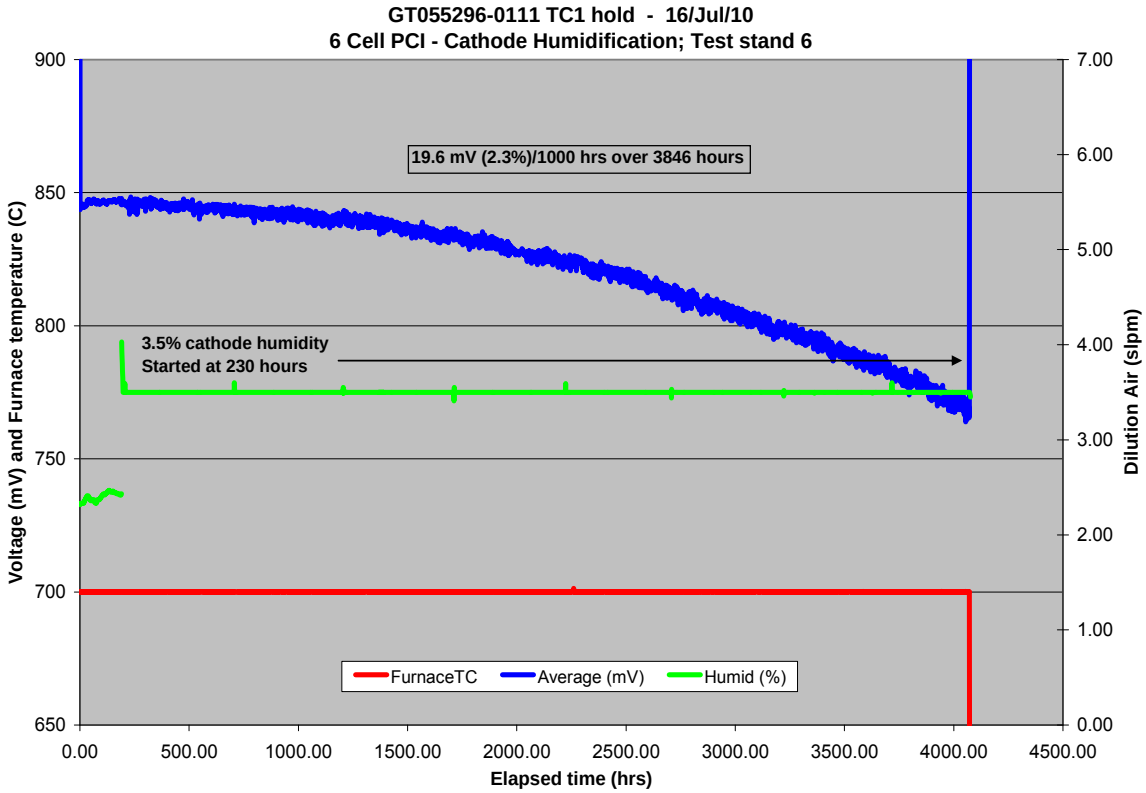

Figure 1-8 Performance Degradation of a TSC-3 Cell Stack During Test with 3.5% Cathode Gas Humidity

To incorporate TSC-3 cells in stacks and operate at system conditions with significant cathode humidity, technology development to minimize the impact of Cr on TSC-3 cells was pursued. One of the strategies employed was coating the cell hardware to minimize Cr species in the cathode. The sub-micron Co coating is effective in reducing Cr species in cathode by forming in situ a dense Co-Mn spinel as the protective outer oxide layer. This spinel layer prevents Cr transfer to the cathode through surface diffusion as well as gas phase transport in air. The impact of Co coating effectiveness in preventing Cr poisoning of TSC-3 cells was evaluated in a single cell test. The stainless steel test jigs (hardware) were coated with sub-micron Co (cobalt) and oxidized in-situ to form a Co-Mn spinel layer on top of Cr_2O_3 layer. The cell was first tested with dry air, and then the cathode gas humidity level was progressively increased to 3.5%, 5%, and 10%. Figure 1-9 shows the test results. Although, the performance decay rates are significantly lower compared to those observed with uncoated stainless steel jig, the cell degradation rate still increased from 0.56% to 2.1% per 1,000 hours with the increased humidity. Upon return to dry air (prior to test termination), the cell degradation rate reduced to less than 1% per 1,000 hours.

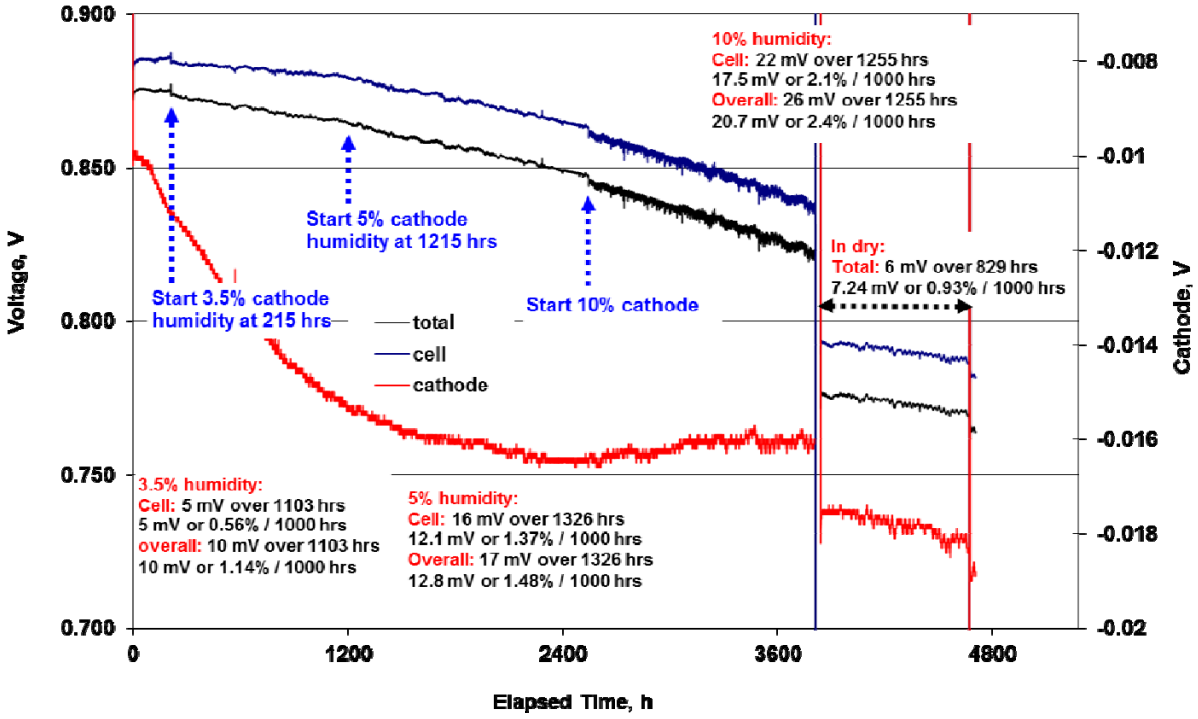

Figure 1-9 Effect of Cathode Gas Humidity Level on Performance Degradation of TSC-3 Cell Glob 101792 Containing Coated Stainless Steel Hardware

In addition to a better coating technology, developing more Cr-tolerant cathodes was a key area of cell development. New methods of incorporating active Cr getters on cell showed some promise. After screening a number of material options, three successful candidates (Ga, Gb, and Gc) were chosen for single cell tests. In order to accelerate the Cr poisoning effects, non-coated stainless steel components were used and tests were conducted at 10% cathode gas humidity level. Among the three candidates, the cell with Gb demonstrated significant improvement. The test at 10% cathode gas humidity level lasted close to 3,000 hours. The Cr tolerance of the cell with Gb was significantly better than the cell without Gb.

The combined efforts from coating and cathode modification directions included a single cell test (Glob101843) evaluating Cr getter Gb and coated hardware. The test ran 1880 hours total,

including 1595 hours with 10% cathode humidity. There was no degradation up to the end of the test (termination resulting from a test-facility component failure). After the test, the microstructure was analyzed by SEM (scanning electron microscope). In Figure 1-10, one picture shows the surface and the other shows a cross-section. The post-test analysis showed that Cr was captured (over 1:1), and Cr getter Gb was sintered as dense phase (and growing particles on cell). The Cr getter seemed to work well to prolong cell life by filtering out Cr before it reached the active sites.

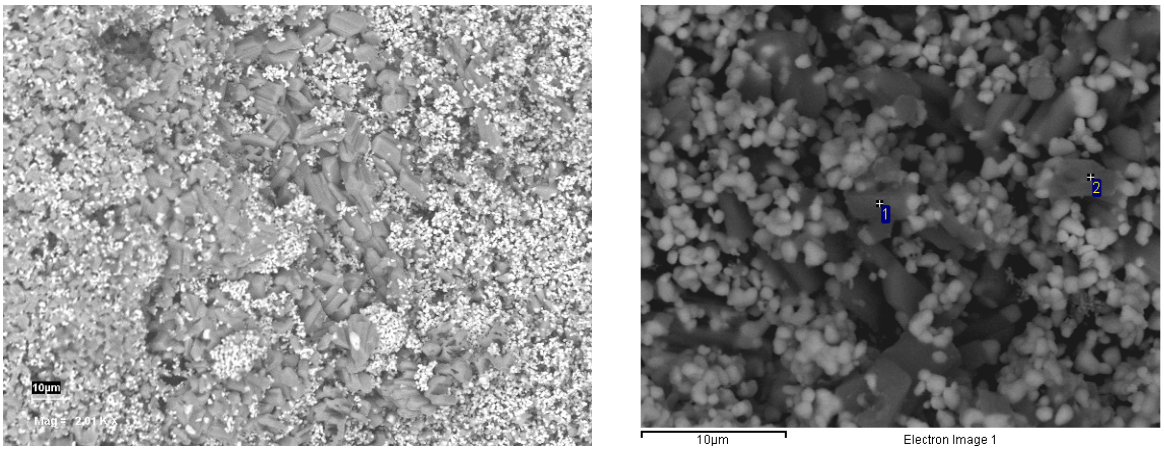

Figure 1-10 SEM and EDX Analysis of Cell Glob101843 Containing Cr Getter Gb after Test at 10% Cathode Gas Humidity

There was another test with Cr getter Gc on cell. The test, Glob101838, used a non-coated 430 steel cathode jig. It operated for ~3200 hours with 10% cathode humidity, showing stable cell performance for the initial 1080 hours. After the test, the microstructure was analyzed by SEM. As shown in Figure 1-11, Cr getter Gc was in dispersed state and remained porous after absorbing Cr species. This is microscopically better compared to the Cr getter Gb.

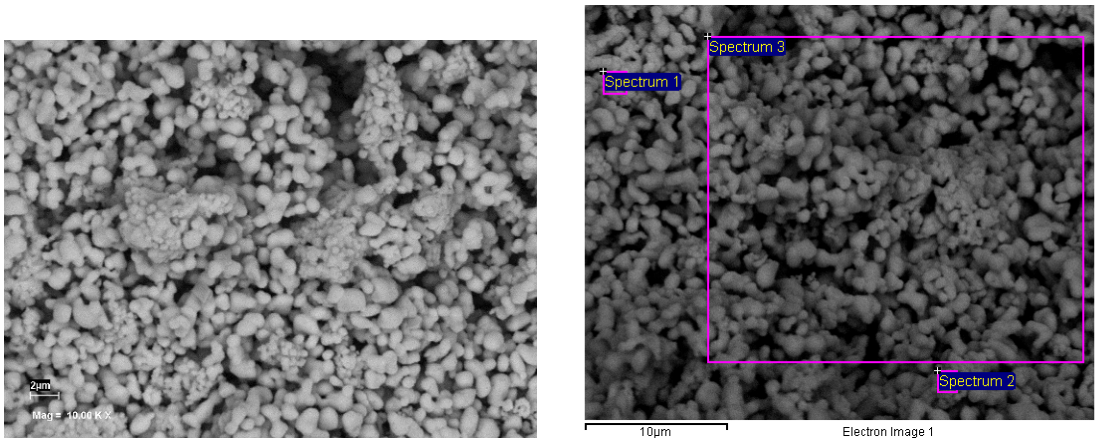

Figure 1-11 SEM and EDX Analysis of Cell Glob101838 Containing Cr Getter Gc after Test at 10% Cathode Gas Humidity

Accelerated (at 10% cathode gas humidity conditions) endurance testing of cells containing cathodes with Cr getter materials was continued. Test results of cells containing Cr getters in combination with coated hardware are presented in Figure 1-12. After introducing humidity, the cells with Cr getters had a stable period of operation followed by a slow degradation compared to the baseline cell degradation. Neither test with Cr getters experienced dramatic degradation as did the baseline, indicating both Cr getters worked effectively. While the degradation rate is

much slower after adding Cr getters, the cells degraded faster after a period of test when the Cr getters were saturated. The test with Cr getter Gb showed a degradation rate of less than 0.6% per 1000 hours with 10% humidity in cathode compared to 2.7% per 1000 hours for Cr getter Gc. It is possible that the compatibility of Cr getter Gb with the hardware coating played a role in reducing Cr poisoning effects at cathode.

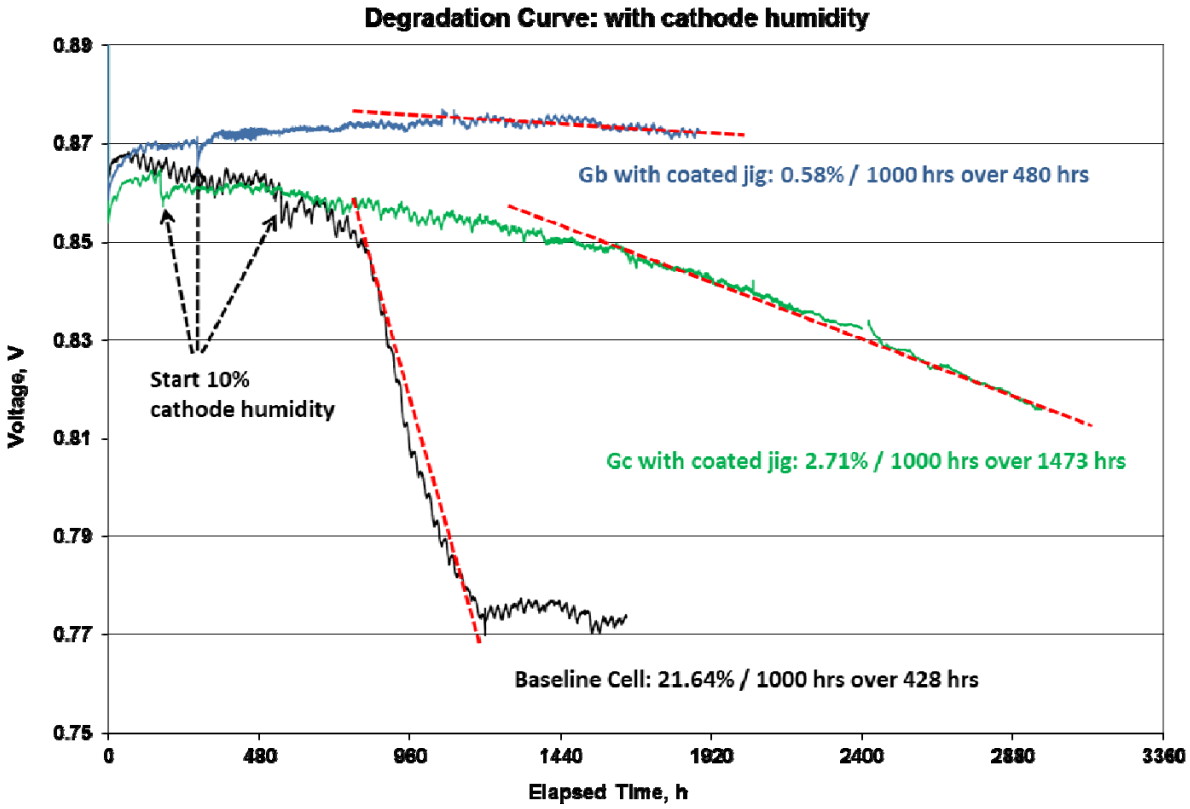

Figure 1-12 Accelerated Single Cell Tests of Cathodes with Cr Getter Materials Using Coated Cathode Jigs

To further improve the cell endurance (Cr getter performance), mixtures of Cr getters Gb and Gc were studied. A single cell test with blended Cr getters Gb and Gc in the proportion of 30% Gb and 70% Gc (Design 2), and cobalt (Co) coated cathode hardware was conducted. As shown in Figure 1-13, the cell performance was very stable even while experiencing a full thermal cycle due to a facility power issue, and a number of facility-induced interruptions. Thermal cycling capability of the cell was also evaluated (toward the end of test period). Ten full thermal cycles were completed successfully. The test was terminated after more than 11,500 hours of operation at 750°C, 0.5 A/cm^2, 50% Uf (hydrogen) and 25% Uo (air with 10% water). The performance degradation rate was 0.6% per 1000 hours over a 10609-h test period with 10% cathode gas humidity.

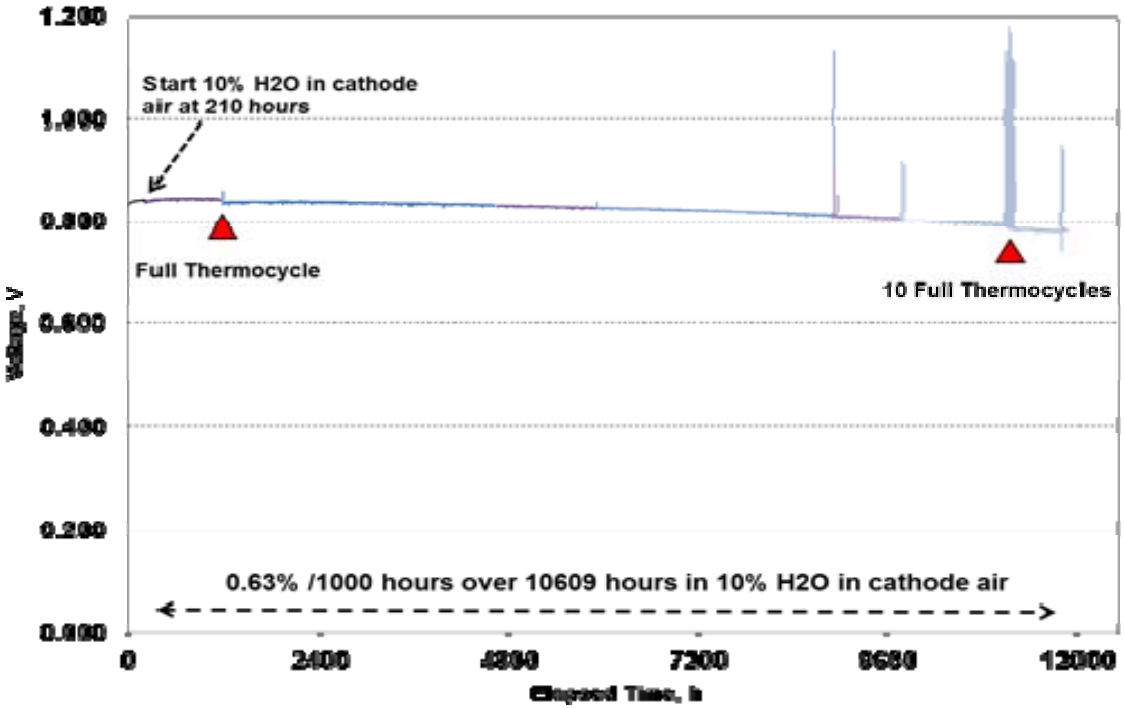

Figure 1-13 Stability and Thermal Cycling Capability of Cell Glob101859 Containing 30% Gb-70% Gc Blend of Cr Getter Materials and Co-coated Cathode Hardware

Another test was conducted with blended Cr getters in the proportion of 70% Gb and 30% Gc (Design 1) and Co coated cathode jig. Figure 1-14 shows the test results. The test was initially run with dry air for over 1000 hours. The cell experienced a voltage improvement period after introducing 10% cathode gas humidity. The cathode to jig contact degradation rate (represented by secondary Y-axis in the figure) was 0.67%/1000h over about 1500 hours.

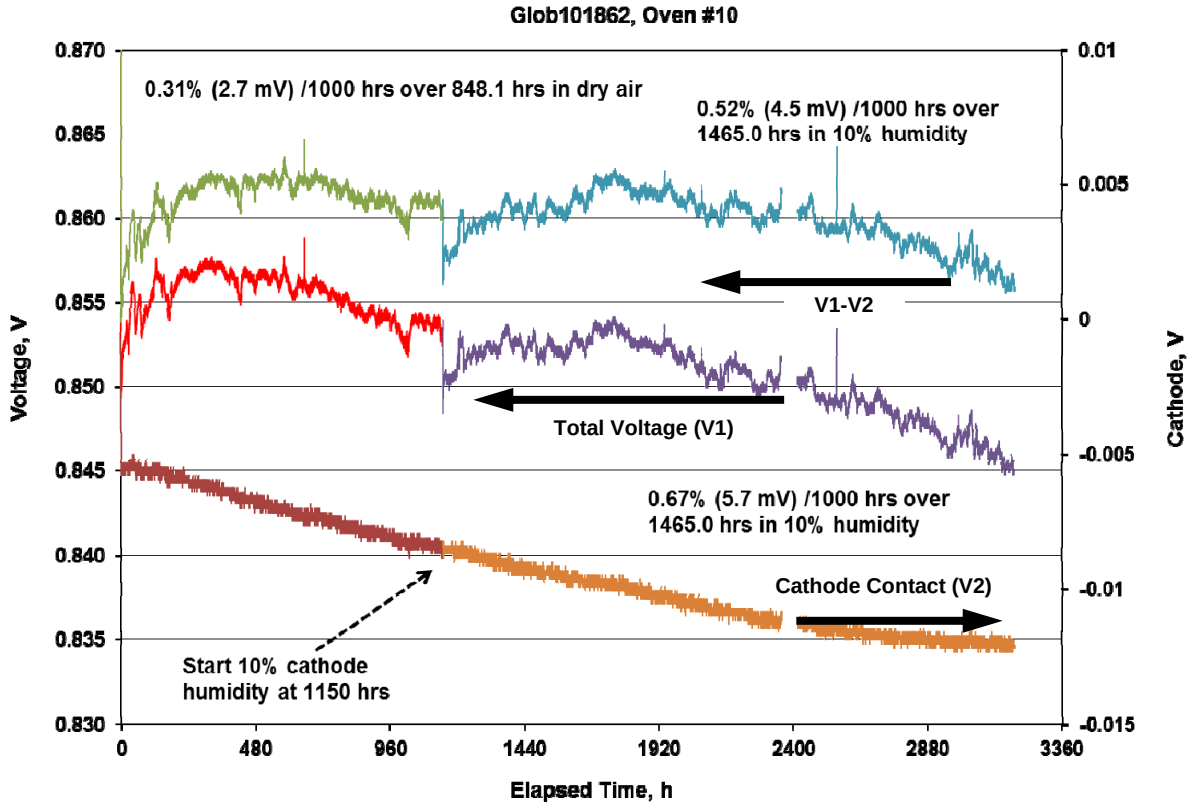

Figure 1-14 Stability of Cell Containing Cathode with 70% Gb - 30% Gc Blend of Cr Getter Materials and Co Coated Cathode Jig

Subsequent to the success in single cell tests, Cr getters were evaluated in six-cell stacks. Stack GT055296-0134 was built with mixed Cr getters (Design 1 in cells 2, 4, and 6 and Design 2 in cells 1, 3, and 5). After operating on dry cathode air for 600 hours, testing with 10% cathode gas humidity was initiated. As shown in Figure 1-15, the performance degradation rates with 10% cathode gas humidity condition were comparable (about 0.6% per 1000 hours) for the two cell groups.

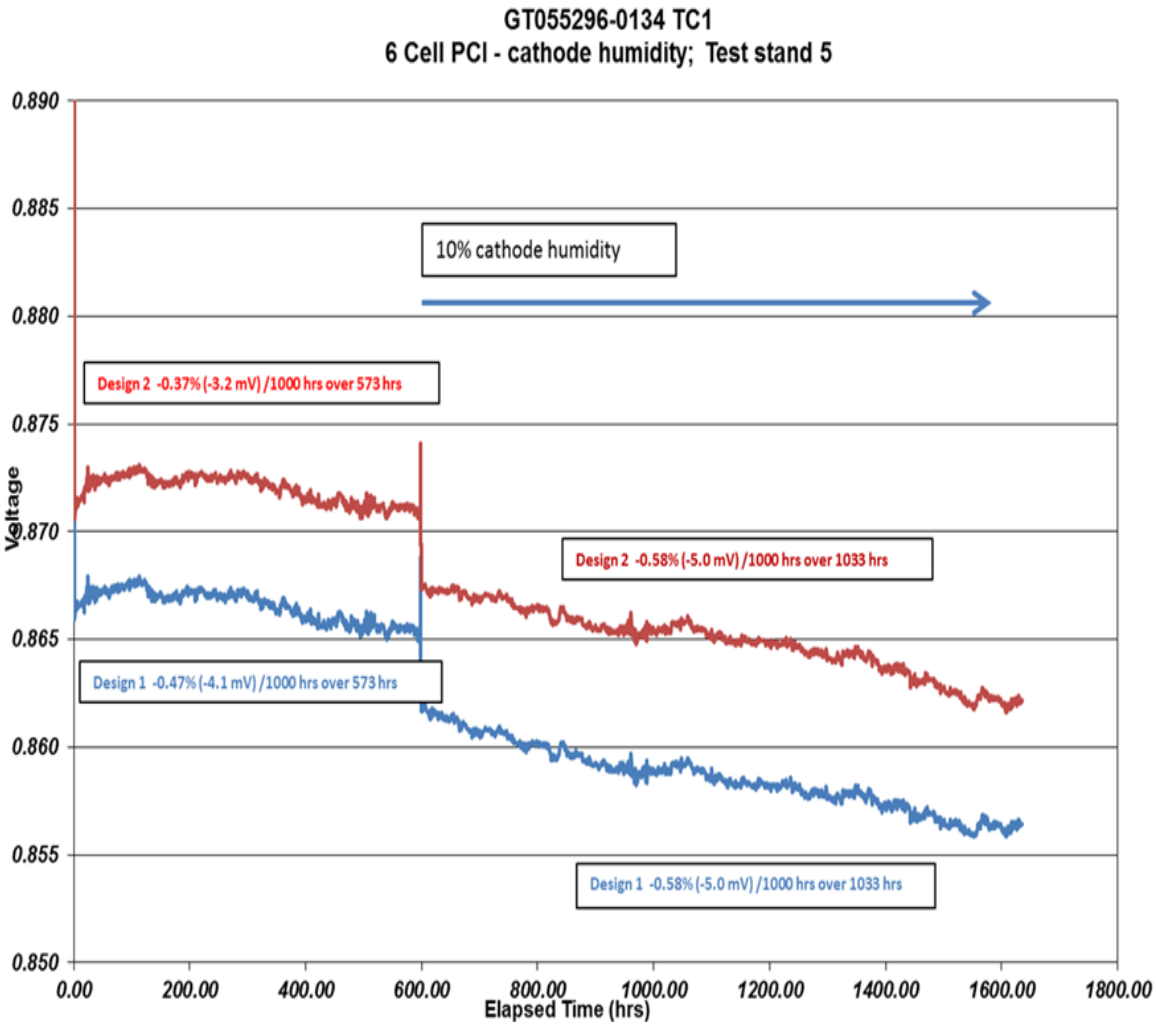

Figure 1-15 Testing of Six-Cell Stack Containing Cathodes with Blended Cr Getters (Design 1 in cells 2, 4, and 6; Design 2 in cells 1, 3, and 5)

The stack was tested with 10% cathode gas humidity for almost 4000 hours. As shown in Figure 1-16, the overall decay rate was 1.7% per 1000 hours. Although this was still relatively high, it compared favorably to 2.3% per 1000 hours decay rate observed in a previous baseline stack test with only 3.5% humidity in cathode air (also shown in Figure 1-16). The overall improvement exceeded the 25% decay rate reduction target at high humidity condition (the main reason for Cr vapor formation) at the cathode.

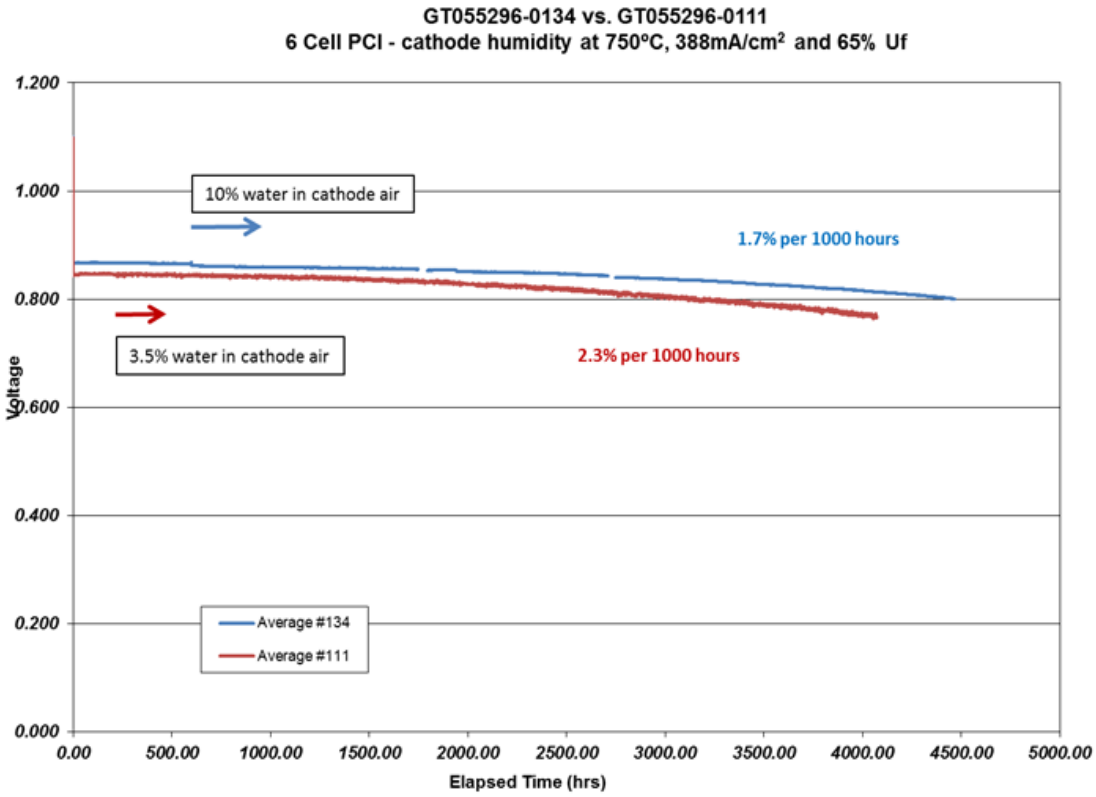

Figure 1-16 Stability of Six-Cell Stack GT055296-0134 containing Blended Cr Getters Gb and Gc Compared with Baseline Stack GT055296-0111

A repeat test with Cr getter blend Design 2 was conducted to evaluate the thermal cycling capability after operation with 10% cathode gas humidity condition. As shown in Figure 1-17, the cell performance was very stable (less than 0.3% voltage decay per 1000 hours) during the 2000-hour period at 10% cathode gas humidity. After about 2500 hours of total operation, the cell was subjected to 10 deep thermal cycles (750°C to 150°C to 750°C) to see if the thermal cycling capability of Cr getter cells is affected. The degradation for the test was only 0.8 mV/cycle with about 10% of the degradation arising from the cathode contact and interconnect combined, and 90% from the cell, anode contact and anode interconnect.

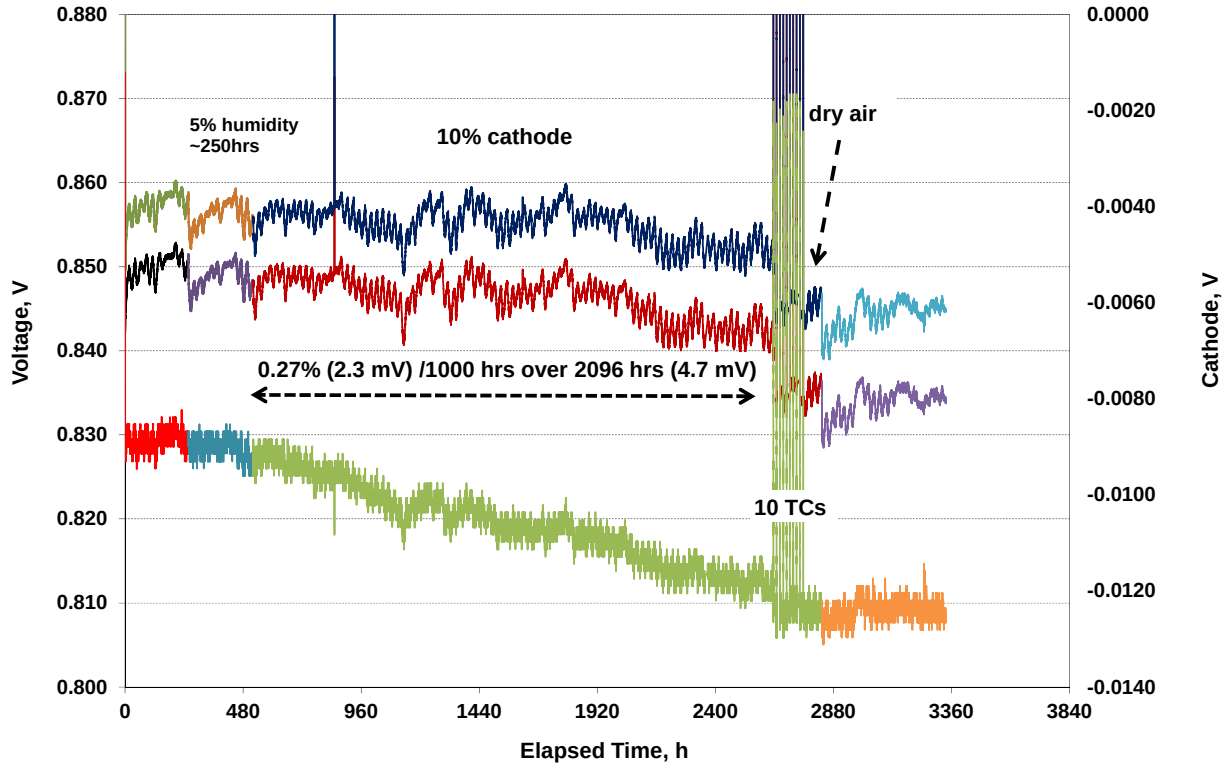

Figure 1-17 Stability and Thermal Cycling Capability of Cell Glob 101875 Containing 30% Gb-70% Gc Cr Getter Blend and Coated Cathode Hardware

Cr getter Design 2 was selected and incorporated into 16-cell large-area stacks for further validation. The test results are reported in Section 2.1.

Long-term Cell Tests: Single cell tests and test results related to the cell material development were discussed above. Results of the long-term steady state tests conducted during the project are presented here. Figure 1-18 summarizes results of material development for performance enhancement and degradation rate reduction. Three long-term single-cell tests with identical testing conditions (750°C, 0.5 A/cm^2, 50% fuel utilization, and 25% air utilization) are shown. The baseline for comparison is the 26,000 hour cell test prior to the current project and conducted from 2002 to 2005. After two years of intense cell material development in Phase I, a long-term single-cell test was initiated in 2008 to validate all the performance and endurance improvements achieved in Phase I. During the steady-state operation of over 28,000 hours (exceeding the past record of 26,000 hours), the overall degradation rate is 0.76% per 1,000 hours (184 mV total loss). A test facility related interruption accelerated the degradation in the final 3,000 hours of the test.

After another year of cell material development and optimization in Phase II, the test of the material system with both TSC-3 cell and alloy coating was started in 2009. This material system offers a superior combination of both performance and longevity. With the linear voltage decay projection shown as a dotted line in Figure 1-18, the cell material system will reach 40,000 hours with a cell voltage of 750 mV. A facility-related interruption cut the test short. The degradation rate was 0.32% (3.17 mV) per 1,000 hours for the entire test duration of 18,300 hours.

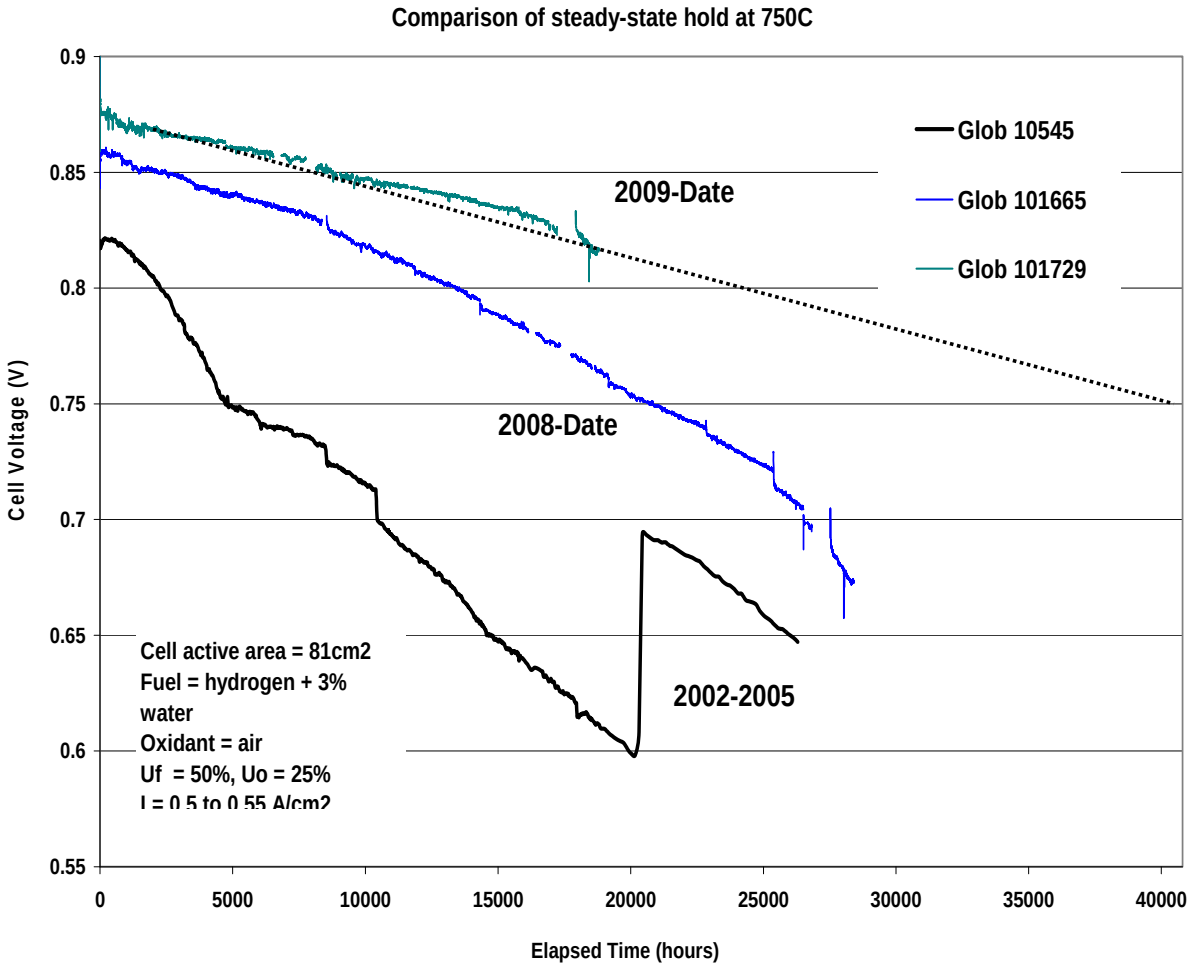

Figure 1-18 Performance Enhancement and Degradation Rate Reduction though Materials Development (Long-Term Single-Cell Testing)

A single cell test conducted at lower operating temperature of 650°C accumulated over 14,000 h. Figure 1-19 presents the test results. The cell performance degradation rate over a 12,666 h period was 0.48%/1000 h.

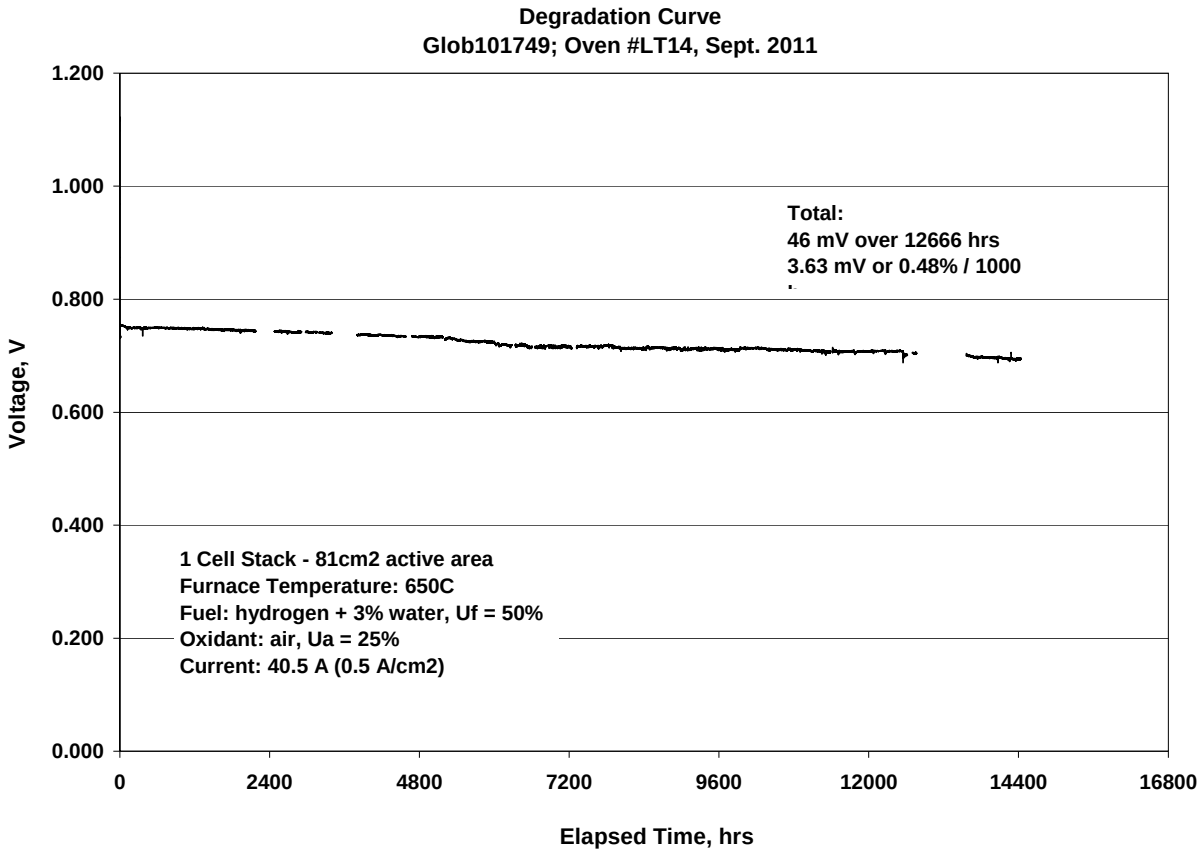

Figure 1-19 Overview of Long-Term Single-Cell Test (Glob101749) at 650°C

A single cell test with up-to-date cell technologies and uncoated jigs was started in Phase III. This test was conducted for over 15,400 hours. As shown in Figure 1-20, the starting voltage of the cell was very good, and the overall degradation rate was 0.34%/1000 h, comparable to the previous long-term test with coated jigs (cell hardware) and half the degradation rate compared to the test with uncoated jigs.

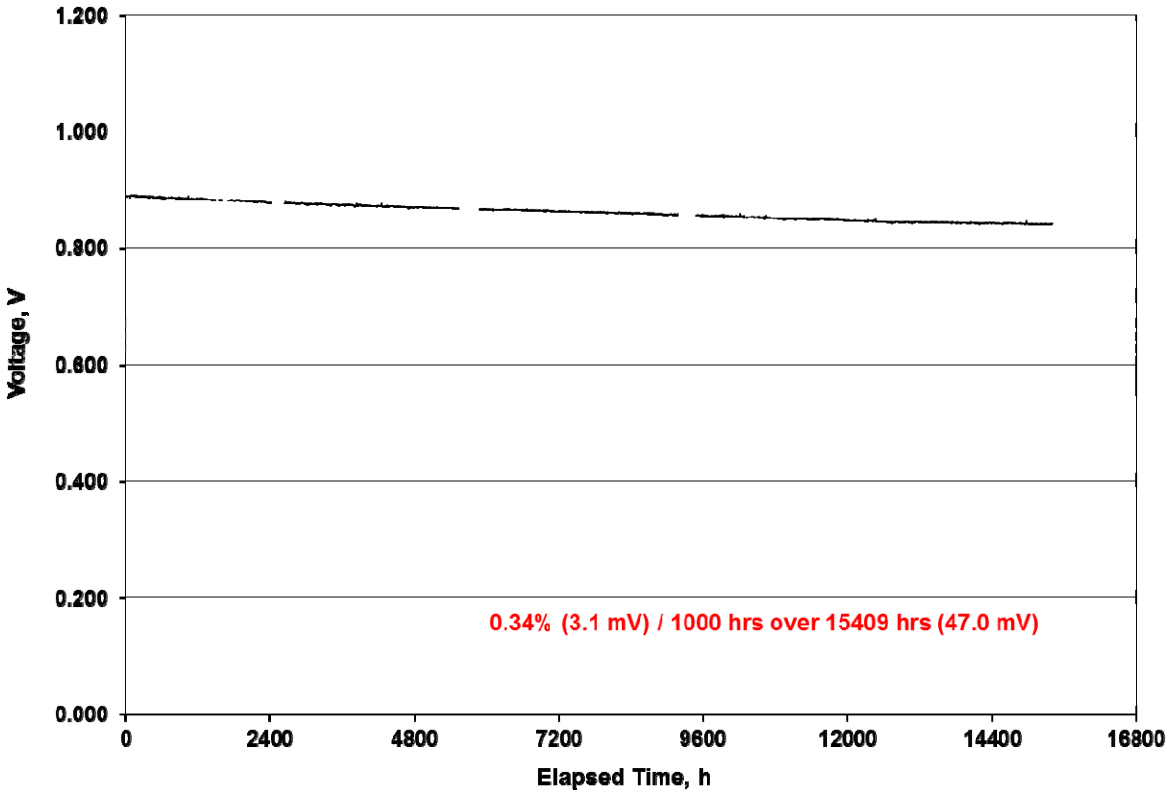

Figure 1-20 Long-Term Single-Cell Test (Glob101837) at 750°C

1.2 Cell Area Scale-up and Cell Technology Integration

Parallel to materials development, significant progress was made in cell area scale up. In order to explore the challenges of ceramic fabrication scale-up, cells up to 33 cm X 33 cm (1090 cm^2 in area) were made using VPS's baseline TSC (Tape casting, Screen printing, and Co-sintering) process. Based on manufacturing engineering and stack design analysis, a cell size down-selection was conducted early in the Phase I. A square cell of 25.4 cm X 25.4 cm, 645 cm^2 overall, with an active area of 550 cm^2, was selected for stack and power module development.

Performance of the scaled up cell was empirically validated. Figure 1-21 compares electrochemical performance of the scaled-up, 550 cm^2 active area, cell to that of the baseline, 81 cm^2 cell. It shows that there is no significant difference in performance (variation in the range of zero to 2.5%). This was further verified through extensive scaled-up stack testing.

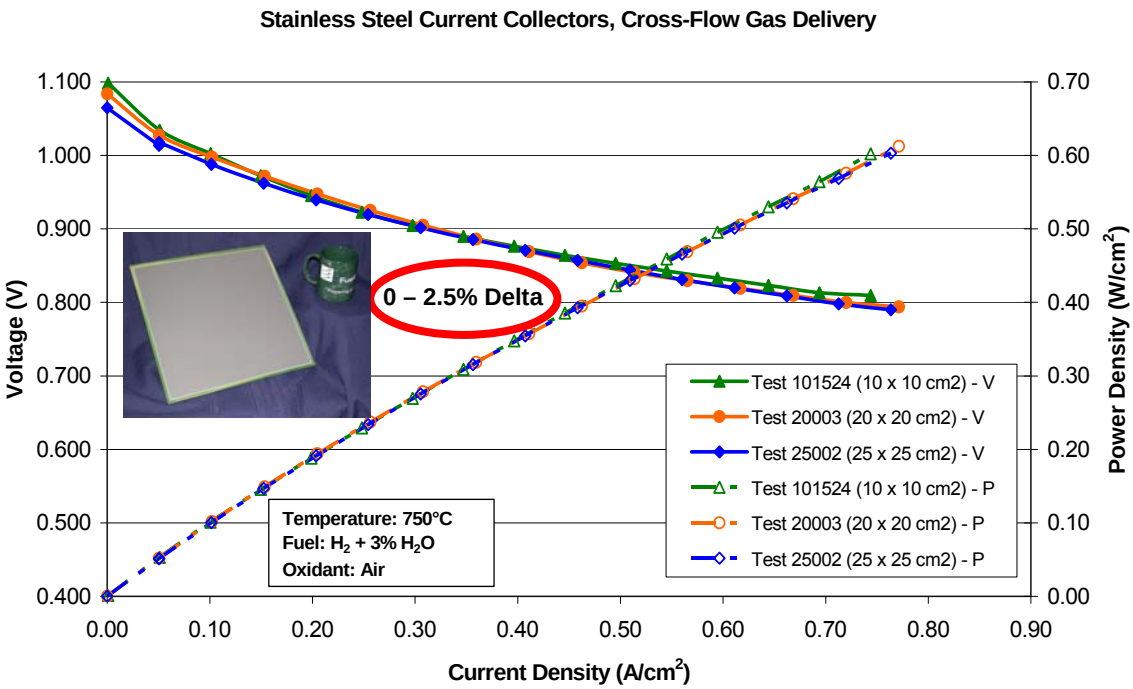

Figure 1-21 Electrochemical Performance of the Scaled-Up Cells vs. the Baseline Cells.

Development activities were carried out to incorporate cell material breakthroughs in the scaled-up cells. The LTS cathode was incorporated in large area cells for further validation. A 25 cm x 25 cm cell (550 cm^2 active area) was tested for more than 4,500 h, demonstrating 0.75%/1000 h degradation rate at 0.5 A/cm^2. Figure 1-22 shows the cell performance during the test. The performance degradation rate was similar to that demonstrated at 10 cm x 10 cm cell size level. The cell also performed well in a fuel utilization test up to 85% utilization level.

Cells with LTS cathodes and modified anodes were scaled up to 550 cm^2 cell area and incorporated in 16-cell and 32-cell stacks. These TSC-3 cells were evaluated in stacks, both with standard 1 mm thick 8YSZ anode substrate and 0.57 mm thick 3YSZ anode substrate (as a part of thin cell development). Table 1-3 shows the performance observed (at 388 mA/cm^2) for a range of fuel utilizations. A performance improvement of ~8%, with ~2% points from anode substrate thickness reduction, was observed compared to the standard thickness TSC-2 cells.

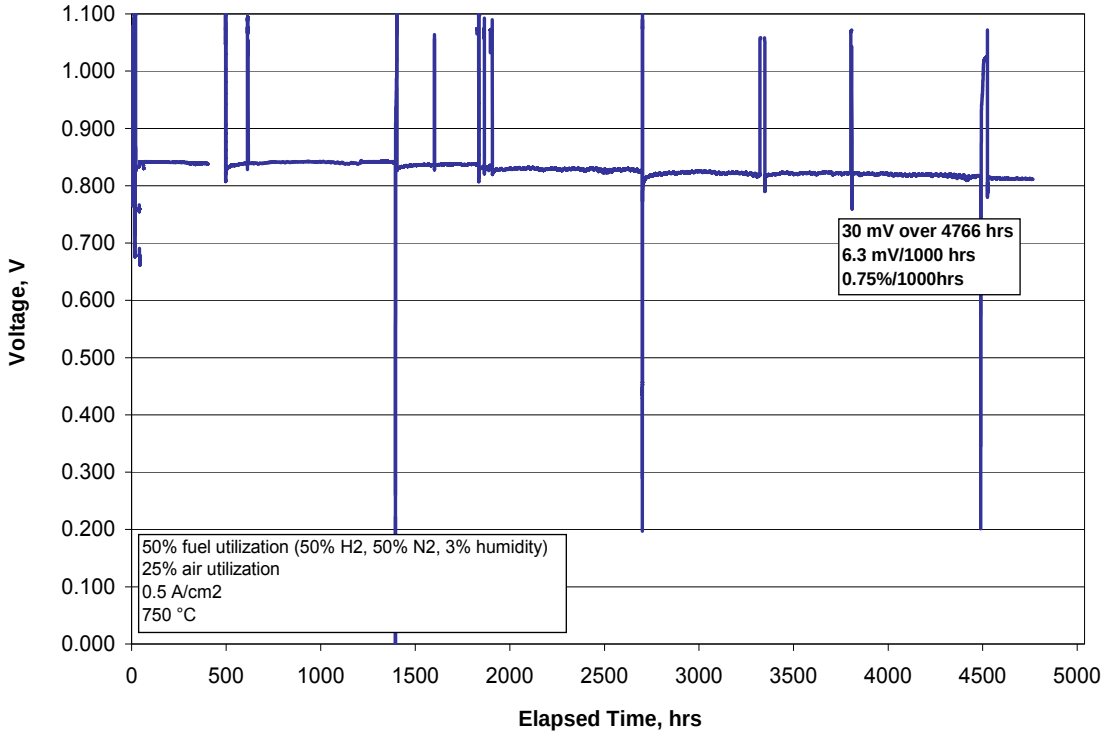

Figure 1-22 Cell Voltage vs Time Trend at 500 mA/cm^2 for 25 cm x 25 cm Advanced Cathode LTS Cell

Table 1-3 Performance Comparison of 16-cell Stacks (550 cm^2 cell area) Containing Baseline 1 mm Anode Substrate TSC-2 Cells and Thin TSC-3 Cells

Fuel Utilization (%)	TSC2 cells 1 mm Stack 057235-0037	TSC3 cells 1mm Stack 057832-0001	TSC3 cells 0.57 mm Stack 057235-0044	Performance Enhancement (vs. TSC2/TSC3 1mm)
50	0.823	0.876	0.886	7.7%/1.1%
60	0.817	0.864	0.879	7.6%/1.7%
70	0.804	0.846	0.866	7.7%/2.4%
80	0.785	0.820	0.847	7.9%/3.3%

Cell scale-up development was continued to evaluate 33 cm x 33 cm cells (~1000 cm^2 active area). A 33 cm x 33 cm cell with LTS cathode was tested for more than 1,900 h with a degradation rate of 1.3%/1000 h (at 520 mA/cm^2). During initial performance testing, the cell produced a peak power of 880 W (915 mW/cm^2) at 1200 A. Figure 1-23 shows the performance characteristics (power curve) of the scaled-up cell. The total test period (~4,000 h) included 2,000 h of additional testing at 500 mA/cm^2.

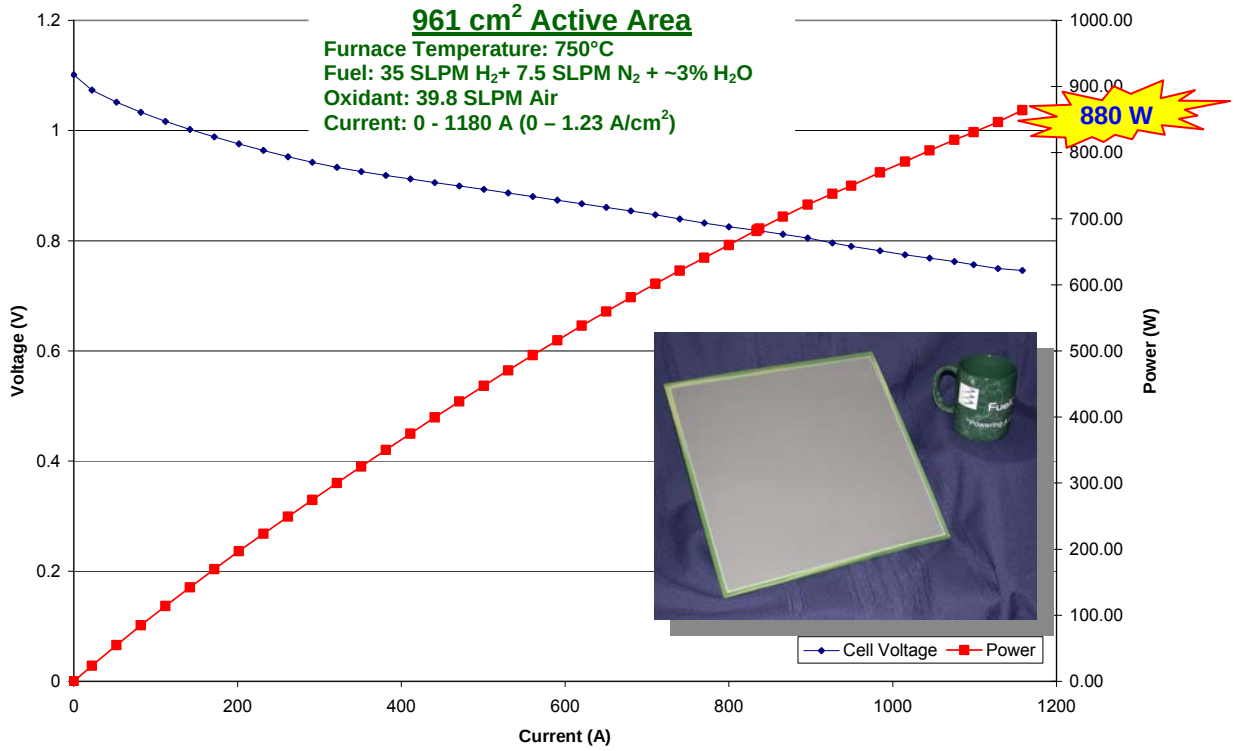

Figure 1-23 Performance Characteristics of 33 cm x 33 cm Size Scaled-up Cell

The 33 cm x 33 cm cells were also tested in short stacks. The effort included stack design to provide an initial investigative platform for evaluation of scaled-up 1000 cm^2 cells in short stacks. Testing of 1000 cm^2 active area cells, in short stacks, was conducted as part of the stack scale-up. A 10-cell stack was built and tested at Phase II normal operating conditions. The stack performed successfully during the fuel utilization test in which the utilization was varied from 50 to 80%. The average cell voltage was 800 mV at 388 mA/cm^2 and 80% fuel utilization. The large area stacks significantly increase cell power output, as the cell voltage level is maintained during the scale-up. As shown in Figure 1-24, a DC power output of 4 kW was observed at 500 mA/cm^2 for the 10-cell stack, during the peak power test. The stack was also thermal cycled twice.

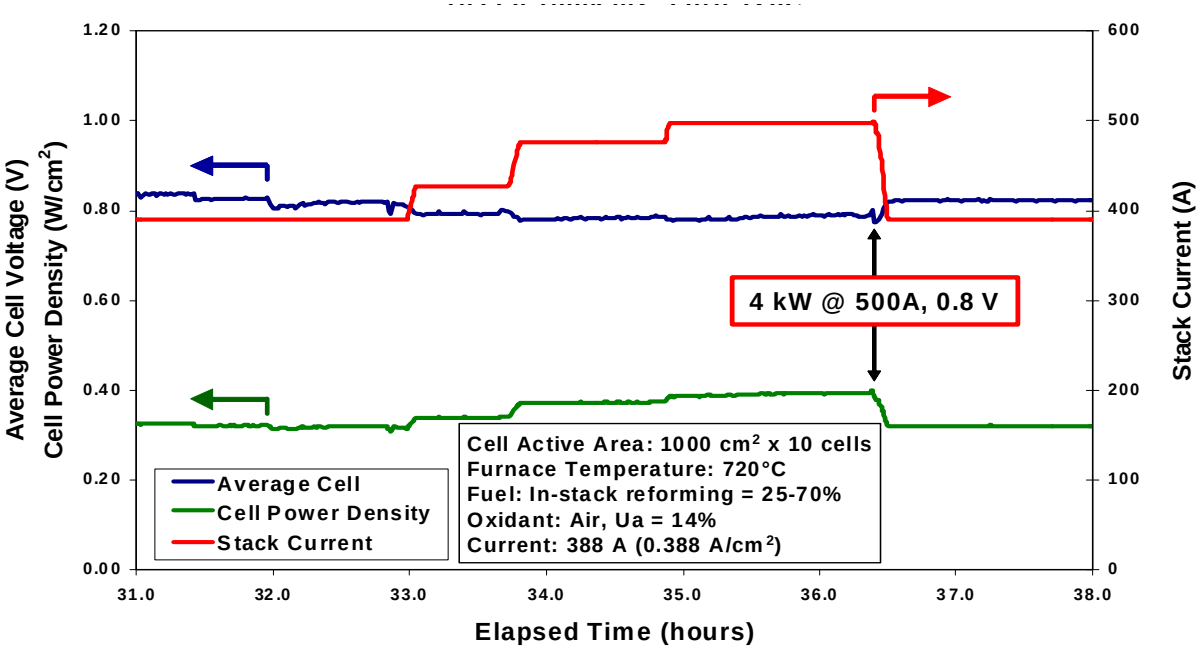

Figure 1-24 1000 cm^2 Cell Area 10-cell Stack Peak Power Test Results

1.3 Cell Manufacturing Process Development

Cell manufacturing process development was conducted to establish a new, scaled-up cell baseline. This included:

- Design development of the scaled-up cell manufacturing process
- Procurement and commissioning of new manufacturing equipment
- Re-tooling of existing equipment
- Completion of scaled-up cell manufacturing trial runs
- Performing engineering analysis on cost, volume and yield
- Applying statistical process control and optimization for yield improvement
- Establishing new detailed manufacturing procedures and specifications.

In Q1 2008, the new VPS cell pilot production facility was upgraded to an annual volume of 1 MW of cell production. Pilot production runs of over 1000 scaled-up cells were conducted and a yield of over 95% was demonstrated.

The cell manufacturing process standardization was conducted for the initial Phase II stack design. A total of 780 cells, 25 cm x 25 cm in cell size, were produced in eight trials. An excellent overall yield of 88% with material yield of 95% was achieved. This completed a key milestone for the project. Further effort in cell manufacturing process development was focused on 25 cm x 25 cm thin scaled-up cells. The standard cell manufacturing process was modified based on the hydrothermally stable anode substrate material developments. The cell manufacturing process yield of >90% was regained. This was based on over 1000 cells (25 cm x 25 cm size) fabricated. The completion of final cell manufacturing process development and pilot trials of the thin TSC-3 cell led to a new baseline cell platform for the Phase II deliverable stack (stack used for end-of-Phase II metric test).

Manufacturing of 1000 cm^2 active area cells (33 cm x 33 cm) proved to be challenging, requiring process development. The challenge was overcome with existing equipment. A large Deltech kiln was procured and made operational in 2010 to support higher volume 1000 cm^2 cell production.

Since large area cells were degrading at higher rates in stacks (test result discussion included in Section 2 Stack Technology Development) than single-cell and small area PCI (pre-commercial integrated manifold) stacks, a review of the differences in cell production between the large area (25 cm by 25 cm) cells and smaller area (10 cm by 10 cm and 12.5 cm by 12.5 cm) cells was conducted. The key differences were in processing of the cathode and contact layers.

A 24-inch screen printer was used exclusively for cathode and contact layers (for large area cells). These layers were the thickest layers printed, especially the contact layers. Typical final combined thickness of these layers was over 50 microns compared with thickness of less than 10 microns for all other screen-printed layers. In reviewing the printer, it was found that the print stage was flexing during printing, resulting in poor thickness uniformity across the cell area. An improved print stage was made and installed. This modification significantly reduced the thickness variation of the layers.

A new insight from the study was that the thickness variation of the cells was larger than the expected total design thickness of the contact layers. In addition, the allowable variation in metallic part thickness can also lead to even larger variation than the total thickness of the contact layers. This meant that the design tolerance of stack parts might not be accommodated by the design thickness of cathode contact paste. A design change of either increasing cathode contact thickness and/or tighter tolerances on other stack components was required to improve cell contact in the large area stack. It was decided to investigate thicker cathode contact layers, and due to the expected thickness proposed, stencil application of contact paste was selected for trials. Three stacks were built to validate the design changes (test results reported in Section 2.1).

The other key area investigated was the cathode sintering process. Large area stacks built during Phase III of the project used cells that had cathode layers sintered in the new, large Deltech batch furnace with new kiln furniture (SiC plates) and a slightly modified heating profile to prevent temperature overshoot in this large batch kiln. Previously, (the initial) TSC-3 large area cells were all processed in a smaller batch furnace with old kiln furniture and a slightly faster heating rate to the maximum sintering temperature. Efforts were made to investigate and separate the effects of the heating rate change and the effects of the new kiln furniture. A study of causes of cell contamination highlighted the new SiC kiln furniture as a potential source of contamination. As a result, stacks were built and tested to see if there was an effect on degradation rate and recommend a path forward. A 6-cell PCI stack was built and tested with three cells processed in smaller batch kiln and the other three cells processed in new large Deltech kiln. Figure 1-25 shows the performance of the two cell groups during the stack test. Cells fired in the new production Deltech kiln had slightly lower performance, but showed very similar degradation rates, even when the furnace temperature was increased from 700°C to 750°C for the last 977 hours. Large area stacks were also built to further validate the cathode firing process equipment (see Section 2.1).

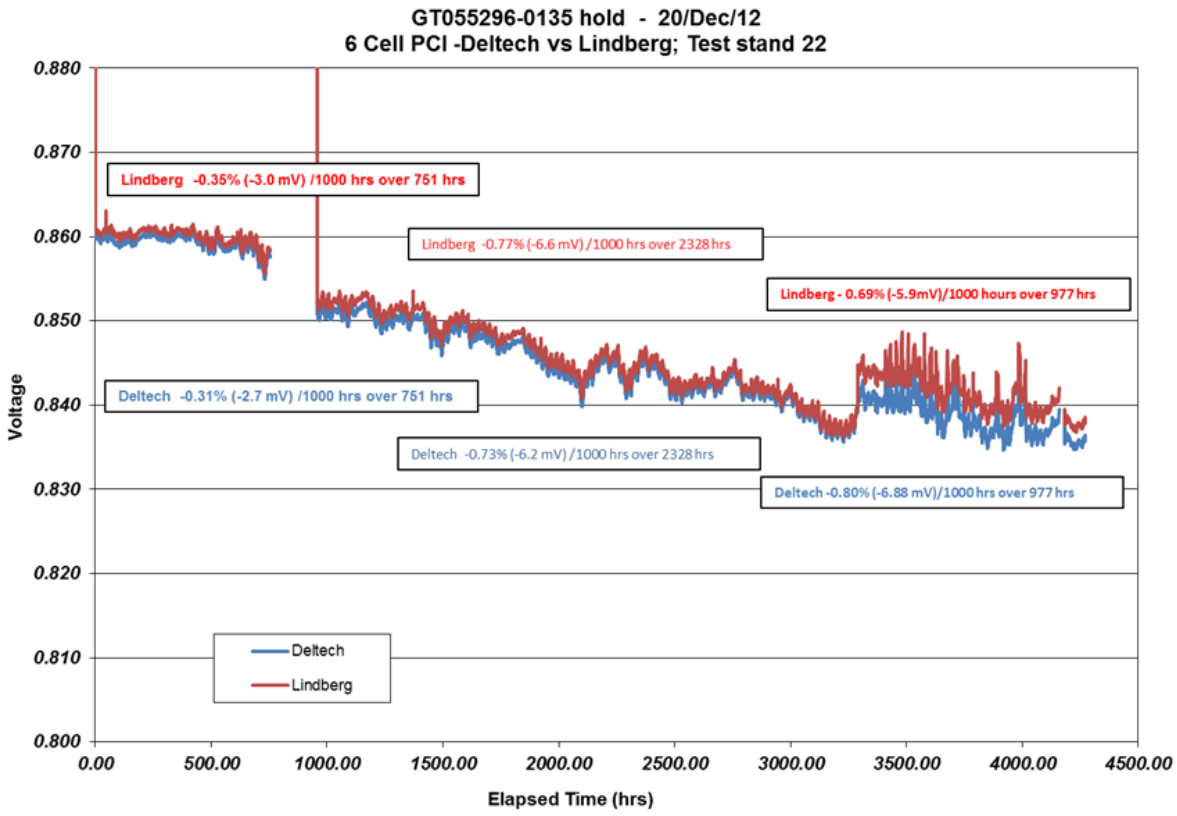

Figure 1-25 Performance Stability Comparison in 6-cell Stack for Cells Fired in Deltech and Lindberg Furnaces

Effort was also focused on developing cell manufacturing technologies for a new and advanced ICM (In-Cell Manifolded) stack design, shown in Figure 1-26. The incorporation of the fuel manifold in the cell presented challenges in the fabrication of cells. Due to the nature of ceramic process change at the substrate level, significant efforts were placed on recalibrating subsequent process steps to regain cell manufacturing yield, especially for the co-firing stage. Production of fully-functional cells was initiated. ICM stack test results are included in Section 2.3.

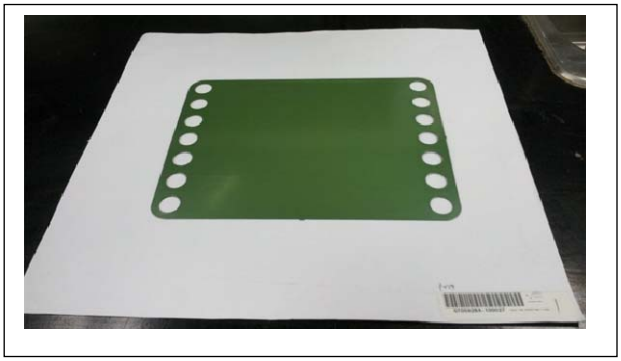

Figure 1-26 In-Cell Manifolded (ICM) Stack Production Half Cell

2.0 STACK TECHNOLOGY DEVELOPMENT

SOFC stack development concentrated on stack block design issues to increase stack reliability and endurance. The highest priority issues included loss of electrical contact, Cr poisoning of the cathode (specifically in system operating conditions), and manufacturing reliability. Stack component development focused on function—performance at various stack operating points—as well as cost impact. Stack tests were conducted to further define and design a standardized stack building block unit and stack tower. In-cell manifolded (ICM) stacks were also developed and tested in parallel with the baseline stack design development.

2.1 Stack Design Development and Testing

Stack design issues associated with the 550 cm^2 active area cell size: primarily, cell component contact, sealing, flow uniformity for taller stacks, component manufacturability/tolerances, and part count were addressed.

A detailed stack/stack tower/stack power module size engineering analysis study was conducted to identify the optimum design with respect to performance, reliability, manufacturability, and cost. Mechanical design focused on repeat part stack hardware as well as non-repeat parts (NRP) such as manifolding and compression systems.

Stack Development in Phase I

Stack design utilized various engineering analysis and computational modeling methods to optimize specifications and design solutions. A step-wise approach was taken with respect to both analysis and actual stack scale-up. This involved development of the basic stack repeat unit, and extension to 6, 16, and 64 cell stacks, and further up to stack towers. With the participation of Pacific Northwest National Laboratory (PNNL), the VPS/FuelCell Energy, Inc. (FCE) team finalized the stack design of a 10 kW stack with 64 scaled up cells, 550 cm^2 active area each, as the primary stack building block [2]. With support from modeling analysis, stack engineering focused on the challenges resulting from thermal and flow management of the scaled-up components. A detailed 10 kW stack block design and 30-50 kW stack tower design analysis were completed in Phase I.

To optimize development efforts, a staged stack development approach was taken. Stage 1 stack development was a platform for early stack component scale-up and validation through stack testing. At the end of 2007, this effort was completed with successful 6-cell and 16-cell short stack tests. The Stage 2 stack development incorporated optimized stack design features, and component scale-up utilizing lessons learned from Stage 1. Using the 16-cell short stack as a key testing platform, most of the major technical issues related to stack scale-up were resolved. Those issues included component repeatability, production tooling, stack manufacturability, stack transport, stack operating conditions, in-cell temperature gradient, new flow field design to enhance cell to cell flow uniformity, and mechanical loading on sealing and contact media. Final scale-up to a 64-cell, 10 kW stack block for Phase I metrics testing was accomplished in Q3 2008.

End-of-Phase I Metric Test: The 10 kW stack metric test was started near the end of Phase I and continued in Phase II. Two 64-cell stacks (each 10 kW) with a cell active area of 550 cm^2 were tested. Figure 2-1 shows a picture of a 10 kW stack building block consisting of 64 cells with 550 cm^2 cell active area. The test started with a high current density (388 mA/cm^2) dwell of more than 24 hours. A power output of 11 kW and power density of 314 mW/cm^2 were achieved. Steady state testing at normal operating conditions (NOC) was then initiated (364 mA/cm^2). The power output at NOC was 10.5 kW. Both stacks at VPS completed the 5000 h endurance requirement. DOE's minimum requirements were successfully met. The 64-cell stack

(GT057382-0002) successfully completed over 9000 test hours. A performance plot showing average cell voltage and stack block power output is included in Figure 2-2. Over the first 5500 h, testing was relatively uneventful and a near linear degradation rate of 2.7%/1000 h was demonstrated. After this point, the stack test was continued for further long-term degradation study and to complete one year of operation. Different stack thermal management strategies were evaluated.

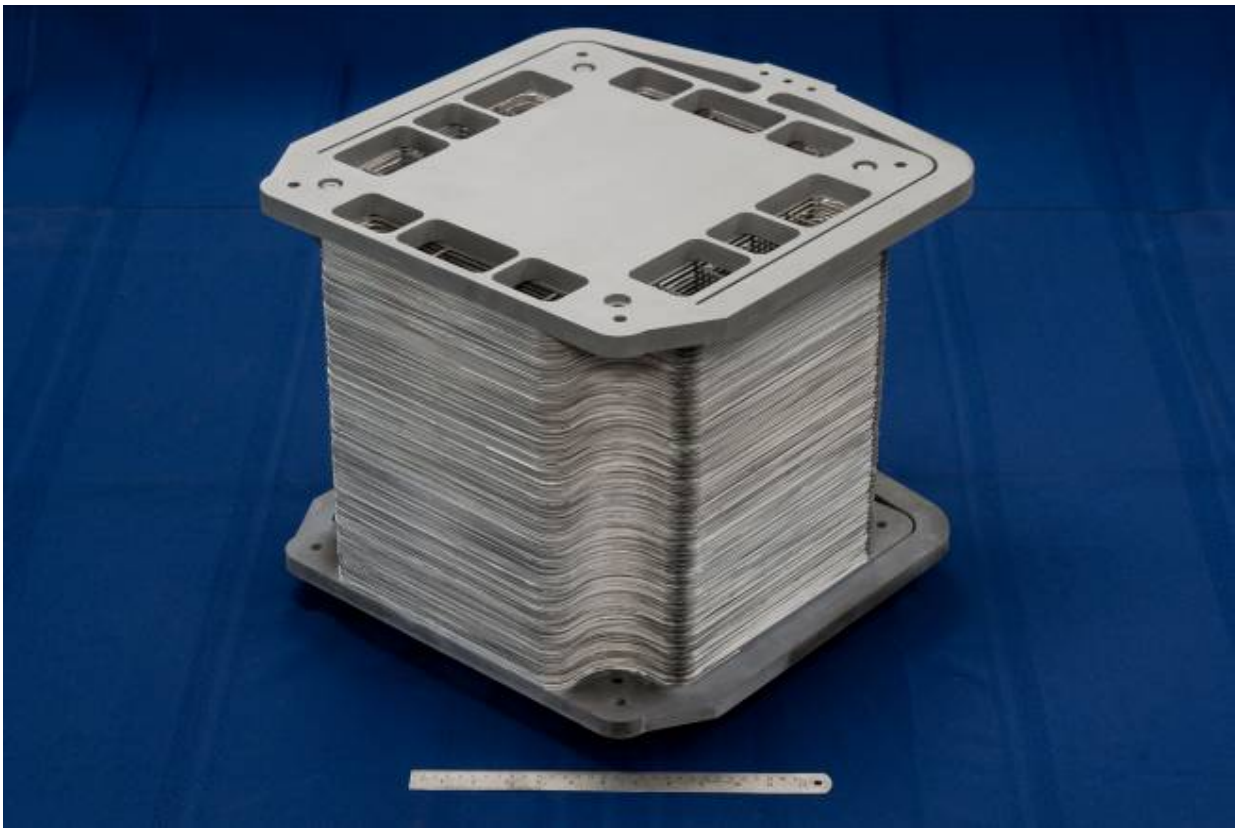

Figure 2-1 10 kW Stack Building Block (64 cells, 550 cm^2 cell active area)

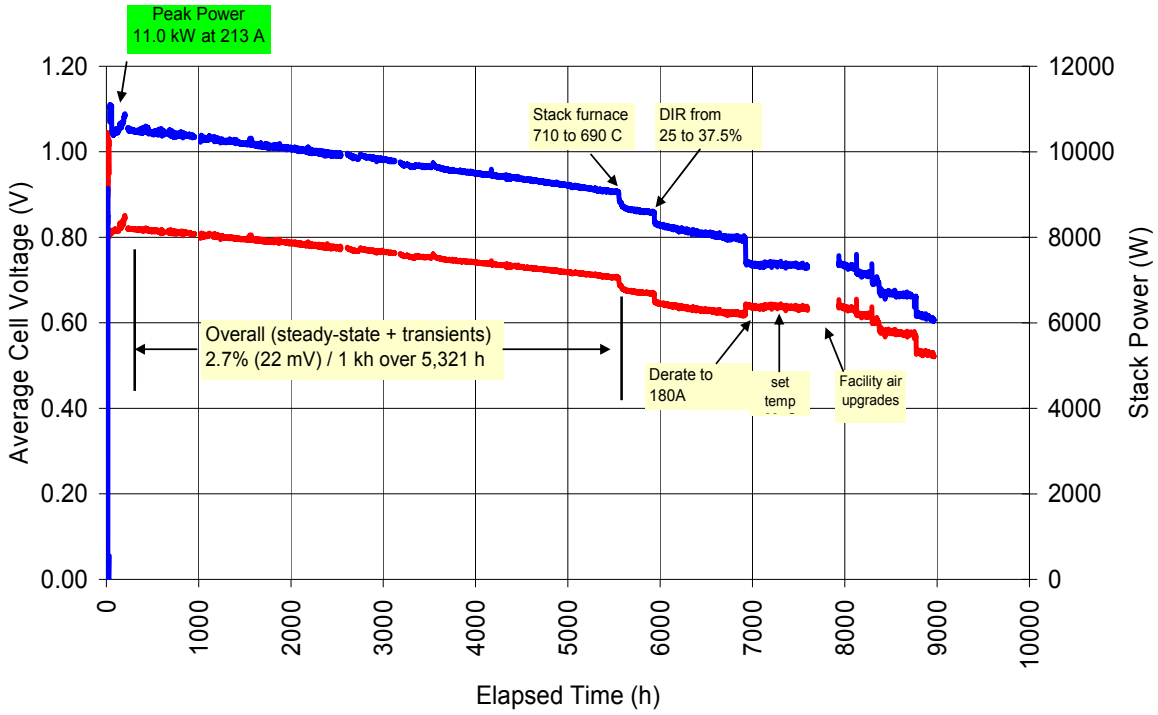

Figure 2-2 End-of-Phase I Metric Test (550 cm^2 cell area 64-cell stack block) - Average Cell Voltage and Stack Power Trends

A 16-cell stack with the same stack architecture and components demonstrated a degradation rate of 1.5% per 1000 h over 1400 h. The test results are shown in Figure 2-3.

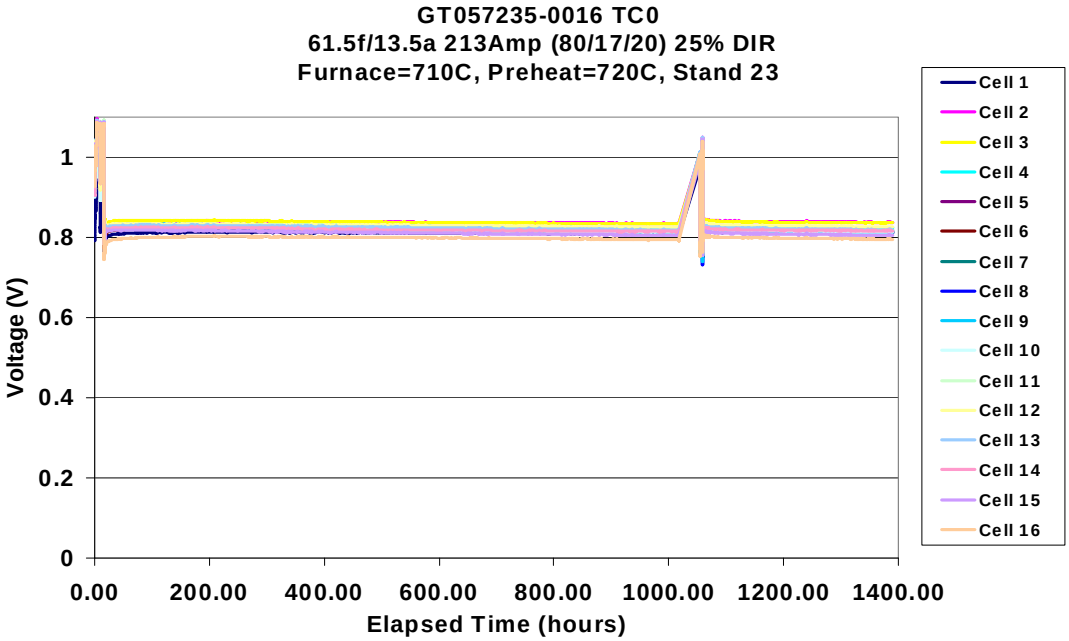

Figure 2-3 Long Term Steady-State Test of a 16-cell, 2.5 kW Stack

Stack Development in Phase II

Stack development focus areas for Phase II were identified and targets were selected to allow the integrated Phase II stack to offer improved system level performance, as shown in Figure 2-4. Significant progress was achieved from Phase I levels, as indicated by the (then) current status points/contour in the figure.

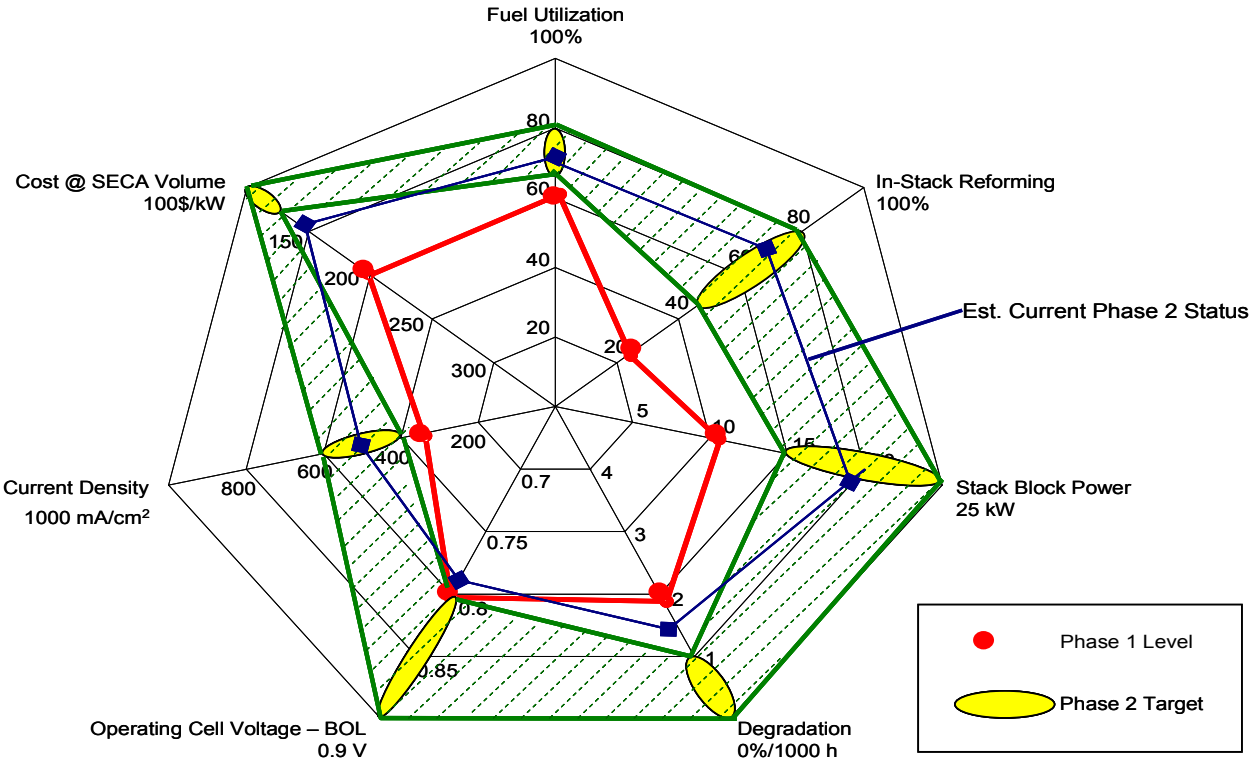

Figure 2-4 Phase II Stack Development Focus and Current Status

The stack building block was scaled-up from 64-cell to 92-cell size in Phase II. Three 92-cell stacks were built and underwent performance testing at VPS. Two of the 92-cell stack blocks were utilized to assemble a stack tower at FCE for a tower test. Figure 2-5 shows a photograph of the 92-cell SOFC stack block consisting of 92 cells with 550 cm^2 cell active area. Table 2-1 is a summary of the 92-cell stack performance achieved. All data presented are 24-hour averages. Performance of all three stacks (at NOC) was quite comparable. The DC output from each was ~18 kW. The stack tower test results are discussed under Section 3.2 Sub-scale Module Tests.

Figure 2-5 92-cell SOFC Stack Building Block (550 cm^2 cell active area)

Table 2-1 Summary of Results from 92-Cell Stack Block (550 cm^2 cell area) Performance Testing Conducted at VPS

		GT57607-001 NOC (248-272h)	GT57607-001 Peak (555-579h)	GT57607-002 NOC(12-36h)	GT57607-003 NOC(4-28h)
Inputs	Fuel Utilization	68.3%	65.3%	68.4%	68.1%
	In-Stack Reforming	70.0%	60.0%	70.1%	70.0%
	Air Utilization	14.1%	13.8%	14.1%	14.0%
	Stack Current (Current Density)	250.9 A (456 mA/cm^2)	281.2 A (511 mA/cm^2)	251.2 A (457 mA/cm^2)	250.4 A (455 mA/cm^2)
	Stack Furnace Temperature	704 C	700 C	705 C	715 C
Outputs	Stack Block Voltage (Average Cell Voltage)	71.823 V (0.781 V)	70.744 V (0.769 V)	72.044 V (0.783 V)	73.939 V (0.804 V)
	Stack Block Power (Power Density)	17,992 W (0.356 W/cm^2)	19,868 W (0.393 W/cm^2)	18,099 W (0.358 W/cm^2)	18,517 W (0.366 W/cm^2)
	Cathode Out Temperature	779 C	780 C	779 C	789 C

Over 40 16-cell stacks were built in Phase II. Sixteen-cell stacks were used for development testing. A 16-cell stack was tested at more aggressive Phase II system operating conditions (500 mA/cm^2, 70% fuel utilization, 75% of fuel from in-stack reforming). Figure 2-6 shows the individual cell performance trends over the 3100-h test period. The average cell performance degradation rate was 1.5%/1000 h. The test emphasis was on implementing the TSC-3 cell technology in combination with the thin anode substrate cell design. Thin TSC-3 cells in stack tests demonstrated a robust performance in fuel utilization tests (50-80% utilization range) before and after a thermal cycle.

Phase II final stack design was fixed and validated to qualify it for the end-of-Phase II metric test stack deliverable. A 16-cell stack representing Phase II final stack design passed an 80% fuel utilization test with all cell voltages well above 0.8 V. The stack also thermal cycled very well, with average cell voltage loss of <5 mV from the thermal cycle. The stack was tested at system representative conditions (including simulated coal syngas composition). These results confirmed the stack design for the deliverable stacks (for Phase II stack tower metric test at FCE). Another 16-cell stack containing thin interconnects was tested to qualify the design for the supplementary (parallel) 120-cell stack metric test planned at VPS. The design was qualified based on excellent results before and after a thermal cycle.

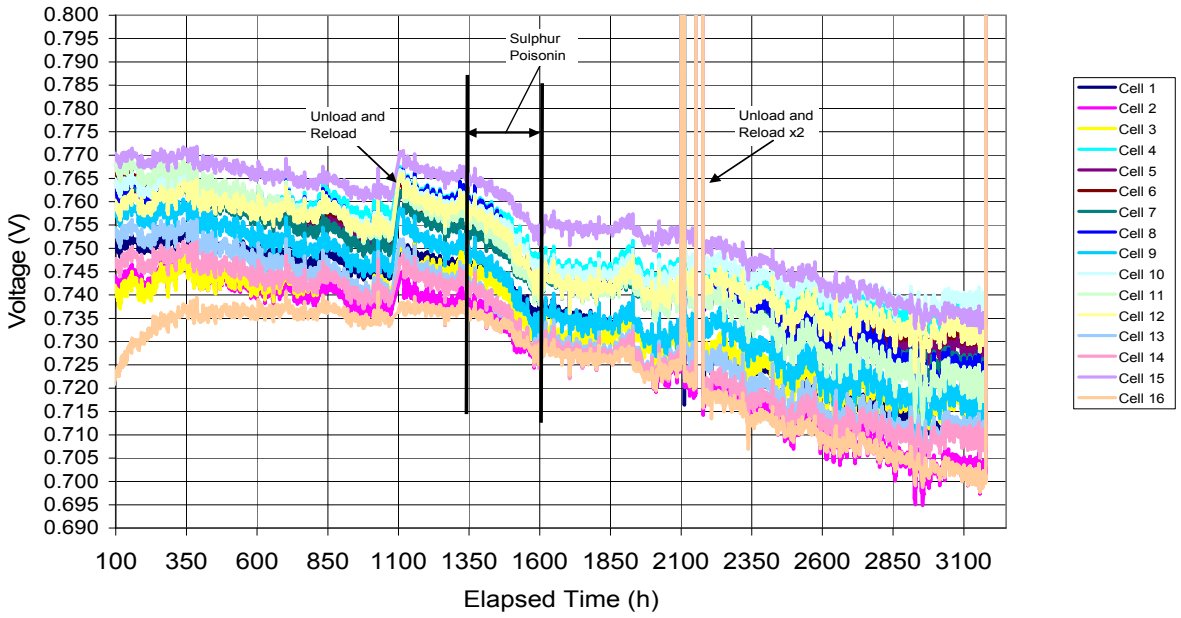

Figure 2-6 550 cm^2 Cell Area 16-cell Stack Test at Phase II Type Conditions

End-of-Phase II Metric Test: Three 92-cell stacks (550 cm^2 active area cells) were built (using TSC-3 cell technology) to provide the two stack blocks required for assembly of the End-of-Phase II metric test stack tower. The stack blocks were successfully performance tested at VPS. The 2 x 92-cell stack tower for the metric test was assembled and instrumented at FCE's facility in Danbury, CT, and the tower test at FCE was initiated (in Phase II). In parallel, a 120-cell stack metric test at VPS was conducted. The stack employed thin TSC-3 cells and thin interconnects. The start-up phase of the test included stack heat up and conditioning. Prior to initiation of the 5000 h steady state test, the peak power test was completed. Over a 22-h peak power test period, the stack generated 25.2 kW (DC power measured in hot zone). This

corresponded to an average cell voltage of 831 mV at 459 mA/cm^2 and a power density of 381 mW/cm^2. Phase II metric of achieving 25 kW peak power was satisfied. A more aggressive peak power test was conducted separately on a 16-cell stack built using the same cell design as the metric test stack tower above, to provide performance basis for the Baseline Plant Power Island Factory Cost Estimate (Section 4.2 of this report). A power density of up to 467 mW/cm^2 was demonstrated.

Following the peak power test on 120-cell stack, normal operating conditions (NOC) were established for the long-term steady state test. The stack performance at NOC corresponded to an average cell voltage of 835 mV at 367 mA/cm^2 (23% CH_4 dry basis) and a DC power of 20.2 kW. The 120-cell stack metric test successfully met DOE's requirement of completing 1500 h of testing before the end-of-Phase II.

The 120-cell stack metric test was continued in Phase III. The test, however, had to be shutdown after ~2,350 h of operation, because of low performance of some cells. Figure 2-7 shows the average cell voltage, power and the performance degradation rate observed over the test period. A performance degradation rate of 1%/1000 h was observed at steady state normal operating conditions (1,640 h period), which is well within DOE's requirement of <2%/1000 h.

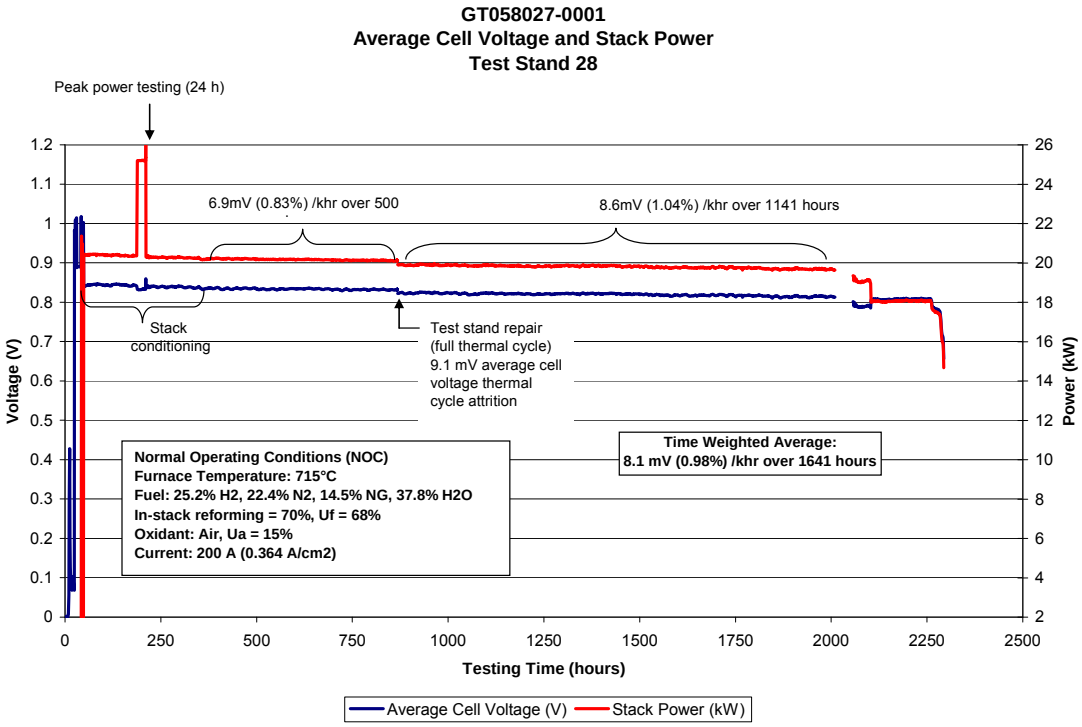

Figure 2-7 End-of-Phase II Metric Test (120-cell Stack) at VPS

The stack tower test (SO-30-4) at FCE tested the tower in a module enclosure environment. The peak power test achieved 30.2 kW DC output at 200 A (and 151 V), with a fuel utilization of 54% and an air utilization of 12.6%. Following the peak power test, during the NOC steady state hold, the stack tower produced an output of 27.0 kW at 185 A (and 146 V), with a fuel utilization of 70% and an air utilization of 13.5%. The stack tower test at FCE was shut down because of low performance of some cells. Overall, the stack tower operated for >1,900 h with a power degradation rate of 1.89%/1000 h, based on linear regression for the NOC portion of the test, achieving the targeted value of <2%/1000 h.

Post-test analyses of the 120-cell stack and the top stack (92-cell block) from the stack tower metric test at FCE were completed. Inadequate cathode contact was found to be the primary cause for the stack performance loss. Patchy cathode contact can result in very high local current density, high cell temperatures and cell degradation. Plans were made to achieve 5,000 h of testing (to satisfy the metric test requirement) early in Phase III, using a 96-cell stack with improvements based on the lessons learned.

A 96-cell (550 cm^2 cell area) stack block (proposed Phase III stack configuration) was assembled for the 5000-h metric test completion. After initial performance characterization and a thermal cycle, long-term steady state testing at system-representative operating conditions was initiated at VPS. In-cell thermal profiles were stable. Approximately 1700 h into the steady state hold the test was interrupted by a power outage resulting from failure of a utility transformer. Cell 72, which had shown performance sensitivity during fuel utilization test earlier, degraded rapidly. The operating conditions were relaxed to 50% fuel utilization, 50% in-stack reforming and 270 mA/cm^2, to stabilize the cell performance. After another 200 h, the stack test was shut down because of a leak in the test stand humidification system. Total hours accumulated by the test were 3120 h. The stack steady state operation test was resumed after the stack repair. The repair constituted bypassing the low performing Cell 72. Performance characterization after the repair indicated that the adjacent Cells 71 and 73 were negatively affected. The stack performance degradation rate after the repair was somewhat high (initially 3%/1000 h and later improving to 1.6%/1000 h). Figure 2-8 shows the test history. Overall the stack test accumulated over 5500 h and achieved 16 kW DC power level during steady state operation.

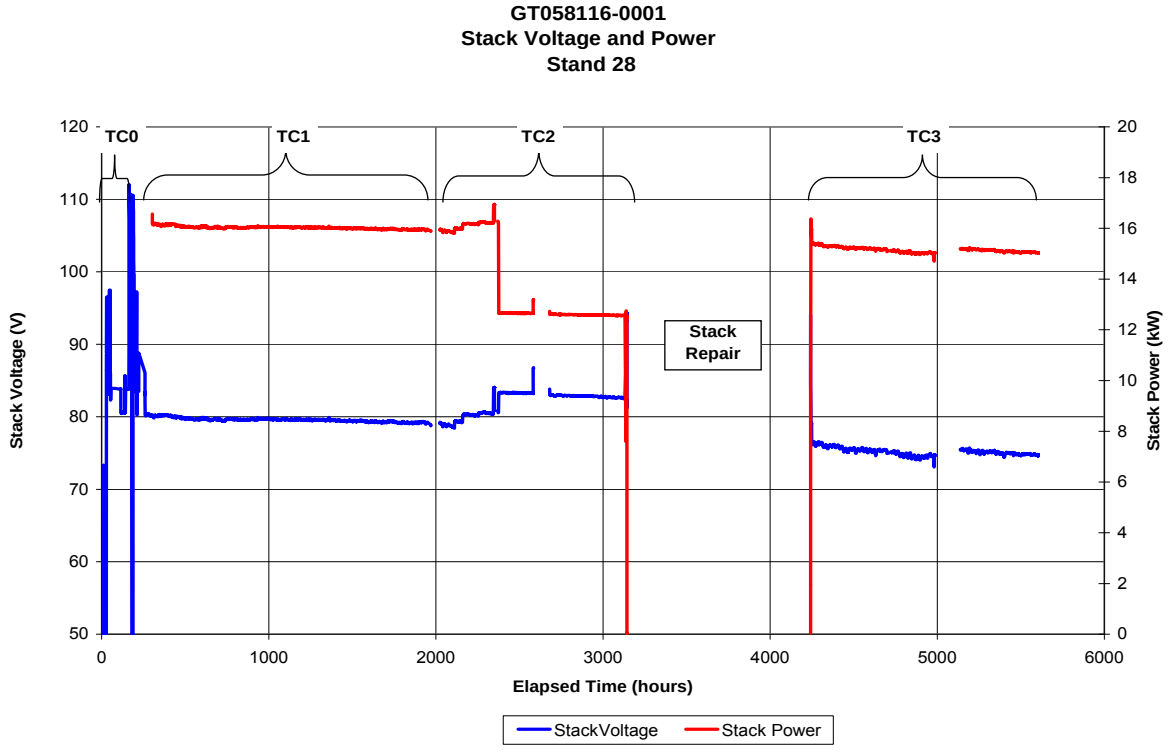

Figure 2-8 Stack GT058116-0001 Performance over the Total Test Period

Stack Development and Testing in Phase III

Stack development in Phase III focused on improving robustness of the SOFC stack. The stack building block size was finalized to 96-cell size. The 16-cell stack tests (and some 32-cell stack tests) were conducted to study the issues related to higher performance degradation rate and cell performance drop observed in 96-cell stack block tests. The stack builds were designed or configured to facilitate parametric studies. Sensitivity to more aggressive (Phase II) system operating conditions (higher fuel utilization, more in-stack reforming) was evaluated. Selected stack test results categorized by the stack size (cell count) are presented here.

16-Cell Stack Testing

Stack GT057235-0081 (Plain Fin Cathode Flow Fields): Stack GT057235-0081 was assembled for evaluating plain fin cathode flow field. Performance testing was good with all cell voltages above 0.70 V at 80% fuel utilization. Following the performance testing, steady-state testing was conducted. Over a 1068-h period, a degradation rate of 2% per 1,000 hours was observed. This was roughly twice the degradation rate of VPS's standard cathode configuration cells in 16-cell stacks. Further testing was not pursued.

Stack GT057235-0083 (Modified Anode Flow Fields, Increased Compression load): A 16-cell stack was built with modified "JV" fin anode flow fields (JV is an internal designation) to see if the issues seen at the 96-cell stack level (high degradation and performance dropping of cells) would occur at the 16-cell stack level. The standard performance testing was conducted on the short stack. Figure 2-9 shows the stack performance during fuel utilization testing after a thermal cycle. Interestingly, Cell 8 showed performance sensitivity at high utilizations. The performance sensitivity was thought to be related to presence of thermocouples in the cell.

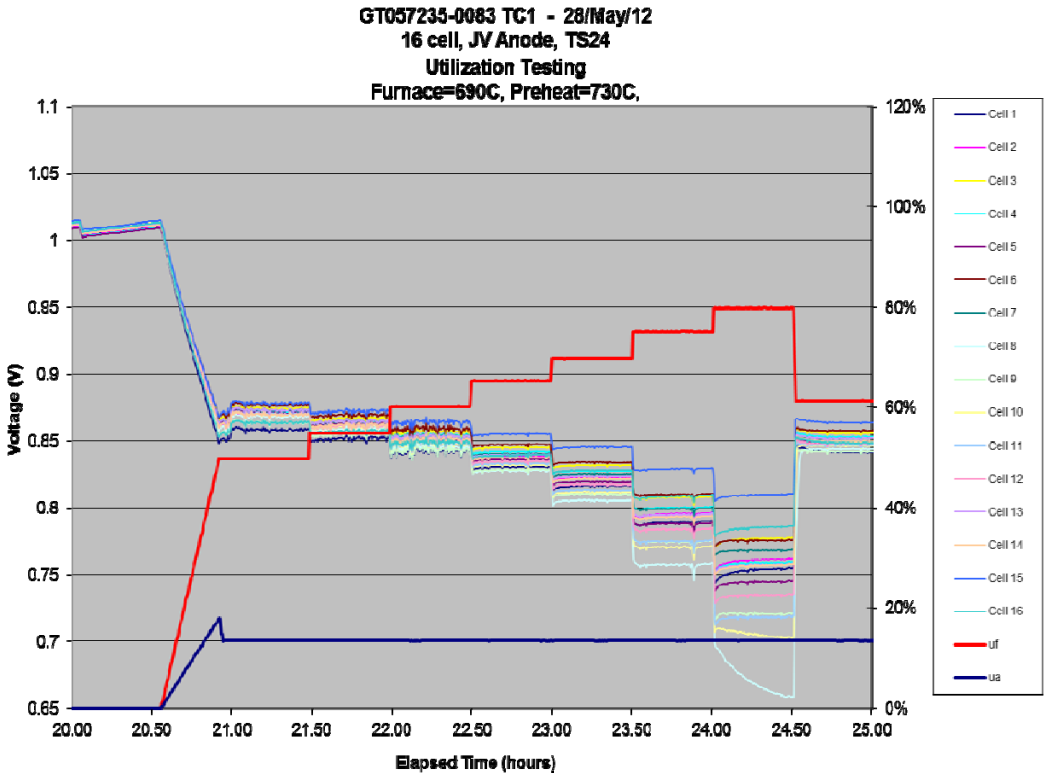

Figure 2-9 Stack GT057235-0083 Performance during Fuel Utilization Testing After Thermal Cycle (TC1)

Following the performance testing, steady-state testing at 62% Uf, 62% DIR (in-stack reforming), and 200 A conditions was conducted. During 1980 hours, the stack had a degradation rate of 1.1% per 1000 hours as shown in Figure 2-10. A decision was made to thermal cycle the stack as a part of further evaluation. During the thermal cycle, top compression load on the stack was lost due to a maintenance-related mishap. On reheat and subsequent loading of the stack, a number of cells showed a significant voltage loss. The test was terminated.

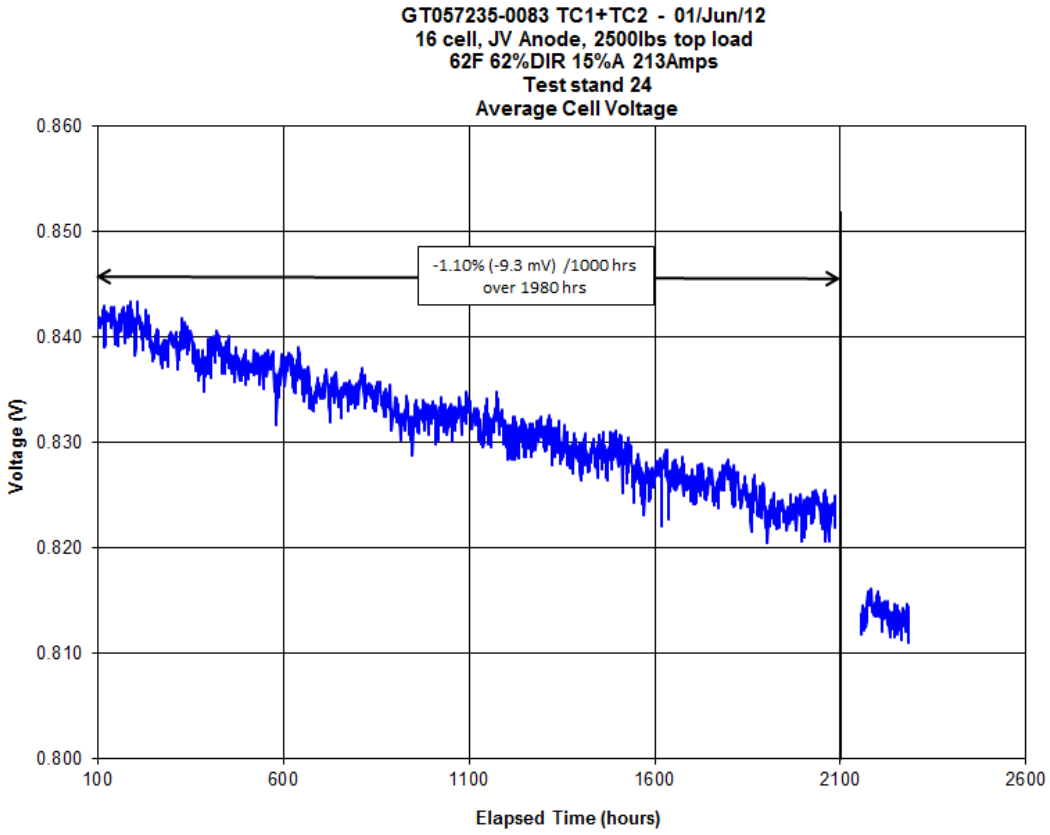

Figure 2-10 Stack GT057235-0083 Steady-State Hold Average Cell Voltage

Stack GT057235-0089 (TSC-3 Cells, New Production Hydrothermally Stable Cells): To improve the chances of finding the cause of higher performance degradation observed in (then) recent stacks, a number of cells were produced with a high level of QA/QC (quality assurance/quality control) so that they can be fully tracked. In addition, all stack components were tracked to a given layer in the stack. This included tracking nominal stack components with more detail such as metallic components and seals tracked to a given stack layer, and cell locations in particular furnaces tracked for batch firing. All cells used in Stack GT057235-0089 were fully-stabilized anode formulations produced with improved manufacturing processes.

The stack performed well in fuel utilization testing before a thermal cycle. However in fuel utilization tests after a thermal cycle, Cell 16 appeared to suffer contact loss from the thermal cycle. With this stack build, endplates were recycled from a previous stack test potentially resulting in a warped endplate.

The stack was placed into a steady state hold (at Phase II system conditions) for ~1500 hours to determine the degradation characteristics. Figure 2-11 shows the average cell voltage over

this hold and the corresponding degradation rate. The stack showed close to double the expected degradation rate. To investigate the effect of operating conditions on degradation rate, the stack was placed into a 110 Amp (0.2 A/cm^2) hold on pure hydrogen at 65% fuel utilization (Uf). As can be seen in the figure, the degradation rate improved by an amount roughly proportional to the current reduction.

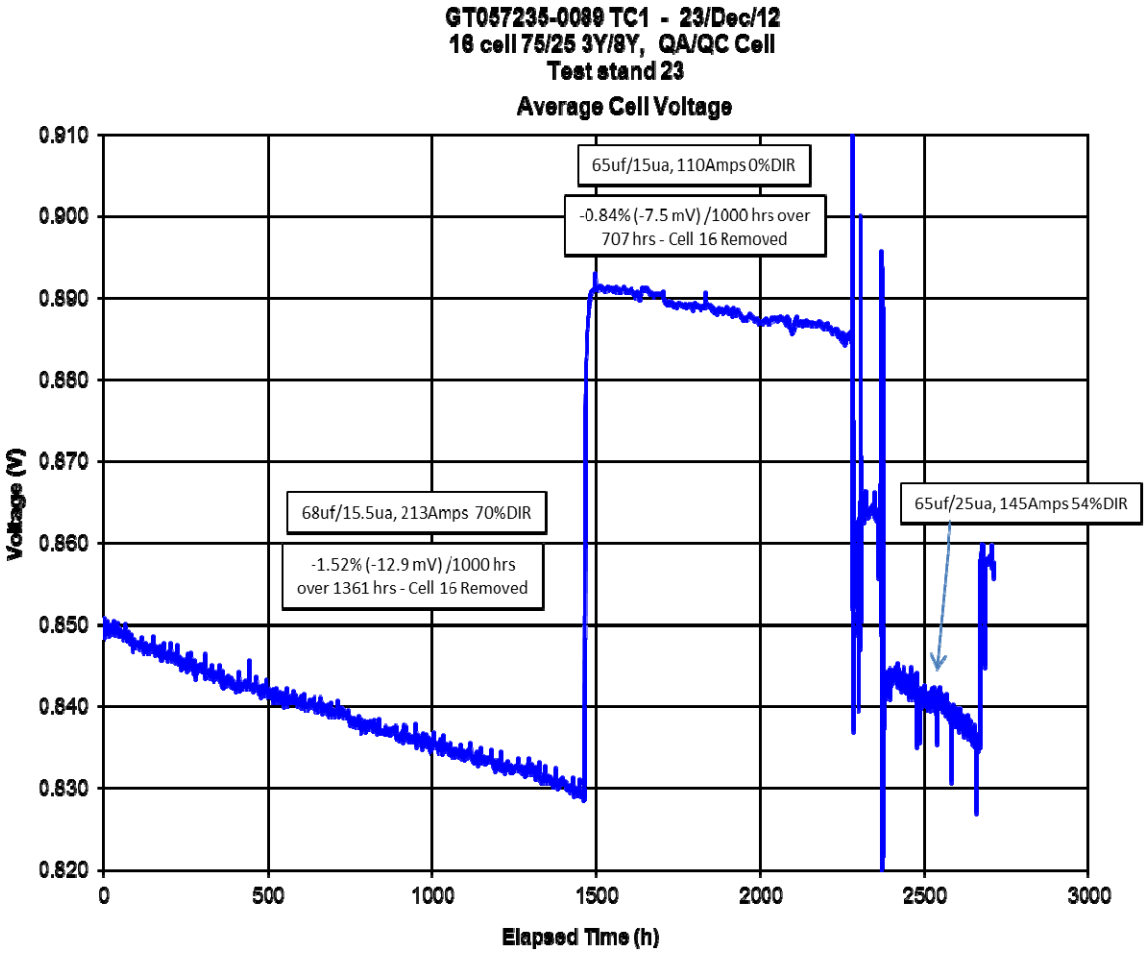

Figure 2-11 Stack GT057235-0089 – TC1 Steady-State Hold Performance

The stack was operated at these conditions for over 700 h and did not show signs of any cell dropping from the pack. The individual cell degradation rate profile is shown in Figure 2-12.

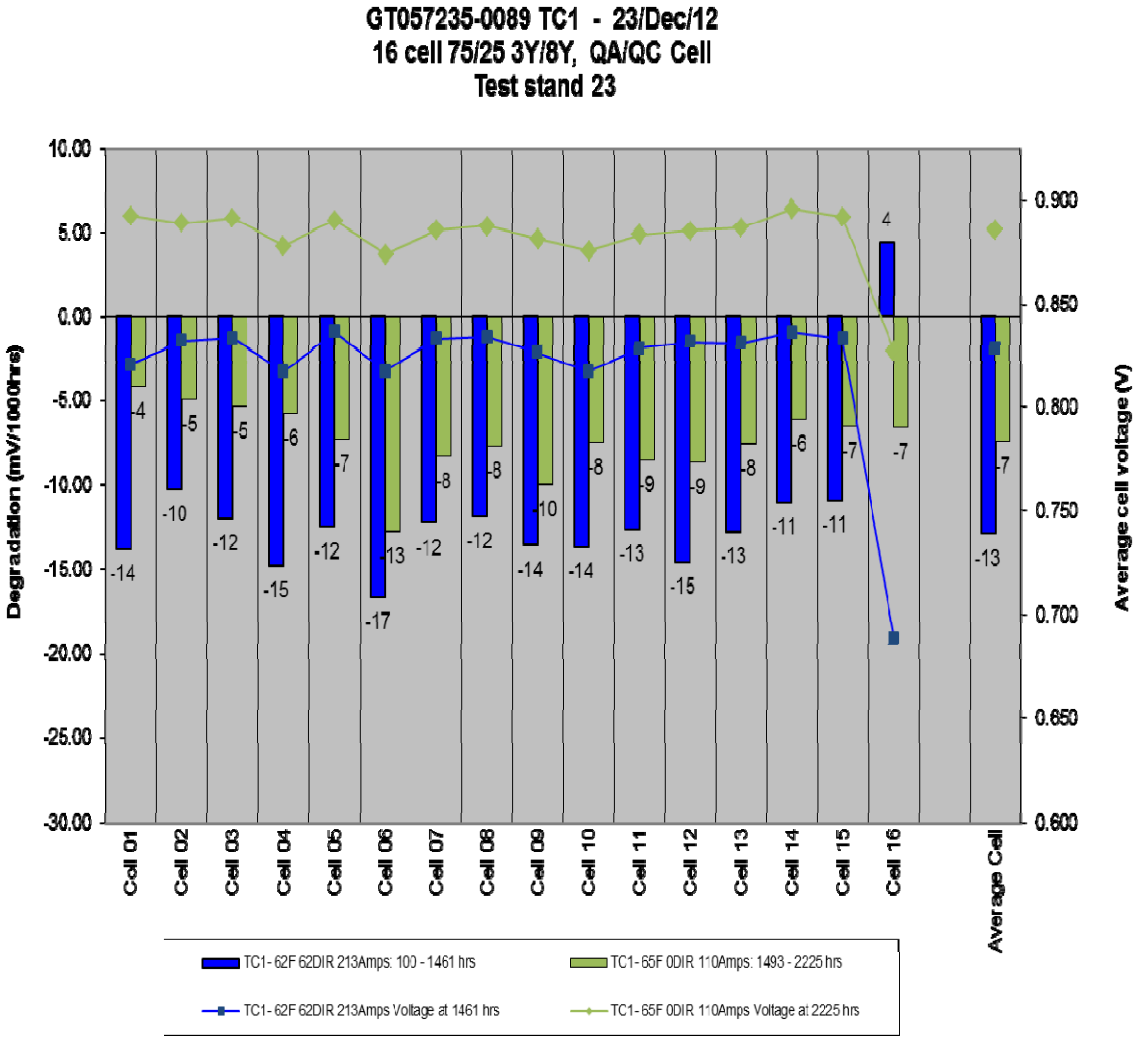

Figure 2-12 Stack GT057235-0089 TC1 Hold Individual Cell Degradation Rates Profile

Following the hydrogen hold, a number of higher current (lower than full 213 Amp) operating points were investigated with higher in-stack reforming level (lower than 70% DIR). The conclusion from this testing was that there were some contact issues/challenges within the stack.

Stack GT057235-0093 (Cathode and Barrier Layer Firing): Stack GT057235-0093 was built to investigate the parameters (variables) of the firing equipment and the cell firing process including both covered (with half-cell) and uncovered (exposed or open to furnace environment) firing. VPS has two types of electrically-heated, bottom loading batch furnaces which are named by the original equipment manufacturers: PSH Canada and Deltech. The PSH furnaces are small batch furnaces. The Deltech is a large batch furnace which has increased forced air cooling for manufacture of a large number of cells and larger area cells. The covered or uncovered cell firing relates to potential contamination from the furnace environment during the high temperature firing.

Fuel utilization testing before (TC0) and after (TC1) a thermal cycle (TC) was performed. Figure 2-13 shows average cell performance trends for the different cell pedigrees during steady state testing after the thermal cycle.

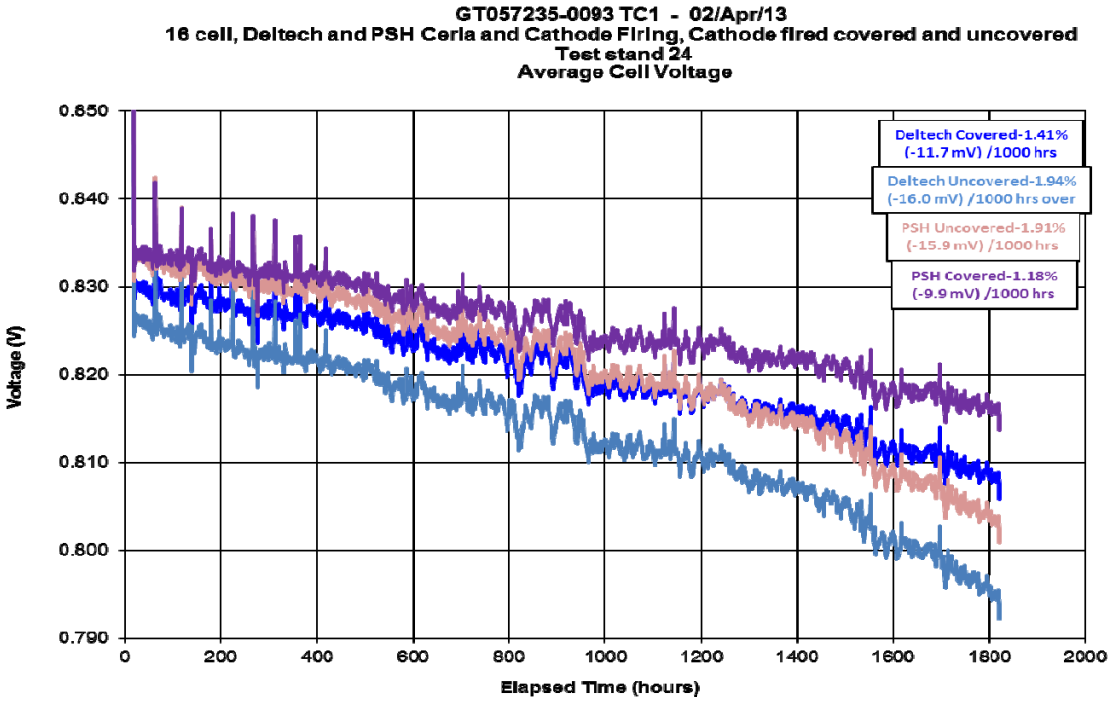

Figure 2-13 Performance Degradation Trends for Different Cell Pedigrees in Stack GT057235-0093

Based on these results, the technical team decided to use the covered cell firing method for both barrier layer and cathode firing for all future cell production.

Stack GT057235-0095 (Thick Contact Paste and Chromium Getters): As outlined in Cell Materials Development section (Subsection 1.1) of this report, excellent progress was made on the subject of chromium getters (adding materials to the SOFC that are preferentially reactive to chromium). This design approach is expected to extend cell life by minimizing degradation related to Cr poisoning. Stack GT057235-0095 was the first stack implementing these materials into the large area stack platform in combination with a thick contact paste. The motivation behind a thicker contact layer in a large area stack was to improve physical and electrical contacts within the stack and to influence degradation characteristics. This was also the first large area stack to include the improved anode flow field parts. The parts were pinch rolled to a high degree for reduced height variation.

Incidents occurred after the first thermal cycle (TC1) affecting the stack testing. The stack was reduced and then a test stand error occurred leading to hot standby condition. In this condition, fuel purge gas (4% hydrogen in nitrogen) was flowed, however, with no air was flowed for 40 hours. The electric load and hot zone flexible current collectors required change out.

Figure 2-14 shows the fuel utilization performance test results after two thermal cycles. The secondary Y-axis represents the fuel utilization. The stack successfully passed the 80% fuel utilization test (all cells >800 mV). This high utilization performance and the close grouping of cells (~20 mV spread) were expected as a result of the anode flow field changes.

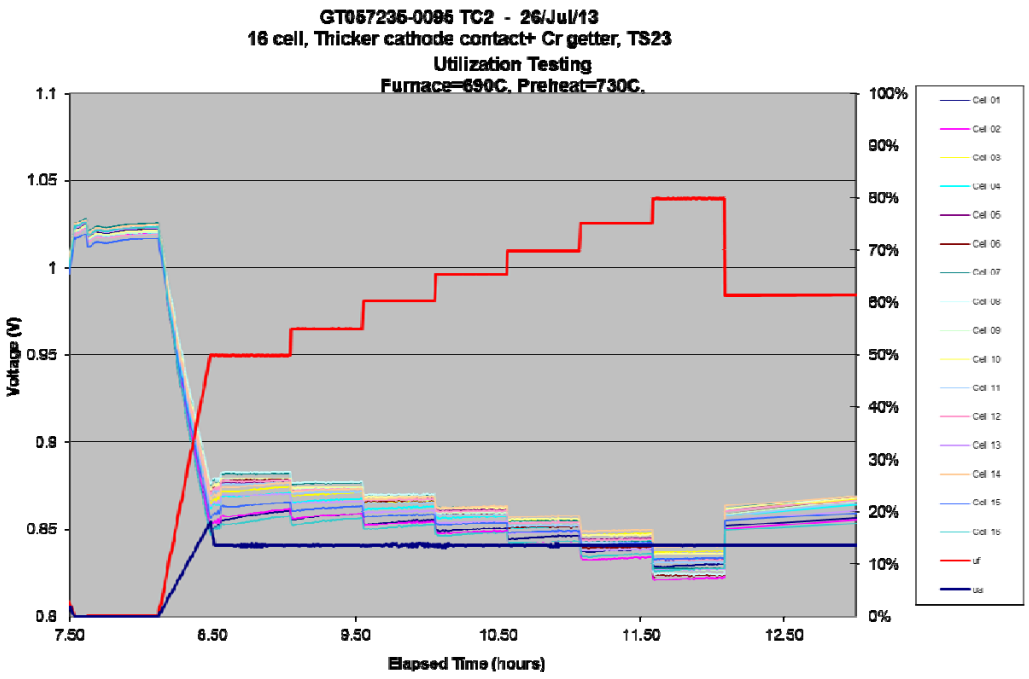

Figure 2-14 Stack GT057235-0095 Performance during Fuel Utilization Testing

Following the qualification testing, the stack was placed into a steady state hold at conditions of 61.5% fuel utilization, 25% in-stack reforming, 13.5% air utilization and 213 A current. Over a short term hold of approximately one week (159 h), the stack performance appreciated (no degradation). Following Phase I system condition hold with high humidity (56% anode inlet humidity), fuel and air flows were transitioned to Phase II system conditions of 68% fuel utilization, 70% in-stack reforming, 15% air utilization and 213 A current. Under these conditions, the stack demonstrated an impressive 0.23% per 1000 hours degradation rate over 713 h. Figure 2-15 shows the stack average cell voltage trend.

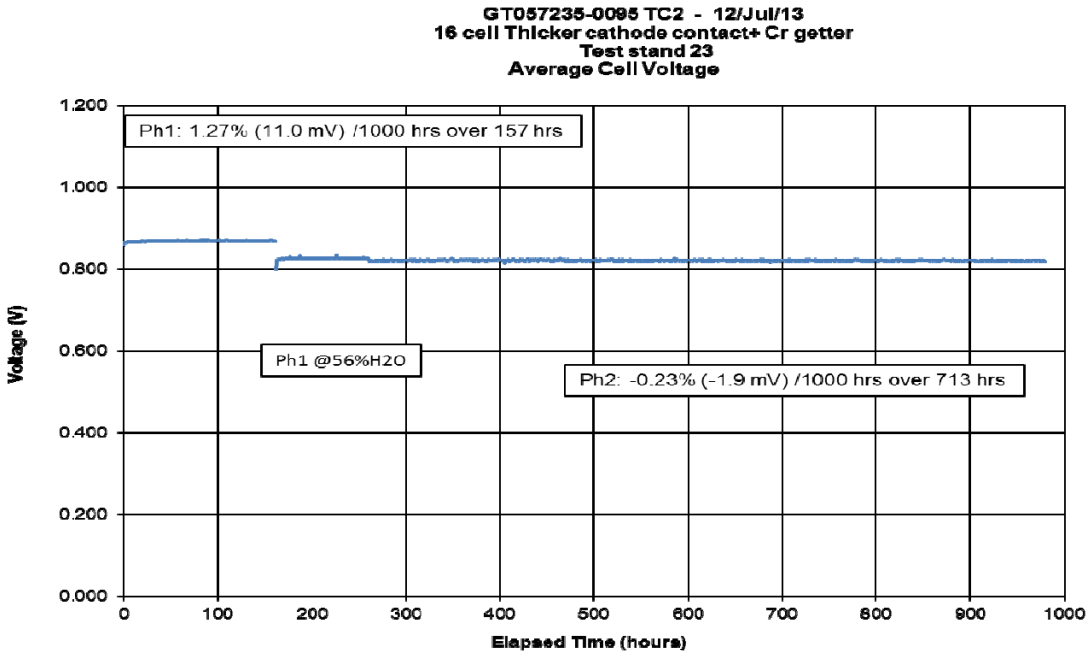

Figure 2-15 Performance of Stack GT057235-0095 at Phase I and Phase II System Conditions

Approaching 1000 hours of testing, there was a test stand incident during which hydrogen flow was inadvertently shutdown and stack load (current) was sustained under no fuel conditions. This oxidized the anodes. The test was terminated and stack was cooled for post-test examination.

In post-test examination, the design and components measured as expected. The variation in height of the anode flow field after rolling was significantly lower than for the previous stack and the large fuel bypass gaps were almost eliminated.

Stack GT057235-0097 (Thick Contact Paste): As a further evaluation of thick contact paste, stack GT057235-0097 was built with a consistent amount of wet contact paste on each cell. The stack passed the 80% fuel utilization test (all cells >800 mV) before (TC0) and after (TC1) thermal cycle. This result was expected and compares well to Stacks GT057235-0095.

Following conditioning and qualification testing, the stack was operated at Phase II system conditions of 68% fuel utilization, 70% in-stack reforming, 15% air utilization, and 213 A (387 mA/cm^2) current. Test results are presented in Figure 2-16. Testing was resumed after the second thermal cycle. The stack demonstrated 0.73% (6.2 mV) per 1000 hours degradation rate over 767 hours after the first thermal cycle and 0.48% (4.1 mV) per 1000 hours over 1985 hours after the second thermal cycle.

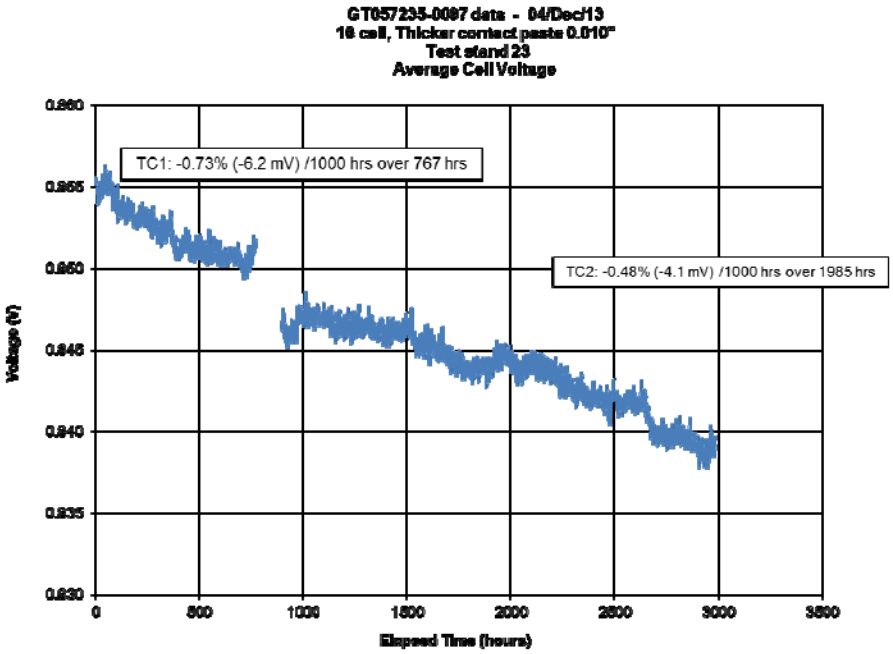

Figure 2-16 Performance Stability of Stack GT057235-0097 at Phase II System Conditions

The individual cell performance trends showed that all cells were grouped together throughout the test duration with less than 20 mV voltage spread.

Figure 2-17 shows the distribution of individual cell degradation rates before and after the second thermal cycle. The cell degradation rates are quite uniform throughout the stack, as desired for the technology.

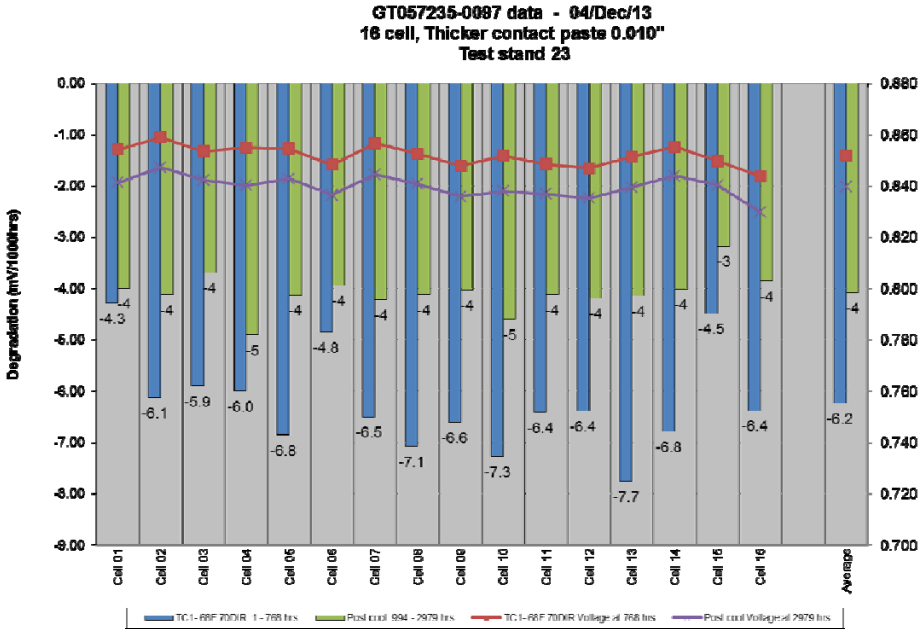

Figure 2-17 Individual Cell Performance Degradation Rates for Stack GT057235-0097 Operating at System Conditions

32-Cell Stack Testing

With the reduced production of 96-cell stacks, the 25 kW test stands were also available for development testing. Given the test facility's large capacity, a 32-cell stack is the smallest stack that can be effectively tested in the stands. As such, 32-cell stacks were used, as required, in these stands to bolster the short stack (16-cell) development testing.

Stack GT057832-0003 (Old Production Full Cells vs. Old Production Half Cells vs. New Production Hydrothermal Stable Cells): As a further investigation into the cause of the recent high stack degradation, three different cell combinations were built into a stack. The first cell type was old production full cells produced approximately two years ago. The second type of cell was old production half-cells (anode to electrolyte) produced approximately two years ago combined with a new production cathode. The third cell type was new production cells. This stack was built to help determine whether the new production cathode materials played a role in stack performance degradation.

Performance during fuel utilization tests before and after thermal cycle was strong, passing 80% fuel utilization in both cases. Following performance testing, the stack was placed in a steady-state hold at Phase II system conditions. Figure 2-18 shows the test results. Looking at the performance of the different cell pedigrees in the figure, the lowest performing cells were found to be those with the old cathode layers. Initially there was very little stability difference between the cell pedigrees. However, after about 1000 hours, the new stabilized cells began to show higher degradation rate. Over the last 900 hours of testing at these conditions, the new stabilized cells had degradation rate roughly three times that of the other cell pedigrees. The higher degradation was primarily driven by three new production cells rapidly dropping from the cell group.

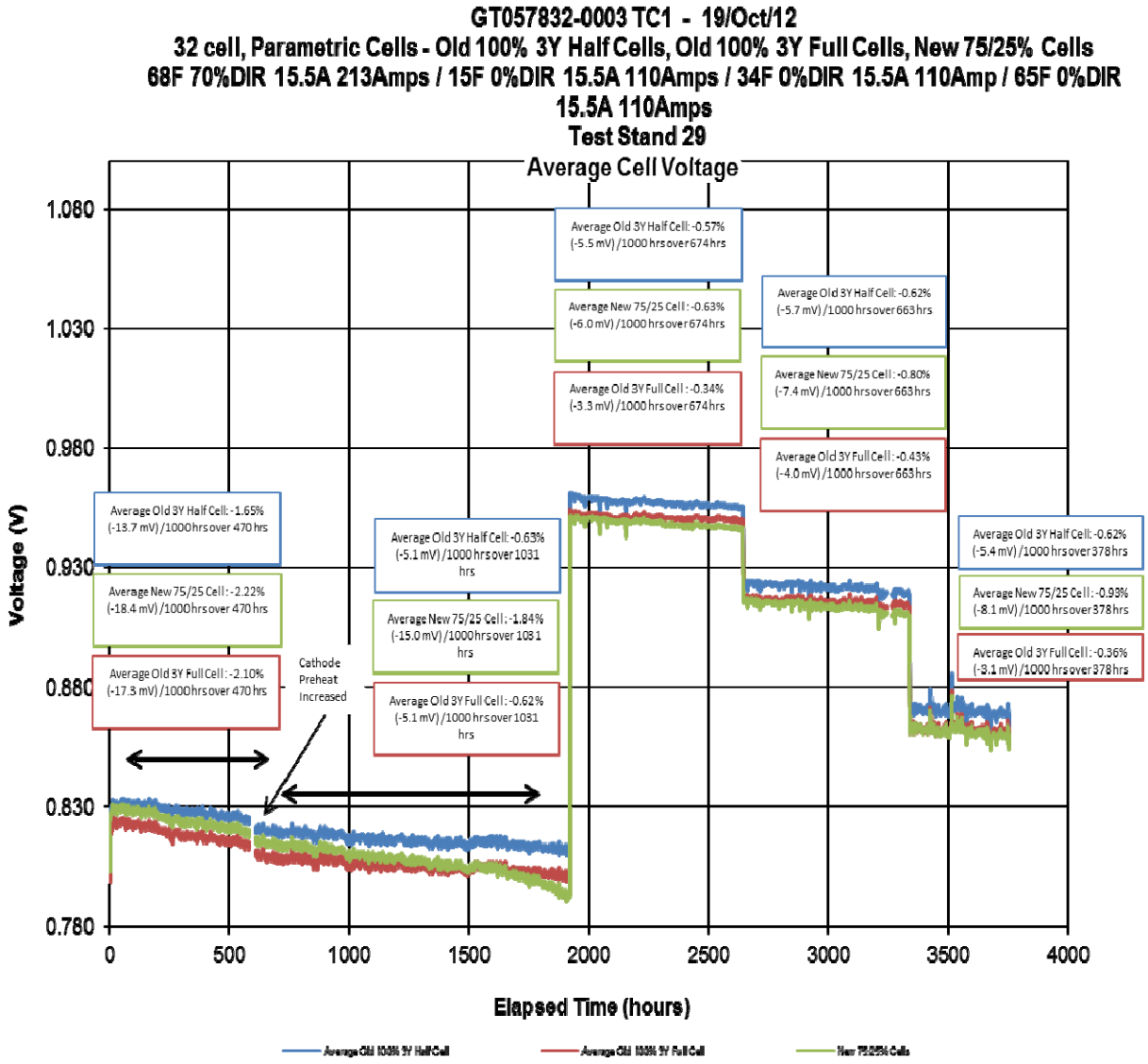

Figure 2-18 Stack GT057832-0003 Performance during Steady State Holds

After approximately 1800 hours of testing at Phase II system conditions, the conditions were relaxed to 15% Uf, pure hydrogen fuel and 110 A (0.2 A/cm^2) to see the effect on degradation and cell drop outs. A major improvement was observed with all degradation rates decreasing below 0.6% per 1000 hours. In addition, the rapidly degrading cells had stabilized. Figure 2-19 shows the individual cell voltage trends.

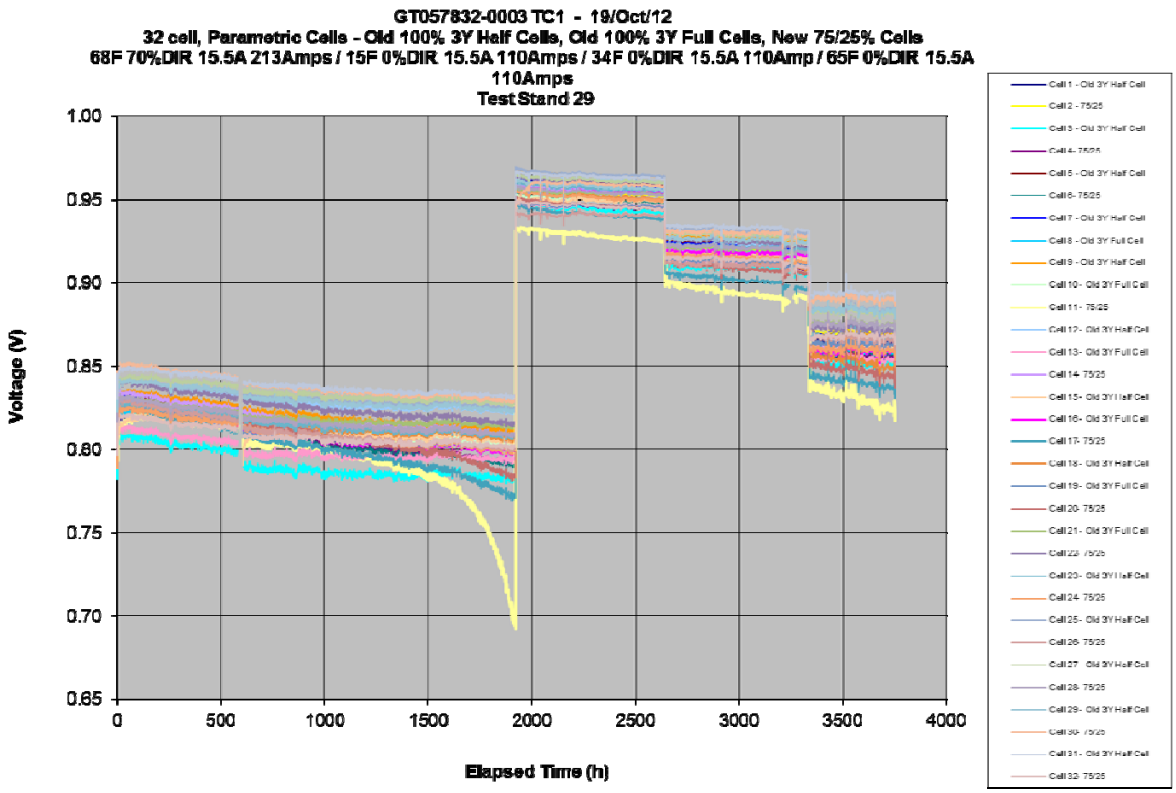

Figure 2-19 Stack GT057832-0003 Individual Cell Voltage Trends during Steady-State Holds

Following about 600 hours of hold time at 15% Uf pure hydrogen and 110 A (0.2A/cm^2), fuel utilization was increased to 34% Uf (pure hydrogen fuel) to see the effect of utilization on degradation. The degradation rate of the new production cells increased slightly to 0.8% per 1000 hours, the other cell groups remained relatively unchanged. Following another 600 hours hold time, the utilization was increased further to 65% Uf (pure hydrogen fuel). The stack was held at these conditions for almost 400 hours. While the degradation rate of the new production cell group increased slightly to 0.9% per 1000 hours, the other cell groups remained relatively unchanged.

96-Cell Stack Testing

The first 96-cell (550 cm2 cell active area) stack block (GT058116-0001), a representative of the manufactured building blocks for large-scale modules (>50 kW), was assembled using TSC-3 cells. The stack was used for 5000-h End-of-Phase II metric test completion. The results have been presented earlier in this report.

Stack GT058116-0003 (TSC-3 Cell Technology Long-Term Testing): Stack GT058116-0003 was a long-term test of the TSC-3 cell technology. The stack underwent full performance testing before and after a thermal cycle (TC0 and TC1), before initiation of a long-term steady-state hold. Figure 2-20 shows the stack performance over the test. The stack demonstrated a performance degradation rate of 1.3% per 1,000 hours over a 3,450-hour period.

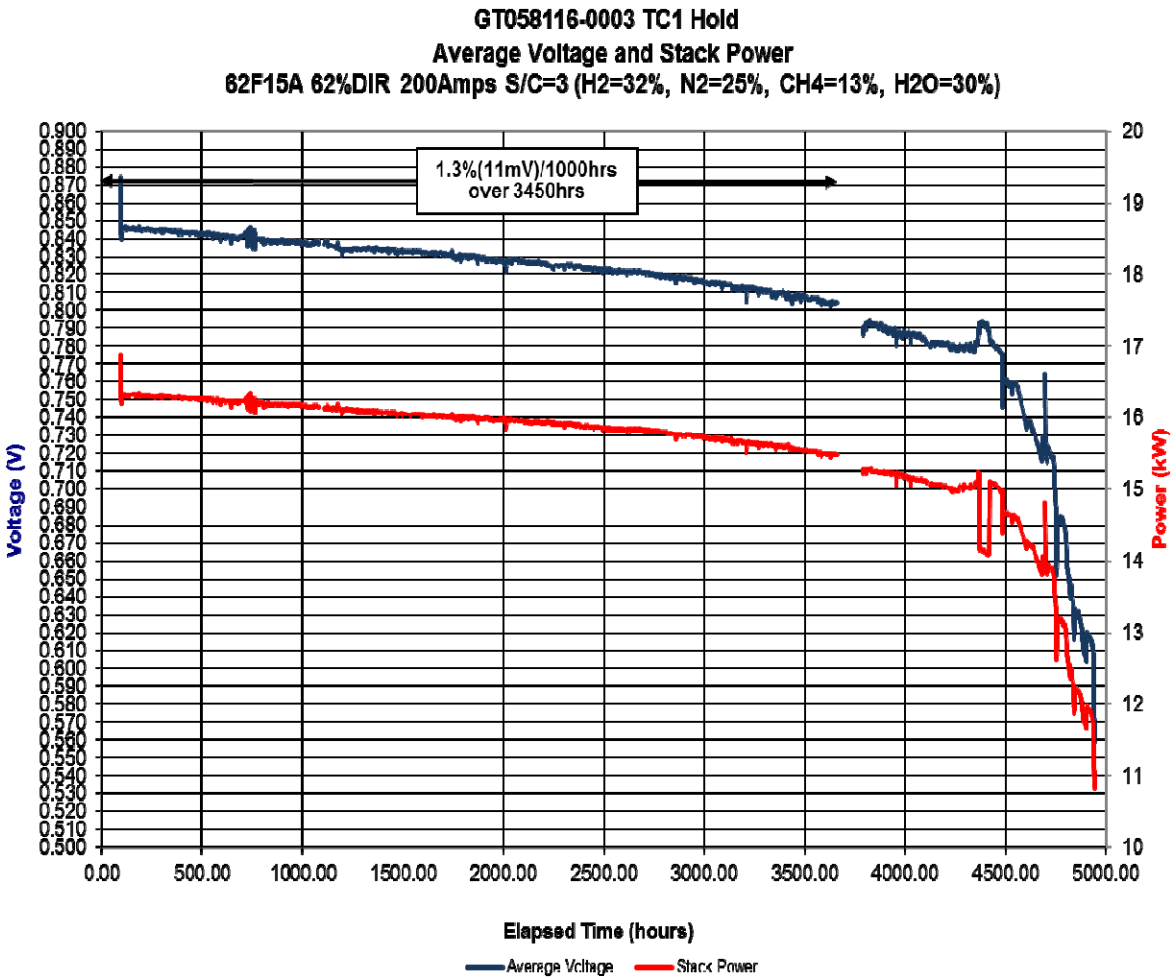

Figure 2-20 Performance of 96-cell Stack GT058116-0003 During Long-term Steady-State Test

As shown in Figure 2-21, performance of Cells 18 and 28 began to degrade faster after 2,000 hours of testing.

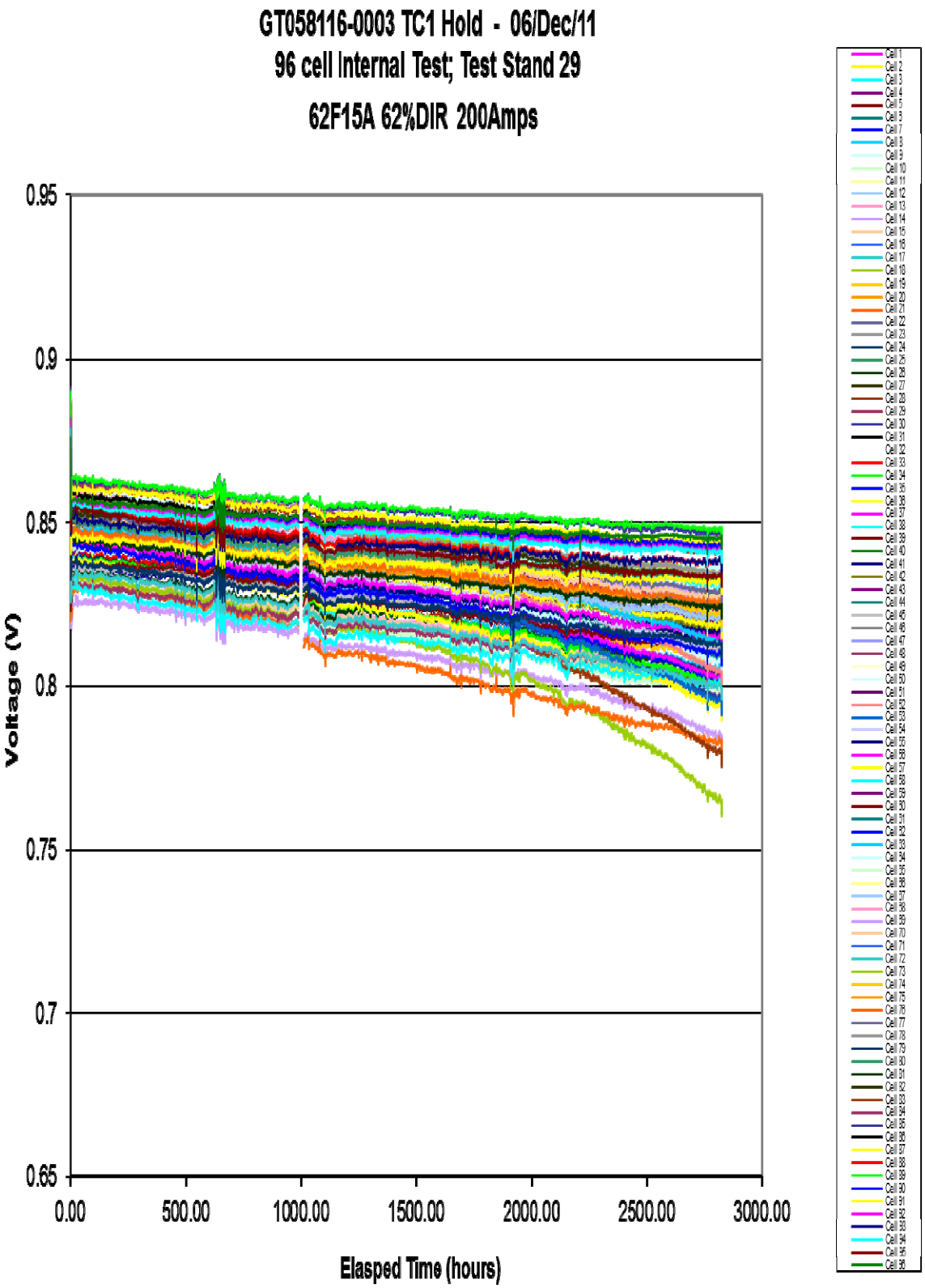

Figure 2-21 Stack GT058116-0003: Performance of Individual Cells

At approximately 3,600 hours, the stack went through a full thermal cycle due to a gas preheater malfunction. Shortly after the thermal cycle, performance of a number of cells began to degrade rapidly. As the target for this stack was 5,000 hours, the steady-state test was continued until the test reached 5,000 hours of run time and then the stack was shut down.

Stack GT058116-0002 and -0004 (FCE Stack Tower Test Deliverables #1 & 2): Stacks GT058116-0002 and -0004, each containing 96 TSC-3 cells, were assembled and performance tested at VPS prior to shipment to FCE (Danbury). The stacks served as the deliverables for 2 x 96-cell stack (block) tower test conducted at FCE (stack tower test results are discussed in Sec 3.2). Results from the stack qualification testing (performed at VPS) for Stack GT058116-0002 are shown in Figure 2-22 as an example. All cell voltages were above 0.75 V at 75% fuel utilization and closely grouped during the short holds.

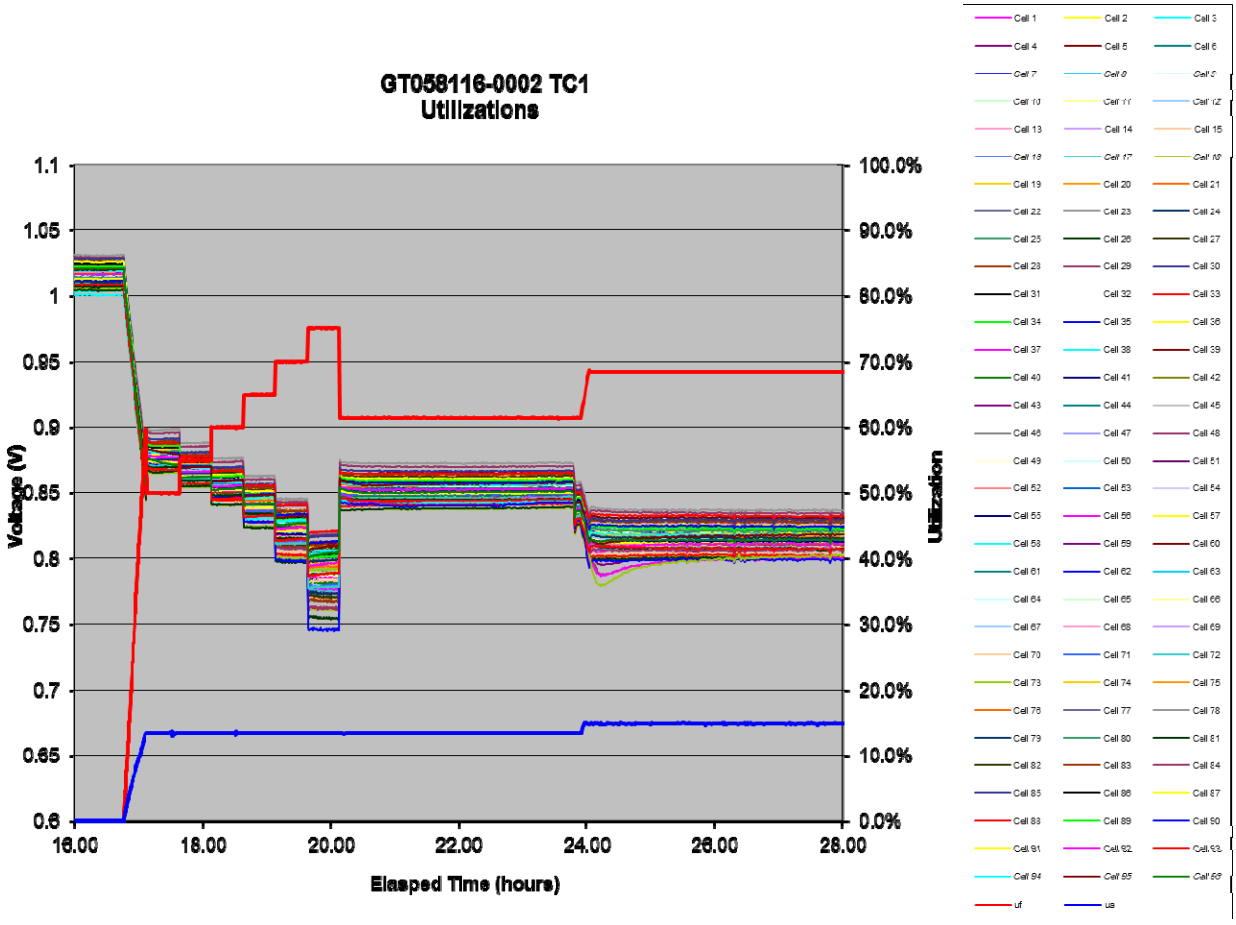

Figure 2-22 Stack GT058116-0002 Performance during Fuel Utilization Test

Stack GT058742-0001 through -0004 (Quad Module Test Deliverables #1 to 4): The four stacks for the FCE quad (4-stack) module test were built in in the period February to May 2012. The 96-cell stacks were assembled and performance tested at VPS prior to shipment to FCE (Danbury). The stacks served as the deliverables for a 60 kW (nominal) quad module test conducted at FCE (SOFC module test results are discussed in Sec 3.2). The fuel utilization tests before and after the first thermal cycle (TC1) were conducted to characterize the stack performance. The performance testing showed good results. Results of the performance

characterization after the thermal cycle are shown in Figure 2-23 for Stack GT058742-0001 as an example.

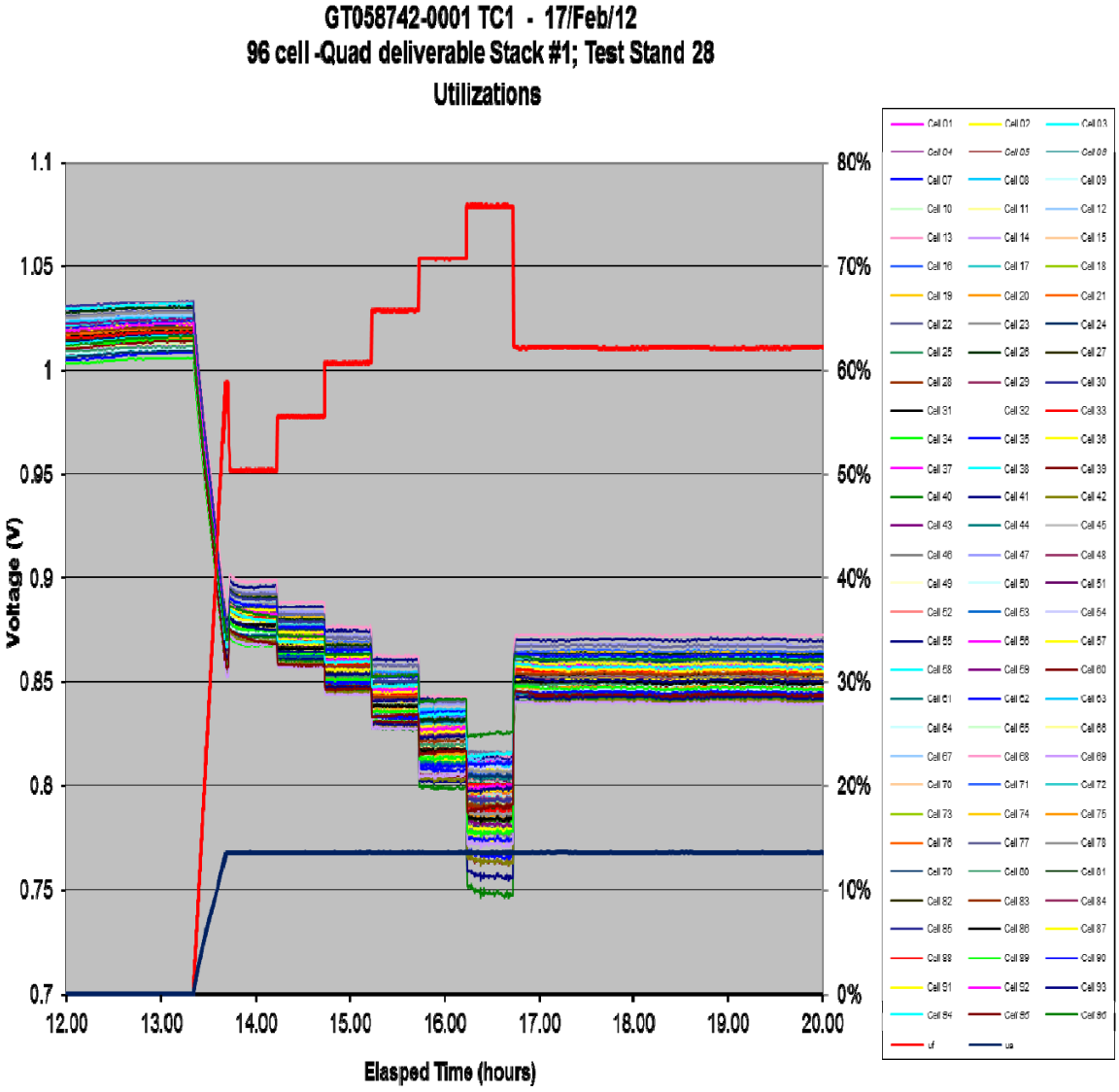

Figure 2-23 Performance Characterization of Stack GT058742-0001 before shipment

The conditioning profile (procedure) for the third and fourth stacks (GT058742-0003 & -0004) was modified to incorporate a longer dwell at normal compression load followed by an increase in the compression by about 30%. The motivation for trying new (increased) compressive load was the feedback (from analysis) of poor cathode contact in the top cells of the earlier 96-cell stacks. An LVDT (linear voltage differential transmitter to monitor stack height change) was installed to monitor stack compression during different load trials. Following the compression trials, the stacks were performance tested successfully yielding consistent results.

A final comparison of the average cell voltage was made between the four deliverable stacks (for the quad module test), as shown in Figure 2-24. The results show good consistency, with Stack GT058742-0003 exhibiting higher performance at all conditions.

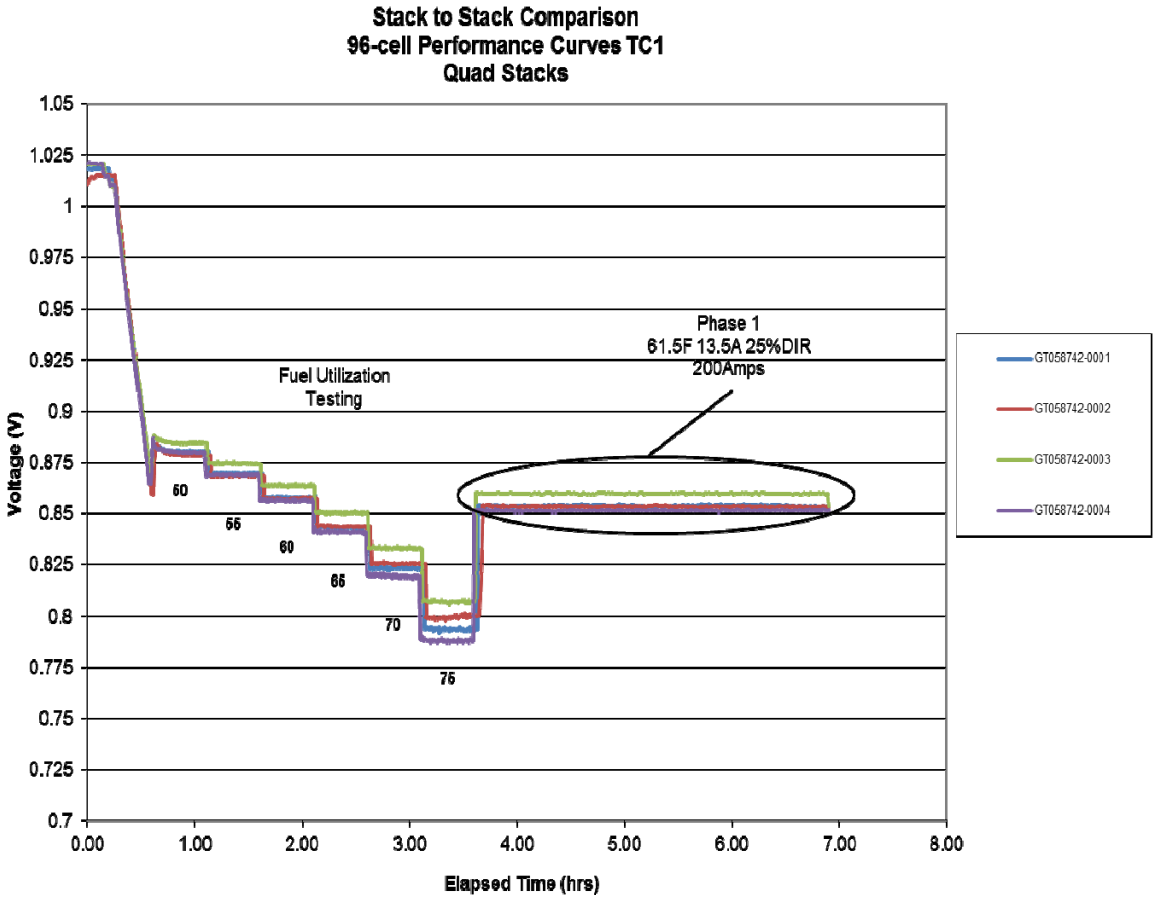

Figure 2-24 Performance Comparison of Stacks Fabricated for Quad Module Test

2.2 Stack Component Development and Testing

Anode Flow Field Improvement: A general review of the anode and cathode flow fields was carried out. The evaluation criteria for alternate geometries were design simplicity, low-cost, better part tolerances, suitability for carrying out in-stack reforming (anode side), low height (for stack compactness) and matching (anode and cathode side) pressure drops. For the anode side, a flow field pattern used by FuelCell Energy (for the carbonate fuel cell product) was selected for further development. A form suitable to achieve the desired in-stack reforming was developed. For the cathode side, a simple plain fin type pattern was chosen for further testing, as the plain fin is much easier to manufacture than a lanced offset fin. The flow media were tested successfully in short stack tests (550 cm^2 cell area). The robustness of the design in fuel utilization tests (up to 80% fuel utilization) and thermal cycles was validated.

The anode gas flow field and cell electrical contact are separate components. Potential cost savings and assembly simplification could be achieved by combining these components. The flow field is made of a ferritic stainless steel while the contact is made of nickel. By coating the stainless steel with nickel, the flow field could become a multifunctional part. An investigation into the methods of applying pure nickel to stainless steel indicated cladding as the most cost effective process. VPS worked with EMS, a premier supplier of metal clad solutions, to produce a suitable nickel clad stainless steel. A sample batch of material was obtained, processed, and fabricated into the anode flow fields for testing.

Anode flow field component inspections and stack post-test examinations revealed several issues. During component preparation, the anode flow field is pinch rolled to correct for “as received” thickness variation. Figure 2-25 shows the pressure mat force distribution indicating height variation of an as-received anode flow field sample. The supplied tolerance is 0.042 ±0.002 inch (0.107±0.005 cm) and the target rolled thickness is 0.039 ±0.0015 inch (0.099±0.0038 cm). It was found that VPS’s quality control method (measuring the four corner heights of the component between metal plates) is not adequate and that the incoming parts had low height areas that were not addressed by the existing pinch rolling specifications. Problematic low height areas affect electrical contact within the stack.

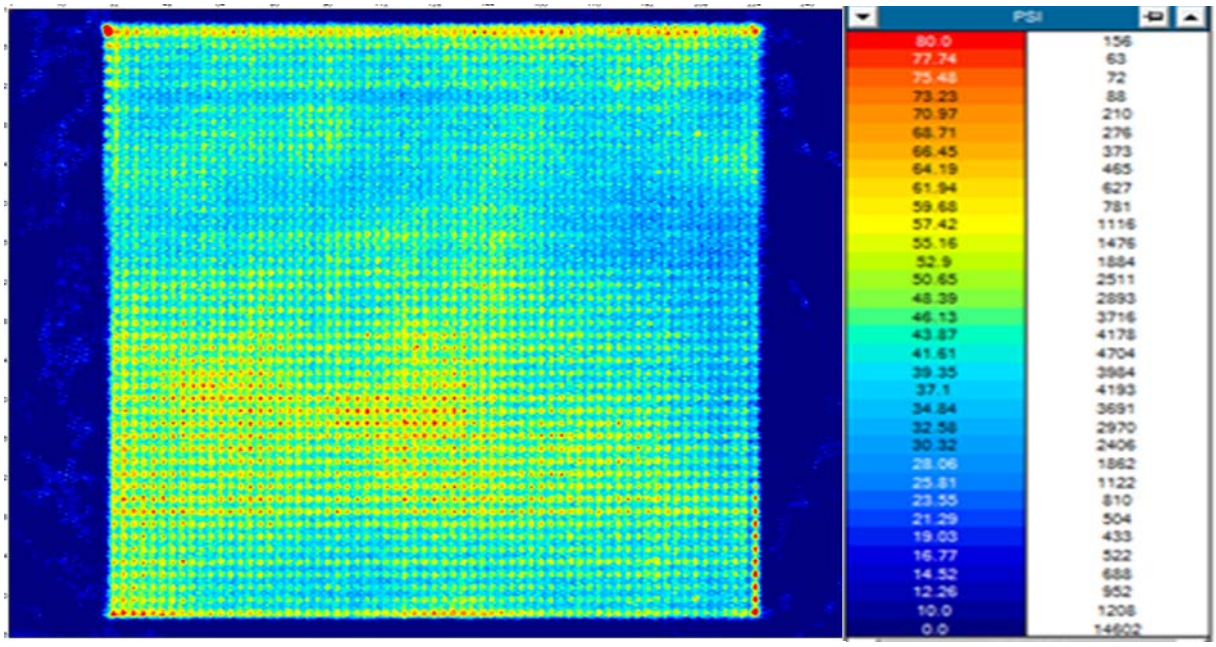

Figure 2-25 Pressure Mat Force Distribution Indicating Height Variation of ‘As-Received’ Anode Flow Field Sample (dark blue – low, red –high)

Also, with the pinch rolling process, there are two feed direction options. Rolling with the feed direction perpendicular to the fin flow direction causes an expansion in the part. Whereas, rolling with the feed direction parallel to the fin flow direction causes crushing of the component and lesser change in part dimensions. Thus, when the fin corresponds to the low end of the height tolerance band, the expansion due to pinch rolling is less than the anticipated (targeted) value which results in a bypass gap along the edge of the flow media as shown in Figure 2-26.

Figure 2-26 Anode Flow Field Fin with Fuel By-Pass Gap

As a solution for stacks built in Q3 2013 and onwards, the rolled thickness target was lowered to ensure part expansion and thickness consistency.

Cathode Flow Field Development: The cathode flow field is formed (a process step) after the coating step, which causes uncoated edges to be exposed to the cathode. This increases the risk of Cr contamination which results in performance degradation of the cell. Some testing of a plain fin cathode flow field was conducted and it was shown to be stable for more than 1,000 hours, with a slightly lower initial performance (about 20 mV lower than the baseline design) and a slight increase in performance degradation over thermal cycles. To fully evaluate this form, as it has exposed uncoated edges, longer-term testing was conducted. Testing of plain fin in a 16-cell (550 cm2 active area) stack is discussed in Section 2.2 of the report.

A new combined interconnect and cathode flow field was developed. Benefits of this design include a reduced part count, essentially combining three parts into one. Additionally, the flow field is a continuous form which facilitates the use of pre-coated steel. Only the cathode side of the steel needs to be coated. The design featured a dimpled cathode flow field. The feasibility of producing such a part was investigated through a prototype stamping vendor. Design considerations included selection of dimple spacing to optimize the flow distribution with low pressure drop while enhancing electrical conductivity. Input from manufacturers was utilized to guide the design of the dimpled part. Past forming work with the desired flow field material showed that the potential elongation available is quite limited making it difficult to produce a form tall enough to get low pressure drop and with dimple spacing close enough to get adequate electrical contact.

The dimpled cathode flow field design was further developed as shown in Figure 2-27. Coupon trials were conducted at a vendor location and a design review was conducted at VPS. Following the design review, a final design was released and a PO (purchase order) was issued to the vendor for a sample production run.

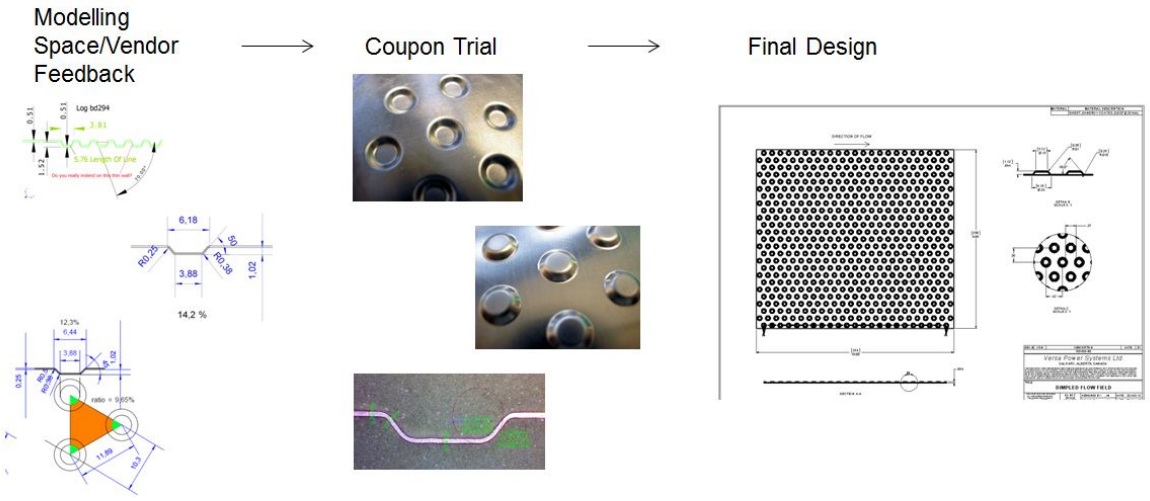

Figure 2-27 Dimpled Flow Field Development

The die for hydroforming the parts was completed. Parts fabricated from a small coil of 0.010" thick 441SS material were received. Finished parts are shown in Figure 2-28. Due to the geometry of the dimple pattern, two orientations of the part are possible for cell flow path: one with a slightly higher pressure drop and one with a slightly lower pressure drop. As the parts support the edge of the cell differently, both orientations were tested.

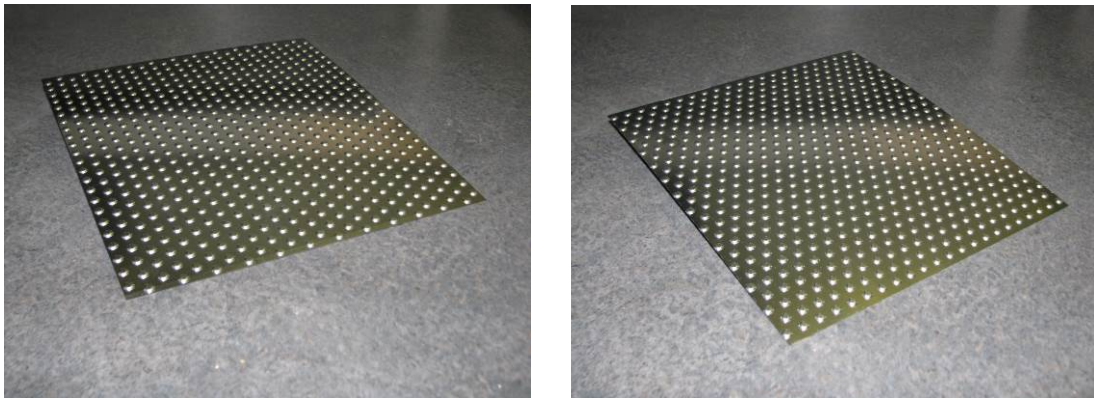

Figure 2-28 Dimpled Cathode Flow Field Finished Parts (Left: low pressure drop direction, Right: high pressure drop direction)

Joined Interconnects: One of the areas for improvement in the stack design is stack leakage reduction. By using a hermetic method of joining shims, the number or non-hermetic sealing layers can be reduced, leading to a reduced overall stack leakage. The effort was primarily focused on a brazed design to join shims. The joined interconnect was fabricated by an outside vendor. The parts received from the vendor had a large variation in quality. The method used for brazing the components involves tacking the components together with TIG welds and then hanging the parts in a brazing furnace. Parts come out of brazing with significant warpage and inconsistent joining of the metallic components.

To enable full qualification of the brazed part, a leak testing device was developed. The leak tester was able to measure fuel manifold leakage and air manifold leakage as well as leakage from the air side to the fuel side (cross leakage). The parts were tested with 1.0 psid (69 mbar) air pressure. From over 50 parts produced, a total of 6 components passed leak testing and had marginally acceptable flatness.

After going through quality control, parts were selected for a six-cell stack assembly. The finished stack can be seen in Figure 2-29 prior to testing. During performance testing, the stack (GT058768-0002) marginally passed 75% fuel utilization level test. Following the performance testing, the stack was tested at Phase I system conditions (61.5% fuel utilization, 25% in-stack reforming) for over 3000 h, showing performance degradation rate of 1%/1000 h.

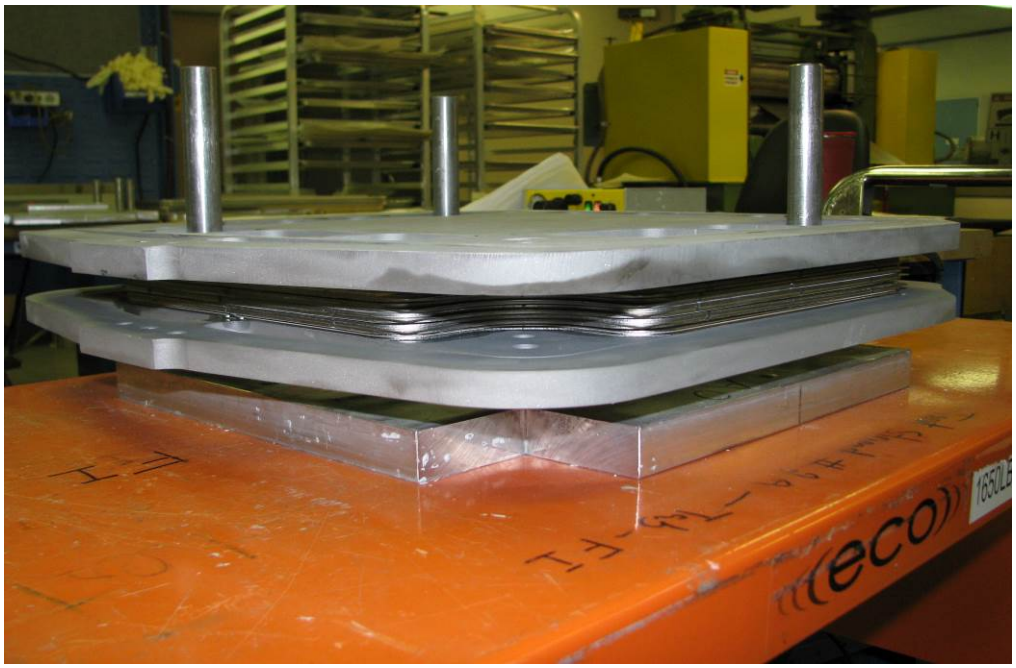

Figure 2-29 Six-Cell Stack Featuring Brazed (Joined) Interconnects

With the clear need for a new approach to brazing, a fixture was designed to better constrain the components during brazing. The jig stacks the components together using guide posts to align the parts. Metallic inserts are used (white plates) to take up the step height in the parts and about 150 pound (68 kg) weight is placed on top of the stacked components to hold them together. The jig was fabricated (Figure 2-30) and the assembly process was tested.

Figure 2-30 Braze Assembly Jig

The first batch of parts was received from the vendor. The parts were manufactured using the new assembly jig and had significant warpage. Figure 2-31 shows a part received from the vendor. In an attempt to make the parts usable, they were placed in a furnace at VPS for annealing. The parts annealed very well, indicating that the brazing process induced stress into the parts. Figure 2-32 shows an annealed part. Communication with the vendor revealed that the furnace was quenched at a very fast rate to reduce cool down time. This quenching could have caused the part warpage.

Figure 2-31 Brazed IC from Vendor

Figure 2-32 Brazed IC after Annealing

In an effort to resolve the part warpage and vendor interface issues, a site visit was made to the brazing vendor. During the brazing vendor visit, the main focus was on analyzing the braze furnace profile and modifying it to minimize stress placed on the IC assemblies. Two runs were conducted over a three day period with thermocouples placed in the braze jig to monitor the thermal stress on the part. Both runs of five parts produced ICs with extremely good flatness, confirming that the warpage was caused by the previous braze furnace temperature-time profile. A picture of a sample part from the final braze run can be seen in Figure 2-33.

Figure 2-33 Brazed IC after Modifying Braze Furnace Temperature-Time Profile

A larger batch (37 parts) of joined interconnects was produced. Overall the parts met flatness specification for the outer and thicker sections in the brazement. In addition to the brazed interconnect, 20 separator plate brazements were produced with enhanced x-y thermal conductivity. These parts were cleaned and inspected for implementation into a stack.

High Temperature Interconnect Development: Sanergy alloy interconnects with cobalt coatings were evaluated for long-term stability in a 28-cell (121 cm^2 cell active area) stack. Over 20,000 h of testing, the performance degradation rate was 0.38%/1000 h. A single cell test (81 cm^2 active area cell) containing Sanergy interconnects (cathode side coated with cobalt) accumulated 7,700 h, demonstrating an even lower performance degradation rate of <0.3%/1000h.

A 32-cell (550 cm^2 cell area) stack test was conducted to evaluate Sanergy HTC (coated) cathode flow field material. The stack was built with alternating layers of SS434LN2 and Sanergy HTC cathode flow field material and had TSC-3 cells. The stack performed well in the standard performance tests (passing 80% fuel utilization test with voltages exceeding 0.78 V). Testing was then conducted at steady state test conditions. Figure 2-34 shows the life-graph with average performance trends for the cell groups containing the two materials. The Sanergy coated material cell group had a degradation rate of 0.9% per 1,000 h compared to the standard alloy cell group degradation rate of 1.4% per 1,000 h, over 9,000 h of testing.

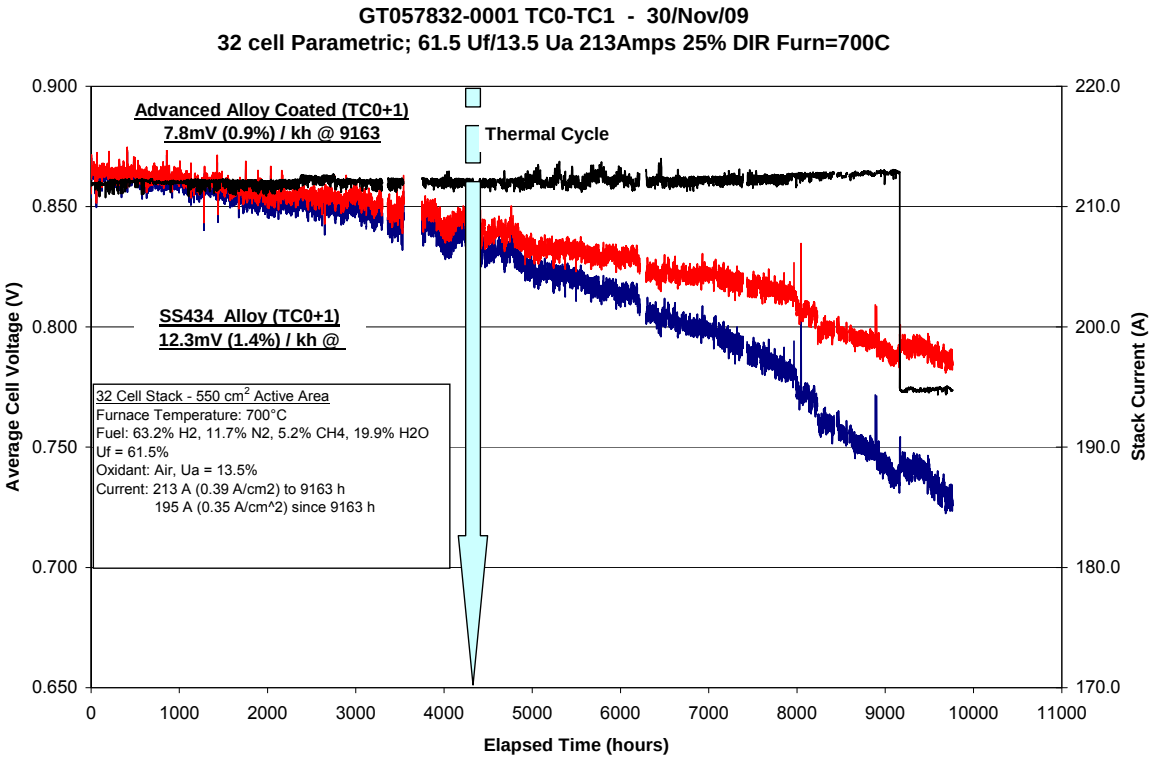

Figure 2-34 Performance Stability of 32-Cell Large-Area Stack Containing Sanergy and SS434 Cathode Flow Fields (TSC-3 Cells)

During Phase III, long-term test evaluations continued for commercially available alloys and new alloys developed specifically for SOFC applications that could be mass manufactured at low cost. In addition, pre-treatment of new and existing alloys as well as functional coatings were evaluated. The advantages of this development are two-fold. First, the upper limit of stack operation can be extended to allow a wider operating temperature window for the materials system. Second, degradation rates under existing operating conditions could be lowered. Several alloys were compared via coupon and stack testing to the baseline steel 434LN2. Table 2-2 is a list of steels in active development. Sanergy alloy, especially with coating, has become the new baseline for the cathode interconnect (IC) in VPS stacks. Other steels, alloys, or coatings were explored to decrease the cost and lead time of procurement. This included a new alloy (ZMG232G10) from Hitachi.

Table 2-2 Main Additive Elements in Steel Compositions

Steel	Cr	Mn	Si	Mo	Nb	Ti	Nb+Ti	W	Cu	La+Zr
434LN2	19	0.16	0.25	1.93	0.35	---	---	-	-	
T444	18.2	0.30	0.45	1.9	0.27	0.13	0.40	-	-	
T441HP	17.5-19.5	1.00 max	0.34	---	0.3+(9xC)min 0.9 max	0.10-0.50	---	-	-	
Sanergy	22	0.5	0.3	1.0	0.75	0.10	---	-	-	
ZMG232G10	24	0.28	0.09	---				2.03	0.95	0.29

A long-term single cell test 101729 was conducted to evaluate coated Sanergy cathode interconnect. As shown in Figure 2-35, the cell exhibited a low performance degradation rate, attributable to the interconnect, over 18,000 hours. The secondary Y-axis represents the anode-side voltage loss in volts. The test was terminated due to facility shut down.

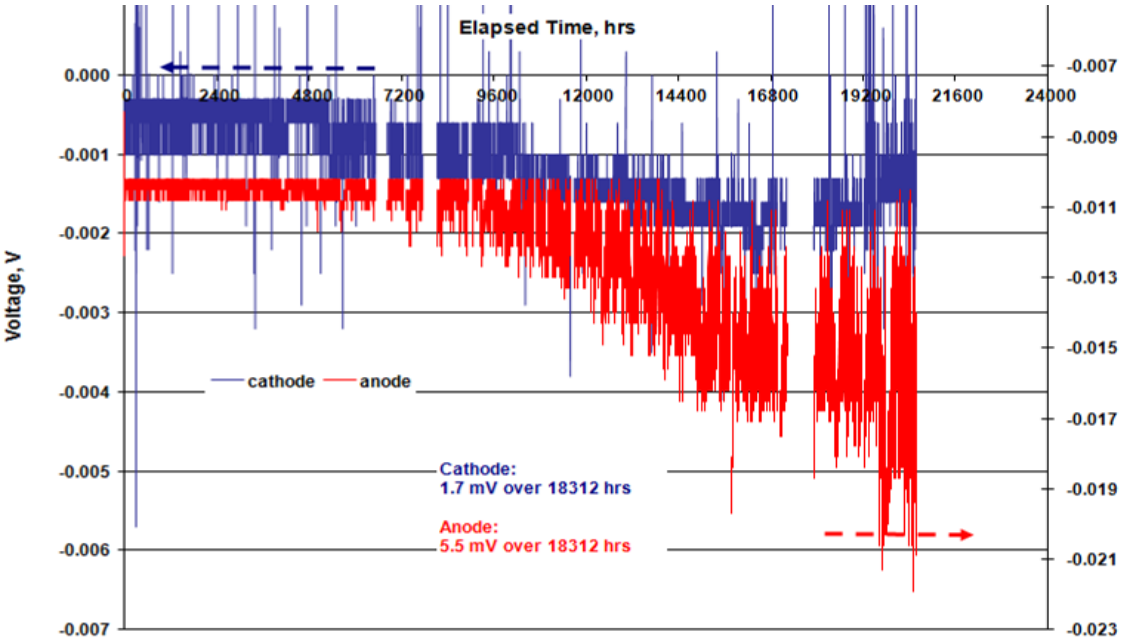

Figure 2-35 Interconnect Related Degradation during Long-Term Single Cell Test 101729

Several multi-metal (interconnect material) stacks were built and tested. Some alloys had coating applied to them. A long-term test of a 28-cell (121 cm^2 cell active area) stack containing Co-coated Sanergy interconnects was carried out. The performance life-graph of the stack is presented in Figure 2-36. The test was terminated after completion of 20,000 h of endurance testing and post-test examination was conducted.

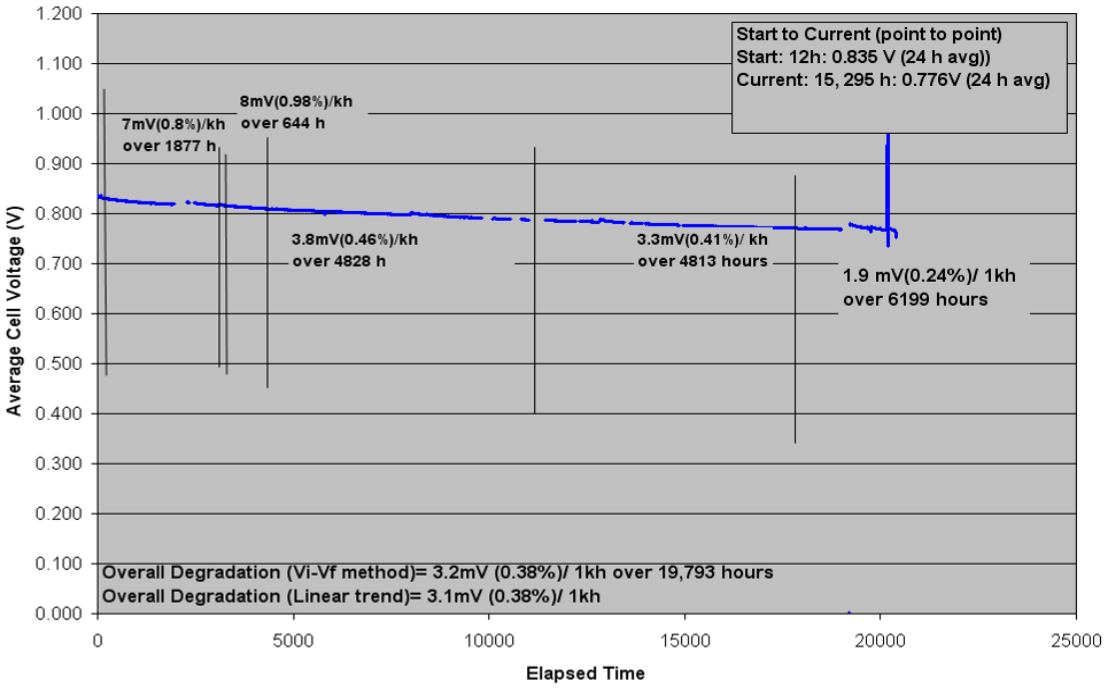

Figure 2-36 Long-term Performance of Stack GT056019-0132 Featuring Co-Coated Sanergy Interconnects

SEM (scanning electron microscopy) analyses of five layers of the stack were performed. Oxide thickness on anode and cathode sides was analyzed. The oxide thickness at anode contact was only 4.5 microns (after 20,000 hours of testing). On the cathode side, the oxide formed on the flow field was a bi-layer as shown in Figure 2-37. The outer layer was CoCrMn oxide with the presence of Fe as well. The inner layer was mostly chrome oxide. At the steel-oxide interface, there was concentration of Si and Ti oxide. The overall thickness was about 5 microns.

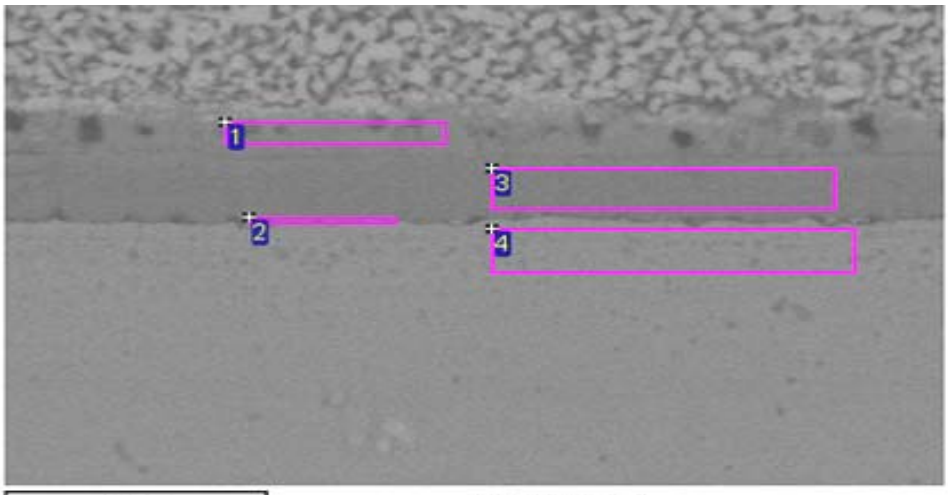

All results in atomic%

Spectrum		O	Si	Ti	Cr	Mn	Fe	Co	Ni	La
1	Yes	55.85		0.03	8.46	6.31	3.69	18.21	6.43	1.01
2	Yes	50.78	3.63	0.51	30.76		14.32			
3	Yes	59.80		0.20	38.08		0.75	1.17		
4	Yes	14.40		1.39	19.01		65.20			

Figure 2-37 Oxide at Cathode Contact

Although the oxide was very thin under the electrical contact area, it was thick at other locations at the cathode. Most of the oxide at non-contact locations was over 20 microns. After 20,000 hours of testing, there was no chrome deposition at contact. The chrome deposition was observed only in flow channel areas as shown in Figure 2-38. This demonstrates the effectiveness of the coated parts. Chrome found in channels could have come from other non-coated steel parts in the stack. The results indicated that coating of the parts helped in achieving a long testing time with a very low degradation rate.

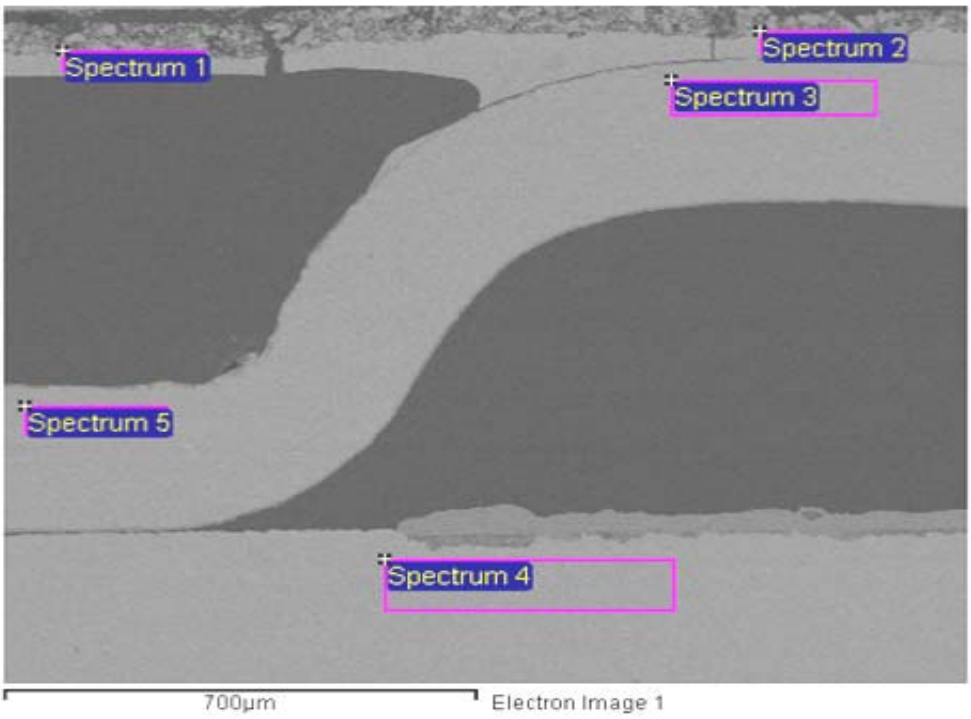

All results in atomic%

Spectrum	In stats.	O	Cr	Fe	Co	Ni	La
Spectrum 1	Yes	59.17	2.11		12.43	7.13	19.17
Spectrum 2	Yes	60.21			11.43	8.19	20.17
Spectrum 3	Yes		23.34	76.66			
Spectrum 4	Yes		20.84	79.16			
Spectrum 5	Yes		22.63	77.37			
Max.		60.21	23.34	79.16	12.43	8.19	20.17
Min.		59.17	2.11	76.66	11.43	7.13	19.17

Figure 2-38 Chrome Deposition Analysis

Three different coated steel samples were tested in a tube furnace with air at 750°C. The test objective was to evaluate the change in composition and structure of the coating with time. The samples tested were:

- Cobalt coated Sanergy with a thickness of 0.150 mm, provided by Sandvik
- MCO (manganese cobalt oxide) coated Crofer with a thickness of 0.264 mm, provided by Nextech
- MCO coated SS441 with a thickness of 0.540 mm, provided by PNNL (Pacific Northwest National Laboratory).

A number of coupons of each sample were placed in a tube furnace. They were taken out at various time intervals. The coupons were analyzed by SEM (scanning electron microscope) to determine the oxidation and microstructure of the oxide. Figure 2-39 shows the SEM images of the cross-sections of coupons as-received and after 1,000 h of testing.

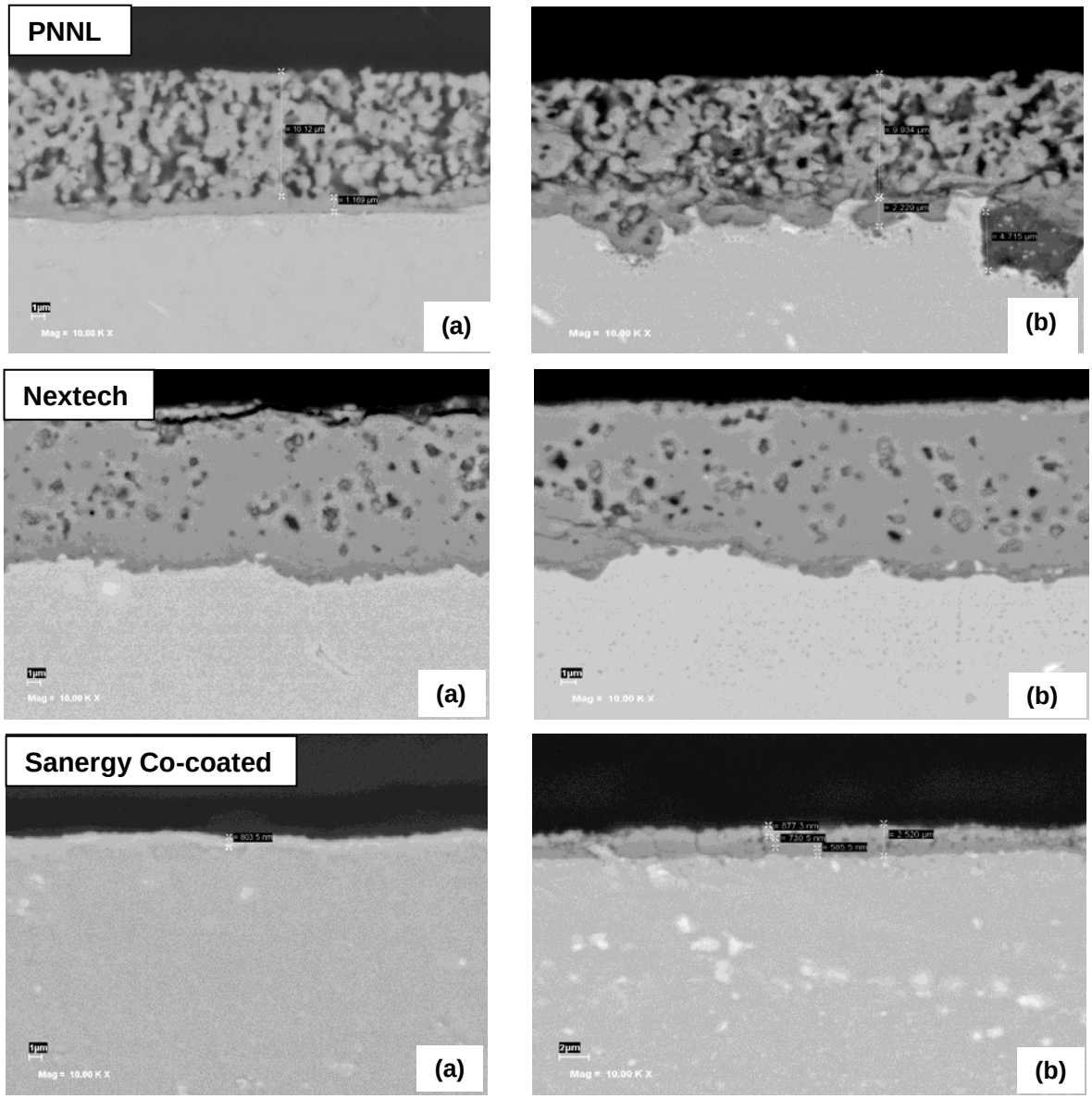

Figure 2-39 Cross Sections of Coated Coupons: (a) as Received and (b) After Testing in Air at 750°C for 1000 Hours

The study revealed the following:

- The MCO coatings were around 10 micron thick with a very stable composition $Mn_{1.5}Co_{1.5}O_4$. The Nextech coating was much denser than PNNL.
- Chromium presence in the MCO coating was minimal but was increasing with time. The chromia layer thickness was growing for the PNNL coupon. It was also the thickest coupon and made of 441 steel.
- Thickness of the Cobalt coating on Sanergy remained the same, at 3 microns, even after 2000 hours of testing.

- The coating composition was changing and evolving towards $(CoMnFe)_3O_4$ obtained after over 1250 hours at 750°C. In a fuel cell stack, the composition $(CoMnFe)_3O_4$ is obtained earlier. Several factors can influence that: Temperature, flowing air, humidity, current, etc.

Nextech and PNNL coatings were applied on a single repeat unit cathode jig for testing. The Nextech coated jig was tested in single cell for more than 10,800 hours. As shown in Figure 2-40, the cell showed a low degradation rate of 0.45% per 1000 hours at 0.5 A/cm^2. The test did not have any major incidents. The jigs were made of ZMG232G10 alloy material and were coated with MCO at Nextech. A gold mesh was included in the cathode contact to measure the contact-cathode interconnect voltage loss. No measurable contact to cathode interconnect loss was observed during the test.

The test was terminated for post-test examination. Both jigs and the cell were prepared for a thorough post-test analysis using SEM (scanning electron microscope).

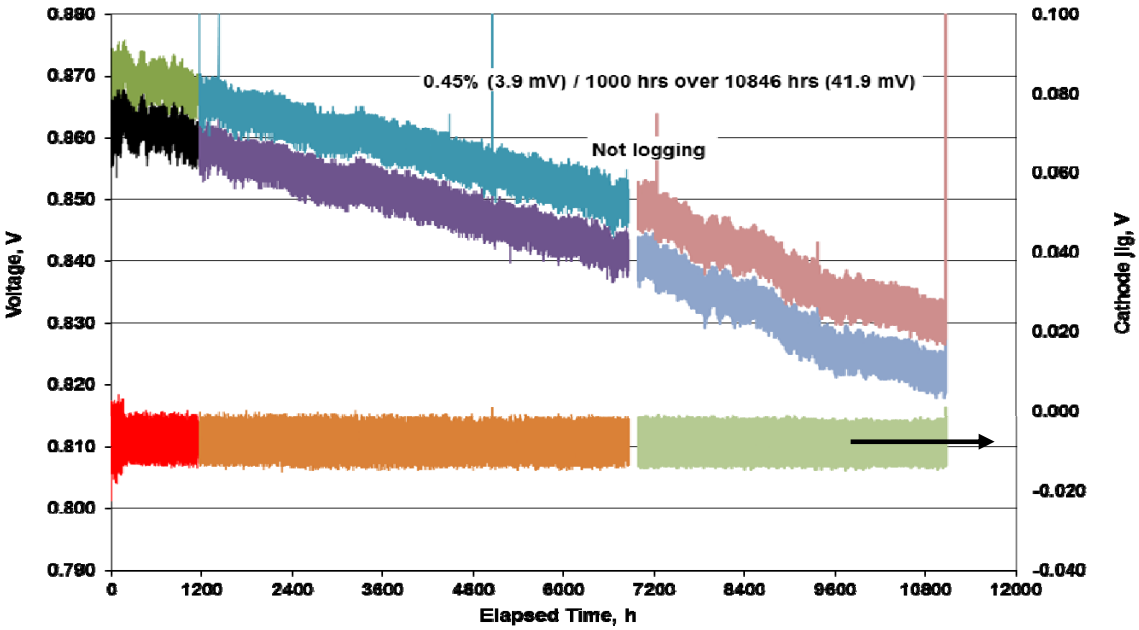

Figure 2-40 Performance Stability of Cell Containing a Nextech Coated Jig (Test Glob 101853)

SEM image of the cell cross-section revealed a nice microstructure with no damage or decay over 10,000 hours of testing. The coating provided good protection as there was no chrome found on the cell.

The PNNL MCO coated jig was tested in single cell for over 10,000 hours. After 1000 hours in dry air, 10% humidity was introduced. The degradation rate in dry air was less than 0.2% per 1000 hours. As shown in Figure 2-41, the degradation rate with 10% cathode gas humidity was 0.48% per 1000 hours over 9,669 hours.

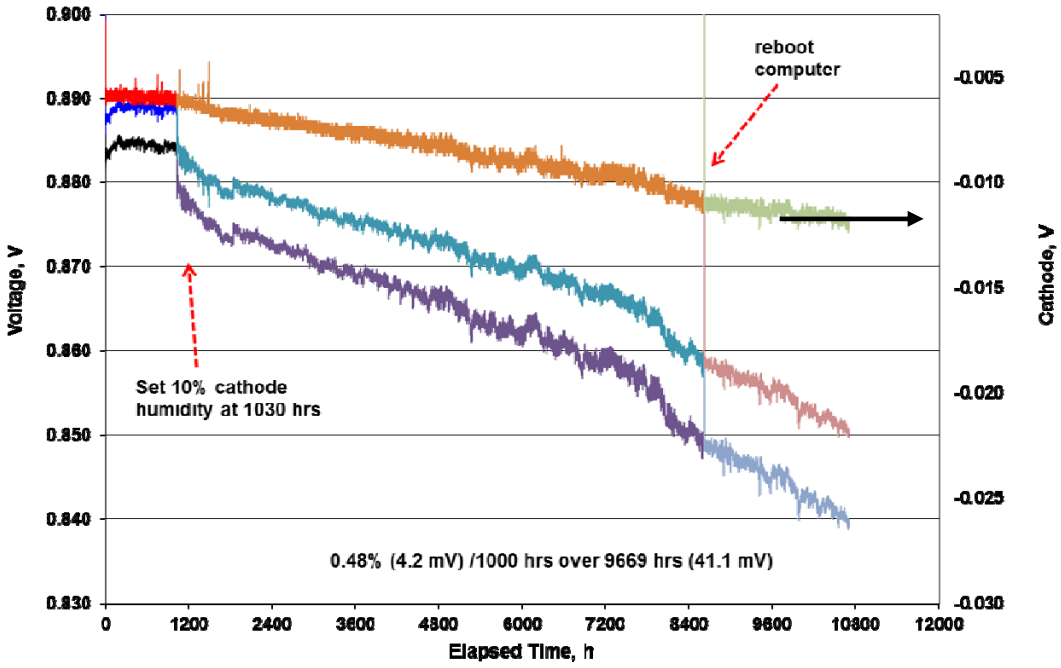

Figure 2-41 Performance Stability of Cell (Test GT101863) Containing PNNL Coated Jig

Another single cell test was conducted with a cobalt coated ZMG232G10 (Hitachi Metals) alloy cathode jig. As shown in Figure 2-42, the degradation rate with 10% cathode gas humidity was 1.23% per 1000 hours over 4,840 hours.

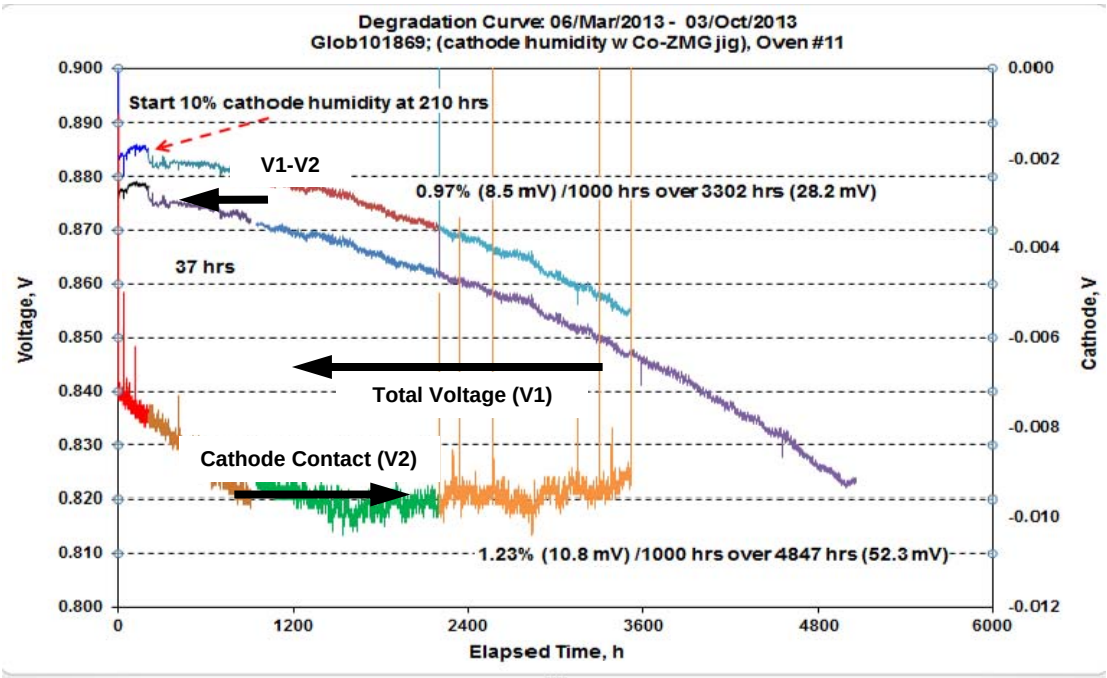

Figure 2-42 Performance Stability of Cell Containing Co Coated ZMG232G10 Alloy Cathode Hardware (Jig)

This is significantly higher than the decay rate of cell with PNNL MCO-coated cathode jig. The test was terminated and the post-test examination was conducted. Both jigs and the cell were then prepared for a thorough post-test analysis using SEM. Figure 2-43 shows the SEM image of the cathode jig. A bi-layer oxide was observed on the jig, with top CoMn oxide in-situ formed from Co coating and Chromia underlayer. The total oxide thickness was about 4.5 microns with an even split between two oxides.

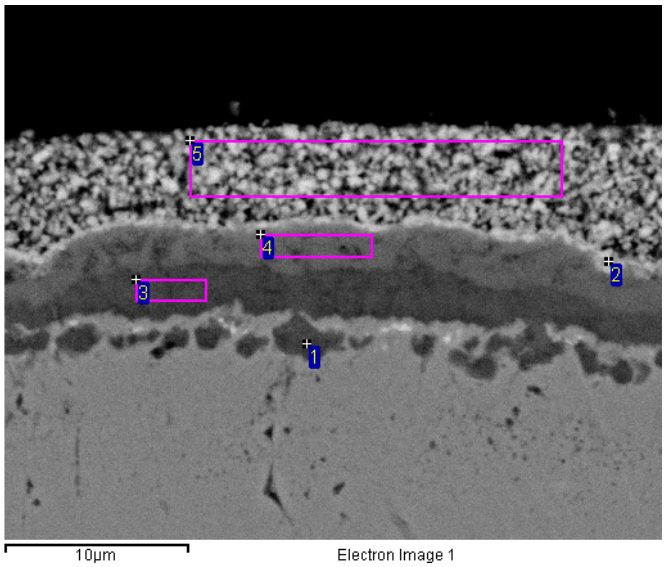

Figure 2-43 SEM of Cathode Jig Showing Oxide Presence (Test Glob 101869)

The cell cross-section samples were prepared. Close examination of the samples showed that there was an obvious difference between the cell sections corresponding to cathode jig rib (contact) area versus those corresponding to channel (non-contact) area. Sections from channel area had chrome present in the cathode and cathode contact layers whereas the sections from rib area were clean, as shown in Figure 2-44. It seems that the MCO coating in-situ formed from the thin Co coating might not provide as good a chrome vapor barrier as an MCO coating.

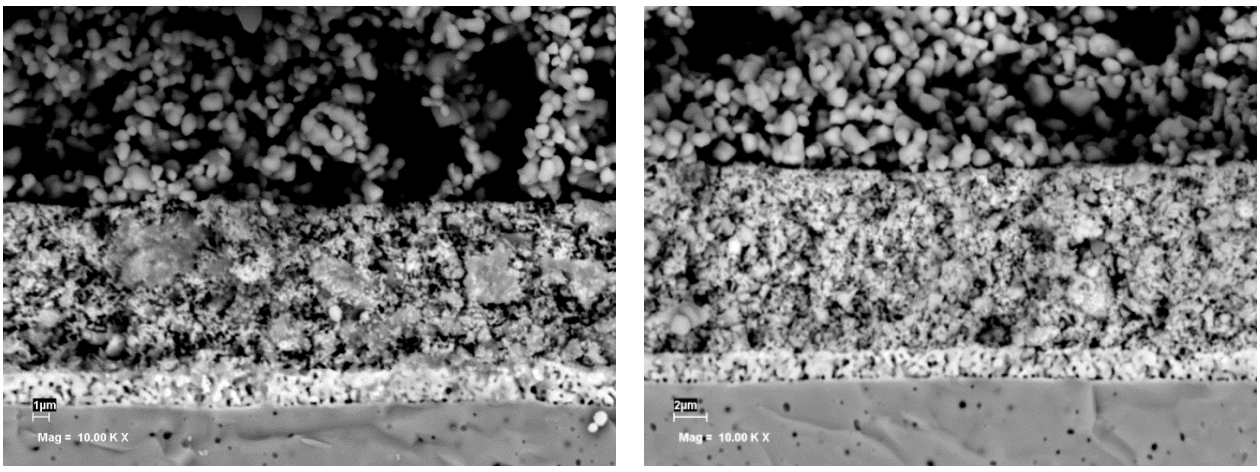

Channel **Rib**

Figure 2-44 SEM of Cell Cross Sections Corresponding to Cathode Jig Channel and Rib Areas (Test Glob 101869)

In addition to the single cell tests, stacks were built and tested with different coatings. Stack GT056019-0155 had layers of 441 steel interconnects featuring Co-Ce coating developed by Sandvik. These layers were placed in alternate cells, with the baseline Co-coated Sanergy layers used in the remaining cells of the stack. The stack did not perform very well but it showed no significant difference in performance degradation rate for the two cell groups (coatings) after 1,600 hours of testing. The test was terminated after over 2,000 h of testing. The post-test examination of the stack revealed that the root cause of the degradation was above-average leakage. Six layers were analyzed further by SEM. There was no evidence of Cr contamination in the cells. Both interconnects formed a bi-layer oxide; chromia and CoCrMn oxide. Ceria particles were observed between the two layers in the 441 steel. Overall the oxide and coating was thicker on the coated 441 interconnects as compared to coated Sanergy interconnects. No chrome was found in the cells with the exception of areas above the flow channels. This indicates that the Chrome source was not in the coated surfaces but rather the flow-plate or the manifolds.

The second 28-cell stack GT056019-0156 had half the layers containing Sanergy alloy coated with MCO by Nextech and the remaining layers with the baseline Co-coated Sanergy. The stack had high degradation and leakage similar to Stack GT056019-0155. There was no difference in performance degradation rates between the two cell groups (coatings) over 1600 hours of testing as shown in Figure 2-45.

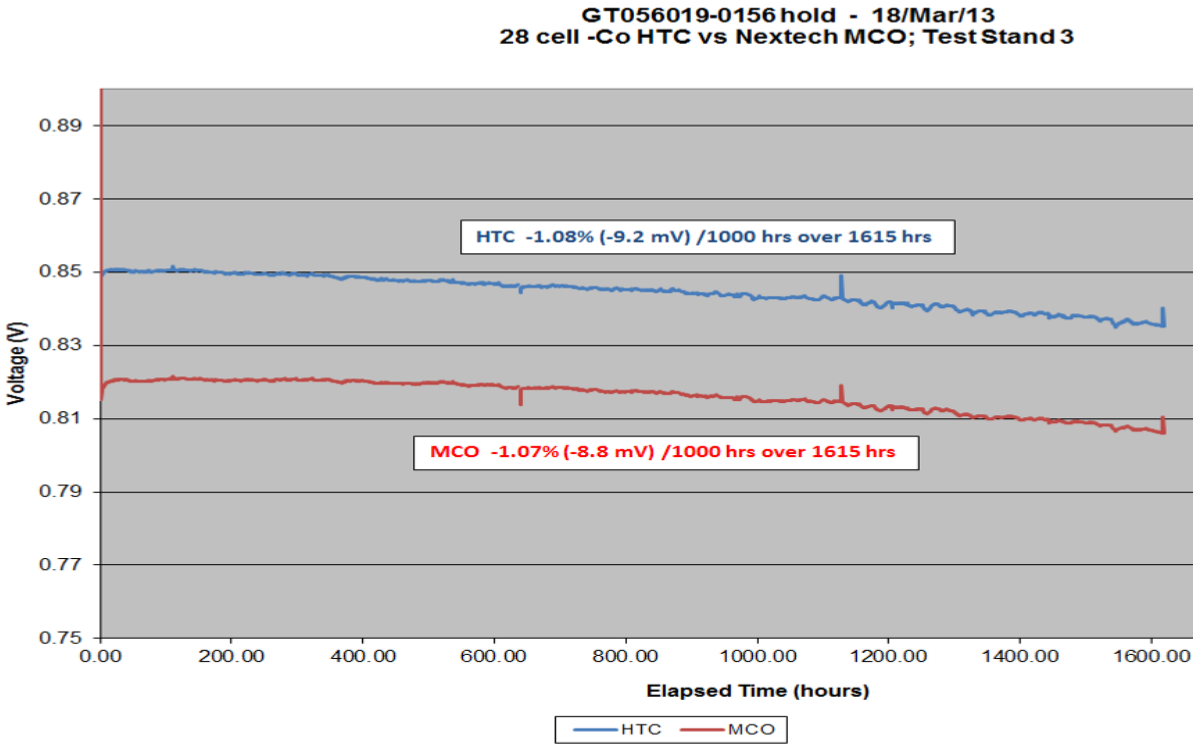

Figure 2-45 Evaluation of MCO Coated (by Nextech) Interconnects in Stack GT056019-0156

Coating Development for Non-Repeat Components: As discussed above, a coating has been applied to the interconnect contact surface in an effort to limit the presence of Cr vapor in the air stream. To further improve the life and decrease the degradation, a parallel effort was carried out by coating the hot balance of plant tubing and piping for protection. Inconel 600 tubing was pre-coated with Al metal then pre-heated to 1000°C to form an alumina

protective layer. The coated tubing was welded to a Co coated cathode single cell jig (GLOB101851). The jig was used in the cell test.

As shown in Figure 2-46, the cell test accumulated over 3000 hours at 10% humidity level in cathode air. The overall degradation rate at 10% cathode gas humidity level was about 1.27% per 1000 hours. The coated tubing showed a significant improvement in degradation compared to the test with non-coated tubing.

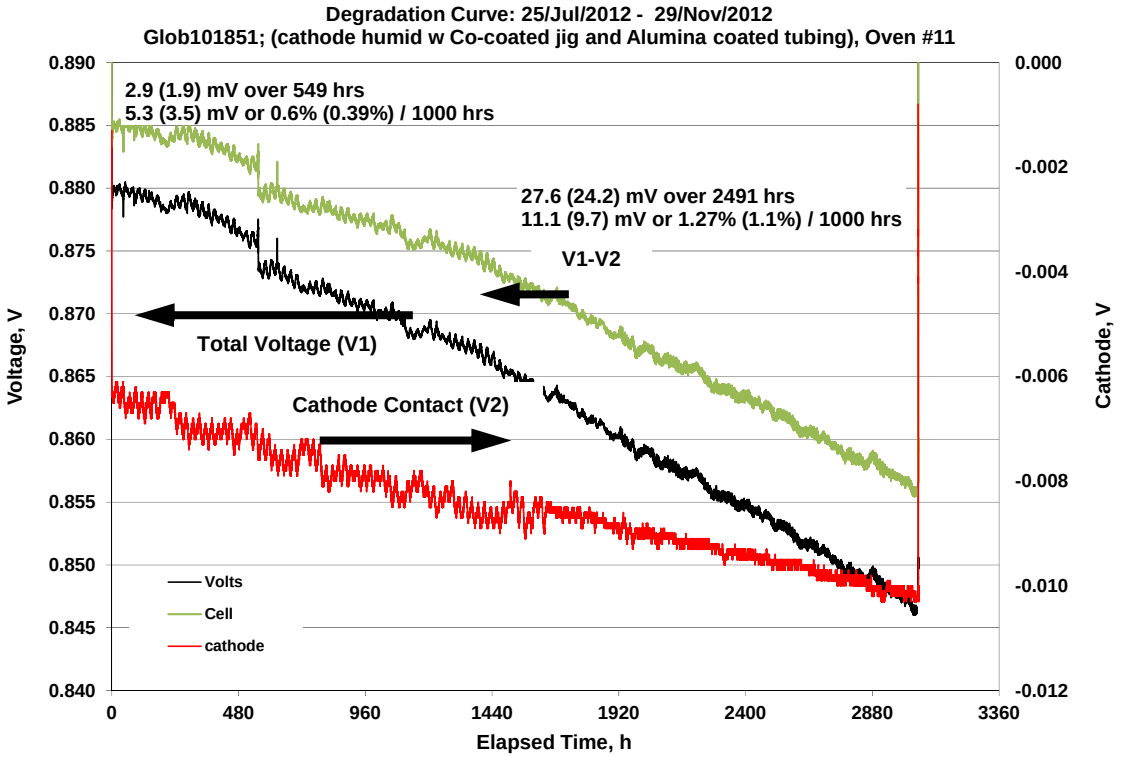

Figure 2-46 Steady-State Test Glob101851 of Coated Jig and Tubing with 10% Cathode Gas Humidity (2491 h with humid gas)

The test was terminated and post-test examination was conducted. The coated tube, cell and cathode jig were cut and analyzed by SEM as shown in Figure 2-47, Figure 2-48 and Figure 2-49, respectively. The pre-coating helped in reducing Cr contamination in the cell by forming a continuous dense alumina layer on the internal surface of the tubing. Some chrome was still found on the cell. Further improvement is needed, including optimization of the coating and oxidation process for the alumina layer.

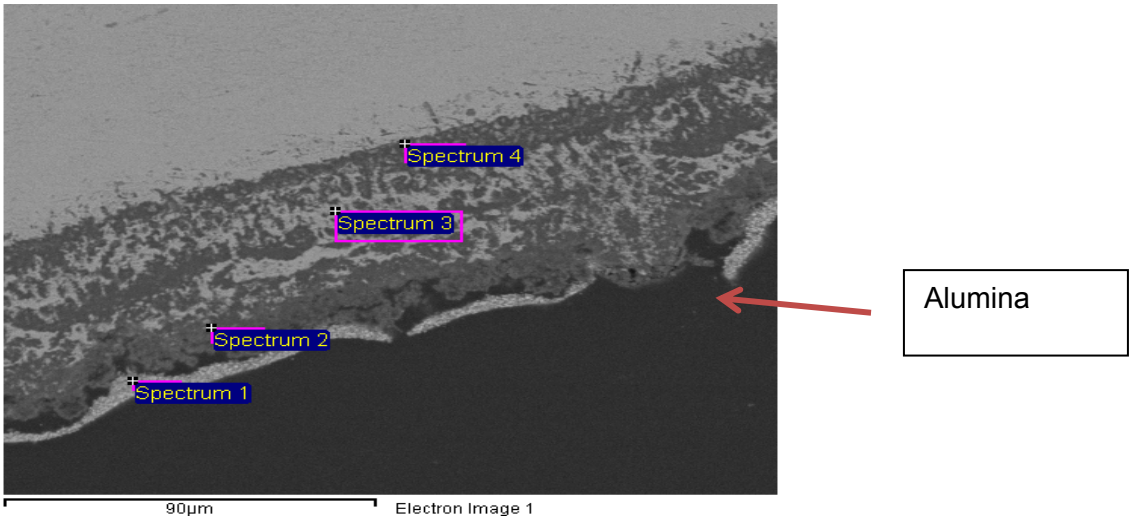

Figure 2-47 Cross Section of the Tested Coated Tubing

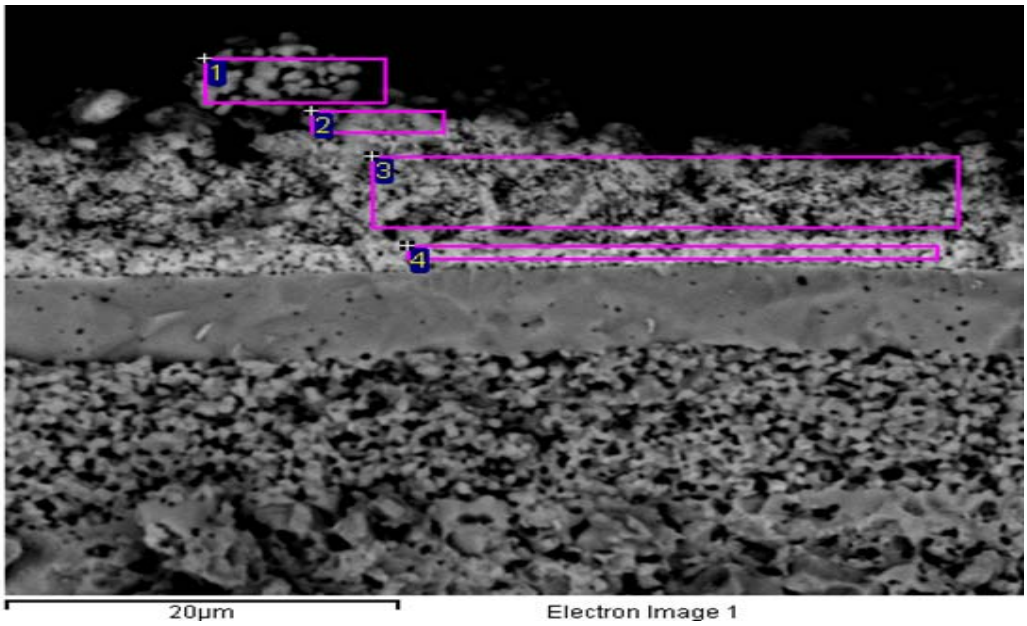

Figure 2-48 Cross Section of the Tested Cell

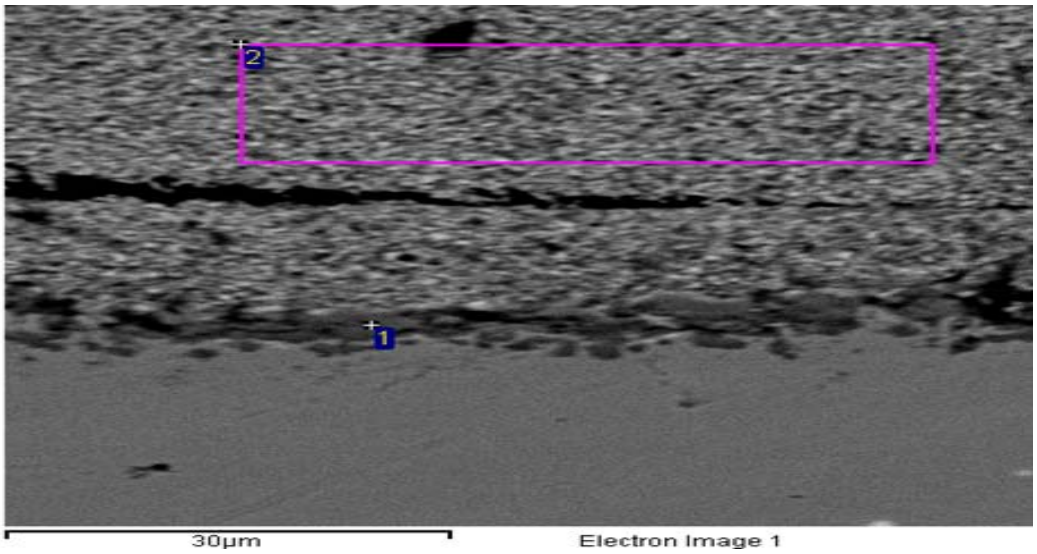

Figure 2-49 Cross Section of the Tested Co-Coated Cathode Jig

Glass-Ceramic Seal Development: A commercial glass-ceramic seal of interest is NYG-353. This glass-ceramic material has physical properties very similar to VPS's in-house glass-ceramic material, but shows improved adhesion to ferritic stainless steel. Since the material was already fully characterized by NYG and the property data provided, it was decided to proceed directly to the in-cell testing stage. Small packages of cell + NYG-353 + ferritic stainless steel (representing the interconnect) and ferritic stainless steel + NYG-353 + ferritic stainless steel showed no measurable leak (less than the 0.05 ml/min detection limit) up to 3 psid (20.68 kPa) with He. One concern with this material is the high boron content (22%) reported in the literature [3]. The cited work, conducted within the SECA program, highlights potential concerns with boron-containing species that are most significant in fuel environments containing moisture (i.e., the anode side gas environment is more of a concern than the cathode side gas environment). In order to check the effects and confirm gas tightness in a larger configuration (10 cm by 10 cm cell test incorporating all of the materials and contact layers in a stack repeat unit), two single-cell tests were run. The first, Cell Glob101878, was heat treated, conditioned, and tested for 165 hours at standard single-cell steady-state test conditions (750°C, 0.5 A/cm^2, 50% Uf, fuel gas containing 48.5% hydrogen, 48.5% nitrogen, and 3% humidity, 25% Uo, and air as oxidant). It was then removed and leak tested to confirm that there was no measurable leakage (with the exception of the leakage from the edge of the anode substrate). The test article was then placed into a test stand suitable for long-term testing and run at the same steady-state hold conditions for 340 hours. It was noticed that the degradation rate was somewhat higher. The bubbler humidifier temperature had risen significantly over time increasing the humidity of the fuel inlet gas (which lowers the Nernst potential and hence cell voltage). The cell was then switched to dry fuel (50% hydrogen and 50% nitrogen) and continues to operate at this condition with a degradation rate of 0.6% per 1,000 hours.

A duplicate test was conducted without removing the test article from the test station for leak testing. This test article, Glob101881, was installed and operated at the same steady-state hold conditions as Glob101878, including 3% humidity in the fuel stream. Figure 2-50 shows the cell voltage vs time trend at 750°C, 0.5 A/cm^2, 50% Uf (hydrogen + 3% water), and 25% Uo (air). The degradation rate was 0.28% per 1,000 hours over almost 4,000 hours operation, indicating that the material is not causing an increase in degradation rate. This material could be used to seal the edge of the cell anode substrate and as a more stable alternative to the commercially-available coating used in Thermicullite 866LS. By applying this material to standard

Thermicullite 866 it may be possible to tailor compressibility and have a stable hybrid seal for the stack.

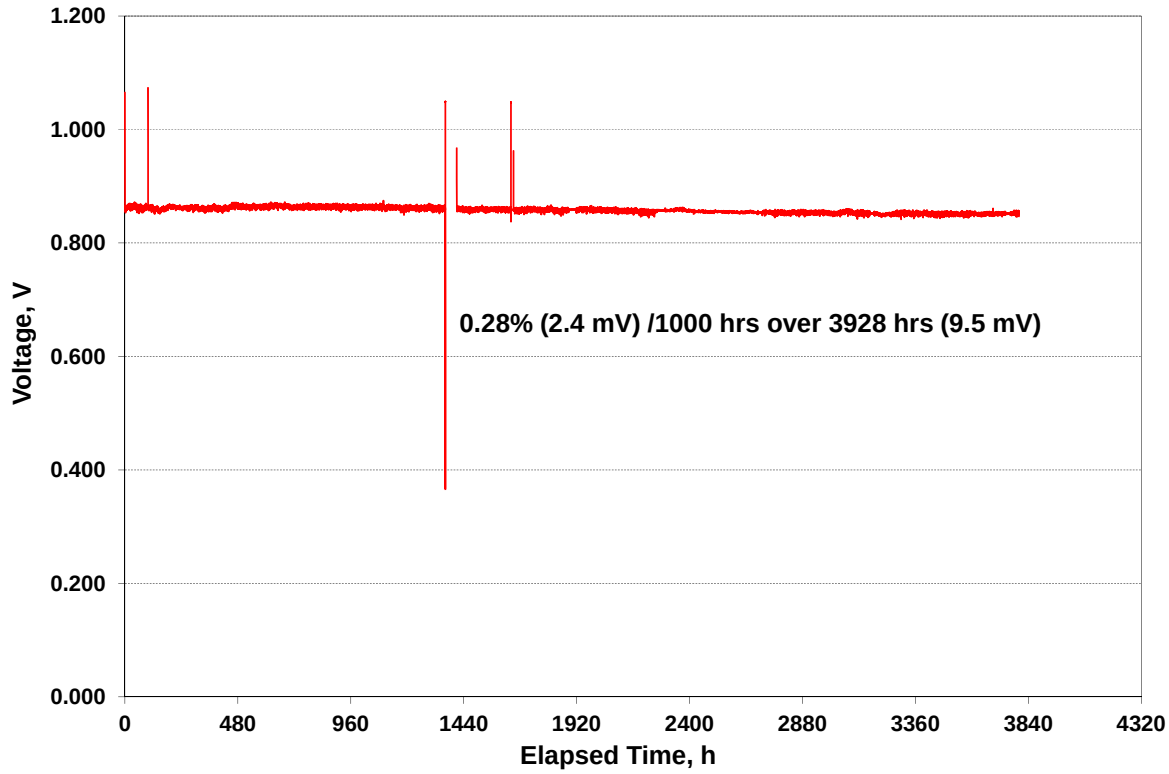

Figure 2-50 Long-Term Single-Cell Test (Glob101881) With Glass-Ceramic Seals

End Plate Current Collection: For the 60 kW quad module design, the stacks were designed to conduct current through the end plates of the stack to the manifold plates of the module. A number of methods were considered to accomplish this, including a conductive seal designed at FCE.

An alternate design developed used various forms of nickel contact to conduct current from the stack end plate, and an alumina seal for gas sealing. To prevent the nickel from oxidizing, cuts in the seal were made (leaving it slightly open to the stack fuel manifolds) as shown in Figure 2-51. The latest design incorporated two layers of nickel mesh, one spot welded to the manifold plate and the other spot welded to the stack endplate.

Figure 2-51 Nickel Mesh Endplate for Current Collection

Testing of this configuration showed very good results. The voltage drop at 200 A, which stayed constant over 1,000 hours of testing, was just 40 mV.

2.3 In-Cell Manifolded (ICM) Stack Development

ICM (In-Cell Manifolded) Stack Design: Current PCI (Pre-Commercial Integrated) stack design has been instrumental in utilizing large area cells in SOFC stack operation. A number of design attributes, however, can be improved. The design considerations for development of a new large area stack design include: simplified (electrical) contact and (gas) seal balancing (low gas leakage), high material utilization (cell active area), compatibility with existing test infrastructure (set-up/configuration), stack-ability for systems (tower of stack blocks), simplified manufacturability and cost reductions.

Following a number of design iterations, a concept stack (ICM) was developed which combines the benefits of internal and external manifolds. Figure 2-52 shows a schematic of the design for a 20-cell ICM stack. The fuel manifold remained internal; however, the design incorporates the fuel manifold within the cell. Both contact and seal balancing are significantly simplified when utilizing an internal (in-cell) manifold. On the air side, an external manifold is used for part simplification and high material utilization. The main drawback of an external manifold is potential for gas leakage. However, in the ICM design, the manifold only seals cathode in and out streams (not between fuel and air), making leakage less of a concern.

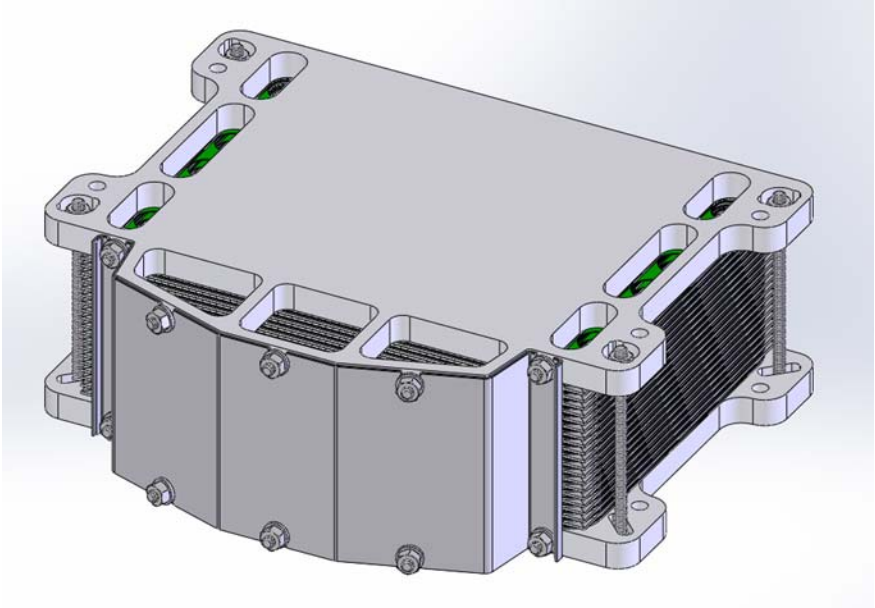

Figure 2-52 20-Cell In-Cell Manifolded (ICM) Stack Rendering

The cell size for development was set at 440 cm^2 active area. This cell size was driven by the size constraints of the continuous tunnel kiln (Harrop Kiln) at VPS's facility. With some fairly simple modifications of the entrance and exit of the Harrop Kiln and the purchase of new kiln furniture, significantly larger cells could be produced.

Detailed design and part procurement were conducted, culminating in an eight-cell mock stack. Figure 2-53 shows the stack in assembly. The mock stack used all real components except for the cells (active components) which were metallic.

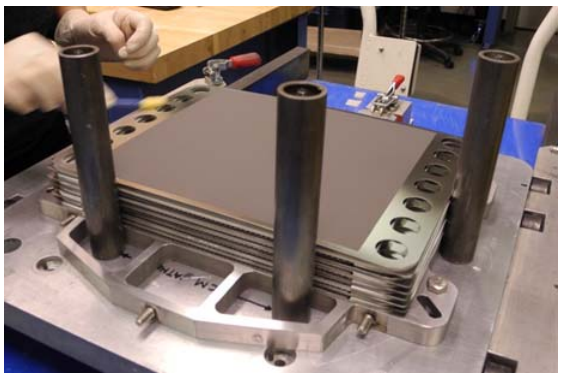

Figure 2-53 8-cell In-Cell Manifolded (ICM) Mock Stack in Assembly

Subsequently, two operational ICM stacks were built and tested. These included an 8-cell stack and a 19-cell stack, discussed later in this section.

Modeling work was performed to evaluate suitability of the ICM stack design for scale up to larger stack blocks. An 80-cell stack was modeled using computational fluid dynamics analysis. The focus was on calibrating the model for different flow field design options which were compatible with this stack design as well as on reviewing the sensitivity of flow distribution (different anode flow field pressure drops with the different options). The ICM stack design results in slightly higher in-manifold pressure drop compared to VPS's PCI stack platform, which makes fuel flow distribution a greater challenge. The stack running on a fuel stream with the gas composition of 16.4% CH_4, 28.5% H_2, 47.2% H_2O, and 7.9% N_2 was comprehensively

investigated for fuel flow uniformity. The stack design criterion for anode flow distribution was selected as ±0.2% mass flow rate deviation for each anode cell in an 80-cell stack.

As a first step, the anode flow field was modeled and calibrated using results from a 19-cell ICM stack test. The simplified porous media model of anode flow field was based on the Ergun equation:

$$dP = C_1 \mu v + \frac{1}{2} C_2 \rho v^2$$

where C_1 is the viscous parameter (1/m^2), and C_2 is the inertial parameter (1/m).

Modeling progressed through cold flow (i.e., room temperature, isothermal) simulations, then hot isothermal flow simulations, and eventually into the computationally intensive fully-coupled flow simulation. Figure 2-54 illustrates baseline anode and cathode flow distributions, showing mass flow rate (MFR) deviations for 80 cells. The anode flow rate varied from -0.5% to 1.8%, which was substantially greater than the design criterion value of ±0.2%.

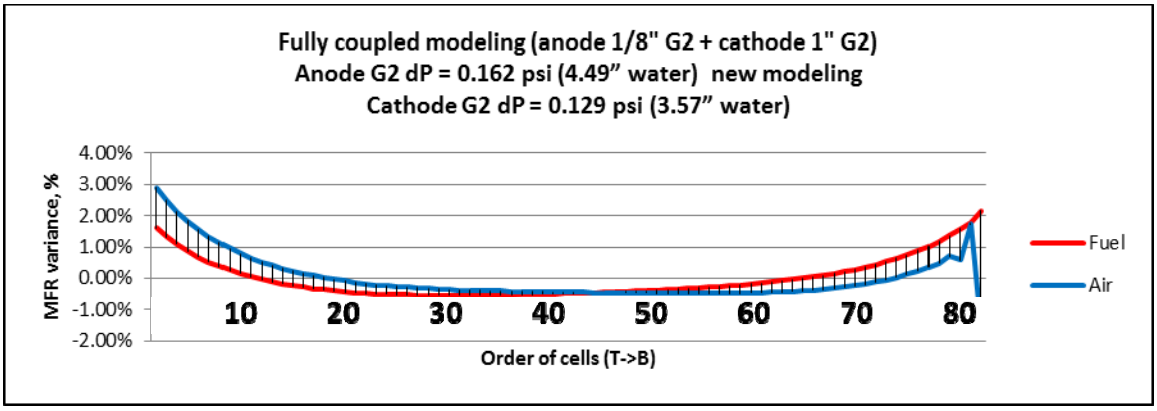

Figure 2-54 Baseline Flow Distribution in 80-cell ICM stack

As an extreme d*P* case, an anode flow field pressure drop of 0.5 psi (3.45 kPa) was considered. By comparing the stack cell pressure drop distribution, temperature distribution and anode flow rate distribution as shown in Figure 2-55, it was concluded that the stack anode flow distribution is dominated by stack thermal profile. With the anode flow at a dP of 0.5 psid (3.45 kPa) , on-cell dP variation was very small but the on-cell dT varied widely (from 80 to 123°C). The large thermal variation led to a variation in mass flow approaching 2%.

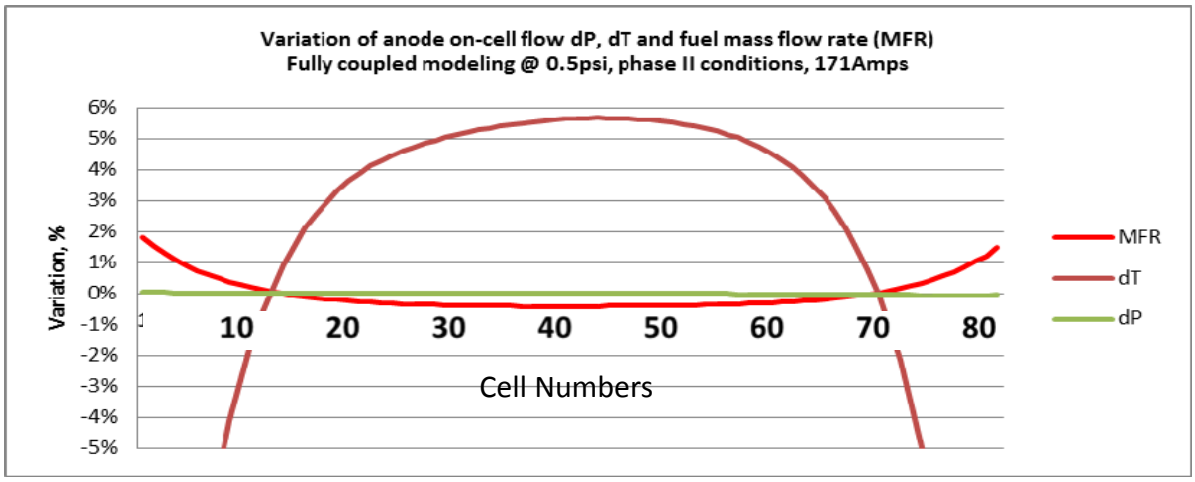

Figure 2-55 Pressure Drop, Temperature and Fuel Flow Variations in 80-Cell ICM Stack

One of the potential design solutions was to improve stack thermal profile by reducing heat loss from both ends of a stack. By setting an adiabatic condition on the stack ends (top and bottom layers), the on-cell d*T* variance decreased to less than ±5% and an anode flow variation less than ±0.2% was achievable. Besides using better insulation materials for the stack end plates, the sensitivity of flow distribution to stack end thermal loads (electrical end heaters) was also analyzed. The results are presented in Figure 2-56.

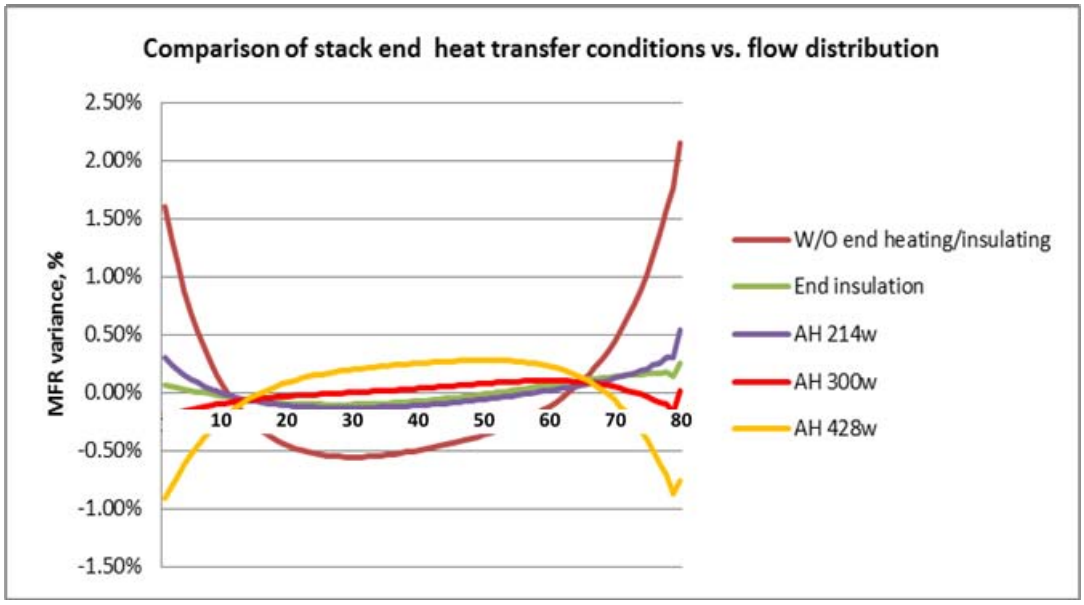

Figure 2-56 Sensitivity of Anode Side Flow Distribution to Stack End Heating Loads

Another possibility to improve stack flow distribution was to reduce the anode flow field cross-sectional area for upper (top) and lower (bottom) anode channels so as to increase the hydraulic resistance and decrease flow rates in these areas. In the model, an equivalent anode media flow resistance change was applied to simulate an anode contact media thickness change. Sensitivity results illustrated that a 4% viscous resistance change resulted in the range of flow rate variance but not in the change of flow variation pattern. To reduce the flow rate variance to within ±0.2%, non-uniform anode contact media thickness (or flow resistance) was

required. However, there are some issues in manufacturing process to achieve the high precision and fine tuning of anode contact media thickness.

In addition to grading pressure drop due to flow field height (or z-direction), it is possible to fine tune anode contact media length in flow direction for each unit cell. This approach may have several advantages:

- Easier to tune flow length vs. precision height dimension
- Limited change of other stack components in z-direction to avoid affecting seal layer thickness

To achieve a ±0.2% flow rate variation, the anode contact media length distribution can be expressed also as a polynomial function. Based on quick analysis, the maximum length difference between the longest and the shortest anode flow field was estimated to be 4 mm as shown in Figure 2-57.

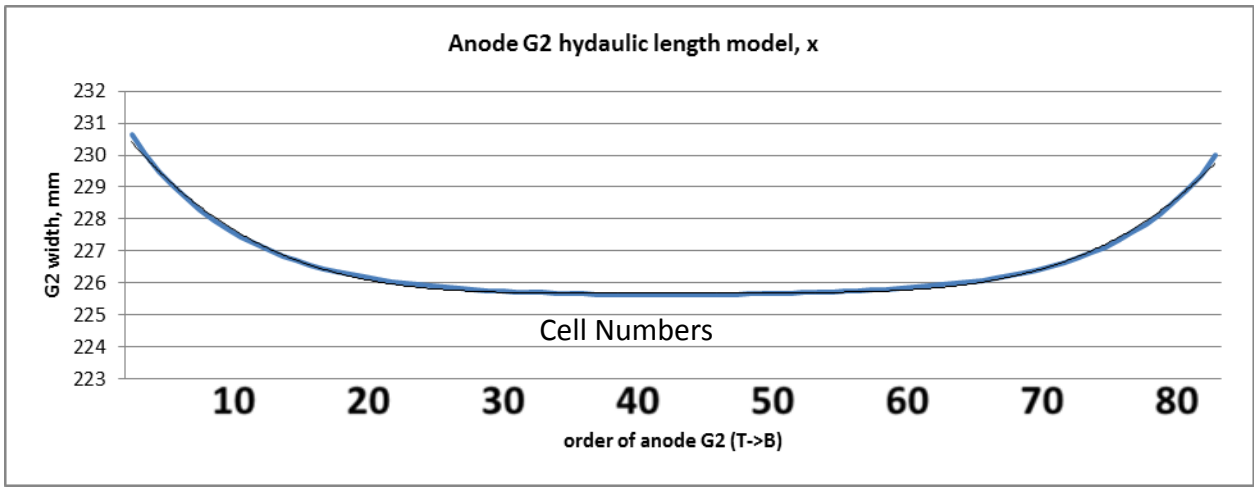

Figure 2-57 Graded Anode Flow Field Contact Media in Hydraulic Flow Direction

Figure 2-58 shows the on-cell temperature profile generated using a fully-coupled SOFC model (reforming, electrochemistry) for central and end cells of an 80-cell ICM stack. Modeling conditions were based on operation at Phase II conditions: 68% fuel utilization, 70% in-stack reforming, and 15% air utilization at 171 A or 388 mA/cm^2. Boundary conditions included top and bottom surfaces at 700°C with emissivity of 0.5 and surrounding walls at 660°C with emissivity of 0.6.

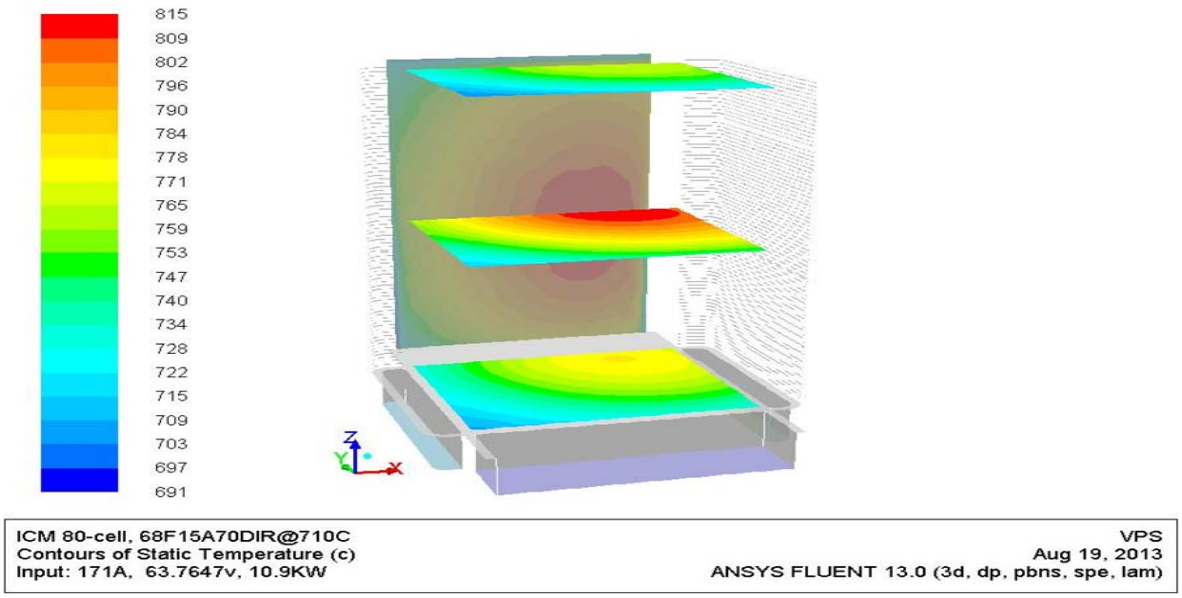

Figure 2-58 Model Predicted Thermal Profile for 80-Cell ICM Stack Operating at Phase II System Conditions

Figure 2-59 shows sample static pressure variation for the fuel domain, which was also generated with the fully coupled SOFC model. As shown, the bulk of the pressure drop was in the flow fields to ensure better flow uniformity throughout the cell layers in stacking direction.

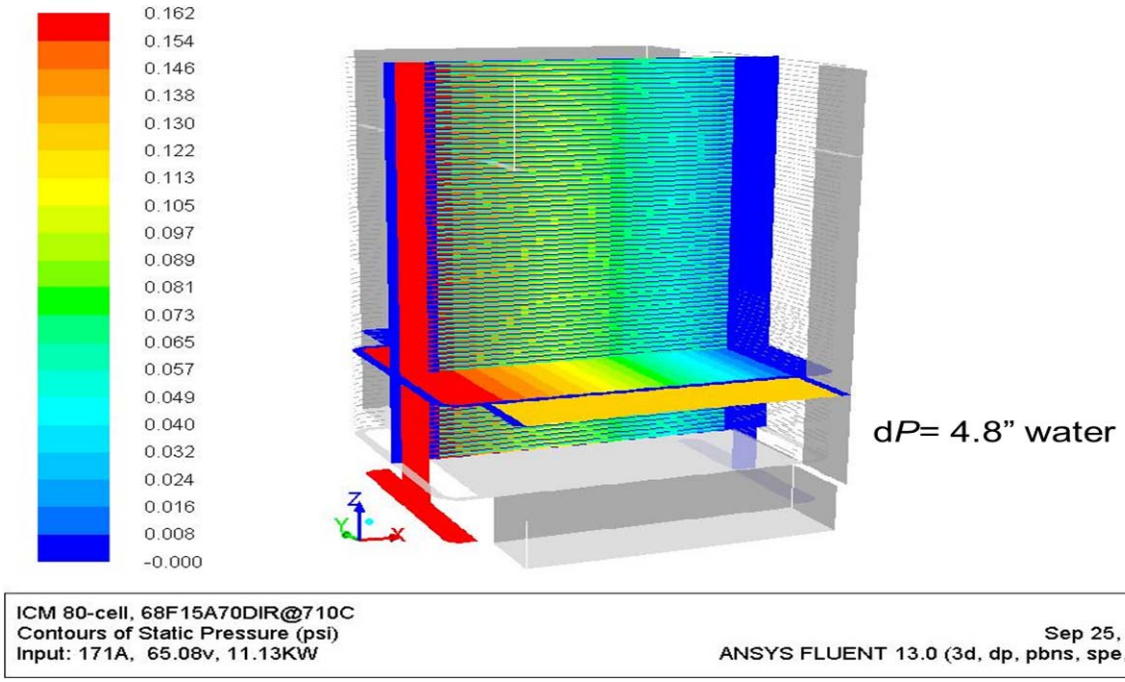

Figure 2-59 Model Generated Static Pressure Profile for 80-Cell ICM Stack Operating at Phase II Conditions (pressure drop per Tested 19-cell Stack)

In-Cell Manifolded (ICM) Stack Tests: Two 8-cell and one 19-cell in-cell manifolded (ICM) stacks were built and tested. Test results of one of the two 8-cell ICM stacks (Stack GT059391-0004) are presented here. Fuel utilization test results before thermal cycle (TC0) are presented in Figure 2-60 as an example. The stack exhibited very good fuel utilization test performance up to 75% utilization during TC0 testing.

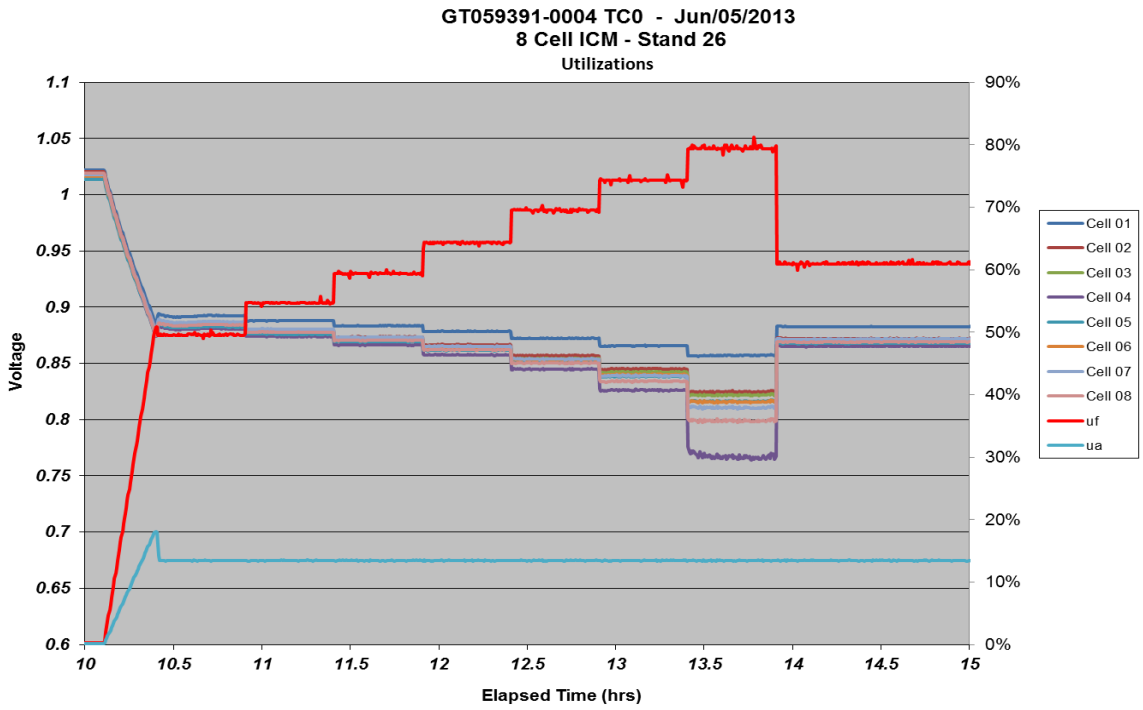

Figure 2-60 Performance of In-cell Manifolded (ICM) Stack GT059391-0004 during Fuel Utilization Testing before Thermal Cycle

Figure 2-61 shows the performance trend during steady state testing at Phase I and Phase II system conditions.

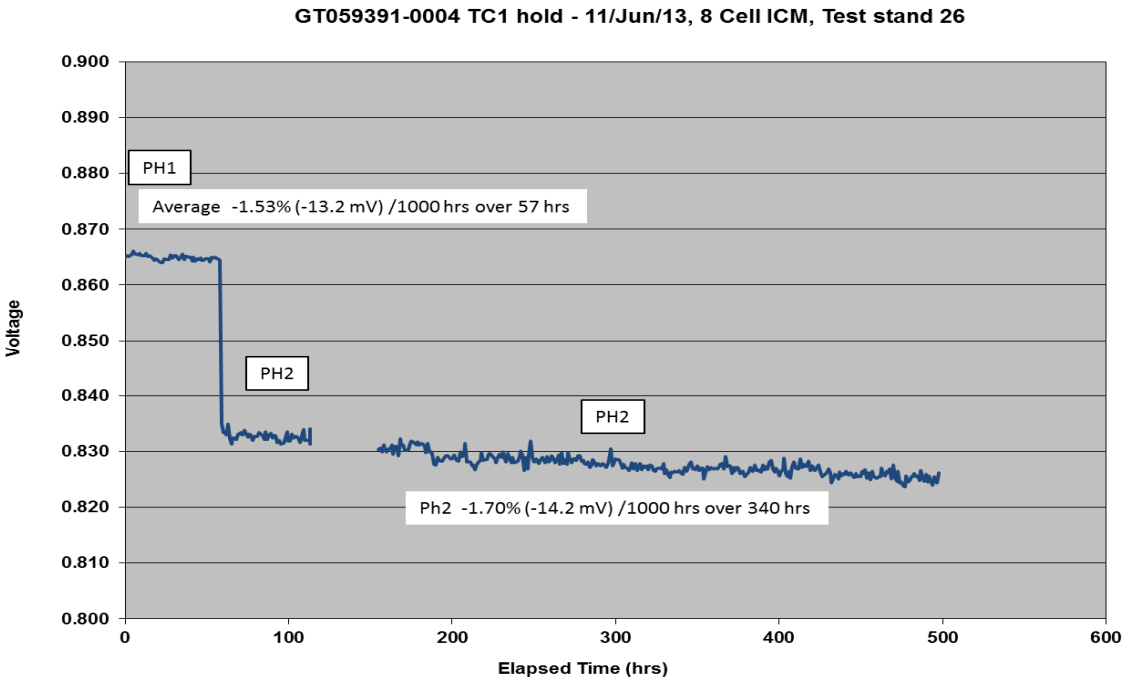

Figure 2-61 Performance of In-cell Manifolded (ICM) Stack GT059391-0004 during Steady State Testing at Phase I and Phase II System Conditions

Following the successful 8-cell stack build, the next step was to scale-up to a 20-cell stack. The scaled-up stack would better represent the thermal profile and challenge of a tall stack. Due to the manifold height and repeat component stack up, a 19-cell stack was built in place of 20-cells. The assembled stack is shown in Figure 2-62.

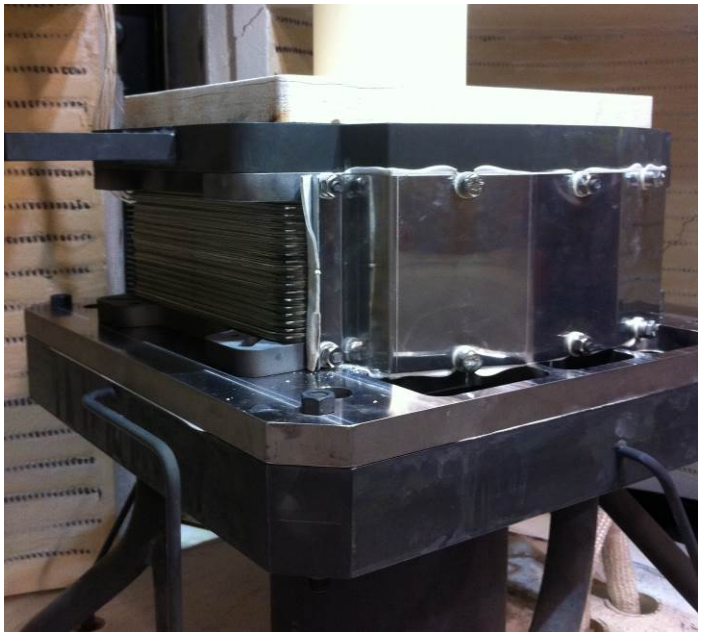

Figure 2-62 19-Cell In-cell Manifolded (ICM) Stack

Figure 2-63 shows the fuel utilization test performance of the stack (with all cells shown) after thermal cycle. The secondary y-axis in both figures represents the fuel utilization. Stack performance was stable at 75% fuel utilization level.

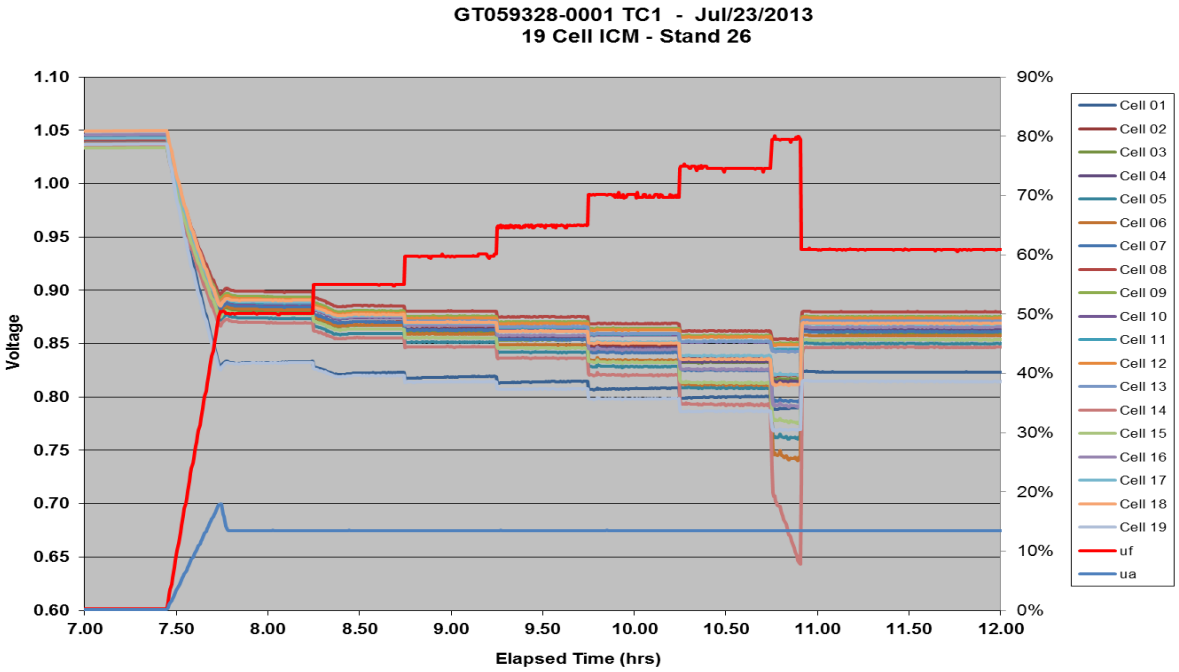

Figure 2-63 Performance of In-cell Manifolding (ICM) Stack GT059328-0001 during Fuel Utilization Testing after Thermal Cycle

For this stack, in-stack thermocouples were placed into the cathode flow field (instead of into the anode flow field which is VPS's normal convention). The initial stack thermal profile is shown in Figure 2-64. The temperature profile shows that the hottest point on the cell is near the center of cathode out manifold.

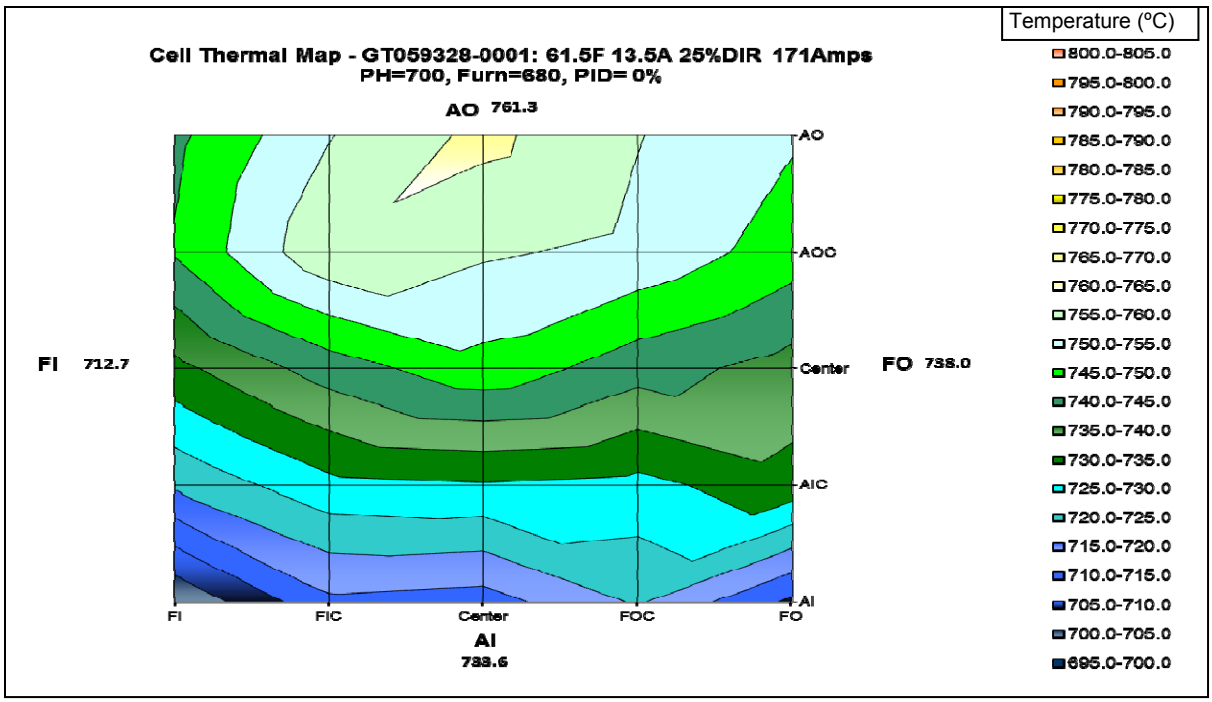

Cell Thermal Map - GT059328-0001: 61.5F 13.5A 25% DIR 171Amps						
	FI	FIC	Center	FOC	FO	ΔTxy
AI	700.4	713.9	712.7	720.6	708.9	61.0
AIC	720.8	728.6	729.5	728.4	733.2	ΔTz
Center	733.6	742.4	748.4	742.2	738.0	28.4
AOC	745.5	759.0	755.6	753.8	747.5	ΔTxyz
AO	743.8	754.7	761.3	755.2	750.5	89.3

Figure 2-64 Thermal Profile of 19-cell ICM Stack GT059328-0001 during Steady State Testing

As shown in Figure 2-65, the stack was further tested at steady-state operating conditions. After a brief test duration of about 300 hours at Phase I system conditions, the stack was operated at Phase II system conditions of 70% in-stack reforming and 68.5% fuel utilization. The average decay rate at these conditions was 0.71% per 1000 hours over a 1,100 h period. Steady state testing was resumed after pressure drop testing at open circuit (OCV) conditions. The average decay rate at Phase II system conditions was 1.15%/1000 hours over the 1,057 h post-OCV period. The test was then terminated to facilitate test stand modifications.

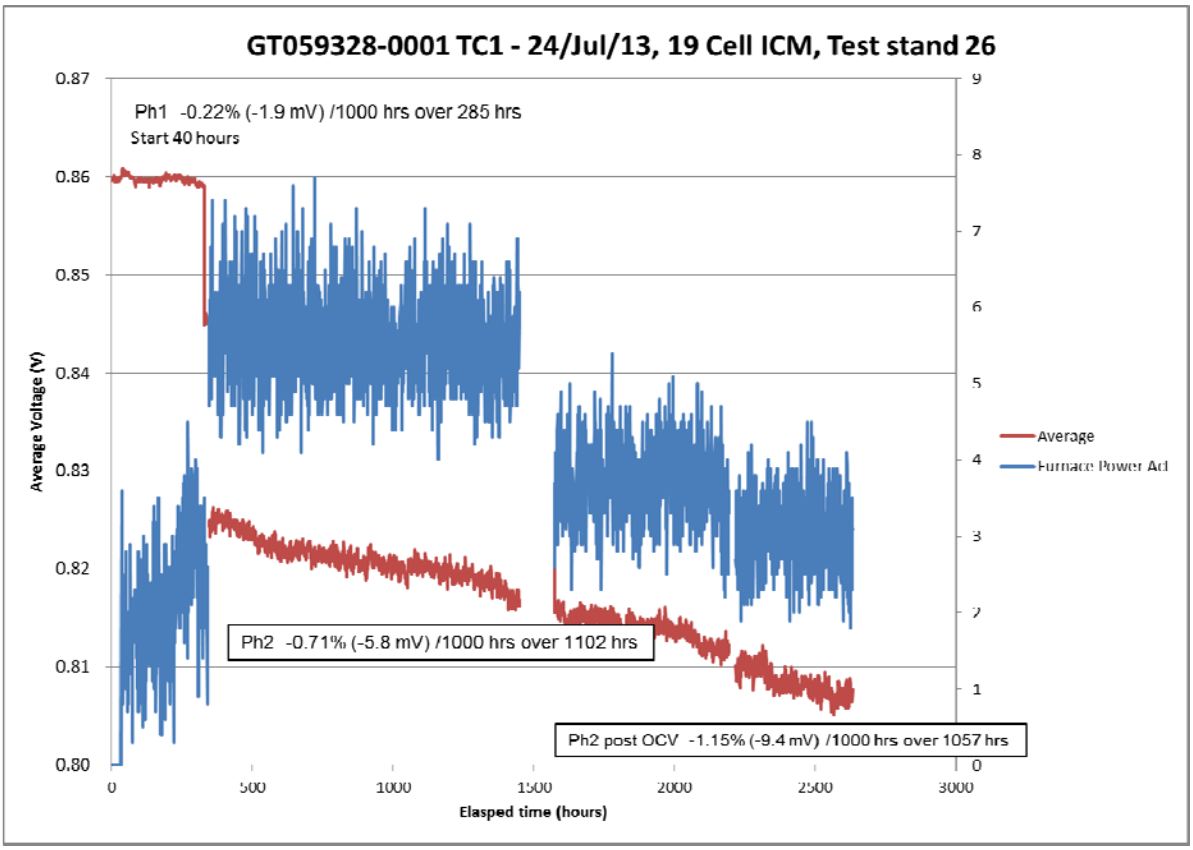

Figure 2-65 Performance Stability of 19-Cell In-Cell Manifolded (ICM) Stack GT059328-0001 at System Conditions

3.0 STACK MODULE DEVELOPMENT AND TESTS

(FCE Technical Lead, support from VPS)

3.1 Stack Module Design

60 kW Module Development

Design of a 60 kW module was developed to facilitate testing of four 96-cell stacks arrayed on a common base. The effort included extensive CFD and FEA of components, assemblies, and the module enclosure. Figure 3-1 and Figure 3-2 highlight some of the CFD analyses that were completed for the 60 kW module. The bill of material and engineering drawings for major non-repeat components were prepared.

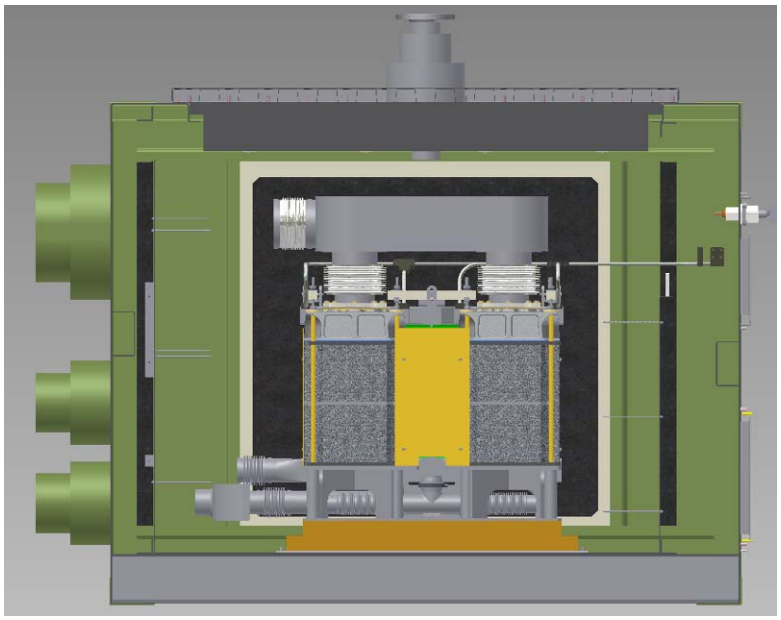

Figure 3-1 Cutaway Side View of 60 kW Module

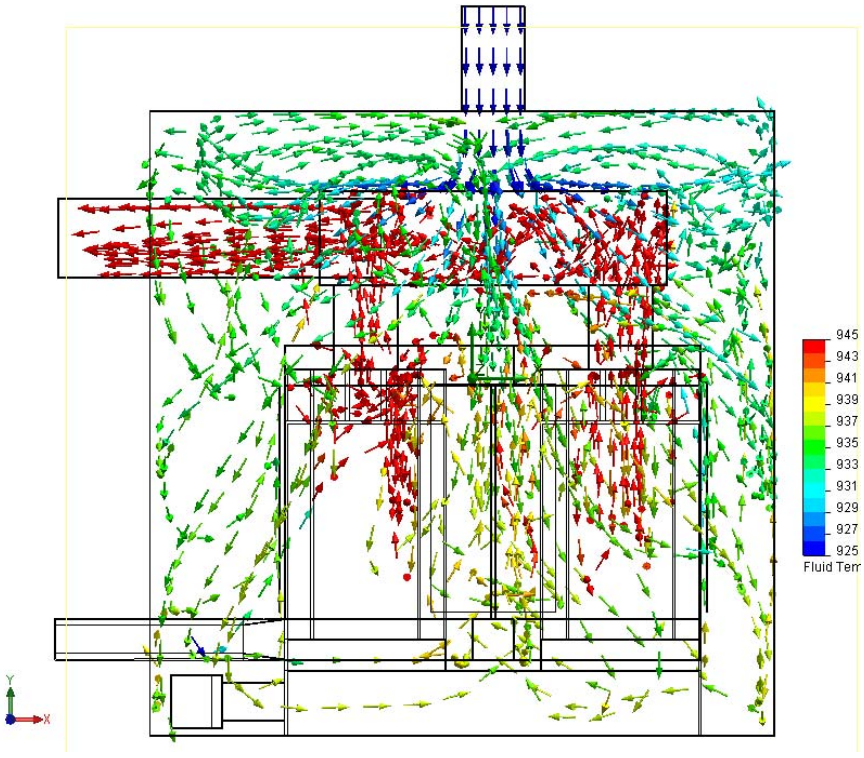

Figure 3-2 CFD Flow Analysis of 60 kW Module

60 kW Mock Stack Module Testing

For the first test of the 60 kW SOFC module, mock stacks were used to evaluate various aspects of the quad-stack design. Components for the 60 kW module were fabricated. These included vessel base (quad base) and enclosure shell, module internal bellows, fuel gas heat exchanger, bus bar and combined compression plate. Four mock stacks were fabricated and orifices were used to ensure the pressure drop through the anode and cathode flow paths within the mock stacks were representative of live stacks. These mock stacks were placed in the quad assembly (Figure 3-3) and put through a battery of tests, both cold and hot. These tests were intended to validate many new design features, concepts, and components. The components were all put together and hot tested to see how they perform as a system.

Figure 3-3 60 kW Mock Stack Quad Assembly Module Prior to Vessel Closure

The hot test was intended to demonstrate the effectiveness of the following major design features of the quad assembly:

1. Current collection path through the quad base and to the outside of the module
2. Dielectric isolation of gas streams, tie rods, and compression system components
3. Conductive interfaces, including stack gaskets and buss bar joints
4. Hot electrical buss bars with novel design features
5. Internal radiative heat exchanger stack cooling performance and fuel heating capability
6. Anode and cathode stack flow distribution (uniformity)
7. Robustness of the stack compression system including tie rods, springs, and cast combined compression plate
8. Sealing performance of bolted flange gas seals in the hot zone
9. Vessel thermal performance

Hot testing was performed through introduction of hot gas flow to both the anode and cathode sides. Voltage and high current were applied to the hot buss system to test the power take off

system and the dielectric isolation performance. Temperature, pressure, voltage and current measurements, as well as gas chromatograph results, were utilized to evaluate thermal heat transfer performance and flow properties.

Electrical Performance Testing: Several design elements of the electrical system were tested. One of the main objectives was to evaluate the effectiveness of the power take-off (PTO) system when hot. This included the hot buss bars, the conductive gaskets, and the quad base itself which acted as both the structural and electrical link between the two stacks in series (Figure 3-12). These systems were tested by passing high current (200 amps) through the PTO system and monitoring voltage drop through each component and its interface.

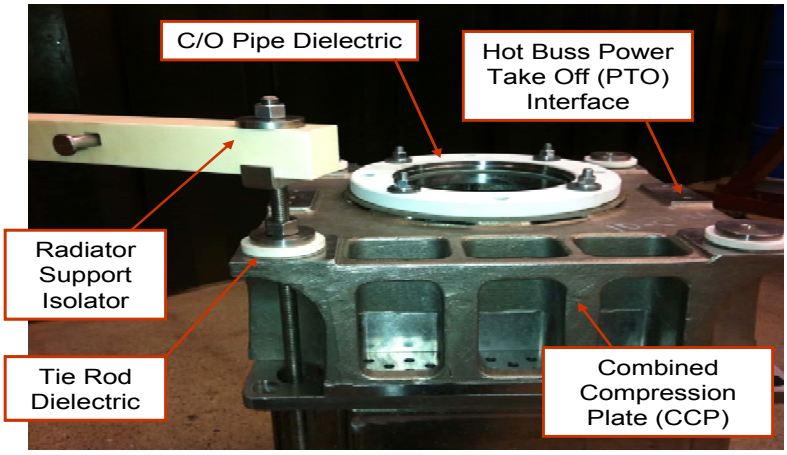

Figure 3-4 Electrical System Configuration for Stack Quad Assembly

The other half of the electrical system comprised the dielectric isolation components. These included the pipe, compression, and structural dielectrics (Figure 3-5). To characterize the hot dielectric performance, high voltage was applied to the other two stacks not used for the high current test. By measuring the changes in voltage at different temperatures over time, the total electrical system was evaluated.

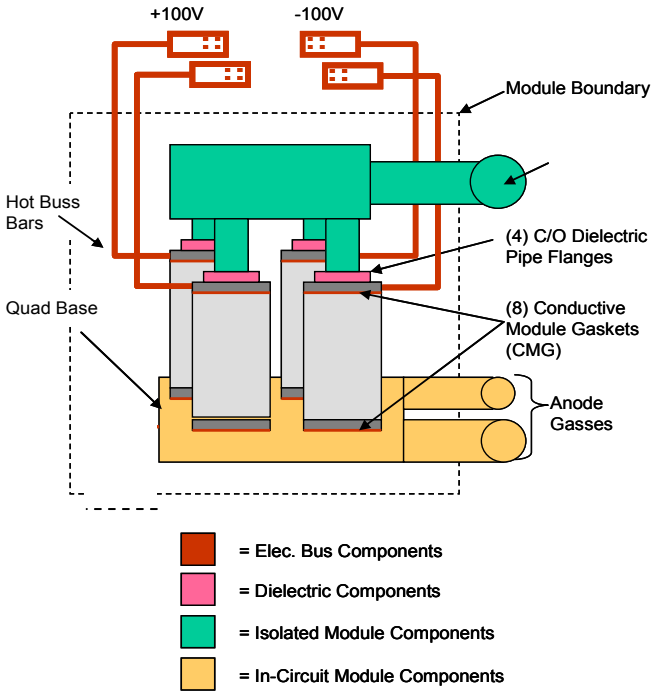

Figure 3-5 Stack Dielectric Isolation Components

The hot test ran for over 400 hours at operating temperatures. During this time, four thermal cycles were completed, resulting in the test spanning nearly three weeks. Figure 3-6 shows the performance of the hot buss bar system (and its interface) over time. The resistance stabilized quite quickly, exhibiting good performance for both the buss bars and the contact losses at the interface. Based on the test results, the expected power loss due to the buss system for the 60 kW module was projected to be approximately 307 W. The total module electrical loss for the 60 kW module is projected to be around 544 W, or <1%.

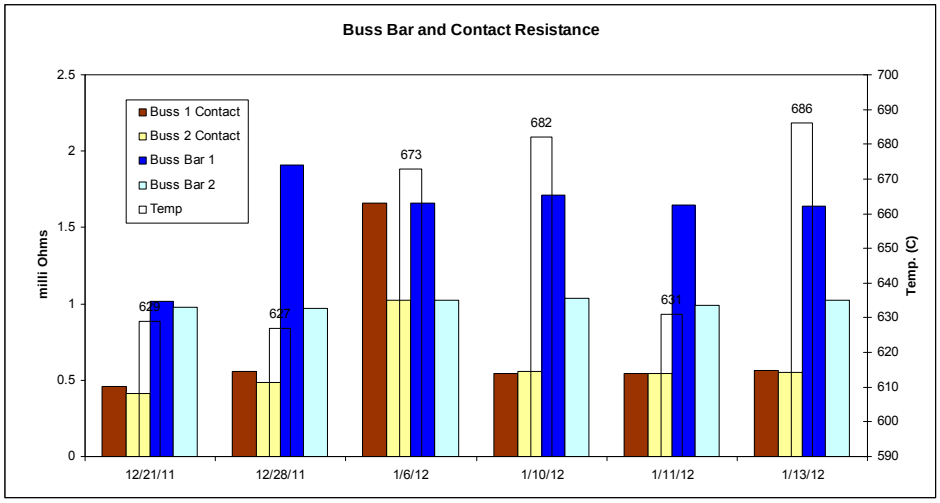

Figure 3-6 Buss Bar System Resistance Change Over Time (During 60 kW Mock Stack Module Hot Test)

Flow Distribution Testing: Anode flow variation between the four stack blocks was engineered to be within +/- 0.5%. The flow distribution design focused on using symmetry when possible. However, collecting the individual anode-out streams and removing the combined stream from a

single side of the quad, some inherent non-symmetry existed (Figure 3-7). The quad base went through several design iterations to minimize the effects of this non-symmetry. Computational fluid dynamic (CFD) analysis confirmed that the final design met the target of <0.5% flow variation. Cold flow testing showed +0.32% to -0.20% variation from the mean. Hot testing showed a range of +0.39% to -0.59% variation from the mean.

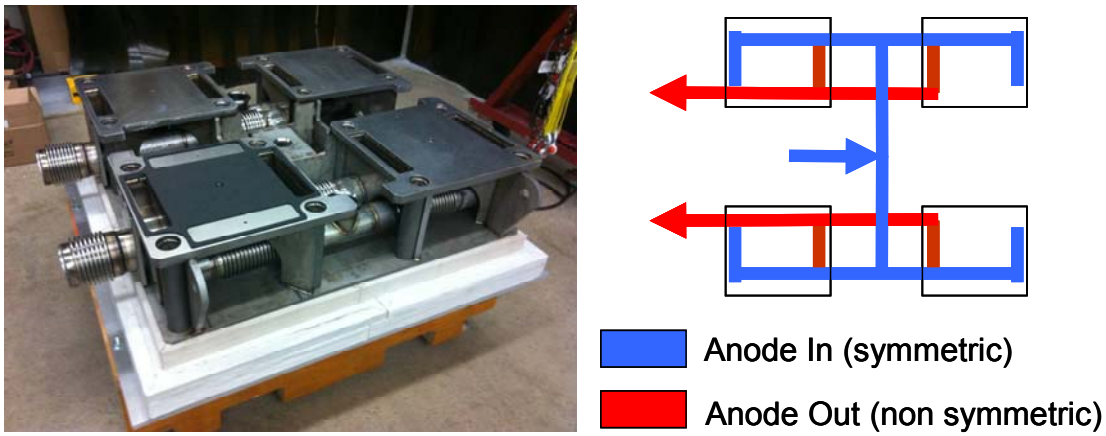

Figure 3-7 Anode Flow Path in Quad Base

Cathode flow variation between the four stack blocks was also engineered to be within +/- 0.5%. Although such tight flow distribution is not deemed as critical on the cathode flow stream as it is on the anode flow stream, the same target for flow variation was used because the cathode side was easier to optimize. Similar to the quad base (anode side flow distribution), the cathode out collector has a non-symmetrical design that was evaluated. According to the CFD, the flow non-uniformity was predicted to be +/-0.18%. Hot testing showed a range of +0.45% to -0.35% variation from the mean on the cathode side.

Overall, given the tight correlation between the CFD, cold test, and hot tests, the design provided very good flow distribution and was not modified.

Anode Gas (Fuel) Heat Exchanger: The anode gas is heated as it passes through the heat exchanger (HX) located inside the module, which collects heat radiating off the hot sides of the stacks. In the mock stack module hot test, the anode and cathode inlet streams were heated prior to entering the module. Because mock stacks do not generate power and heat (like actual operating stacks), these process gases are the only sources of heat. The gas streams cool as they go through the module, compensating for the heat losses to the surroundings. With live stacks, the stacks would generate heat, causing the gases to exit at higher temperatures. Since the mock test does not use stacks that generate heat, the effects of radiation to the heat exchanger are much different.

The intent of the hot mock test was to measure the actual performance of the radiator by measuring gas temperatures and surface temperatures on the HX and the stacks. A computer model that matched the actual geometry, process conditions, and results of the test was then developed. The model was refined until the predicted results matched the test data. The process conditions in the model were then changed to match the actual operating conditions representing live stacks case to predict the actual HX performance in an operational module. The results of this analysis are shown in Figure 3-8.

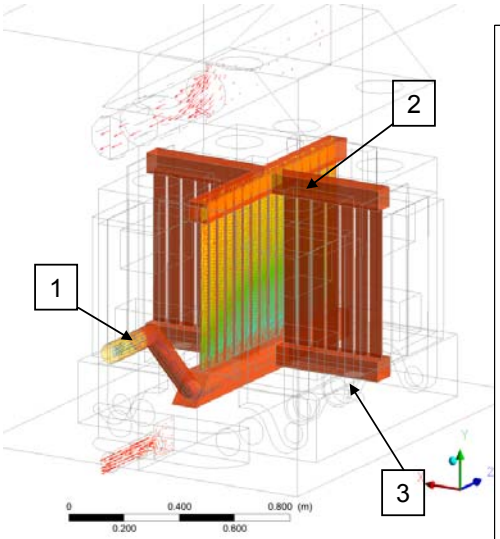

1. Fuel Entering the HX
2. Through First Pass of Radiator
3. Fuel Exit from HX (into SOFC)

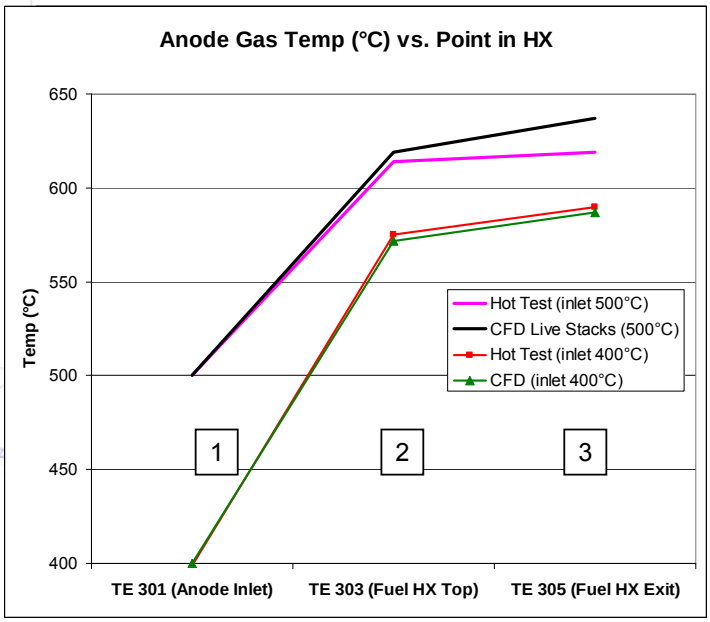

Figure 3-8 Fuel HX Performance: Mock and Live Stack Module Cases

To get good heat transfer between the stacks and the HX during the mock test, the anode inlet gas temperature was lowered such that the stacks would be hotter than the radiator (HX). Tests were run using anode inlet temperatures of 400°F (204°C) and 500°F (260°C). Examining the 400°F (204°C) data in the figure (the red and green lines) shows that the model and the test were tightly correlated. Using the validated model, the HX performance could be evaluated at the nominal operating condition of 500°F (260°C). The pink line shows the test results of mock stacks at 500°F (260°C). The black line uses the validated model to predict the performance of the HX when live stacks are used. The temperature at point 3 is the expected outlet temperature of the HX (anode inlet temperature to the stacks). Based on these results, the actual performance of the HX is expected to exceed the design target. This will result in better cooling of the stack hot faces, which is anticipated to give a better overall thermal profile to the stacks and increased performance overall.

Cross-leak Testing: During operation, any communication of gases between the anode and cathode sides results in a loss of efficiency. It increases risk of degrading stack performance and reducing life. The quad assembly uses several joints that utilize gaskets and bolted flanges that are potential sources of leaks. Some of the potential leak points are shown in Figure 3-9.

Bolted joints were engineered to provide adequate clamping force when hot, with stresses low enough such that creep will not be an issue. First the module was leak tested with the vessel shell not installed. This allowed for the inspection of any leak sources. The cold leak test involved blocking off the outlets of the anode system and pressurizing the anode to 20 “H2O (4.92 kPa) over ambient, which is four times the expected dP. A total leak rate of <0.9 lpm was measured, which corresponds to approximately 0.06% of the total anode flow during operation. Since this is not a hot test, it mainly serves as a workmanship validation of the design.

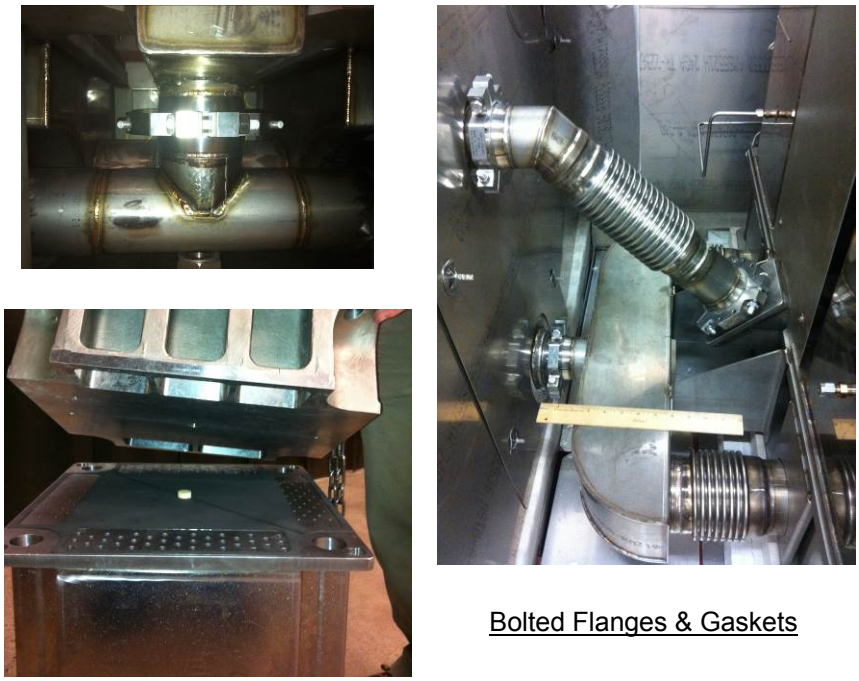

Figure 3-9 Potential Leak Sources Inside the Stack Module

A hot leak test was performed on the module to indicate if there was any significant cross leak from anode to cathode, which is of primary concern. To evaluate the hot sealing efficiency of the module, the cathode stream composition was altered to include 10% CO_2. The anode flow was then decreased such that the cathode pressure was approximately 9 in H_2O (2.214 kPa) greater than the anode pressure. The anode exhaust was then analyzed using a gas chromatograph (GC) to determine the concentration of CO_2 to characterize leak. The GC analyses indicated that there was minimal rise in the CO_2 concentration in the anode-side stream. The increase was on the order of 10 ppm, which was well within the error of the instrument. Worst-case testing correlated to a leak equivalent to approximately 0.1% of the anode stream. This was at a higher differential pressure than what would actually be seen during operation and, compared to the anticipated leak rate of live stacks, was deemed a negligible amount of cross leak.

Vessel: The vessel acts as the cathode inlet manifold to the four stacks, so flow uniformity is important. It must also provide a uniform thermal environment to all sides of the stacks. To achieve this, the 60 kW module vessel had varying degrees of insulation on the sides, as well as strategically placed inlets/outlets to minimize any non-symmetrical features contained within. Additionally, as an added margin of safety, it was designed to contain a deflagration event.

To assist with assembly and to validate design features that are part of the rapid scale-up plan for larger 100 and 200 kW modules, the pipe penetrations, power buss pass-throughs, and instrumentation routing were uniquely designed in this vessel. The first article build went to plan, and these design elements greatly improved manufacturability.

The vessel itself must be leak tight relative to the ambient. This particular vessel was pressure tested and shown to have a very small total leak, approximately 10 times less than allowed on similar-sized commercial FCE vessels (for carbonate fuel cell applications).

Vessel thermal performance was evaluated in the mock stack hot test. It is important to ensure that any exposed surfaces likely to come in contact with personnel are touch-safe. Also, there must be enough insulation that the thermal balance of the system is maintained. FCE has commercial experience designing rectangular vessels similar to this design, and several of the design elements used in those vessels were incorporated in this design. This SOFC vessel is exposed to different process gas conditions (temperature and composition) which drove the unique design. Figure 3-10 illustrates the progression from modeling the thermal profile of the module to comparing it to actual infrared imagery of the module during hot operation. An energy balance was performed to determine the actual thermal performance as a system. The computer model predicted 3.34 kW of heat loss from the module. The energy balance test was based on the dT of the inlet and outlet gases and the mass flow. Since there were no chemical reactions occurring in the mock stacks, any losses were attributed to heat leaving the module/nozzle boundaries. The total heat loss was calculated to be 3.44 kW, within 3% of the predicted value.

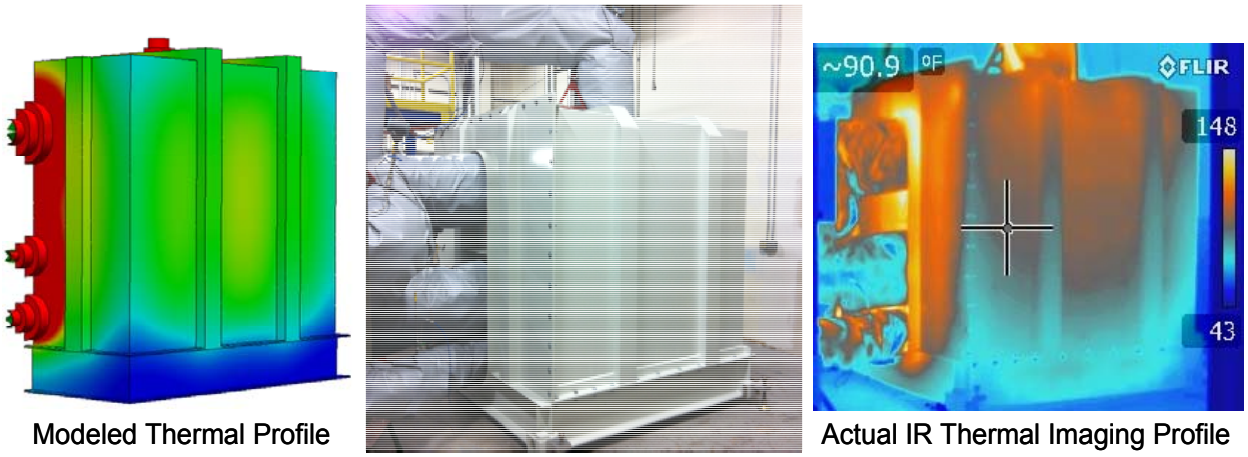

Modeled Thermal Profile

Actual IR Thermal Imaging Profile

Figure 3-10 60 kW Vessel Thermal Characterization

Results of the 60 kW module test with live stacks are discussed in Section 3.2.

2nd-Generation 50kW (net AC) Module Design: A 2nd-generation quad base module was designed for future integration with the 50kW PCM system (discussed in Sec 5). The SOFC module design improvements included integration of system balance-of-plant components into the module (design) to reduce cost and increase the efficiency of the plant. Figure 3-11 shows the thermally integrated module containing system components along with SOFC stacks. The integrated design improved thermal performance, reduced total system size, reduced cost, while still leveraging the design of critical quad-base components validated during the 60 kW module demonstration performed in Phase III.

The most notable design improvement is installation of a multifunctional catalytic oxidizer/cathode heat exchanger within the module thermal transition boundary. The combining of the oxidizer with the heat exchanger resulted in a compact design which was also more effective. This single device eliminated the need for two separate pieces of external equipment, and it leveraged the existing insulated volume of the module. The placement of the heat exchanger between the hot and cold areas of the module utilized very little space and eliminated external piping and equipment, thereby decreasing the size of the power plant. This change allowed near-ambient temperature cathode air to be sent directly to the module without any external heat exchanger. Conversely, this heat exchanger also cools the exhaust gas before leaving the module. In addition, the elimination of high temperature nozzles (for

penetration) into and out of the module further reduced heat losses, and increased the thermal efficiency of the plant.

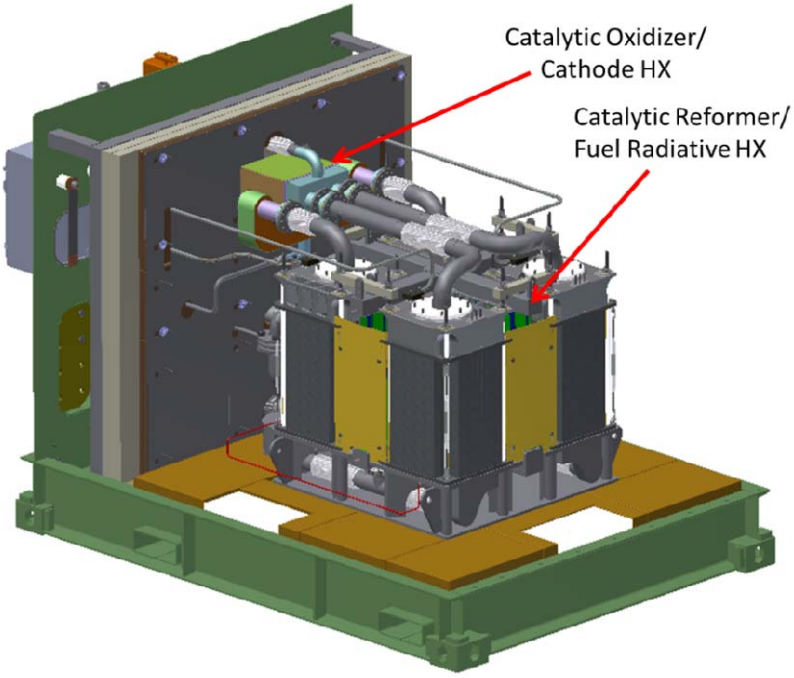

Figure 3-11 Thermally Integrated 50 kW SOFC Module

Another significant improvement was the integration of the anode pre-reformer and the anode radiative heat exchanger. Figure 3-12 shows the combined catalytic fuel reformer and radiative heat exchanger unit. This also benefited the packaging of the plant by eliminating an external piece of equipment in a similar manner as the integrated catalytic heat exchanger. This change further enhanced thermal management of the SOFC stacks by increasing the active cooling of the hottest surfaces of the stacks, resulting in lower thermal gradients.

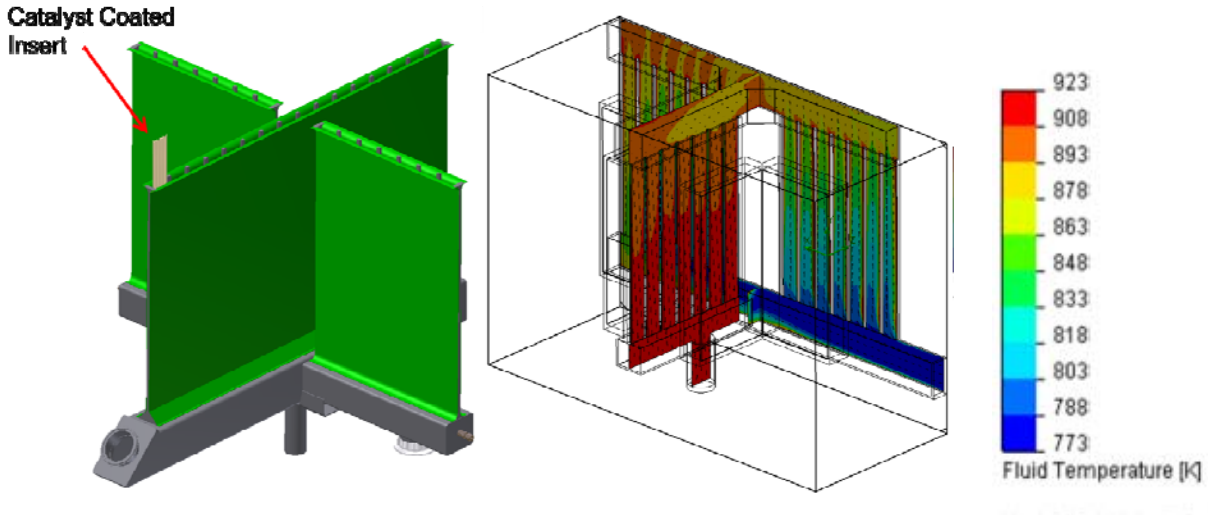

Figure 3-12 Catalytic Fuel Reformer and Radiative Heat Exchanger (Temperature Scale Shows Fluid Temperature in Kelvin)

As a further refinement of the stack module design, the vessel and insulation were remodeled to a smaller size that is easier to assemble in the plant and allows more tolerance between the module and the electrical balance-of-plant (EBoP) cabinet. The width and length of the module were reduced 6" and 3", respectively, by using insulation with a lower thermal conductivity and aligning the lifting feet flush with the side of the vessel. Design work was performed for the anode exhaust line to add an averaging pitot tube and a backpressure valve. The averaging pitot tube (flow meter) was added to measure the exhaust flow. The anode backpressure valve was redesigned to allow thermal expansion movement of the valve relative to the actuator.

3-5 kW Test Module Development

A small scale 3-5 kW module platform was designed, assembled, and integrated into the 30 kW SOFC test facility (Figure 3-13). This module allowed for the quick stack turnaround needed to test multiple stacks with minimal down time between tests. A stack can be removed and replaced with a new stack in ~1 day.

Figure 3-13 3-5 kW Module (Containing 16-cell SOFC Stack) Integrated into the 30 kW Test Facility

This new module also acted as a test bed for several new design features developed to promote more compact, lower cost, and more efficient SOFC modules. For example, it did not require the use of any expensive super alloy materials such as Inconel or A286. This was accomplished by reassigning the functionality of all tensile or high stressed members to other components outside the hot region of the module. An electrical buss bar was also eliminated by designing the gas flow conduits to perform both functions of directing process gasses and conducting current. Thermal improvements included new thinner insulation schemes, as well as redesigned one-piece spun nozzles that used less material to conduct less heat (less thermal losses) as well as accommodated the thermal gradients between the process pipes and the vessel. The module had a 32" x 32" (0.81 m x 0.81 m) footprint, which is four times smaller than the initial single-stack SOFC module tested at the beginning of the SECA program. All these features and design improvements are elements that could play an important role in future module development, especially for much larger modules where power density and cost become primary drivers of the design.

The first test of the new module, designated SO-3-01, was successfully completed. The module performed well during the 3-month test. The test results are discussed in detail under Section

3.2. The post-test examination of the stack indicated a potential reaction of the conductive gasket with SS347 base plate material. Since this alloy is also used in the 60 kW module, further testing was conducted to characterize the conductive gasket performance. Related discussion follows.

Conductive Gasket Development: The small scale 3-5 kW module platform was used to test various conductive gasket configurations. The purpose of a conductive gasket is to form an electrical connection from the stack end plate to module base/top plate for current collection, while also providing gas sealing. It was found that the FCE-developed Conductive Module Gasket (CMG) demonstrated inconsistent results. Some tests showed good operation: stable resistance and good integrity. Other tests exhibited a less stable design, and possible reaction with the 347 SS base material.

To further develop a suitable conductive gasket, a test fixture (Figure 3-14) was designed that could be used to rapidly test various gasket designs in a simulated SOFC module environment.

Error! Reference source not found.

Figure 3-14 Sub-Scale Stack Conductive Gasket Test Fixture

This permitted many different designs to be tested in a single set-up, for long durations. In addition to different conductive gasket designs, various alloys, such as 310 SS, 625, 430 SS, and 347 SS could be tested to characterize/quantify the stability of these materials for use in non-repeat components.

The gasket test fixture was used to develop the CMG, as well as other gasket/conductor designs, for long term use. The CMG has certain benefits for commercial application, such as simplicity, and possibly better stability over very long term applications. However, the CMG exhibited some problems with repeatability in the module tests conducted. It appeared to be somewhat sensitive to conditioning, yielding various results in the test modules. Figure 3-15 shows a representative comparison of the conductive module gasket with an alternative gasket design that utilizes a combination of nickel mesh and a standard gas sealing gasket.

The 3-5 kW test bed modules were tested at FCE with both types of gaskets. Although the tests were limited in duration, VPS has had positive experience with the nickel mesh design. Therefore, the two-piece Ni mesh and gasket design was selected for the 60kW SOFC module.

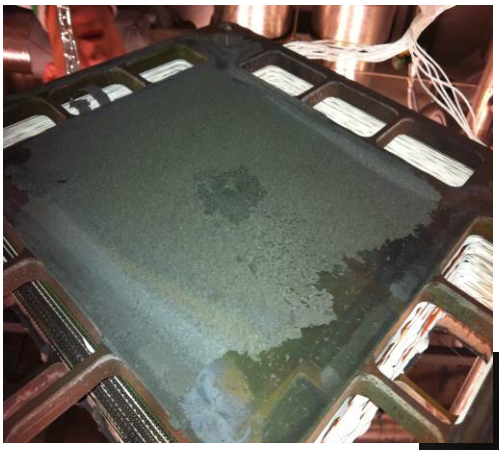

One-Piece Conductive Module Gasket (CMG)

- Gasket structural breakdown
- Variable resistance
- Inconsistent results
- More process sensitive

Two-Piece Conductive Gasket

- Standard VPS manifold seal
- Nickel mesh conductor
- More stable over test duration
- More robust

Figure 3-15 Comparison of Two Conductive Gasket Configurations Evaluated

3.2 Sub-Scale Module Tests

30 kW Stack Tower Testing at FCE: The SOFC test facility at FCE was modified for stack tower tests. Three stack towers were assembled at FCE, consisting of multiple stack building blocks provided by VPS. All stack towers utilized the scaled-up cells with a cell active area of 550 cm^2. The initial tower test was conducted on a stack tower built using three 64-cell (stack building) blocks and representing Phase I stack technology. The tower was tested in a module enclosure environment, with fuel compositions representative of the system (simulated baseline power plant fuel gas). It served as the proof-of-concept test of the SOFC tower. Facility upgrades for testing capacity and stability were also validated. The subsequent tower tests were conducted on stack towers built using two 92-cell stack blocks and representing early Phase II stack technology. Figure 3-16 shows a picture of a completed stack tower. The stack tower test accumulated over 1,000 h of operation. A DC power output of 30.2 kW was achieved at 210 A (382 mA/cm^2) and 59% fuel utilization.

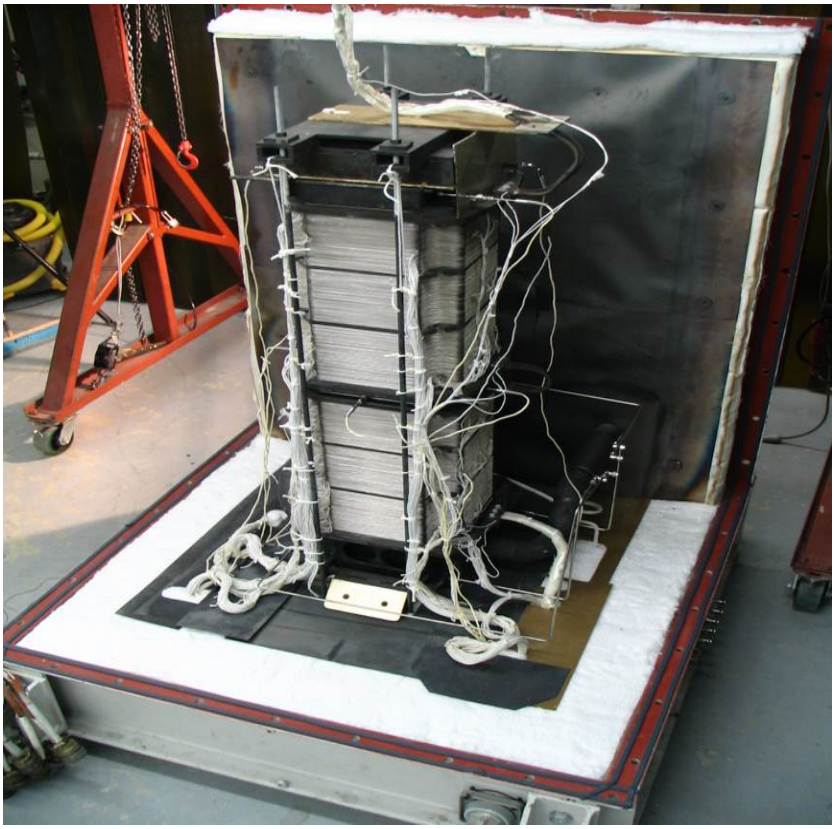

Figure 3-16 Stack Tower Assembled at FCE Using Phase II Stack Blocks from VPS (Two 92-cell Blocks, 550 cm^2 Active Area Cells)

The third SOFC stack tower (SO-30-5) test was conducted using a tower assembled from two 96-cell stack blocks (GT058116-0002 and -0004 received from VPS). The stack blocks were factory tested at VPS before shipment to FCE, Danbury. Cold flow testing of the stack blocks was performed in Danbury prior to their assembly into a vertical tower formation (as shown in Figure 3-17) and incorporation into the 30 kW stack tower test module. Cold flow testing results showed that flow uniformity was very good, with +/- 0.29% flow variation (deviation from the mean) on the anode side, and +/- 0.86% flow variation on the cathode side. The GT058116-0002 stack exhibited lower pressure drop (dP) for both the anode and cathode sides (compared to -0004 stack) at the nominal operating flow rates. The single tower 30 kW module design utilizes a U-flow configuration, with the bottom stack expected to receive slightly more flow. In order to balance the flow as much as possible, the higher flowing stack (-0002) was located at the top of the tower.

Figure 3-17 SO-30-5 Stack Tower (Two 96-cell Blocks, 550 cm^2 Active Area Cells) and Module Enclosure Assembly

The test achieved 3,308 hours of operation on load and accumulated 3,513 hours of hot runtime. An overview of voltage and current over time is shown in Figure 3-18. The test duration was limited by one low performing cell (out of 192 cells) in the stack tower. This cell was located as the 60^{th} cell from the top of the tower, near the middle of Stack -0002 (Stack 1). Halfway through the testing, the stack positions were swapped within the tower, therefore moving the stack containing Cell #60, (Stack 1), to the bottom of the tower.

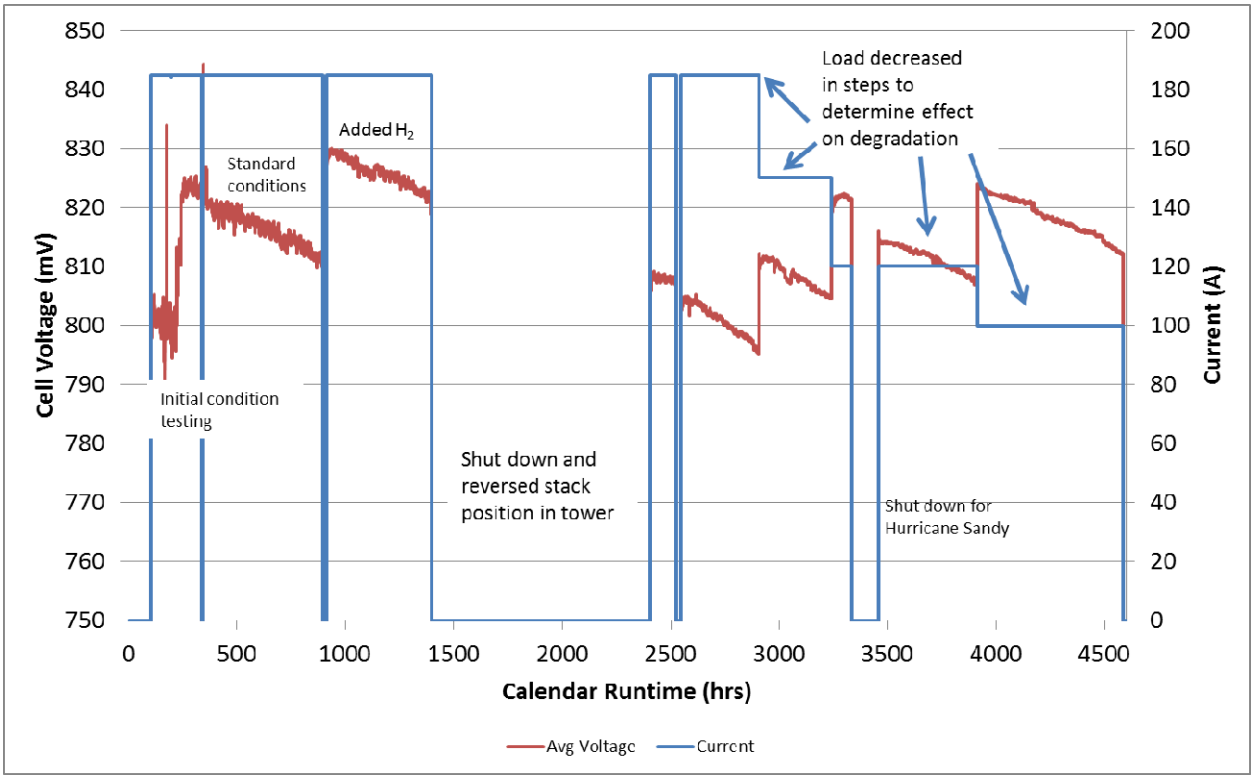

Figure 3-18 30 kW SOFC Stack Tower Average Cell Voltage and Current over the Course of Testing

Before swapping the stacks, the top stack (Stack 1), was degrading at a faster rate than Stack 2. This observation led to the hypothesis that the top stack was a less favorable position in the tower. If this was correct, upon swapping the stack locations, Stack 1 would improve in the bottom position and Stack 2 would begin to degrade more rapidly. Figure 3-19 shows the average cell voltage of each stack before and after the stack swap. Although there was a step-change loss in voltage in both stacks from the thermal cycle, the relative stack performance of the stacks remained constant. The degradation rates in Stack 1 and Stack 2 increased 1.17%/1000 hrs and 0.97%/1000 hrs, respectively, when comparing prior to the swap and after the swap. Not only were these degradation rate increases very similar, Stack 1's increase was slightly larger, indicating that the position of the stack in the tower did not affect the cell voltages or degradation rates.

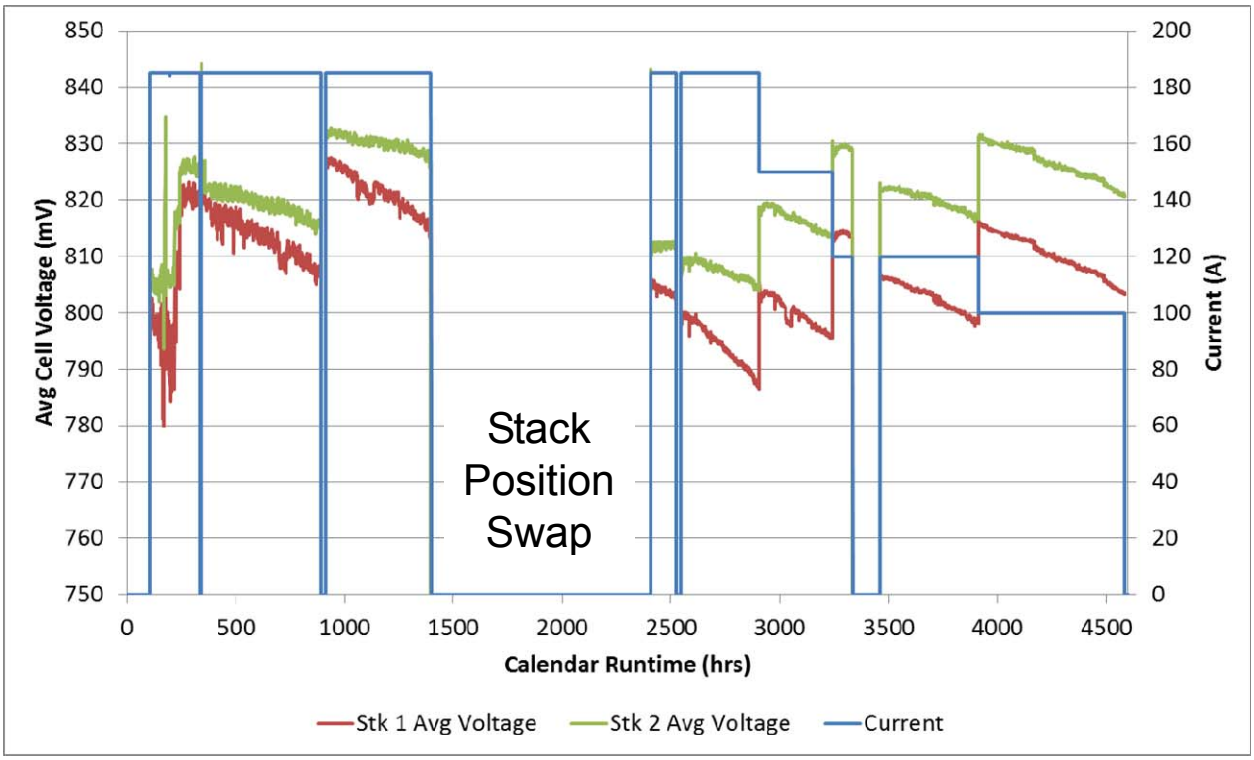

Figure 3-19 30 kW Stack Tower Individual Stack Average Cell Voltage and Current Over the Course of Testing

In addition to the cell voltages, the cell temperatures and in-cell differential temperatures (dTs) were also analyzed and can be seen in Figure 3-20 (cathode out temperature is designated as avg CO). It can be seen that prior to the stack position swap, Stack 1 (the top stack) had higher cathode outlet temperatures than Stack 2, but Stack 2 had higher in-cell dT's than Stack 1. Since the cathode outlet temperature is typically the hottest temperature in the cell, Stack 2 must have had a lower cold temperature than the cells in Stack 1, in order to have the larger dT. It was believed that this was not a tower position effect, but rather caused by a lower flow resistance for the anode gas in Stack 2 cells, allowing for more internal endothermic reforming. It was also believed that Stack 1 was hotter than Stack 2 due to manifold heating, where the fuel cell stack acted as a heat exchanger and the cathode gas carried heat to the top of the tower.

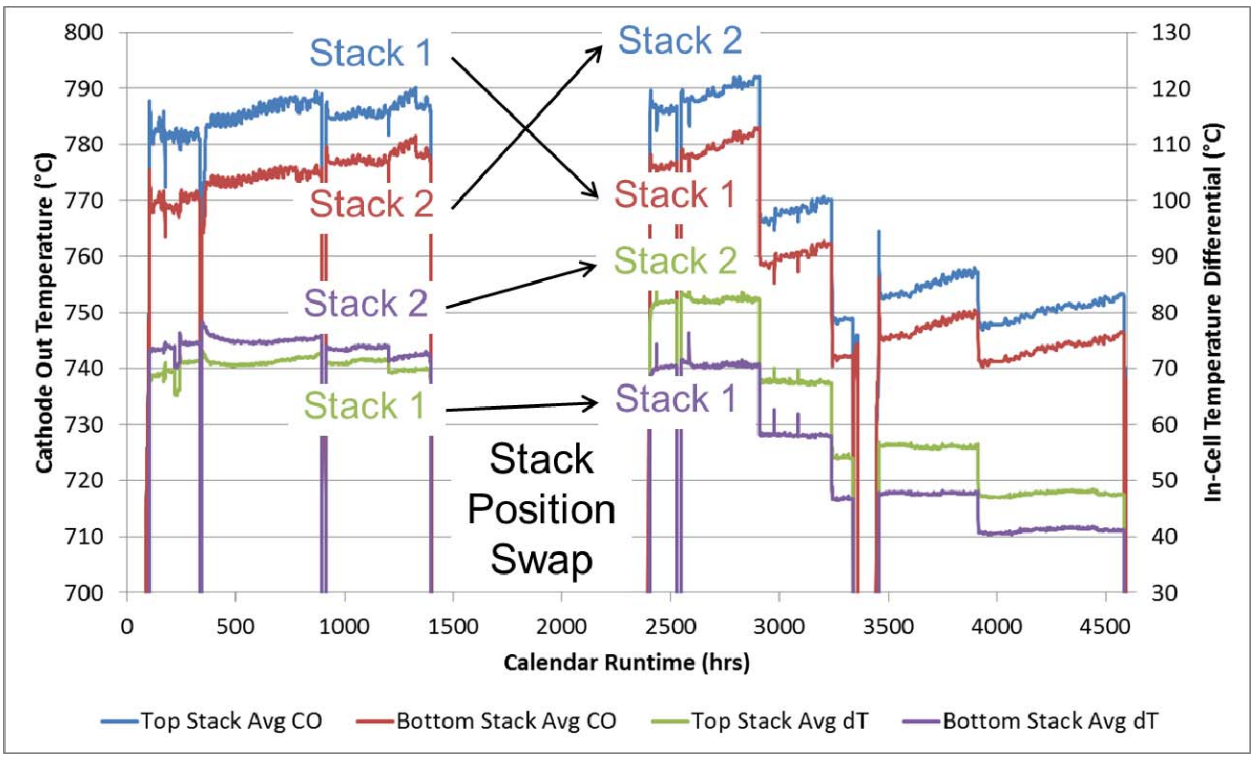

Figure 3-20 30 kW Stack Tower Individual Stack Average Cathode Outlet Temperature and In-cell dT over the Course of Testing

Once the stacks were swapped, it could be seen that Stack 2, which was then the top stack, had a higher cathode outlet temperature than Stack 1 and continued to have a higher in-cell dT. These observations confirmed both of the deductions described above. The fact that Stack 2, as the top stack, had a higher cathode outlet temperature and continued to have enhanced internal reforming explains the increase in relative in-cell dT's between stacks. As additional confirmation, temperature contour charts of the center cell in each stack were created before and after the stack position swap. These can be seen in Figure 3-21. The temperature scale is in °C. Labels AI, AO, CI, and CO indicate anode in, anode out, cathode in and cathode out edges of the cell, respectively.

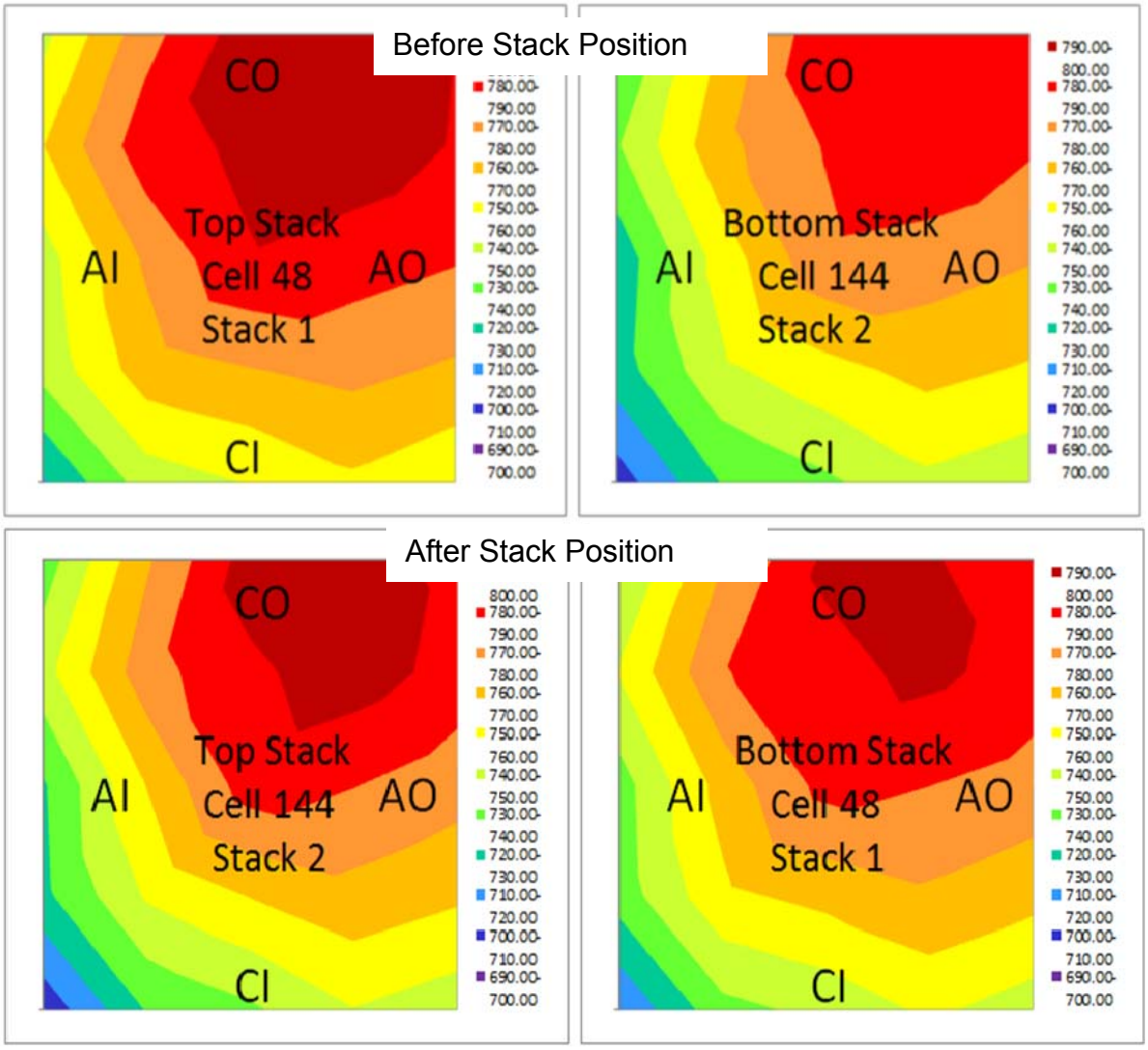

Figure 3-21 30 kW Stack Tower Individual Stack In-cell Temperatures of the Center Cell before and after Swapping the Stack Positions

From these contour charts, it can be seen that the top stack always had the higher cathode outlet (CO) temperature. It can also be seen that Stack 2, regardless of position in tower, always had lower temperatures along the anode inlet (AI) face and anode inlet/cathode inlet (CI) corner, where internal reforming would occur.

Based on this analysis, the stack tower configuration was validated. The stack position within the tower had no significant effect on the stack performance or stack endurance.

After the stack swap within the tower, the load was decreased in steps to study the effect of load on cell performance degradation rates. The load was reduced in steps from 185 A, 150 A, 120 A, to 100 A, and the rate of degradation was calculated at each load. This can be seen in Figure 3-22. The trend labeled 'high voltage avg' represents the average cell voltage of the 96 high performing cells as a group. The trend labeled 'low voltage avg' represents the average cell voltage of the 96 low performing cells as a group. The linear fit equations for the four load test periods are also shown where the slope represents the performance degradation rate in mV/1000h.

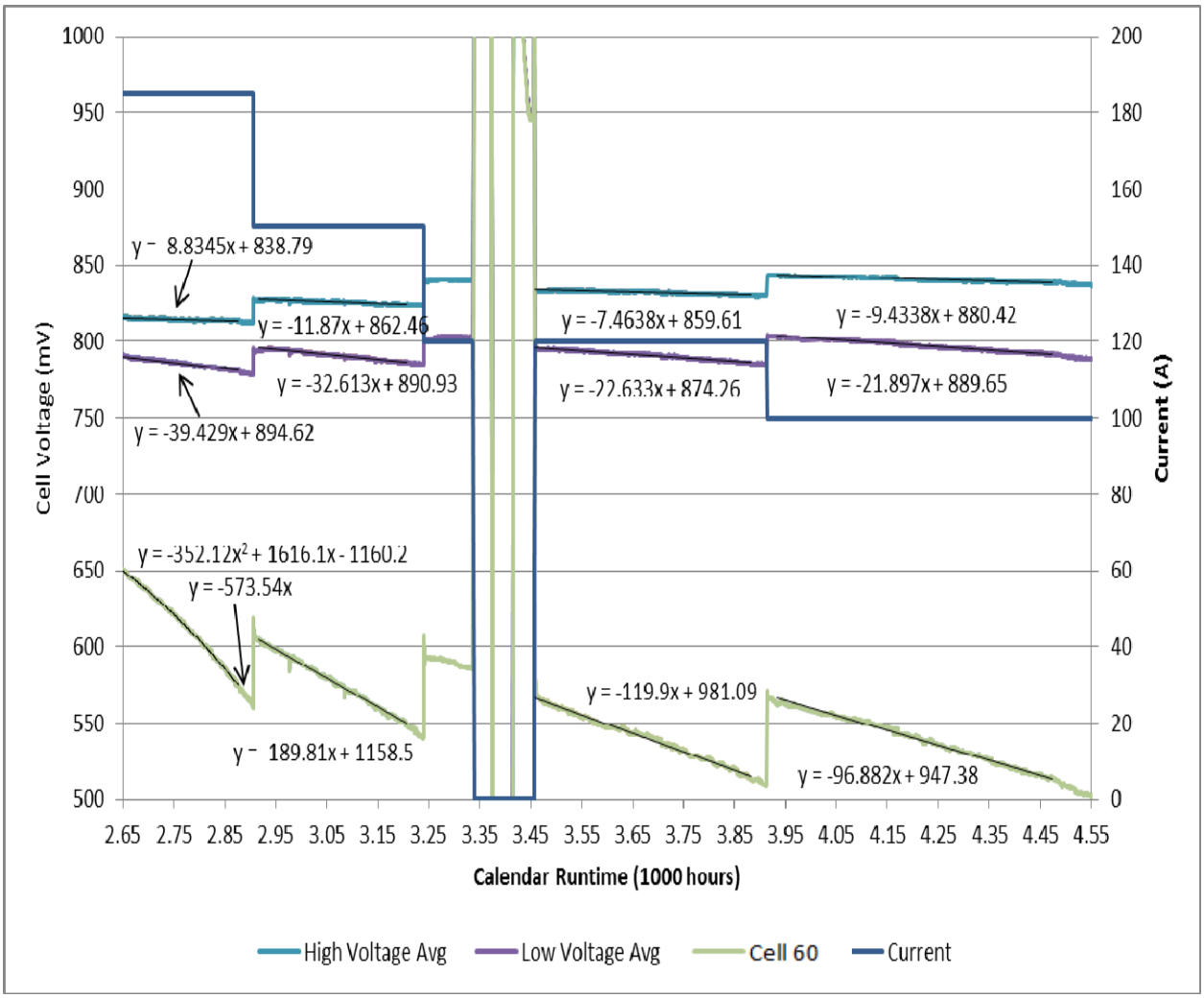

Figure 3-22 Performance Degradation Rate Characterization during 30 kW Stack Tower Test

From Figure 3-22, it can be seen that the '96 high performing cells' group did not have a consistently improving degradation rate trend as the load was decreased, although these cells did benefit by having boosted voltages. In the final 600 hours of operation, this group of cells, on average, was degrading at a rate of 9.4 mV/1000 hours (~1%/1000 hours). The '96 low performing cells' group not only benefited from a voltage boost at each load decrease, but also had decreased degradation rates as the load was decreased. As the load decreased from 185 A to 150 A, then to 120 A, and finally to 100 A, the degradation rate decreased from 39.4 to 32.6, then to 22.6, and finally to 21.9 mV/1000 hours (~5%/1000 hours at 185 A and ~2.7%/1000 hours at 100 A). Cell 60 experienced the same trend as the '96 low performing cells' group overall (within which Cell 60 is included), experiencing greatly decreased degradation rate and increased voltage at each step down in load.

In addition to the cell voltages, the cell temperatures also experienced changes resulting from the decrease in load. The temperature profile contour plots of the center cell of each stack at various loads were generated and analyzed. As expected, the temperature decreased as the load decreased. The contour plots show that as the stacks ran steadily at a constant load, the cell temperature gradually increased and the 'hot spot' at the cathode out edge became larger and spread to the center of the cell. The contour plots also showed that the top stack center cell

(Cell 48) was generally hotter than the bottom stack center cell (Cell 144). The test was terminated after 3,513 hours of hot runtime.

60 kW SOFC Module Test: Testing of the 60 kW Quad-Base SOFC module was conducted using four 96-cell stacks, each with a peak power rating of 15 kWdc, positioned on a Quad Base and connected in parallel flow arrangement. The four stack blocks used were factory tested at VPS (GT058742-0001 through -0004) before shipment to FCE, Danbury. The stacks were cold flow tested, prior to installation into the module, to determine the best position to place each stack in the quad-base arrangement. Anode flow uniformity is of primary concern. Stacks GT058742-0003 & -0004 had slightly lower pressure drop (ΔP). The quad base has four stack positions, and two of them (#2 and #3) flow slightly more. These two stacks were placed in those positions for uniformity of gas flow distribution between stacks. The picture in Figure 3-23 shows the four-stack arrangement on the Quad Base before installation of the module enclosure.

Figure 3-23 Four Stacks on a Quad Base in the 60 kW SOFC Module

The four stacks were electrically connected in a series-parallel configuration as shown in

Figure 3-24. Stacks 1 and 3 were in parallel and the group was in series with the group containing Stacks 2 and 4 which were in parallel with each other. The individual current through each stack varied with stack voltage however the sum of the current through Stack 1 and 3 equaled the sum of the current through Stacks 2 and 4.

The cathode exhaust temperatures of the four stacks during module heat-up were very uniform which showed that the flows and heat loss within the module were uniform. The uniformity of the Open Circuit Voltages (OCV) of the four stacks, at the end of initial start-up, also indicated uniform flows and temperatures. On-load operation was initiated successfully. The cell performance, within the stack as well as from stack-to-stack, was fairly uniform. The bar chart in Figure 3-25 shows the on-load performance at 75% power level (50.9 kW DC power with overall fuel utilization of 87% and a per pass fuel utilization of ~60%) as an example.

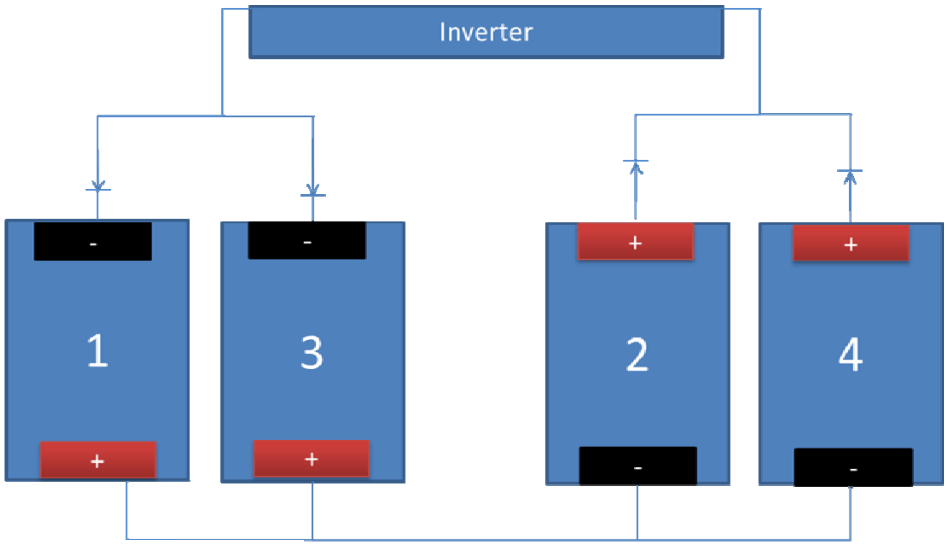

Figure 3-24 60 kW Module Stack Electrical Configuration

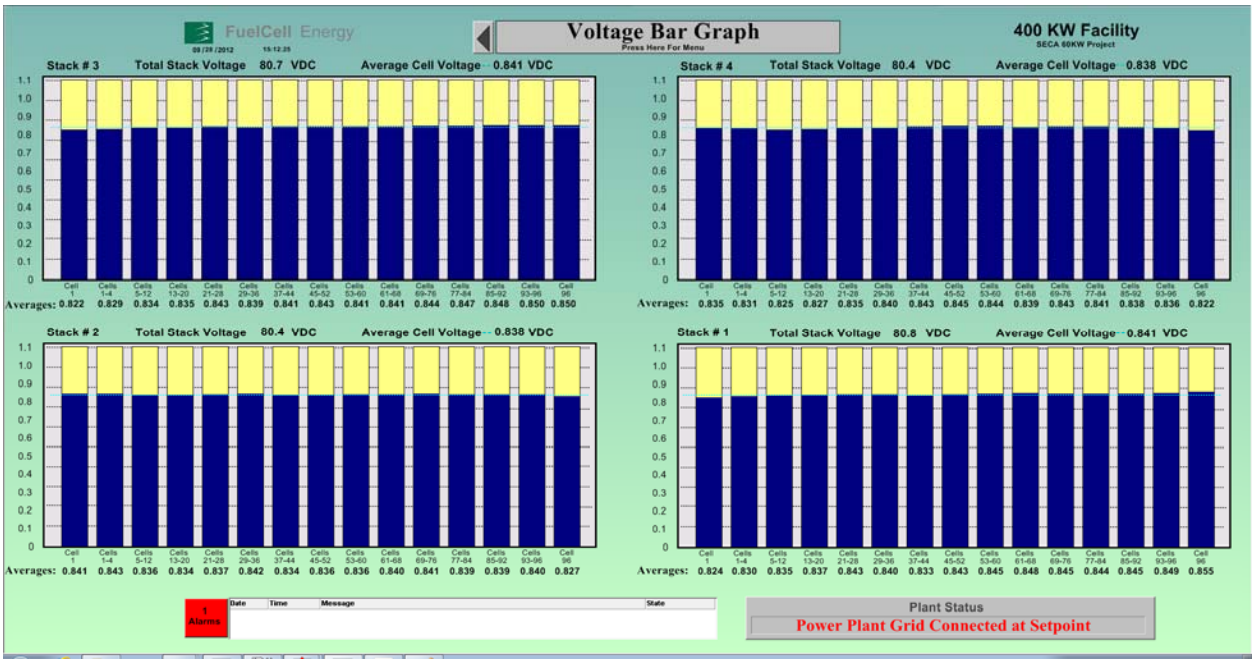

Figure 3-25 60 kW Module Stack Performance at 75% Load Level

Overall, the module operated for 1,130 hours on load, accumulated 1,645 hours of hot runtime, reached a max power level of 60.6 kW, and generated 51.2 MW-h of electricity. The 100-hr averaged BOL (Beginning-of-Life) operational characteristics and performance of the module is shown in Table 3-1. An overview of voltage and current history can be seen in Figure 3-26.

Table 3-1 Beginning-of-Life (BOL) Performance and Operational Characteristics of the 60 kW Stack Module

	BOL Performance (100-hour average)
Stack Current	187.4 A
Cell Voltage	819 mV
Stack Voltage	78.64 V
Gross Module Power	58.96 kW
Fuel Utilization - System	81%
Module Efficiency (LHV)	64%

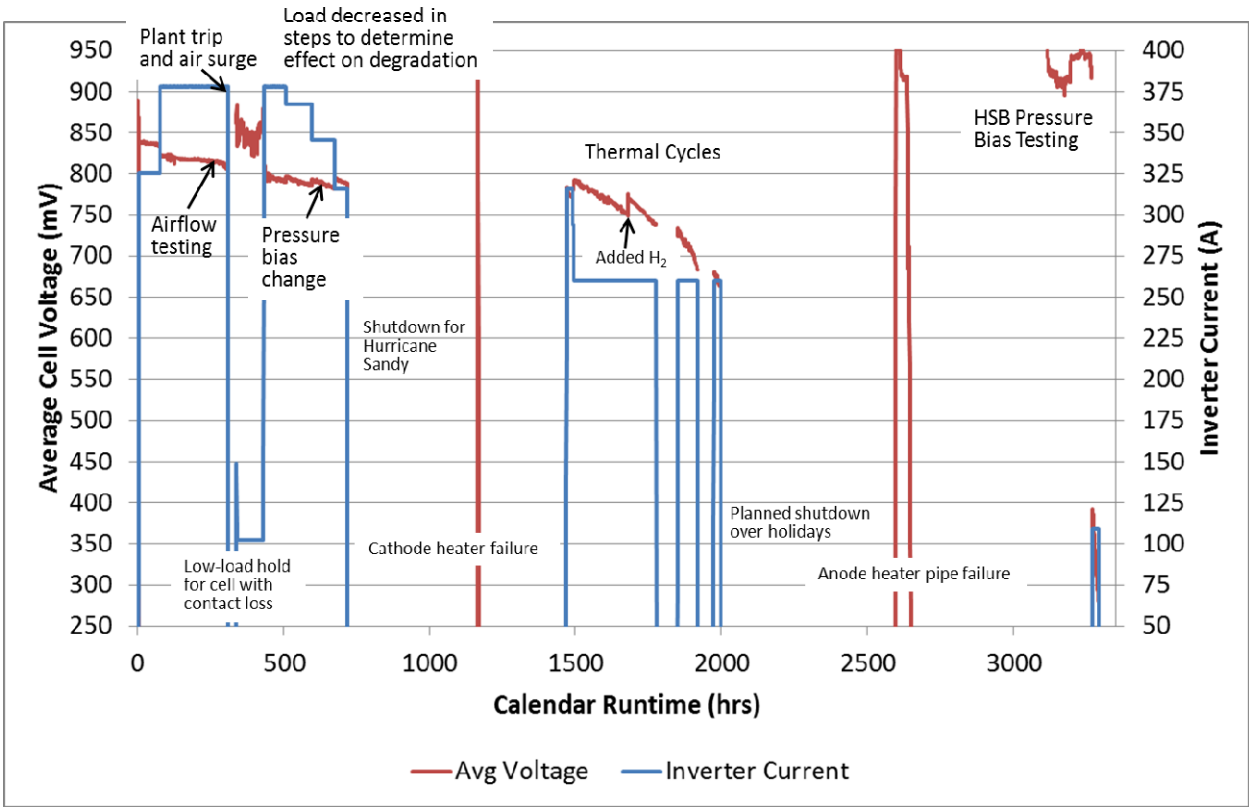

Figure 3-26 60 kW SOFC Module Average Cell Voltage and Current over the Course of Testing

Cell group voltage trends for Stack 1 are shown in Figure 3-27 as an example. The cell numbering in the figure represents cell groups of 8 cells each, except for the cell 001 and cell 095 end cells, and cell groups 004 and 096 which consist of the last four end-cells in each end of the stacks.

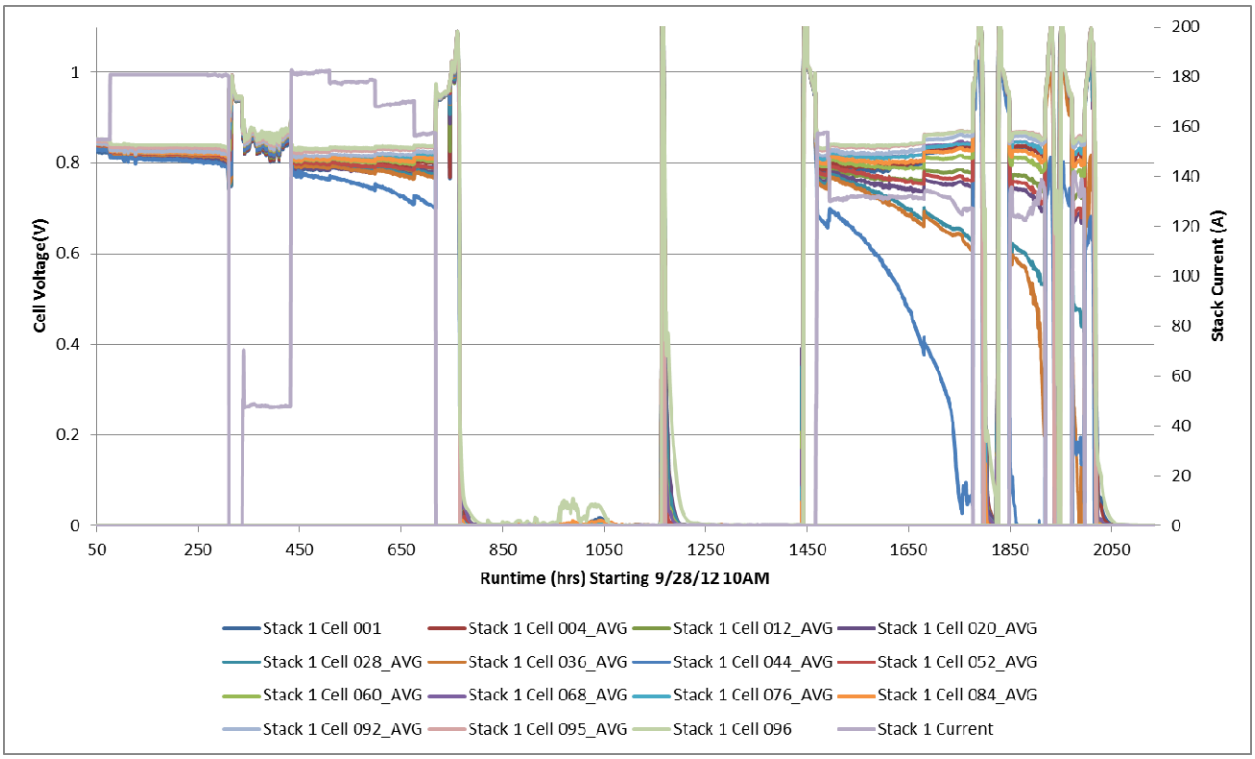

Figure 3-27 Cell Voltages and Stack Current of Stack 1 during 60 kW Module Test

As can be seen from Figure 3-27, at around 500 hours, rapid degradation of some cells was observed in the stacks. The accelerated degradation at the early stage of operation was attributed to an upset (at ~300 hours) in the test facility causing a brief pause in the flow of reducing gas (hydrogen) to the fuel cell anodes. The interruption of the reducing gas flow to the anode may have caused oxidation of nickel in the anode and, possibly, resulted in change in the anode structure and/or delamination of the anode from the electrolyte. At that point, the load was reduced in steps to determine whether the degradation rate decreased with load, which it did not. At 720 hours, the cathode heater began to fail and the system was shut down. A replacement heater was installed (at 1150 hours runtime), but it experienced an electrical short during the heat-up process. A second replacement heater with modified design was then developed and installed two weeks later. Upon the system restart, testing was performed at hot-standby conditions and then on load. However, even under low load conditions, the cell voltages were too low and the cell temperatures were too high to continue testing.

It was observed that the top half of each stack experienced high degradation rates, which is believed to be initiated by the accidental oxidation of the anode active layer in cells at the top of each stack. This was caused by a combination of several facility and operation related incidents. Primarily, there was insufficient anode purge flow during system trips. In conjunction, there was a cathode to anode pressure differential, which was highest at the top of the stacks where the cathode gas enters. In addition, there was no physical disconnect between the stacks and the inverter. The inverter, instead, was given a set point of zero Amps and is now believed to have been drawing a slight amount of current from the stacks during system trip. The constant current trickle would utilize the small amount of hydrogen in the cover gas and therefore hydrogen was not available to protect the anode from cathode air leakage due to the cathode-to-anode pressure differential. Performance loss was propagated to the rest of the stack by high temperatures in the damaged cells during subsequent testing.

Prior to reaching full power, there were several trips associated with the development and implementation of a brand-new control system in the newly renovated facility. After the last system trip, voltage spread (variation from top to bottom within stack) was observed and can be seen in Figure 3-28. The y-axis represents cell groups. Most of these are 8-cell groups (e.g. cell group designated a '12' constitutes cells 5-12). There are two 4-cell groups, one at each stack end. Also, there are two single cell voltages (stack end cells).

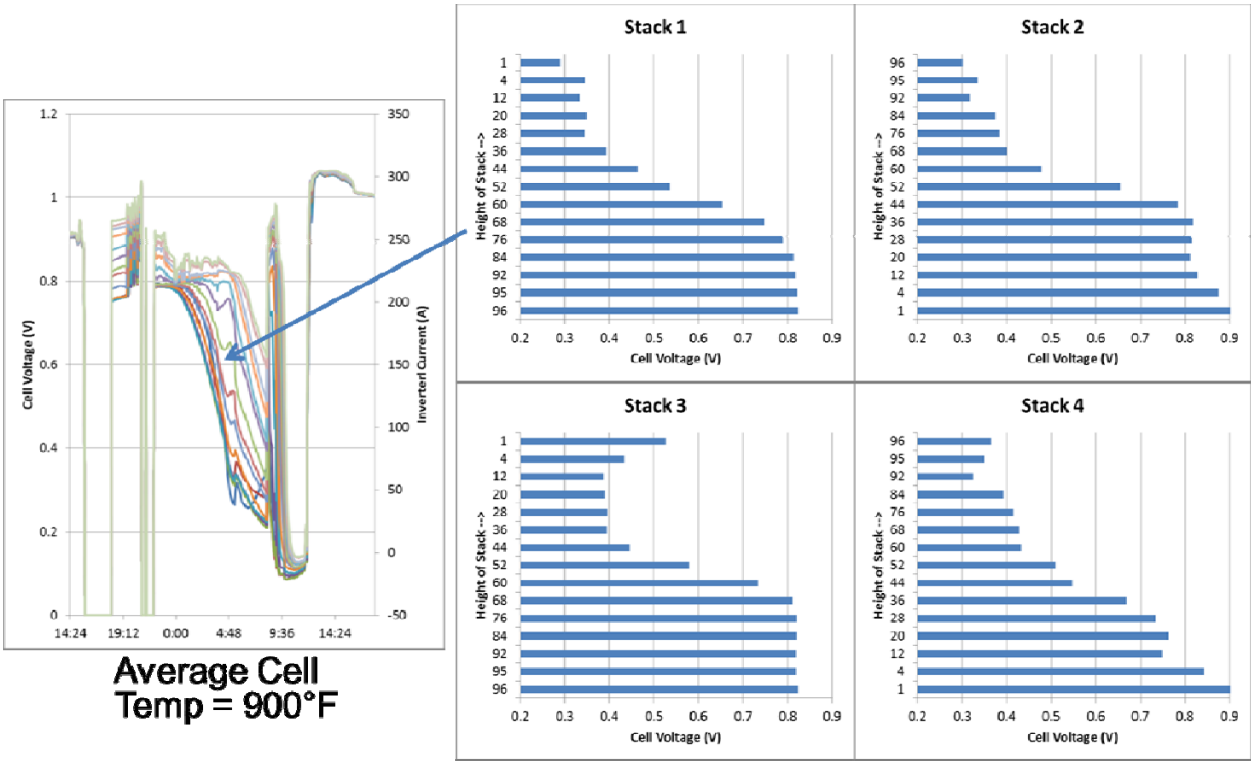

Figure 3-28 Cell Voltage Spread while Flowing Purge Gas during a System Trip of 60 kW Module

On the left side of Figure 3-28, a chart of cell voltage during purge flow period can be seen. Relating to the point marked by the arrow, the four charts on the right are the cell group voltages (average) of each stack along the height of the stack. These charts show that the average cell voltages are all much lower at the top of each stack than they are at the bottom.

The high degradation rates were first noticed upon restart after a trip on October 11, 2012. The events of the trip and the resulting voltage spreading can be seen in Figure 3-29.

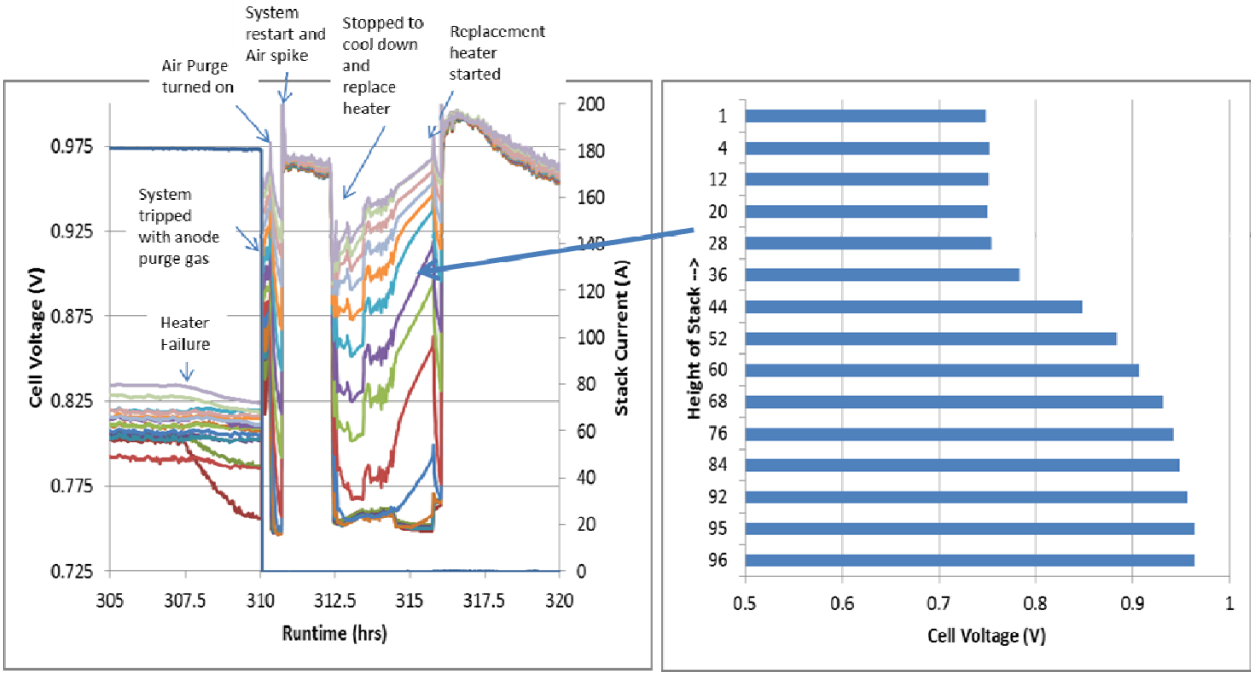

Figure 3-29 Cell Voltage Spread (During Purge Flows of a System Trip on 10/11/12) Indicating Oxidation of the Anode Active Layer at the Top of Each Stack in 60 kW Module

Once again, it was seen that the top cells had a lower voltage than the bottom cells in all four stacks. This time, however, the top cells all stopped declining at ~0.75V; the expected voltage corresponding to nickel oxidation.

It was then planned to perform several thermal cycles (starting at 1780 hours runtime) to evaluate the cells that were not yet rapidly degrading. The thermal cycles were also used to determine the relationship of cathode air flow rate to cool down rates and in-cell temperature differentials. A plot of air flow and cathode module temperature with time is shown in Figure 3-30.

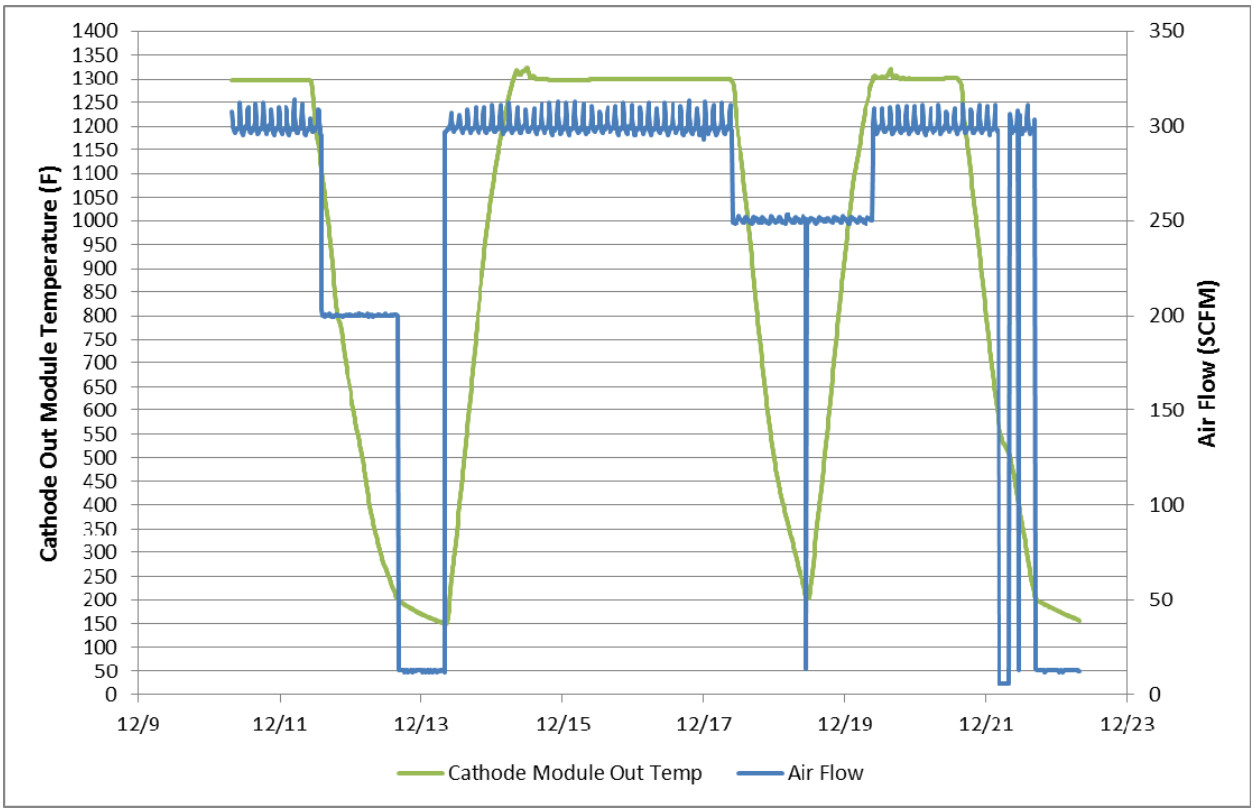

Figure 3-30 Cathode-out Temperature and Air Flow during 60 kW Module Thermal Cycles

Three cool-downs were performed with airflows of 200 SCFM, 250 SCFM, and 300 SCFM, respectively. The cool down rates and in-cell temperature differentials can be found in Table 3-2. As expected, the cool-down rate increased with the flow rate.

Table 3-2 Effect of Cathode Airflow on the 60 kW Module Cool-down Parameters

Air Flow Rate, SCFM (std m^3/min)	Cool Down Rate, °F/hr (°C/hr) 1165°F-1018°F (629-548°C)	Avg of Cell 48 ΔT During First 3 hours, °F (°C)
200 (5.66)	50.9 (28.3)	23.4 (13)
250 (7.08)	53.6 (29.8)	26.8 (14.9)
300 (8.50)	55.7 (30.9)	23.8 (13.2)

The third thermal cycle was ended due to high in-cell temperatures. The cathode-out temperature of Cell 24 in Stack 3 went above 1550°F (843°C). In addition to the cell voltages, the voltage losses across the stack gaskets, junctions, bus bars, and base plate were also measured. From these data, the resistance was calculated and plotted in Figure 3-31.

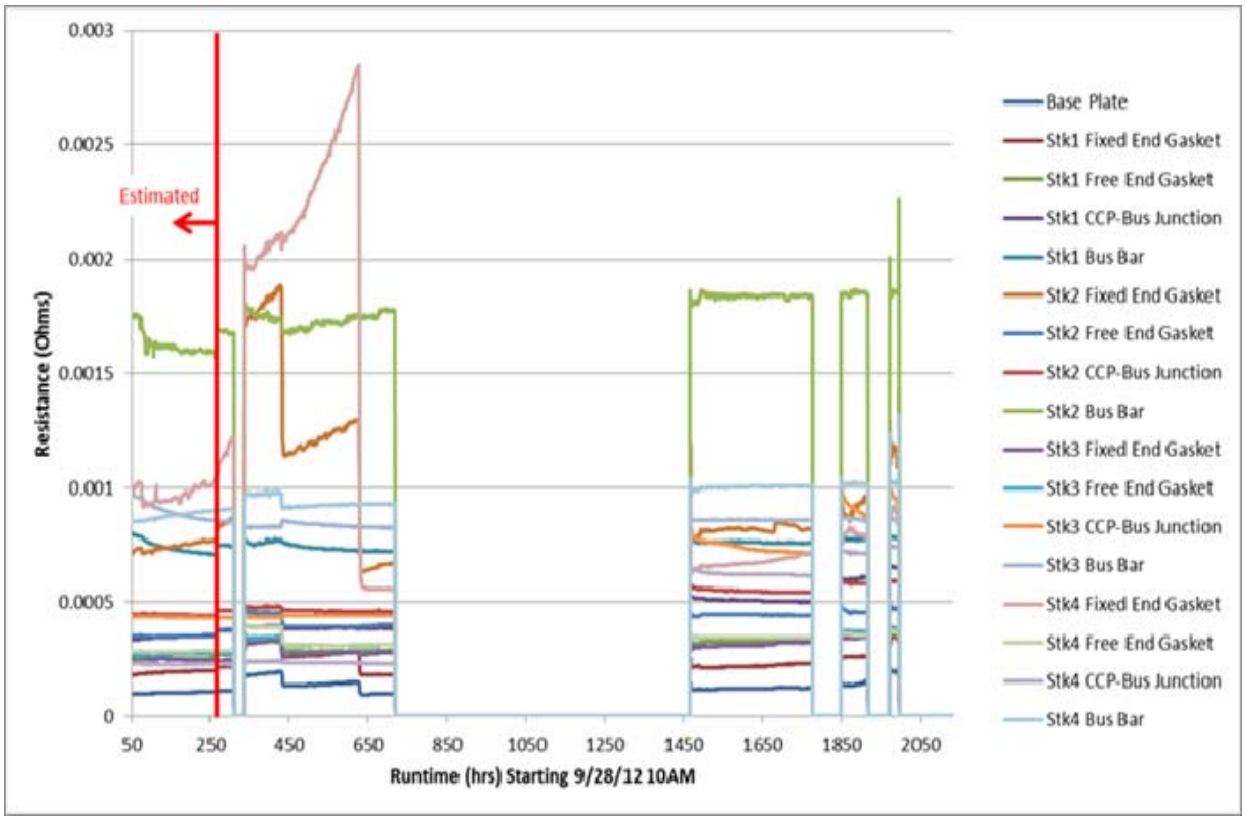

Figure 3-31 Electrical Resistance of the Conductive Stack Gasket, Bus Bar, and Base Plate Components during 60 kW Module Test

From Figure 3-31, it can be seen that the electrical resistance for many of the buss components remained stable, although it also increased for some components. The highest peak was the fixed end gasket on Stack 4, which increased (from the beginning of testing) to almost 0.003 Ω. The sharp drop in resistance occurred as the pressure bias in the system was adjusted from 'cathode pressure greater than anode pressure' mode to 'anode pressure greater than cathode pressure' mode at 640 hours runtime. This result indicates that the gaskets potentially became reversibly oxidized and once the oxidant leakage was decreased, the oxidized gasket was reduced back to a lower resistance state.

Overall, the 60 kW stack module tests showed the importance of system control and off-design operating conditions on the longevity and dynamic performance of the stacks. The root cause of performance degradation was not related to the module configuration, but rather to the operation of the facility. Therefore, through this testing, the quad-base module configuration was validated and lessons were learned to minimize stack damage in the future.

16-Cell Stack (3 kW) Tests at FCE (Danbury): Sixteen-cell (550 cm^2 cell active area) short stack tests were conducted at FCE to study the effect of key system operating parameters on stack performance and endurance in a modular environment. Modifications of the 30 kW test facility (where the Stack Tower Test was performed) to prepare it for testing of 16-cell stacks were carried out. Many modifications were required to operate an SOFC stack more than an order of magnitude smaller in size and power output. Figure 3-32 shows a picture of the facility with the 16-cell stack size module installed.

Figure 3-32 Modified 30 kW Facility with a 16-cell Stack Module Installed for Testing

Once the major facility modifications were completed, a facility checkout procedure was performed along with modifications to the HMI (Human Machine Interface) and data acquisition system.

A 16-cell stack test was conducted initially to validate the modifications to the SOFC test facility and the new test module, including the conductive gasket used for current collection through the supporting manifold base plate. The stack performed well, and further testing was performed on the stack beyond validation of the test fixtures. The test results are discussed below.

A variety of tests were performed evaluating various fuel and oxidant conditions, as well as different heat-up procedures. A chart showing the power output of the stack is included in Figure 3-33.

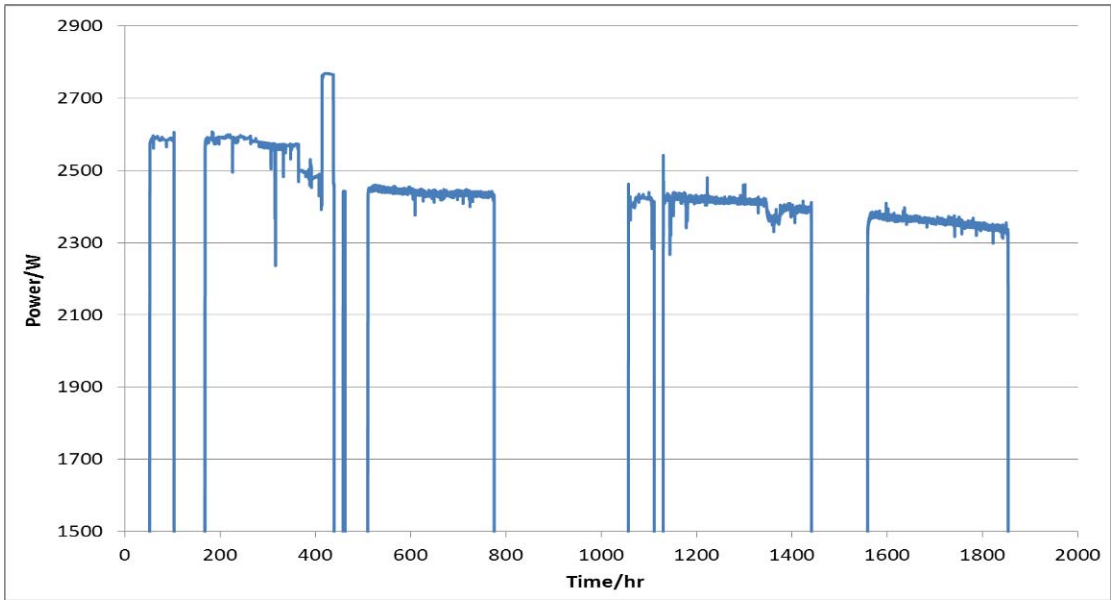

Figure 3-33 Power Output of the 16-cell Stack during Testing History

Tests performed on this stack were focused on understanding the effects of system gases on the performance of the cells. Variances in the simulated anode recycle ratio, per pass fuel utilization and air utilization were evaluated via on-load electrochemical testing of the 16 cell stack. Additionally, heat-up scenarios that would be encountered in a field test/operation were tested, as compared to a laboratory style heat up, i.e., cover gas approximating simulated reformed natural gas was used in lieu of a N_2/H_2 blend, which is typically not available outside of testing laboratories.

Table 3-3 Fuel (Anode) Recycle Ratio Test Conditions

Anode Recycle, %	Anode-In Gas Composition, mole%				Total Anode-In Flow Rate, SCFM (SLPM)
	H_2O	CO_2	CH_4	H_2	
66.8	**33.0%**	**30.7%**	**11.4%**	**25.0%**	**1.76 (49.8)**
64.3	**32.1%**	**30.3%**	**12.7%**	**24.8%**	**1.65 (46.7)**
61.8	30.9%	29.5%	14.8%	24.8%	1.49 (42.2)
59.3	32.4%	28.2%	16.2%	23.2%	1.42 (40.2)

Two tests were performed to determine the effects of fuel parameter variations on voltage and on-cell temperatures. The first evaluated a series of compositions, simulating a variance in anode recycle, albeit at a constant per pass fuel utilization. A summary of the resultant gas composition and the correlating recycle rate is shown in Table 3-3. The primary effect of this variance is an increase in methane fed to the stack (with decrease in anode recycle), and a resulting decrease in steam to carbon ratio and an increase in % DIR (in-stack reforming). The steam feed for the lowest recycle rate case was adjusted from the process simulation values to maintain a minimum steam to carbon of 2.

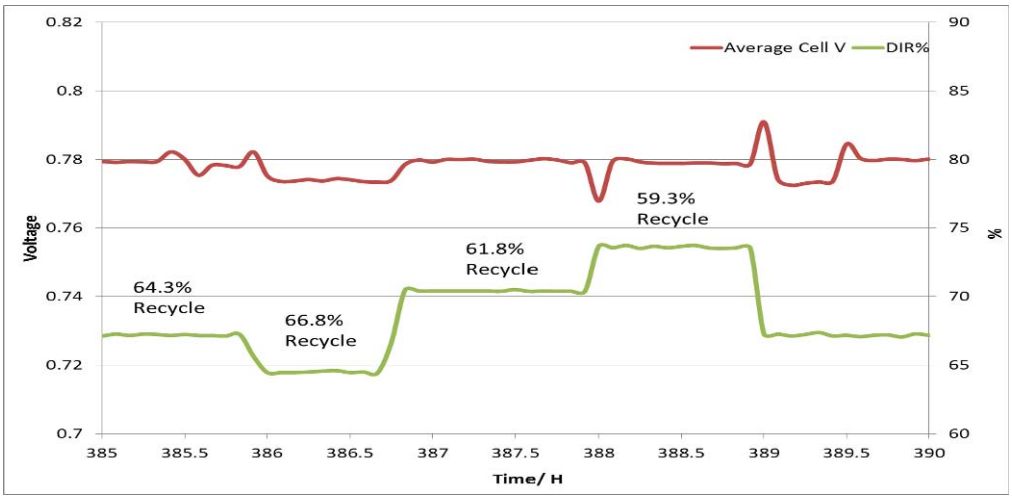

Figure 3-34 Anode Recycle Ratio Test Results

The stack voltage response to the variance in fuel condition is illustrated in Figure 3-34, along with the effect of the fuel variance on % DIR (in-stack reforming). Stack output remained fairly constant throughout this test, and was influenced more by thermal effects caused by the increased DIR, than it was by the fuel composition. This is best illustrated by the hysteresis observed for the baseline 64.3% recycle rate condition. By comparing the stack output for the

initial 64.3% anode recycle period shown in the graph, with that upon return to 64.3% recycle at 389 hours. The performance gain from the reduced recycle rate is offset by stack cooling. It was determined from this test that the 64.3% recycle rate is appropriate for testing and system simulations.

A further demonstration of the thermal effects caused by variance in the recycle rate is illustrated in Figure 3-35, based on temperatures measured during this test. The figure shows on-cell temperature maps for 59% and 66% anode recycle conditions. The temperature scales are in °C. As illustrated by the 59% recycle chart (on left), the higher DIR associated with lower recycle rates resulted in lower on cell temperature, and increased temperature differentials (ΔTs), as expected. The increased ΔT was caused by reduction in temperature at the anode inlet-cathode inlet corner.

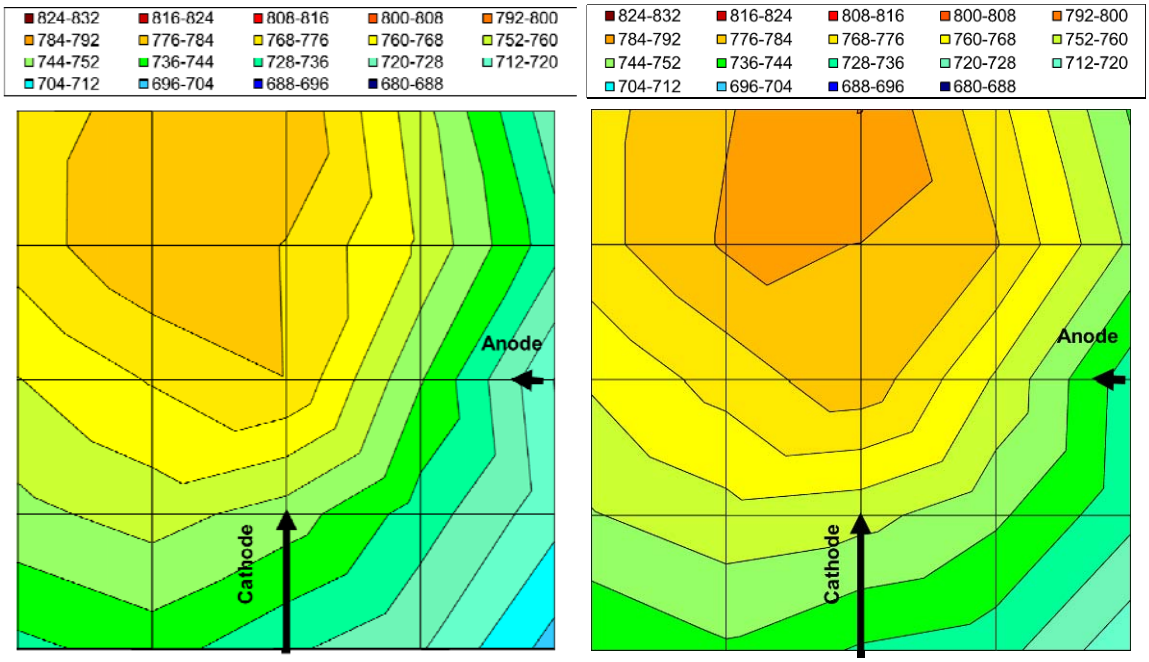

Figure 3-35 On-Cell Temperature Maps for 59% (Left) and 66% (Right) Anode Recycle Ratio Conditions

The fuel recycle rate study was followed by a study of the effect of fuel utilization. The components of the anode feed were varied (in flow rate) proportionally to achieve a range of utilizations, albeit at a constant inlet composition. Fuel utilization (Uf) conditions of 62%, 65%, 71% and 74% were evaluated, along with the 68% baseline condition. As with the recycle ratio test, it was demonstrated that the thermal effects of increased on-cell reforming dominate the effect of additional fuel. Increase in performance was observed during the extended hold at 68% Uf (shown in Figure 3-36), beginning around 391.5 hours, following the low utilization test. The cell voltage increased gradually as the average stack temperature recovered from the low levels caused by the higher cooling from the increased internal reforming during the low utilization test.

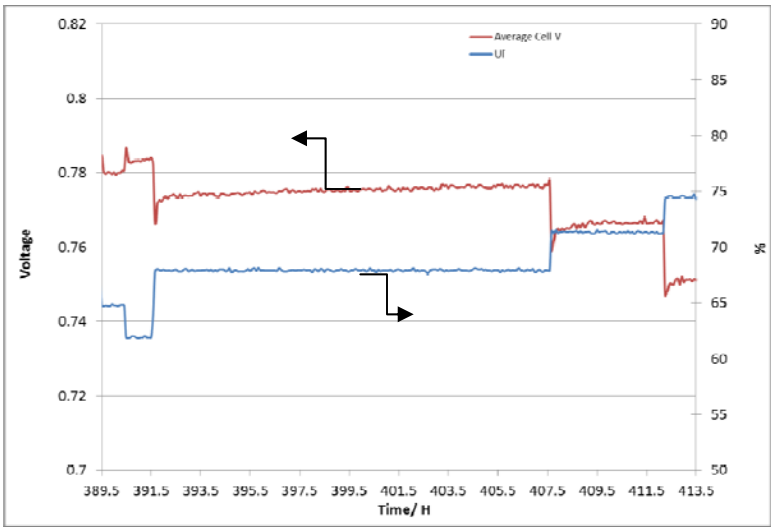

Figure 3-36 Fuel Utilization Test Results

It is anticipated that appropriate varied preheating of inlet gases at the lower utilizations would increase marginally higher performance above that reported in the figure, however this test demonstrated that 68% per pass Uf is appropriate for further testing and system simulation. The penalties observed for the higher utilizations demonstrate that the 68% baseline is approaching the optimal per pass fuel utilization as well. The thermal effects of the test, observed via on-cell temperature measurements were in line with expectations and similar to those observed for the anode recycle ratio tests. Figure 3-37 shows thermal maps for the high and low utilization conditions. The increased internal reforming resulted in higher temperature gradients by reducing the lowest temperature, at the anode in-cathode in corner.

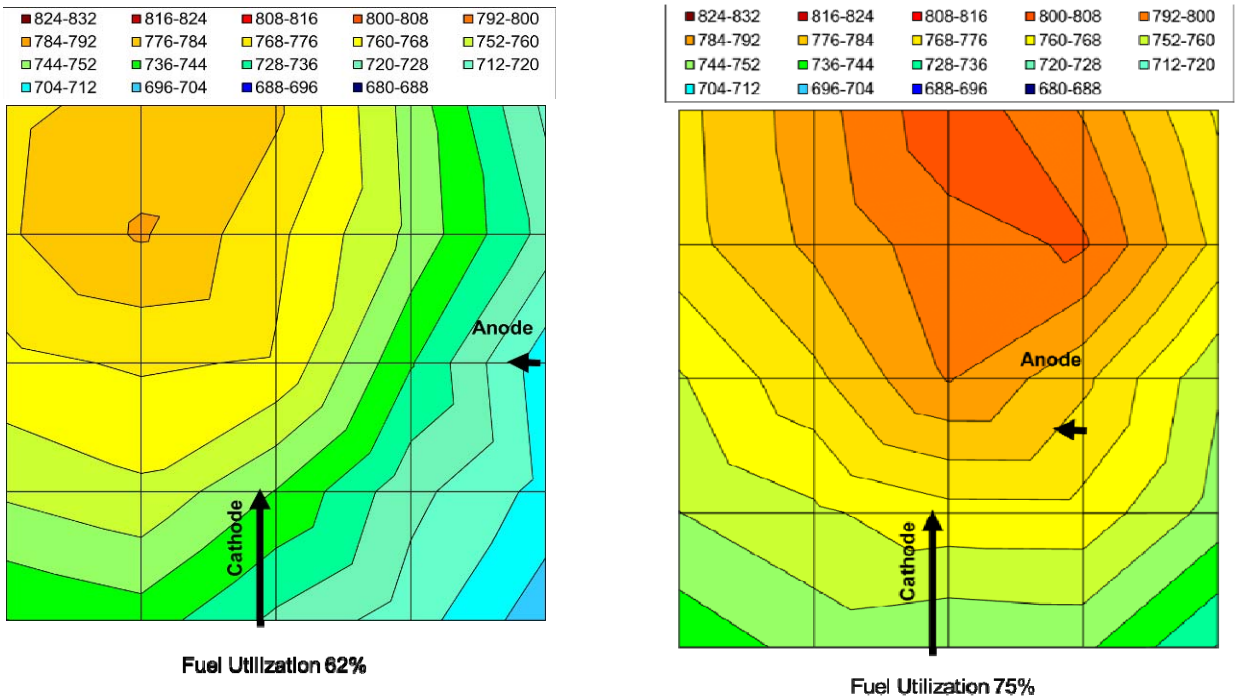

Figure 3-37 On-Cell Temperature Maps for 62% (Left) and 75% (Right) Fuel Utilization Conditions

Tests evaluating thermal effects of air utilization levels were also performed on this stack. While under operation, stack air utilization was adjusted up from 13.5% to 25%. Module inlet temperature was adjusted downwards as well during this time, to maintain a similar temperature at the entrance to the stack. Performance losses from increased air utilization were minimal, and were eclipsed slightly by a performance boost from cell operating temperature effect. Temperature gradients were very similar in this test, in terms of absolute difference between the hottest and the coolest locations, however the location of the hottest measured temperature moved from the cathode out edge to the center of the stack at higher utilization. This was due to the increased external cooling, resulting from a cooler module inlet temperature and longer residence time of incoming cathode air in the module before entering the stack manifold. This effect caused the temperature gradient, in terms of degrees per unit length, to be higher than for the low air utilization case, despite the difference between the minimum and the maximum remaining very close. This is illustrated in the temperature maps of Figure 3-38.

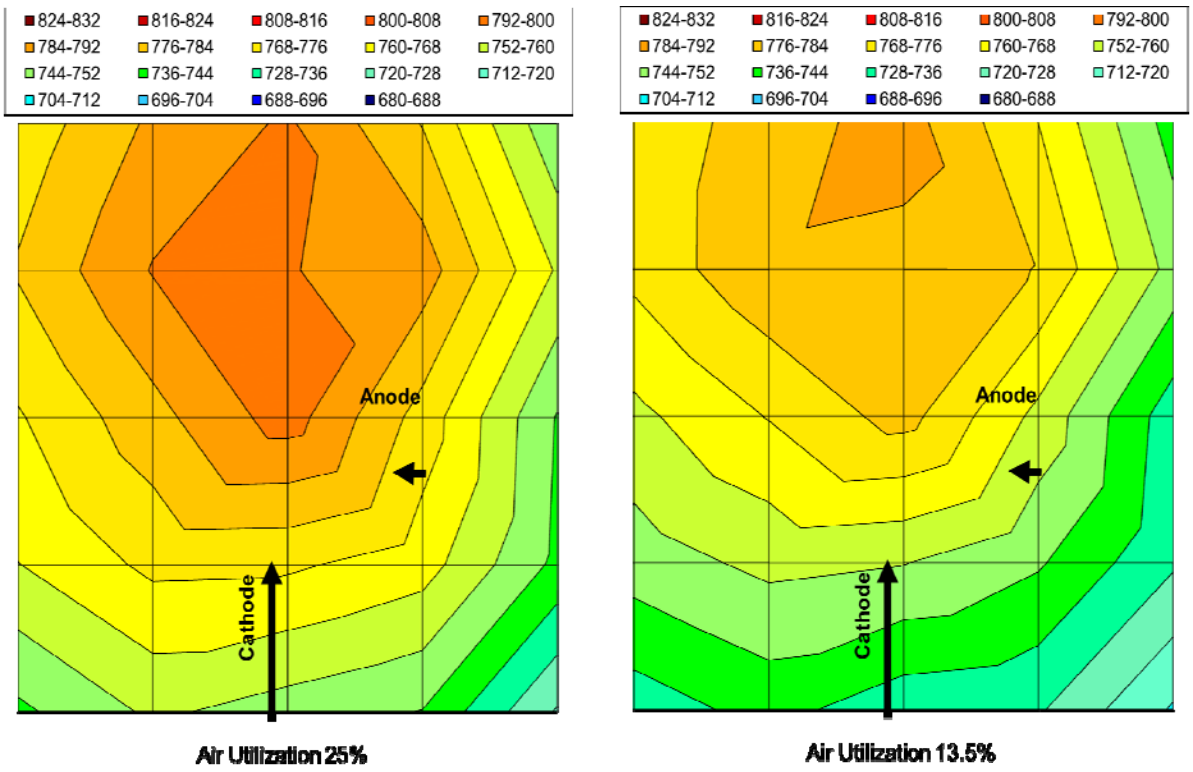

Figure 3-38 On-Cell Temperature Maps for 25% (Left) and 13.5% (Right) Air Utilization Conditions (Temperature Contours in °C)

In another 16-cell stack test (Test SO-3-03), a system-style stack heat-up procedure was evaluated. The stack was initially started using laboratory-style anode cover gas (to provide baseline for comparison), a blend of 96% N_2 - 4% H_2, and followed by on-load testing. The electrical load was then removed and the stack was thermal cycled to a temperature below 100°C, and re-heated using a cover gas expected to be used in a field system. The cover gas consisted of nitrogen from 200 to 425°C, and a blend of CO_2, H_2, H_2O and low concentration of CH_4 (to be representative of a high-recycle, reformed natural gas feed). There was no obvious loss to performance by heating the stack in this manner, as shown by Figure 3-39.

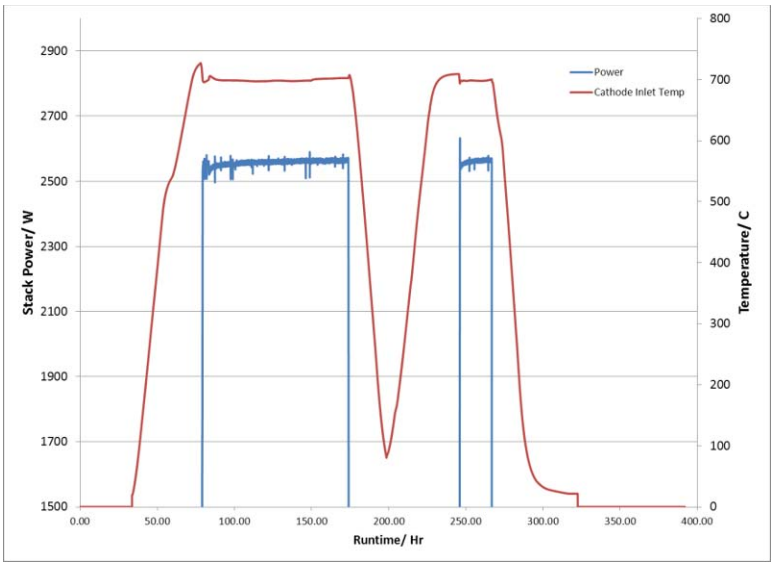

Figure 3-39 Stack Performance Before and After System-style Heat-up (SO-3-03 Test)

A 16-cell (550 cm^2 cell active area) stack test was conducted to examine what effect endothermic direct internal reforming (DIR) of methane has on cell and stack performance and endurance. It is hypothesized that high levels of DIR cause higher rates of degradation by increasing the in-cell temperature differential. Testing began by evaluating the stack at 386 mA/cm^2, 25% DIR, 61% fuel utilization (Uf), 13% air utilization (Ua), conditions (matching to those used in VPS Calgary facility when the stack was commissioned). Compared to the VPS data, the average cell voltage (excluding cell 16) measured was 6.5 mV lower, which is reasonable considering that the stack underwent a thermal cycle (before shipment), shipment from VPS to FCE, and was being operated in a different facility. Cell 16 (the fixed-end cell) experienced a decrease of nearly 150 mV. Once this baseline characterization was completed, the stack was tested at Low DIR condition (200 mA/cm^2, 11% DIR, 68.5% Uf, 15% Ua) for 1000 hours. The stack testing was then switched to High DIR condition (200 mA/cm^2, 68% DIR, 68.5% Uf, 15% Ua). The High DIR condition testing continued for 300 hours. The Low DIR condition was then restored for another 250 hours before finally terminating the test. The stack performance (and sequence of events) can be seen in Figure 3-40 with the average cell voltage in red, the average cell voltage excluding cell 16 in green and the current in blue. Although cell 16 had a lower cell voltage, it did not degrade at a faster rate than the rest of the stack.

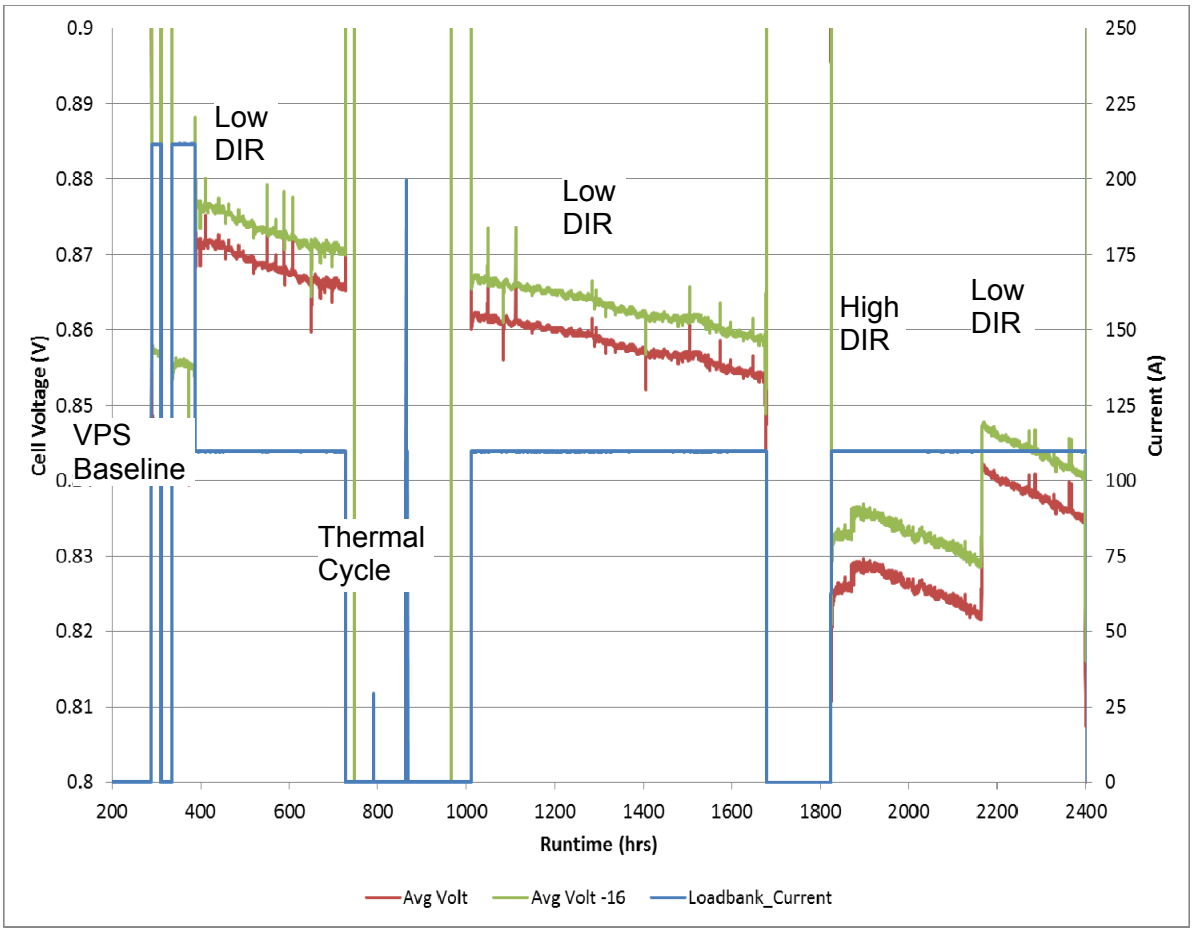

Figure 3-40 16-Cell Stack Testing at Low and High DIR (In-stack Reforming) Conditions

The Low DIR condition period of 1000 h was interrupted by a thermal cycle due to facility shutdown. Figure 3-41 shows the individual cell voltages at the end of the 1000 hour Low DIR evaluation period along with the degradation rates during the steady state hold after the thermal cycle. The blue bars represent the voltage, shown on the left y-axis, while the red bars represent the degradation rate in mV/1000 hours, shown on the right y-axis. The chart titles refer to the test condition along with the period of runtime for which the degradation rate was calculated over. The voltages correspond to the end of the time period. At the Low DIR condition, the average degradation rate was around 13 mV/1000 hours (1.5%/1000 hrs). The figure confirms that cell 16 was not degrading faster than average.

Test results from the High DIR evaluation period are also included in Figure 3-41. The stack experienced a decrease in average cell voltage of ~25 mV during the transition from Low to High DIR condition (the current density and fuel and air utilizations were held constant between the two conditions). The degradation rate increased from 13 mV/1000 hours at the Low DIR condition to 23 mV/1000 hours at High DIR condition.

The stack was returned to the Low DIR condition (after 300 h) to see if it would recover back to where it had been prior to High DIR testing. Once the stack stabilized at the final Low DIR condition, it could be seen (Figure 3-41) that the average cell voltage was 13.6 mV lower than it was when previously at the Low DIR condition. In addition, the voltage degradation rate continued to increase to 28 mV/1000 hours.

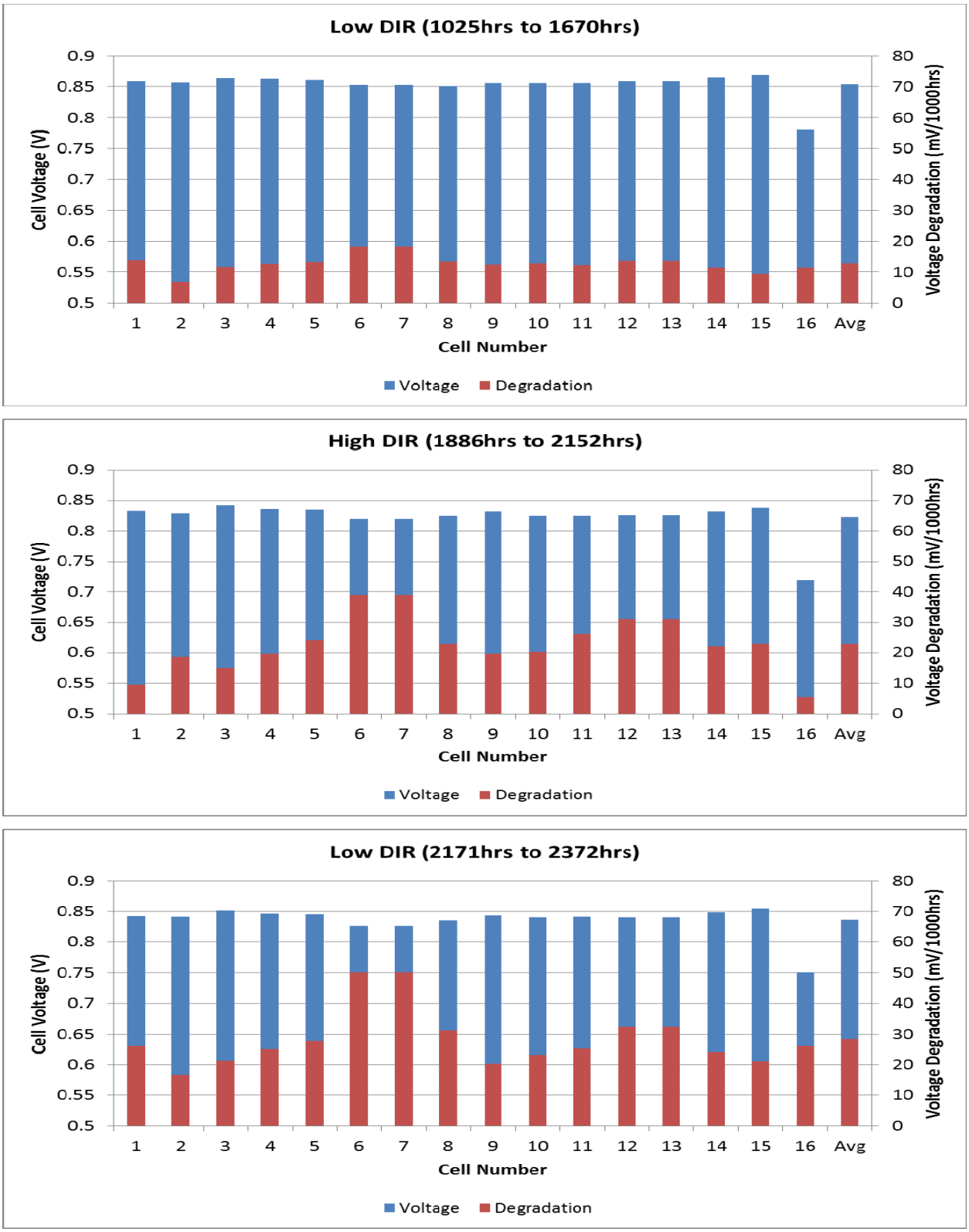

Figure 3-41 Individual Cell Voltages and Degradation Rates at Low and High DIR Conditions During 16-cell Stack Test

From these bar graphs, it can be seen that nearly all cells experienced an increase in performance degradation rate, with cells 6 and 7 experiencing the highest increase. Figure 3-42 shows the difference between individual cell voltages and the stack average. Although the performance weakened significantly once the High DIR condition started, it is clear from the Low DIR (1025 h to 1670 h) period in the chart that these cells were already beginning to drop out. It is therefore inconclusive whether the high rate of degradation was caused by the High DIR condition or whether the stack happened to be at the High DIR condition at the time the degradation began to accelerate.

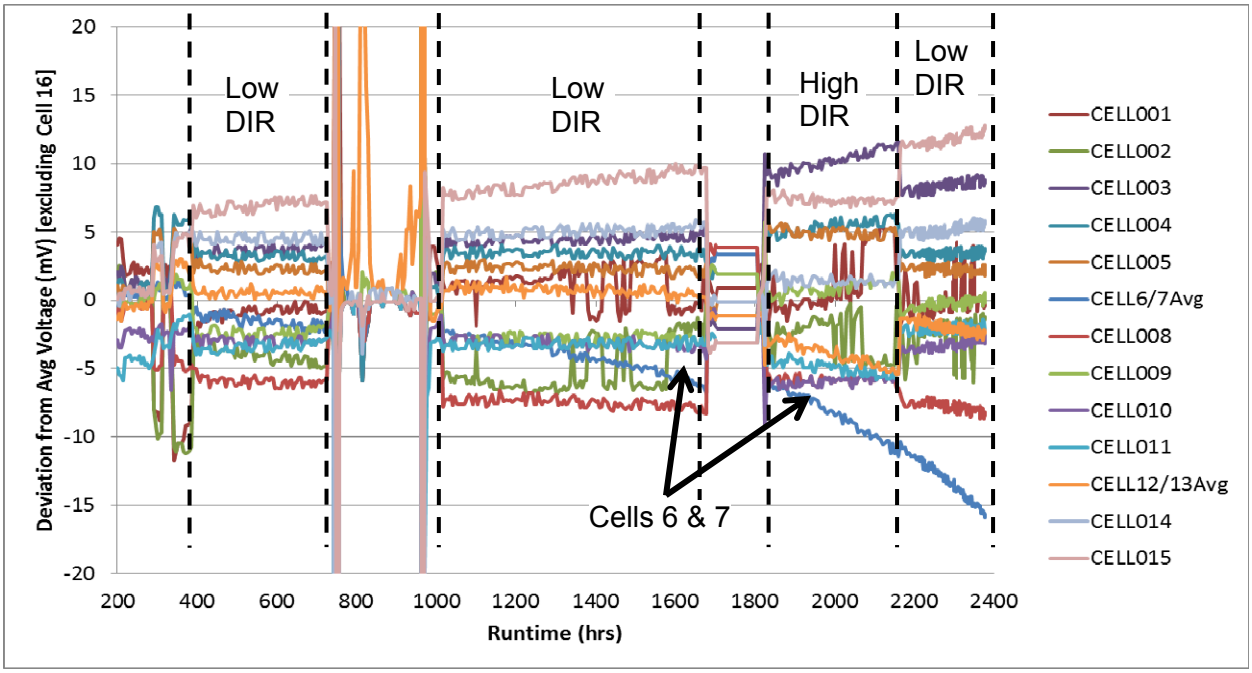

Figure 3-42 Difference Between Individual Cell Voltages and Stack Average Cell Voltage

Cells 6 and 7 experienced “voltage sharing” from the beginning of testing, which means that their voltage measurement leads were shorted together. This caused one of the voltages to increase while the other decrease by the same amount. In the figure, Cells 6 and 7 are averaged together, since the sum of their voltages is more representative than their individual readings. The average cell voltage was calculated excluding Cell 16. A positive deviation from average refers to a cell that is performing better than average.

In addition to differences in cell voltage, each testing condition resulted in a unique in-cell temperature profile, as shown in Figure 3-43. The temperature numbers in the figure are in °C.

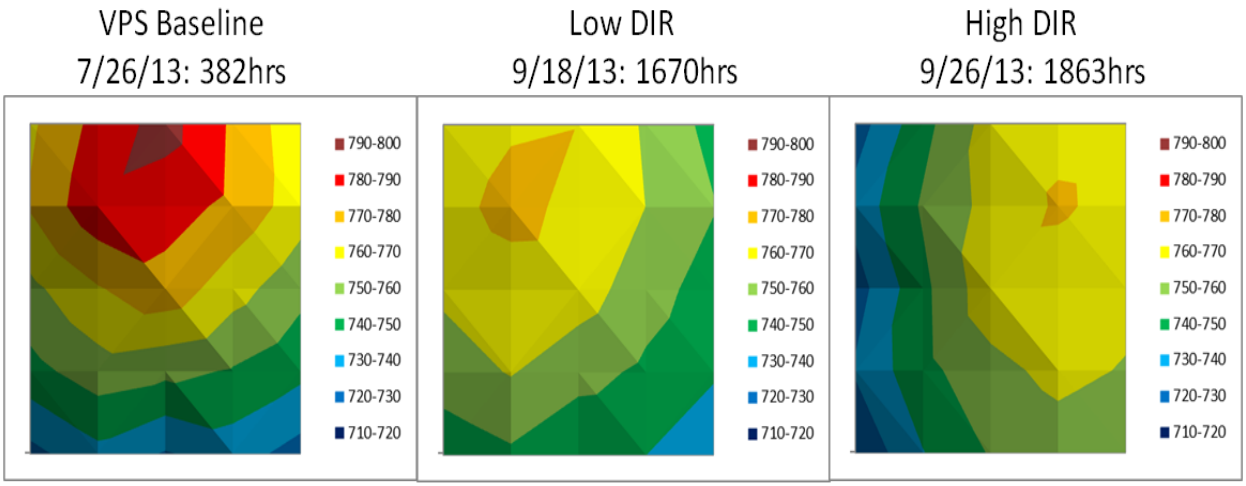

Figure 3-43 Effect of In-stack Reforming Level (DIR) on Center-Cell Temperature Profile (Anode Inlet Face is on left, Cathode Outlet Face is at Top)

The stack at VPS baseline condition showed higher temperatures due to the higher current density. It can be seen that the hot spot is near the center of the cathode outlet (top) face. The hot spot moved closer to the anode inlet (left) in the Low DIR condition and moved closer to the anode outlet (right) in the High DIR condition, due to the varying levels of endothermic methane reforming. It is clear that the higher DIR level decreases the voltage and results in higher in-cell temperature differentials.

4.0 BASELINE POWER PLANT SYSTEM DEVELOPMENT

(FCE Technical lead, support from VPS)

4.1 Baseline System Conceptual Design and Plant Layout

Effort during Phase I was focused on the development of a utility scale, high efficiency baseline coal gasification / SOFC power plant which utilized commercially-available balance-of-plant equipment. As part of the development process, commercially available gasifiers were evaluated relative to metrics that supported carbon separation requirements, cold gas efficiency, auxiliary energy requirements, etc. [4]. In addition, commercially available gas clean-up technologies were evaluated with relation to the type of gasification process they most synergistically supported. Various process configurations were developed and evaluated that included: anode recycle alternatives, cathode recycle alternatives, various turbine configurations, and high temperature blower and high temperature heat exchanger configurations. Conceptual designs for two baseline power plant configurations were developed. These configurations were designated as Configurations A1 and B. Configuration A1 integrated an indirectly fired gas turbine (IFGT) into the cathode air supply, while Configuration B was a simplified system without a gas turbine. Both Configurations had identical gasification and syngas processing islands. Figure 4-1 presents a simplified process flow diagram for Configuration B system, as an example. Preliminary cost analysis was also performed for the two systems. Key design features of the commercial scale Gasification / SOFC systems for baseline power plants are presented in Table 4-1.

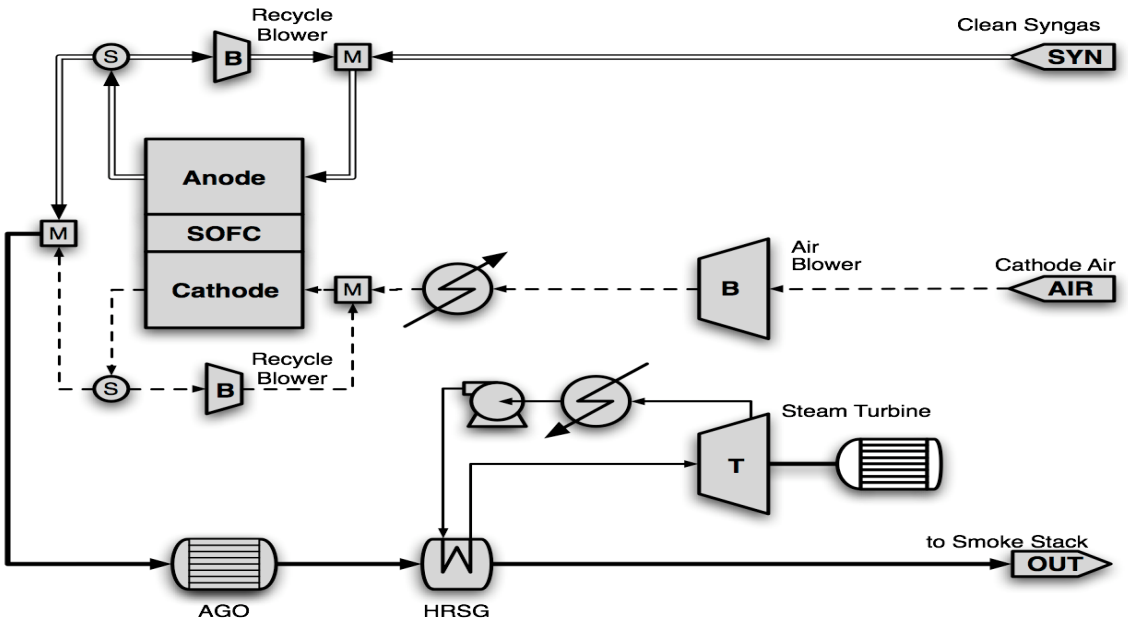

Figure 4-1 Configuration B System Featuring Steam Turbine

Table 4-1 Baseline Commercial Gasification / SOFC System Summary

Parameter	Units	Configuration A1	Configuration B
Output			
Gross Electric Power (ISO conditions)	MW	485	483
Net Electric Power (ISO conditions)	MW	424	408
Net Efficiency (coal Higher Heating Value (HHV) to AC power)	%	44	42
CO_2 Captured (based on C in syngas)	%	90.2	90.2
Consumables			
Coal, bituminous 10% AF moisture	TPD	3,500 (3,175 Tonne/d)	3,500
Oxygen, 95 mol%	TPD	2,490 (2,259 Tonne/d)	2,490
Water, deionized	GPM	4,000 (15,140 LPM)	4,000
System Configuration			
Gasifier		ConocoPhillips, 3500 TPD	ConocoPhillips, 3500 TPD
Acid Gas Removal		Selexol, double stage physical absorption	Selexol, double stage physical absorption
IFGT System		5 compressors, 4 HXs, 4 expanders, 19 MW Net	None
Steam Turbine		One unit (43.7 MW)	One unit (60.4 MW)

Development of the preliminary design of an advanced catalytic gasification / SOFC system was also initiated in Phase I. A Block Flow Diagram, heat and material balance, and performance summary were generated for a conceptual SOFC system, based on catalytic gasification. Preliminary results indicated that 56% system efficiency (coal HHV to AC power) can be achieved. Advanced baseline system configuration development was continued in Phase II. The baseline system employed catalytic gasification and warm gas cleanup technology to provide coal syngas fuel for SOFC.

The baseline power plant system simulations and analyses continued to guide the system development in Phase II. Alternate configurations for the system utilizing Warm Gas Cleanup (WGCU) process in conjunction with Direct Sulfur Recovery Process (DSRP), and WGCU in conjunction with Flue Gas Desulfurization (FGD) were evaluated. The FGD option was incorporated in the system as it offered higher system electrical efficiency. The system further employs oxy-combustion of the anode exhaust for CO_2 capture using a portion of the oxygen from the air separation unit at the gasification site. Figure 4-2 presents the block flow diagram for the Baseline Power Plant system [5]. An Excel-based SOFC performance model was developed to replace the simplified model of Phase I. The detailed model allowed the computation of cell voltage based on cell material properties and system conditions. The model was validated with cell test results at Phase II system conditions. The SOFC operating conditions (current density, fuel utilization, gas stream temperatures, etc.) were revised for simulations, based on the latest stack test results. These changes lowered the system electrical efficiency to 50% (based on higher heating value of coal). After a comprehensive system optimization effort, the system efficiency was restored to ~59%. The optimization included modification of subsystem operating conditions and updating of equipment performance parameters/assumptions. Figure 4-3 highlights the system development progress in Phase II.

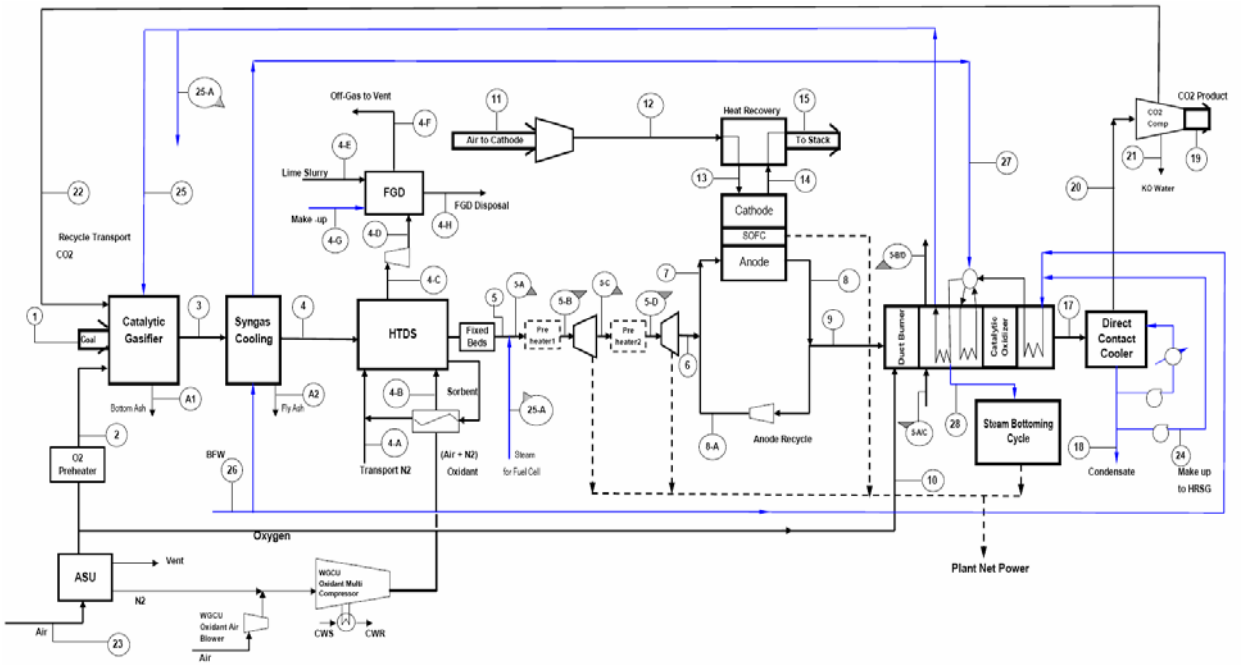

Figure 4-2 Block Flow Diagram for Integrated Gasification Fuel Cell (IGFC) Baseline Power Plant

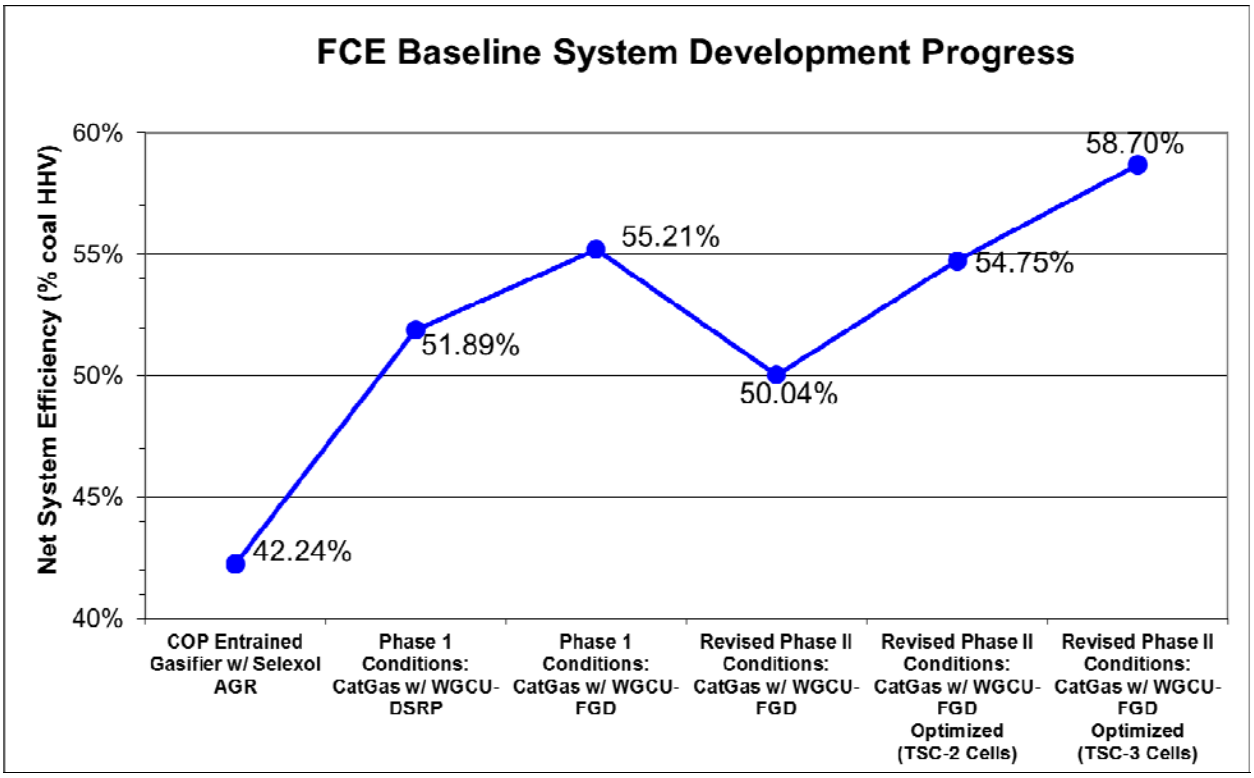

Figure 4-3 Baseline System Development Progress in Phase II

System analyses effort for the Baseline Power Plant system also focused on defining normal operating conditions (NOC) and peak power conditions (PPC), and evaluating the corresponding system/plant performance. At the NOC conditions selected for high efficiency (400 mA/cm^2), a system electrical efficiency of 58.7% was estimated. Table 4-2 summarizes the Baseline Power Plant performance at NOC operating conditions, based on system simulation results. This is while the system captures >99% of carbon (as CO_2) in syngas. The fuel cell performance was based on TSC-3 cell technology. The system process models developed provided the input required for the end-of-phase (Phase II) DOE-approved metric test plan, and also the fuel cell power island factory cost estimate work.

Water balances were generated to analyze the Baseline system water usage. The water consumption of the Integrated Gasification Fuel Cell (IGFC) system was compared to that of the competing technologies such as Integrated Gasification Combined Cycle (IGCC) and Pulverized Coal Boiler Steam Cycle (PC) power plants. The SOFC system consumes 75% less water compared to PC plants using scrubbing technology for carbon capture. The IGFC systems have significantly less water consumption because of their higher system efficiency.

A conceptual layout of the Baseline plant (general arrangement of the power island) was developed. Figure 4-4 shows the layout. The layout included eight sections, each with 42 fuel cell modules. The SOFC module sections were grouped with four sections on each side of the centralized power island equipment. The centrally located equipment included syngas expander, oxy-combustor, heat recovery steam generator (HRSG) and steam turbine. Piping from the centralized system equipment to the fuel cell modules was located between groups of fuel cell clusters. Clean syngas is distributed and anode exhaust is collected by the centralized power island equipment. The footprint of the IGFC plant was found to be slightly smaller (5.5 acres or 22,407 m^2) than a comparable IGCC plant (5.6 acres or 22,814 m^2).

Table 4-2 SOFC Power Plant Performance Summary – Normal Operating Conditions

POWER GENERATION SUMMARY	kW	% Q input	% MW gross
Fuel Gas Expandors Gross Power @ 20 kV	49,750	*7.04%*	*10.96%*
Fuel Cell Inverter AC Gross Power @ 20 kV (0.818V, 400mA/cm2)	362,134	*51.28%*	*79.78%*
WGCU Off Gas Expander Gross Power @ 20 kV	7,024	*0.99%*	*1.55%*
Steam Turbine Gross Power at Generator Terminals @ 20 kV,	35,019	*4.96%*	*7.71%*
Total Gross Power Generation @ 20 kV	453,927	*64.27%*	*100.00%*
ASU (including air and production compression)	11,977	*1.70%*	*2.64%*
Gasification: Coal Prep, Recycle Compressor	1,495	*0.21%*	*0.33%*
WGCU Blower & Compressor	902	*0.13%*	*0.20%*
WGCU Oxidant Compressor	7,505	*1.06%*	*1.65%*
FGD Pumps, Agitators, and Lime Handling	2,441	*0.35%*	*0.54%*
Cathode Air Blowers	9,059	*1.28%*	*2.00%*
Anode FG Recycle Blowers	1,873	*0.27%*	*0.41%*
Steam Turbine Cycle Auxiliaries (BFP, CT, CWP)	3,200	*0.45%*	*0.70%*
Miscellaneous Loads	74	*0.01%*	*0.02%*
Transformer Losses	817	*0.12%*	*0.18%*
Total Auxiliary Load	39,342	*5.57%*	*8.67%*
Net Power Output at 345 kV	***414,585***	***58.70%***	***91.33%***

Net Efficiency Excluding CO_2 Compression & Thermal Input

Coal feed, lb/h	202,980		
Coal HHV (AF), Btu/lb	11,872		
Coal Thermal Input, kWth	706,255	*100.00%*	*155.59%*
Net Plant Efficiency (HHV)	**58.70%**		

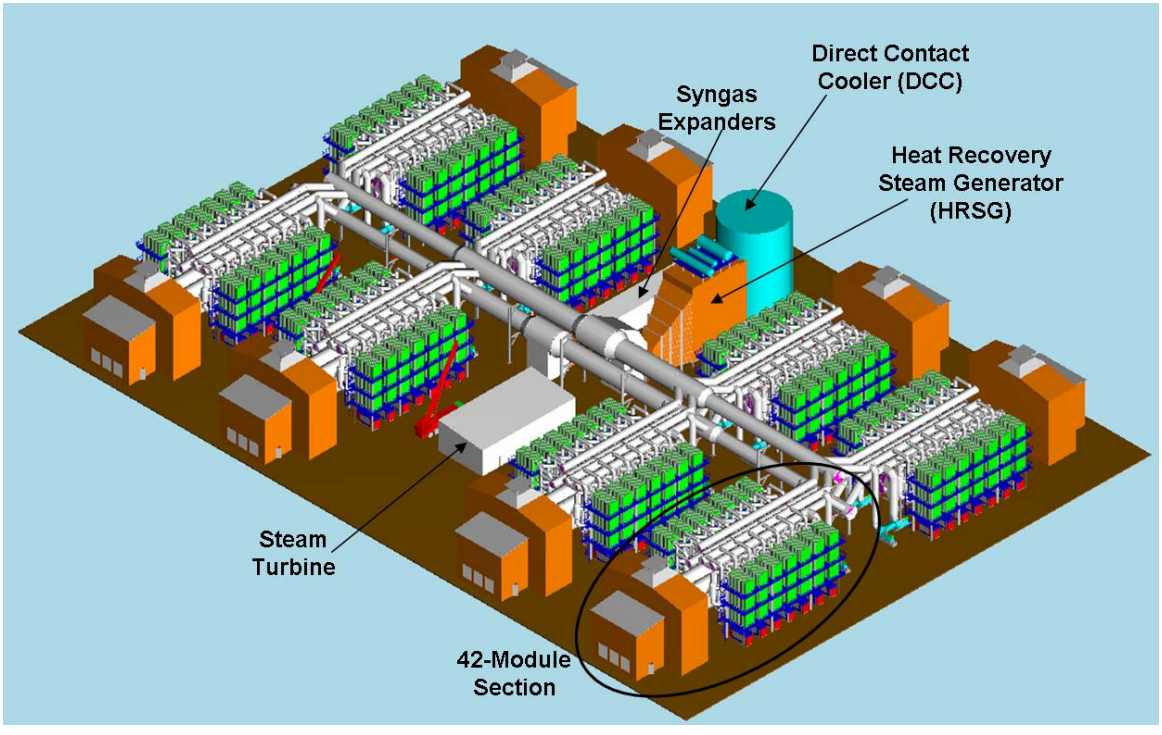

Figure 4-4 Power Island Layout for Coal-Based SOFC Baseline Power Plant

4.2 IGFC Power Island Factory Cost Estimate

Factory cost analysis was completed near the end of Phase I. Phase I SOFC stack cost was estimated to be $197/kW and the power island (for Baseline Power Plant) Factory Equipment Cost was estimated to be $597/kW. The estimates are in Year 2002 US dollars (USD) and assume a production rate of two power plants per year. Both costs were lower than SECA project Phase I targets of 225 $/kW and 600 $/kW for stack cost and power island Factory Equipment Cost, respectively. The power island factory equipment cost was based on advanced catalytic gasification - SOFC system configuration and MW-scale SOFC module concept. The Baseline Power Plant system was estimated to generate 526.6 MW of power at net electrical efficiency of 51.9% (based on coal HHV). Figure 4-5 shows a conceptual design developed for the 1 MW SOFC power module. The module consisted of 20 SOFC stack towers. Each stack tower was comprised of five 10 kW stack building blocks. Each building block was comprised of 64 cells with 550 cm^2 of active cell area. This design utilized a manifolding concept where the cathode inlet face of the stack was open to the vessel interior. This arrangement simplified the piping and ducting designs and was a cost effective approach to providing air to the towers while achieving superior thermal management. The Phase I Factory Cost Estimate Report was prepared. The report was revised based on input from the cost auditor. The report met all the DOE requirements.

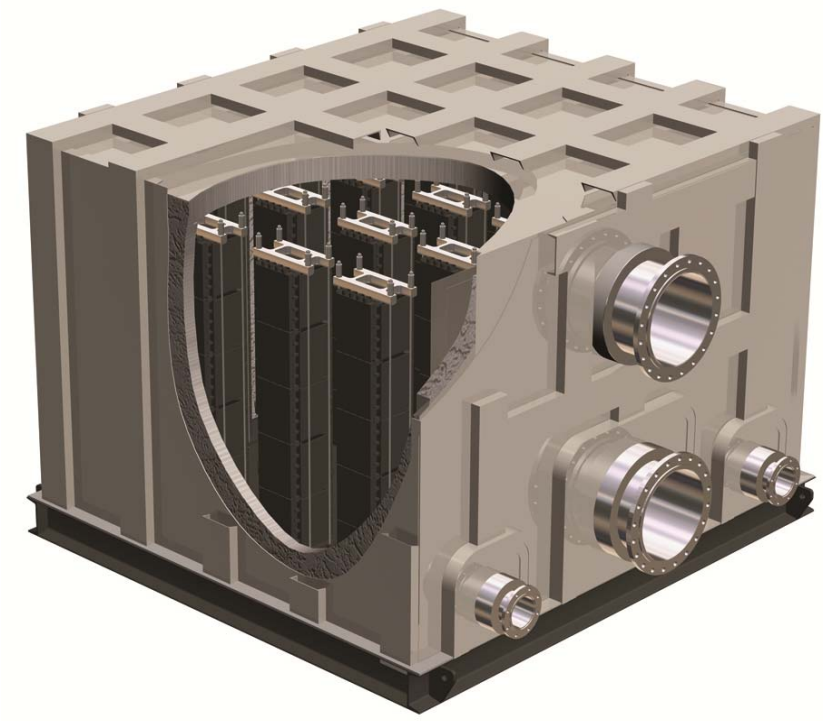

Figure 4-5 1 MW SOFC Stack Module

Cost analysis for the Phase II Factory Cost Estimate Report was performed near the end of Phase II. The SOFC stack cost was estimated to be $85/kW and the power island (IGFC plant) Factory Equipment Cost was estimated to be $371/kW ($286 balance-of-plant cost). The cost estimates are in Y2000 USD (for consistency with DOE cost targets). The cost numbers were based on a peak power output of 671,819 kW net AC and assumed an annual production level of two 671.8 MW size Baseline Power Plants per year. This required the production of 43,008

stacks (stack building blocks) per year. The peak power output estimate was derived from Aspen Plus process simulation models. The SOFC operational and performance parameters used for the system simulation were derived from metric test results. The power island layout shown earlier in Figure 4-4 and the conceptual design of compact MW-class SOFC module shown in Figure 4-6 facilitated the cost estimation. The module concept was developed to accommodate 16 stack towers arranged in a horizontal configuration to provide better thermal performance and a compact footprint. Each tower consists of four 96-cell (550 cm^2 cell active area) stack building blocks. The factory cost estimate, consistent with past SECA practice, did not include shipping, site preparation and on-site assembly. SECA project Phase II requirements of ≤$100/kW and ≤$400/kW for stack and power island costs, respectively, were met.

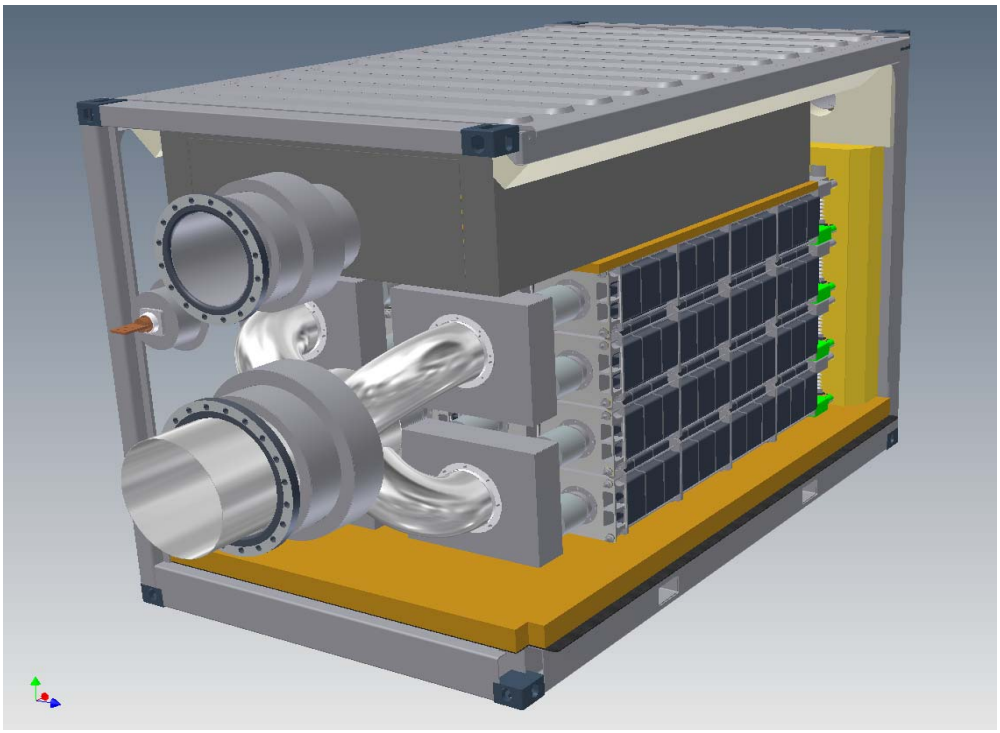

Figure 4-6 Compact MW-class SOFC Module

Figure 4-7 shows how the overall stack cost was distributed. Repeat stack components (all the components of a repeat cell unit excluding the cell and seal), which are all procured, represented the largest proportion of stack cost. Materials accounted for 78% of the total cost while labor and other costs accounted for the remaining 22%. The low labor content was due in part to the fact that only cells and seals are fabricated in-house.

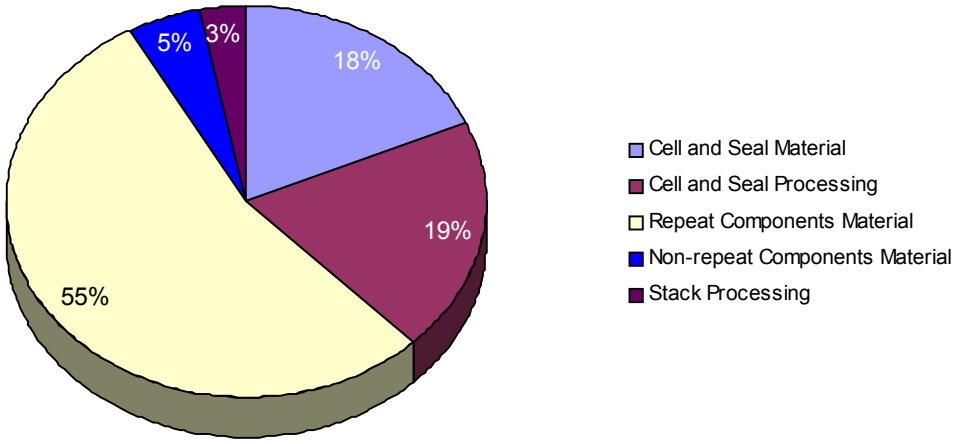

Figure 4-7 Contribution to Fuel Cell Stack Cost ($85/kW) by Functional Area

Figure 4-8 shows the distribution of stack costs by cost category. As discussed above, the procured parts group was the most significant contributor. The commodity materials group represented the raw materials that went into cell and seal fabrication.

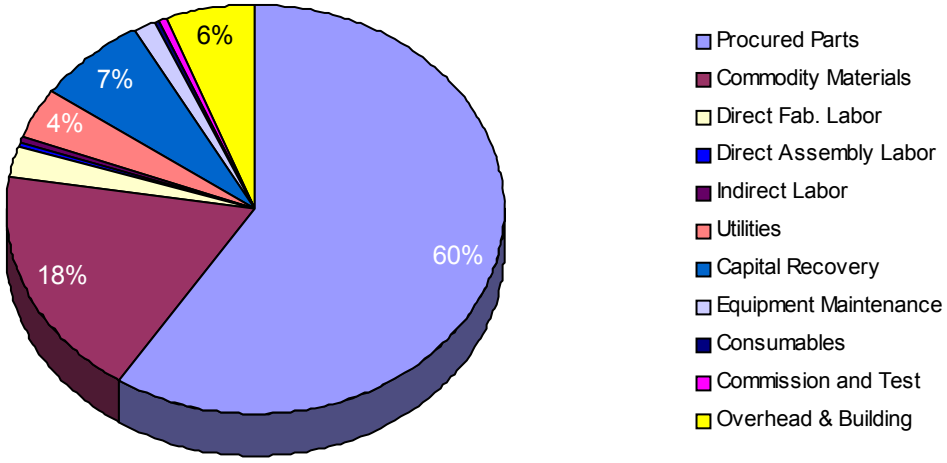

Figure 4-8 Contribution to Fuel Cell Stack Cost ($85/kW) by Cost Category

The distribution of the cost components of the balance-of-plant (BOP) equipment is shown in Figure 4-9. The results indicated that the HRSG, heat exchanger equipment, expanders, and dc-to-ac inverter costs accounted for about two thirds of the overall BOP cost.

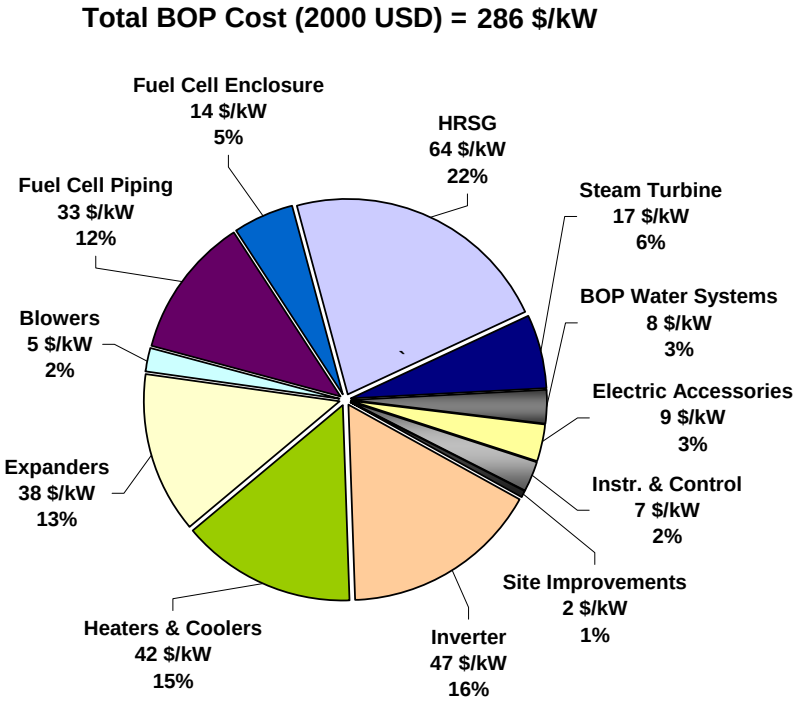

Figure 4-9 Contribution to Balance of Plant (BOP) Cost by Cost Category

The Phase II Factory Cost Estimate Report was prepared, and was reviewed by a DOE-approved auditor. The report was revised per the cost auditor's review comments. A modified approach for estimating the fuel cell module (factory equipment) cost was adopted. The final cost estimates were $85/kW (Y2000 US dollars) for SOFC stack and $372/kW for IGFC power island (factory equipment cost). Both estimates met DOE SECA Phase II requirements of $100/kW and $400/kW, respectively. The cost auditor concluded that the revised report positively met DOE's requirements.

The factory cost report was later revised to update the SOFC stack block, stack module and balance-of-plant factory equipment costs. The costs were previously expressed in Year 2000 US dollars. The updated estimates (early in Phase III) were based on Year 2007 US dollars for easy comparison with DOE's updated cost targets. The revised stack block cost estimate was $147/kW and the power island Factory Equipment Cost is $635/kW. Both costs meet the SECA Phase III requirements of $175/kW and $700/kW for stack cost and power island Factory Equipment Cost, respectively.

Figure 4-10 shows a summary of the progression of stack cost estimates developed throughout the project. The trend towards decreasing cost (accounting for dollar basis adjustments) is attributable to the previously-discussed achievements in both cell/stack design and system optimization.

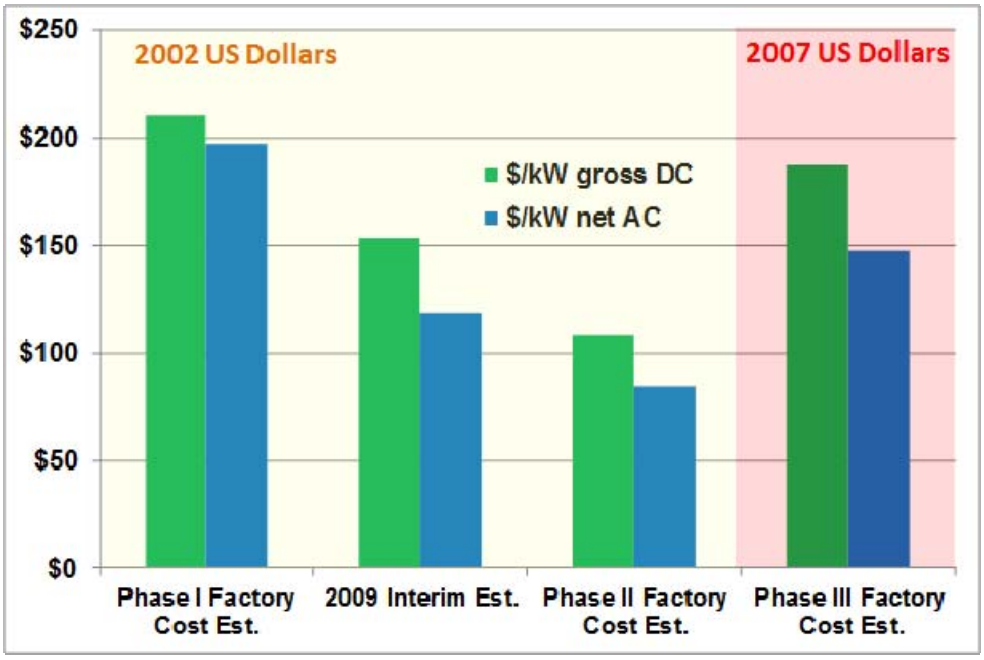

Figure 4-10 SOFC Stack Cost Reduction Progress

5.0 PROOF-OF-CONCEPT MODULE (PCM) SYSTEM DESIGN

(FCE Technical Lead, support from VPS)

5.1 Early-Stage 1-5 kW System Development

During 1998 (prior to the subject project start) through 2006, system development occurred on 1-5 kWe integrated SOFC systems. Initial work focused on a 1 kW thermally self-sustaining laboratory system. The bulk of product development and system testing focused on a steam reformation (single fuel pass, no anode recycle) system design. This system design was targeted for high efficiency, low cost markets where water was available (i.e. residential cogeneration). The RP-2 system was the first system to demonstrate significant advances in system design and configuration as well as performance. Collectively, five RP-2 natural gas fuel cell power plants operated approximately 21,500 hrs in 2002-2003 and demonstrated a peak net electrical (AC) efficiency of 31% LHV. The RP-2 design featured a cylindrical hotbox with an integrated module component (steam reformer, air pre-heat, and afterburner functionality), surrounded by 4 stack towers (see Figure 5-5).

Figure 5-1 RP-2 (Residential Prototype 2) System with Skins Attached (Left), CAD Representation of Hot Balance of Plant (Right).

Building on the RP-2 experience, a next generation Aurora design was developed that demonstrated significant advances in thermal integration, thermal management, performance and control flexibility. As shown in Figure 5-2, the Aurora configuration utilized a single 84 cell tower that is comprised of four 21-cell stack blocks. Radiative heat exchangers were integrated with the vertical faces of the stack to assist in stack thermal management and temperature control. Stack thermal management was accomplished mainly by way of radiative cooling and some internal reforming (25 to 35% in-stack reforming). In December 2003, the first 2 kW Aurora system was commissioned. A second 2 kW Aurora system was commissioned at the end of June 2004.

Figure 5-2 Photo of Complete Aurora System with Skins (left) and 84-Cell Stack Tower and Integrated Module (Rad HX removed) (right)

Figure 5-3 Picture of 3-1 SOFC System Module

The 3-1 System, shown in Figure 5-3, was the first complete system development under the SECA project. It evolved from Aurora "engineering learning" units, with a design objective to meet SECA performance metrics. The system was highly thermally integrated, and utilized pipeline natural gas fuel with on-board desulfurization and on-board fuel processing. Input natural gas and water was partially converted into hydrogen and carbon monoxide rich reformate for the fuel cells. The DC power produced by the fuel cells was converted to single-phase AC power by a Power Conditioning Unit (PCU). Unused fuel and air passing out of the fuel cells is mixed and burned, generating heat to bring the incoming process streams up to a suitable temperature for the fuel reforming and SOFC stack processes. An automated CANbus control system managed the entire process, allowing the system to run unattended during normal operation.

The 3-1 System consists of two main functional assemblies: the Cold Zone and the Hot Zone. The Hot Zone's primary functions are to produce DC electricity in the stacks, convert water and natural gas into a suitable fuel feed for the anode of the stacks, preheat the incoming air for the cathode of the stacks, and complete the combustion of the exhaust from the stacks before release to the atmosphere. The 3-1 System utilized a single 112-cell SOFC tower, comprised of four 28-cell stack blocks. The Cold Zone's main functions are to provide the flow control for all fluids, convert the DC power from the stacks into standard AC power, control all of the processes of the generator and provide the interface between the prototype and the external environment.

A formal performance test of the 3-1 system was completed to meet minimum performance metrics for the Phase I testing defined by the DOE. The testing results exceeded all metric test performance requirements, as shown in Table 5-1.

Table 5-1 Summary of Phase I Metric Testing Results for 3-1 System

Characteristics	Measured	Target
Steady state Net DC power degradation	1.2%/500hr	≤2 %/500hr
Net DC power degradation over 10 transients	0.7 %	≤1 %
Peak Net DC power	5.10 kW	3 to 10 kW
Peak Net DC electrical efficiency at NOC	38.4 %	≥35 %
EOL Net DC electrical efficiency at NOC	35.3 %	≥35 %
Availability	98.6 %	≥80 %

The Phase I performance testing was carried out at Versa Power Systems Ltd. facility starting December 5, 2005. Performance testing was successfully completed on March 31, 2006 after executing 1500 hours of steady state, 10 transients and peak power operation. Critical instrumentation and computation methodology was successfully audited in January 2006 by a third party auditor, selected by the DOE. An overview of the test results are shown in Figure 5-4.

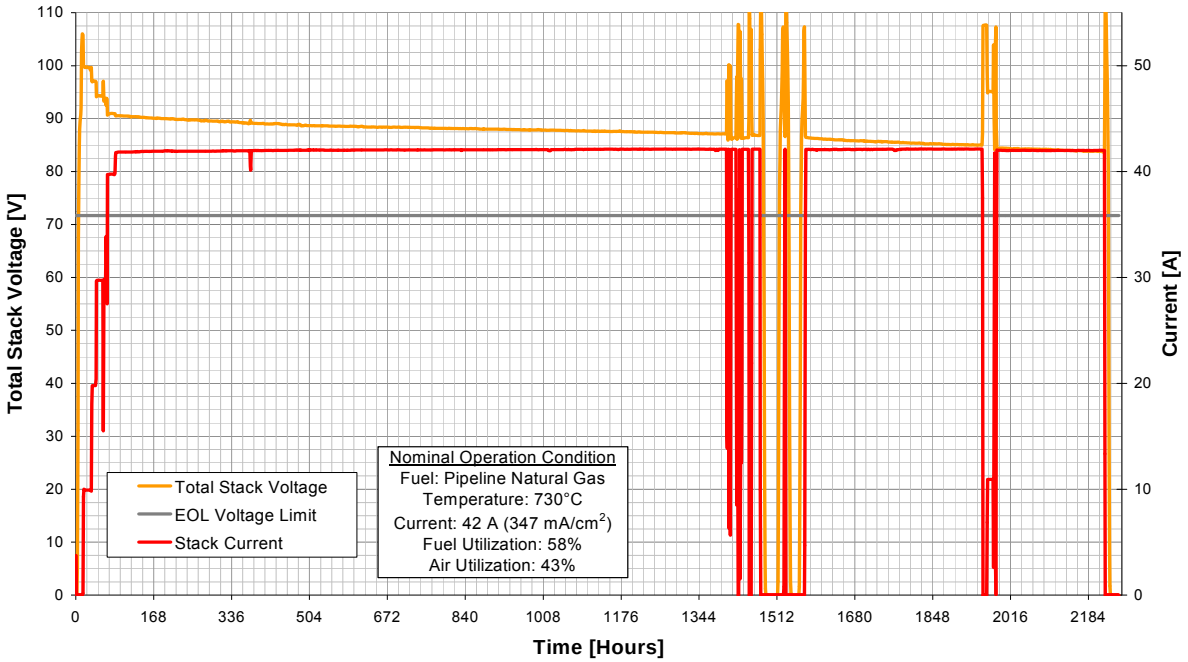

Figure 5-4 3-1 System Test Results: Stack Voltage (Tower) and Stack Current – Formal SECA Phase 1 Test

5.2 50 kW PCM System Preliminary Design

System Design

During Phases II and III, a pipeline natural gas (NG) fueled SOFC PCM system was developed [6]. The design activities focused on mechanical and electrical balance-of-plant (BOP) systems that will serve as a platform for PCM tests. This plant will have a 60 kWdc SOFC module and the BOP supporting the fuel cell module. The PCM system will be a stand-alone, modular (skid-mounted, shippable), outdoor-rated design. A system configuration improvement was implemented to increase the combined heat and power (CHP) capabilities of the 50 kW (60 kW peak) PCM system. High temperature heat available in the SOFC plant exhaust stream is an important attribute when considering the overall system efficiency and plant economics. A simplified block flow diagram of the PCM system is shown in Figure 5-5. The system configuration utilizes anode recycle to increase system efficiency and provide water neutrality during full-power operation.

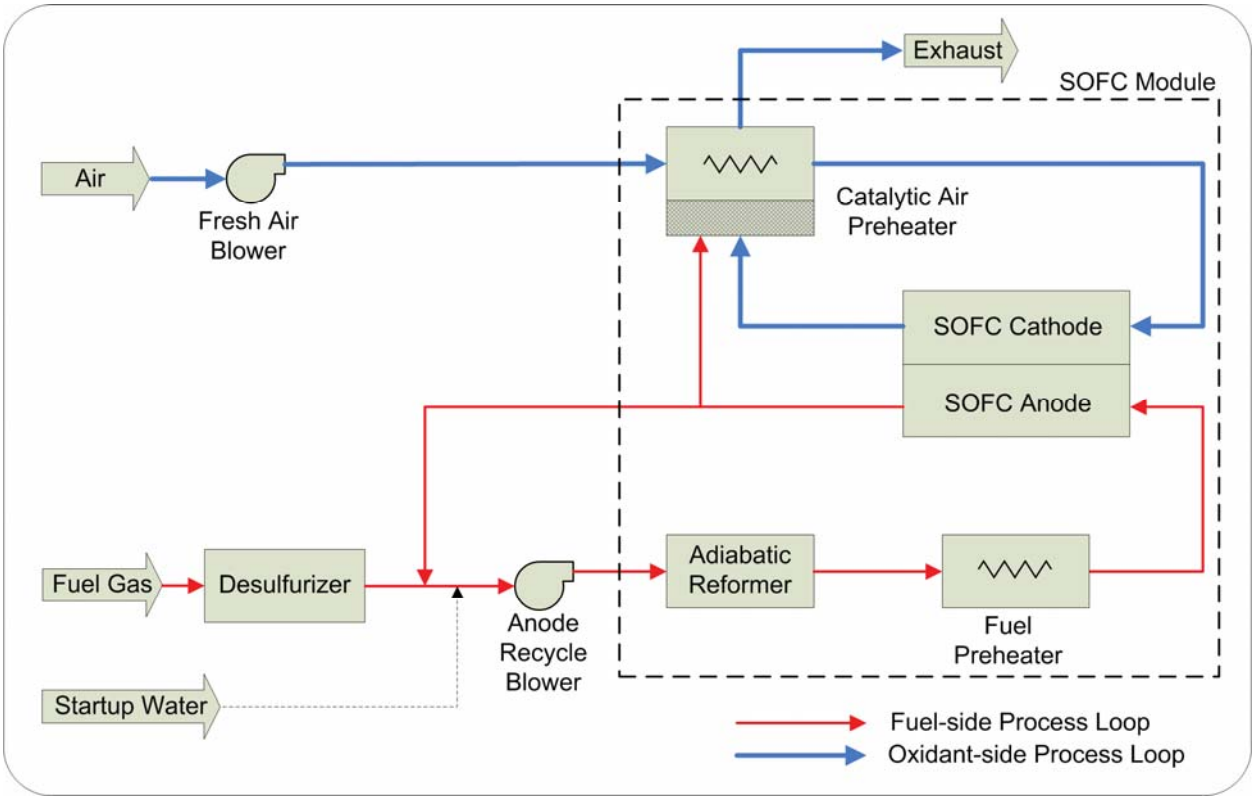

Figure 5-5 Block Flow Diagram of 50 kW PCM System

Process modeling of the improved PCM system was performed for full power, rated power, and heat-up modes of operation. Table 5-2 shows a performance summary of the improved 50 kW PCM system, for the normal operating conditions (250 mA/cm^2) case and the rated power (275 mA/cm^2) case. The electrical efficiency was estimated at 61.9% (LHV natural gas) with the potential for nearly 84% overall thermal plus electrical efficiency (in CHP applications) for the NOC case.

Table 5-2 Performance Summary of 50 kW PCM System

SOFC Gross Power	Normal Operating Conditions		Rated Power	
DC Power	**55.1**	**kW**	**60.3**	**kW**
Energy & Water Input				
Natural Gas Fuel Flow	4.9	scfm	5.4	scfm
Fuel Energy (LHV)	80.8	kW	88.9	kW
Water Consumption @ Full Power	0	gpm	0	gpm
Consumed Power				
AC Power Consumption	2.6	kW	2.7	kW
Inverter Loss	2.5	kW	2.7	kW
Total Parasitic Power Consumption	**5.1**	**kW**	**5.4**	**kW**
Net Generation				
SOFC Plant Net AC Output	**50.0**	**kW**	**54.8**	**kW**
Available Heat for CHP (to 120°F)	**17.8**	**kW**	**19.5**	**kW**
Efficiency				
Electrical Efficiency (LHV)	**61.9**	**%**	**61.7**	**%**
Total CHP Efficiency (LHV) to 120°F	**83.9**	**%**	**83.7**	**%**

Preliminary Engineering Package Development

The PCM system design activities included development of the Preliminary Engineering Package documentation. System simulations and design activities were focused on the PCM system size. Process flow diagram (PFD), piping and instrumentation diagrams (P&IDs), preliminary control philosophy, and the alarm list were generated. All of the long-lead items (LLI) were configured. The equipment specification documents were generated and vendors were contacted to solicitate quotes. The PCM system Hazard and Operability (HAZOP) analysis was conducted.

Piping Pressure Drop Mapping

A piping and equipment arrangement model was developed using *Pipe-Flo Professional* software. This software calculates pressure drops and flows in piping networks. The model developed covers the air, anode recycle gas, and plant exhaust gas for the cathode and anode process streams. The model results were used to:

- Verify or modify the line sizing,
- Define specifications for control valves and orifice plates,
- Refine specifications for the Fresh Air Blower and Anode Recycle Blower,
- Refine maximum pressure drop allowances for the fuel cell modules, heat exchangers, process vessels, and reactors,
- Evaluate whether further control is needed for the pressure differential between the anode and cathode loops.

Power Conversion System

Major component design features and plans/strategies are summarized below.

DC/DC Converter: The front end DC/DC Converter is based on an existing resonant DC/DC boost converter for solar applications. The converter is compatible with the SOFC fuel cell input voltage and allows for independent stack pair loading per the PCM operational requirements. Components were selected and a packaging model was assembled for the DC/DC Converter in SolidWorks format and has been adapted to fit the allocated geometry of the Control System/PCS cabinet.

DC/AC Inverter: The back end DC/AC Inverter is also based on an existing design from a separate vendor. Components for the DC/AC Inverter were selected and a preliminary packaging model was assembled in SolidWorks. A commercial off-the-shelf Insulated Gate Bipolar Transistor (IGBT) module was selected and auxiliary components including: harmonic filter, protective components, and gate drive boards were selected by the principal vendor.

PCS Packaging: The power conversion subsystem for the PCM system will be packaged by the FCE-selected vendor. Figure 5-6 shows the Electrical Balance-of-Plant (EBOP) enclosure comprised of the power electronics (DC/DC converter at the top and DC/AC inverter on the left side). The remaining space is occupied by the Central Control System (CCS) equipment. The Central Control System (CCS) sits on the right side of the EBOP Enclosure. Figure 5-7 shows the CCS layout.

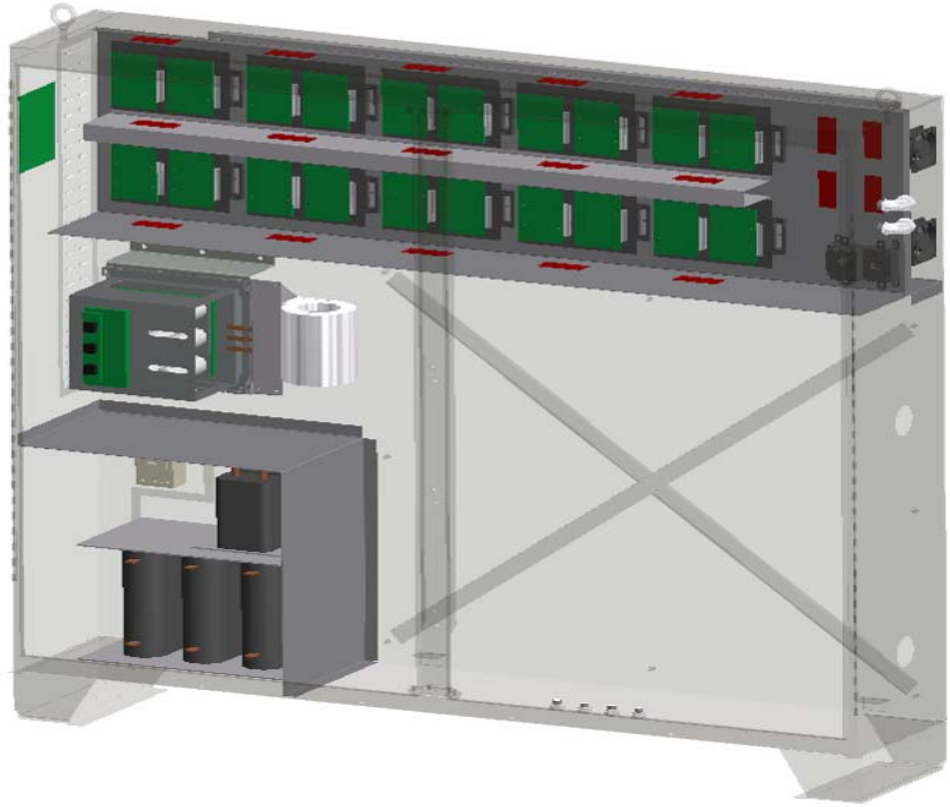

Figure 5-6 Electrical Balance-of-Plant Enclosure Showing DC/DC Converter and DC/AC Inverter

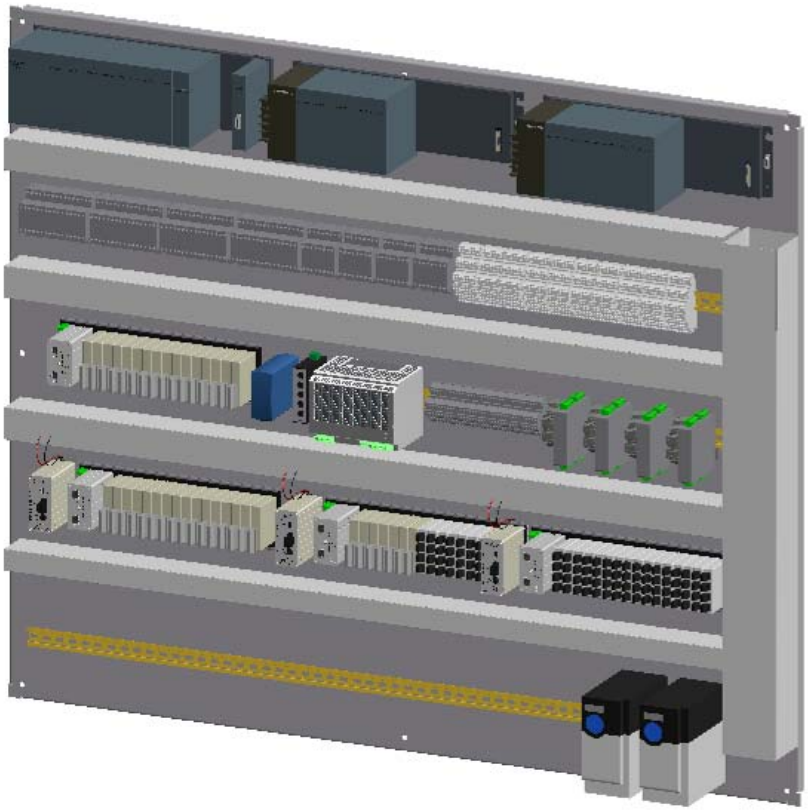

Figure 5-7 Central Control System Layout within EBOP

Control System and Instrumentation

PCM System Control Philosophy: As a part of the 50 kW nominally rated (60 kW Peak) PCM system design, a full control philosophy was developed and finalized. The system was designed for an unattended operation that will be managed remotely. The control sequence included 13 steps; From Off mode through Idle, checkup, heat-up and power generation. A list of all the system alarms and corresponding correction actions including the trip conditions; Hot Standby (HSB), Cool-Down, Non Recycle Cool-down (NRC), Shutdown (SD) and Emergency shutdown (ESD) was prepared. The control philosophy integrated the experience gained from the 60 kW quad test conducted in the 400 kW test facility and finalized the front end engineering design (FEED) package.

Logic Diagrams: Subsequent to the completion of control philosophy document, control logic diagrams were developed to guide PLC programming activities. The diagrams followed a philosophy of remote and automated operation of the fuel cell module, mechanical, and electrical components. The diagrams are in two subsets – Analog Logic (formerly known as SAMA diagrams) and Digital Logic (also known as Binary Logic diagrams).

The logic diagrams were constructed from functional blocks along the lines described in ISA standard ANSI/ISA-5.1-2009. The diagrams display:

- Transmitters, thermocouples, and other analog signals,
- Discrete signals of status or alarm from field devices,
- Modulating controller signals to valves, speed controllers, etc.
- Discrete controller signals for start/stop and open/close,

- Signal monitoring for announcement of alarms,
- All the logic which processes the above.

The functional blocks are, in effect, a programming language. The logic is executed in the Programmable Logic Controller (PLC), but the symbology is generic and not specific to a particular manufacturer's platform. The logic diagrams therefore serve as a key tool for communication between the process engineer, the control engineer, and the PLC provider as well as reference documents for operators and operator training.

Instrument Index: The instrument index was completed, containing 338 items, including:

- 142 temperature elements
- 77 voltage transmitters
- 15 remote operated control valves and block valves
- 15 pressure and differential pressure transmitters
- 9 flow transmitters
- 2 level transmitters
- 78 remaining controllers, sensors, analyzers, switches, and local gauges.

Instrument Specifications: Detailed instrument specifications were completed for:

- Control valves
- On/off/solenoid valves
- Safety relief valves
- Flow sensors
- Flow transmitters
- Pressure transmitters
- Pressure gauges
- Pressure regulators
- Restriction orifices
- Combustible gas analyzer

Humidity measuring instruments were included to detect moisture level in the incoming cathode air stream.

Hardware: The PCM plant control system will be located on a 50" x 60" (1.27 m x 1.52 m) section inside of the control cabinet. The space is shared with a DC-DC Converter and an inverter. A GE Rx3i PLC will be used to control and monitor the system. There will be a 12-slot main rack and two 10-slot expansion bases which will hold the PLC cards. The PLC will also receive voltage and temperature readings from the fuel cell stack through OPTO 22 cards. There will be four racks of OPTO 22 bases which are capable of holding 16 cards each. These cards are fully isolated and communicate over Ethernet to the PLC.

A 46-page electrical drawing package was completed for the control system including point-to-point wiring as well as layout packaging. A description of the Input/Output (I/O) modules follows:

PLC I/O Counts

38 Analog Inputs, 4 Analog Input Cards

10 Analog Outputs, 2 Analog Output Cards

25 Digital Inputs, 2 Digital Input Cards

15 Digital Outputs, 3 Digital Output Cards

41 Thermocouples, 6 Thermocouple Cards

OPTO 22 I/O Counts

81 Analog Voltage Inputs, 40 Analog Voltage Input Cards

96 Thermocouples, 24 Thermocouple Cards

General Arrangement

The 50 kW PCM Power Plant has design features that make it easy to ship, install, and service. The power plant uses outdoor rated equipment and has a removable façade that will allow access to the equipment. The entire plant has been reduced in size due to improvement related to packaging and integration of components, while also improving access and serviceability of the system. The plant will be assembled and shipped on a standard 20 feet (6.1 meter) shipping container sized skid (20' x 8' x 8' 6" or 6.1 m x 2.4 m x 2.6 m) with the façade assembled after installation and commissioning at the customer site. A 3D model of the packaged system is shown in Figure 5-8 with some of the key equipment of the system identified.

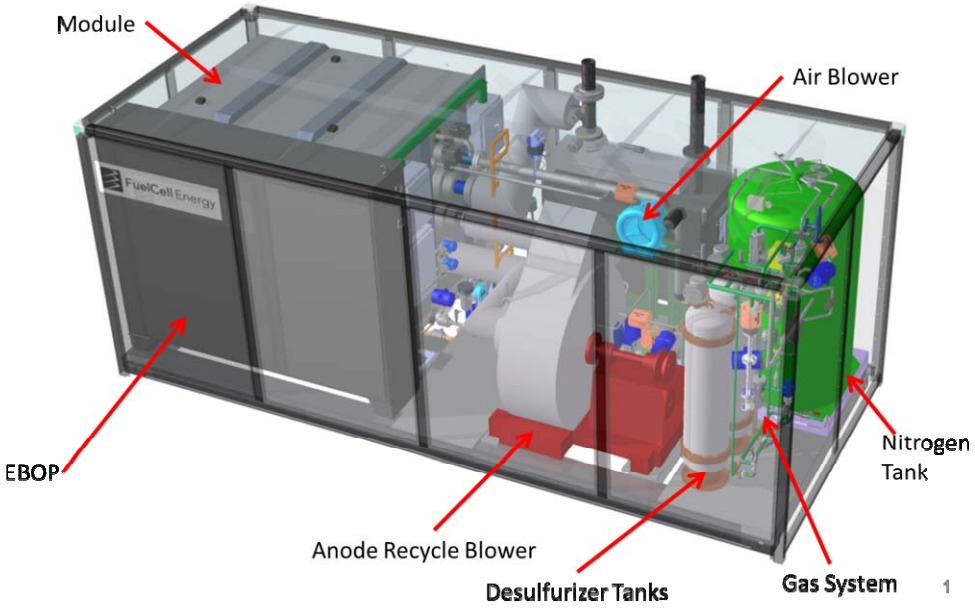

Figure 5-8 Schematic of Packaged 50 kW PCM Power Plant Showing Key System Equipment

The entire plant will be assembled at the manufacturing facility and shipped to the end user. This reduces the amount of time and labor needed on site at each installation. This packaging approach was selected over the alternative of using three skids (Fuel Cell Module, MBoP, EBoP) that are assembled and shipped separately. The PCM Power Plant design integrates the power plant components onto one skid but still allows accessibility because of a removable façade. The façade is composed of an aluminum frame and architectural panel that enhance the aesthetics of the plant. Each frame piece and panel can be removed individually to allow fork truck access to equipment that may need to be replaced in the field. Once the panels are removed all equipment connections are accessible and there is room to work inside the plant. Allowing extra space to work in the packaged unit will allow the Fuel Cell Module to be replaced at the end of life without shipping the entire plant back to the manufacturing facility. The removable façade design is possible because all equipment in the 50 kW PCM Power Plant is outdoor rated. Using outdoor rated equipment eliminates the need for a sealed enclosure and vent fans.

5.3 Balance-of-Plant (BOP) Component Development and Testing

Startup system: A startup system fueled by natural gas is included in the PCM power plant to facilitate the start-up of the power plant.

Detailed design of the system was developed. The completed design elements of the subsystem included Process Flow Diagram, Bill of Materials, Operating Philosophy, Alarms and Interlocks, and General Arrangement Drawing.

Fabrication of the system was completed. Figure 5-9 shows a picture of the packaged unit. Factory acceptance tests with natural gas were conducted successfully. The system was installed in FCE's 400 kW-class facility and integrated with the Catalytic Heat Exchanger (procured from another vendor) for testing.

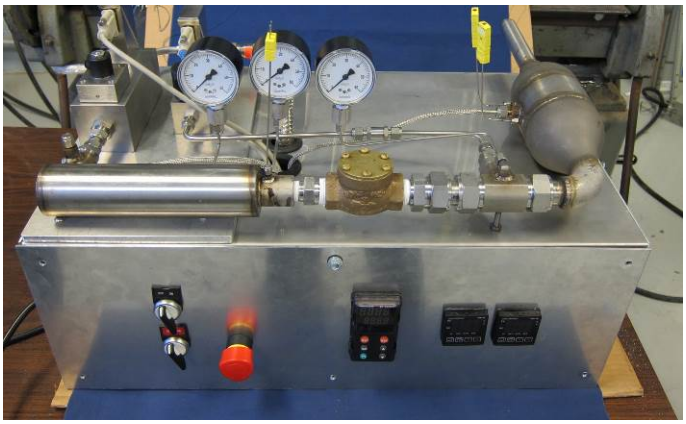

Figure 5-9 Packaged Unit for Supplying Startup Gas for the 50 kW PCM System

Catalytic Heat Exchanger: The catalytic heat exchanger in the PCM power plant combines the functionality of two pieces of equipment (the catalytic oxidizer and cathode air heat exchanger) into a single high-performance multi-functional device. Design of the catalytic heat exchanger was completed. Preliminary General Arrangement schematic is shown in Figure 5-6. Computational Fluid Dynamics (CFD) analysis showed acceptable air- and exhaust-side flow distributions through the heat exchanger.

The design effort and CFD analysis also focused on achieving uniform mixing of anode exhaust (fuel) and cathode exhaust (oxidant) upstream of the catalyst-coated hot-side of the heat exchanger. Results of the Computational Fluid Dynamics (CFD) analysis for the mixing chamber design are shown in Figure 5-7. The mixing plenum receives exhaust gas from the cathodes entering on the left and right. The “shower head” nozzle in the middle introduces anode exhaust. The entire flow is then divided among 23 parallel tube rows. In the final design, a fairly uniform mixing resulted in a minimum stream composition at 8% below average and maximum composition at 12% above average. The design case pressure drop for the air side and exhaust side combined was estimated to be 2.35 kPa, which is within the design allowance of 2.99 kPa (12“H_2O).

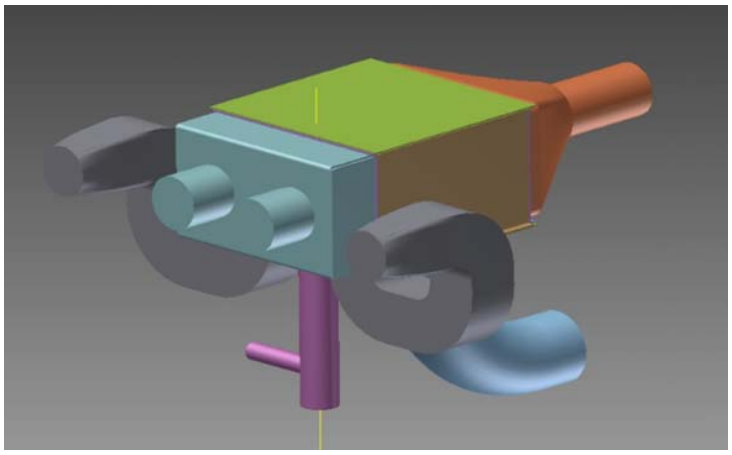

Figure 5-10 Schematic of Catalytic Heat Exchanger

The catalytic heat exchanger fabrication was completed by the vendor. The unit was received at FCE and was installed in the 400 kW Facility in Danbury to conduct performance testing for fuel conversion, heat transfer and pressure drop.

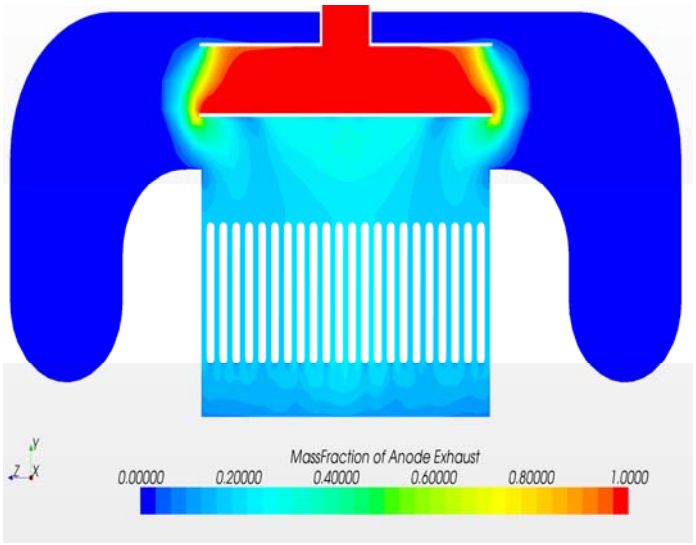

Figure 5-11 Cathode and Anode Exhaust Mixing in Catalytic Heat Exchanger – Computational Fluid Dynamic Modeling

Testing at simulated normal operating condition was conducted to evaluate the heat transfer from the hot combustion product to the cold inlet air. The testing consisted of simulating a hot oxygen-depleted cathode outlet gas and simulating a hot anode outlet gas using hydrogen, carbon dioxide, and water. These two streams were then combusted in the catalytic heat exchanger while a representative amount of room temperature air flowed through the cold-side of the heat exchanger. The thermal stability and heat transfer capabilities were evaluated by increasing the fuel flow rate while maintaining the air flow rate constant, by increasing the air flow rate while maintaining the fuel flow rate constant, and then increasing both flow rates equally. The results are summarized in Table 5-3. At all of the conditions tested, the catalytic heat exchanger exhibited excellent thermal stability in the combustion zone. The PCM system design requires the cathode inlet temperature to reach at least 1200°F (649°C). The table shows that this design criterion was exceeded at all conditions except when the air flow was increased without increasing the fuel flow. Approximately 95% of available heat was transferred from the combustion side to the cold air side at normal operating conditions.

Table 5-3 Catalytic Heat Exchanger Performance for a Range of Normal Operating Flows

Condition:		NOC (100% Fuel & Air)	100% Fuel 150% Air	150% Fuel 100% Air	150% Fuel & Air
H_2 Flow	slpm	107.6	107.6	164.2	164.2
Cold Air Flow	Std m^3/min	2.83	4.25	2.83	4.25
Catalytic Heat Exchanger Catalyst	°C	740	697	799	743
Cathode Inlet	°C	710	632	776	678

Anode Recycle Blower: The Anode Recycle Blower is a key component in the 60 kW power plant (PCM unit) design. A specification for the Anode Recycle Blower was prepared. A key requirement in the specification was a blower head rise of 20 iwc (4.92 kPa) at a flow rate of 114.4 acfm (3.23 actual m^3/min) and inlet gas temperature of 1040°F (560°C). The blower circulates a low density (0.02 lb/ft^3 or 0.32 kg/m^3) stream composed of 10.8% H_2, 44% H_2O, 16% CH_4, 24% CO_2, 5% CO and (balance) unreacted higher hydrocarbons (from the natural gas fuel). Companies that market gas blowers were contacted. The challenge in selecting the anode recycle blower is to achieve desired performance in static head at high temperatures with equipment that fits in a limited space. Proposals were received from 2 companies for existing blowers with ~32 inch (0.81 m) diameter wheels operating at ~3600 rpm and near the maximum pressure point, and requiring 2.3-3 hp (1.72-2.24 kW_{eq}). Proposed costs were significantly high and there was a significant concern for excessive heat loss related to the size of the blower . One proposal was received for development of a small high speed (50-100k rpm) blower requiring significant non-recurring engineering effort and 12 months for development.

Based on these initial responses to the request for proposal and the difficulty in identifying an acceptable blower model, it became clear that the 20 iwc (4.92 kPa) head rise at a flow of only 114 acfm (3.23 actual m^3/min) requires either a large diameter wheel at normal motor speed or a small diameter wheel at very high speed requiring foil bearings. For this reason other equipment in the power plant system was modified to reduce the head rise requirement for the blower to 15 iwc (3.69 kPa). A revised specification with this new head rise was prepared.

CONCLUSION

Advanced cathodes and modified anodes led to cell performance enhancement of up to 18% (compared to baseline TSC-2 cell technology) at lower operating temperature (650°C) and reduction in performance degradation rate of more than 50% in 81-cm^2 (active area) single cells. Degradation rates of <0.7%/1000 h (at ~500 mA/cm^2) were achieved for the operating temperature range of 650°C to 800°C.

Cell size was scaled up from 10 cm x 10 cm (81 cm^2 active area) to 33 cm x 33 cm (961 cm^2 active area) while maintaining the performance level. Cell size of 25 cm x 25 cm (550 cm^2 active area) was selected for stack technology development. The cell technology improvements were implemented in the scaled up cell (550 cm^2 active area) and the TSC (tape casting, screen printing and co-firing) cell manufacturing process achieving production yield of 95% based on over 1000 cells fabricated. VPS cell pilot production facility was upgraded to an annual production volume of 1 MW.

Thin anode substrate cells with improved mechanical strength, offering cost reductions of ~25%, were fabricated and test validated in scaled up (550 cm^2 active area) single cells and 16-cell stacks maintaining the performance level. The new 0.6 mm thick anode substrate has resulted in significant materials cost reduction and better performance at high fuel utilization.

Chromium-tolerant cells were developed. An accelerated cell (81 cm^2 active area) test (performed with 10% cathode gas humidity), evaluating a 30% - 70% combination of Cr getter materials Gb and Gc (Design 2) along with coated cathode side hardware, accumulated over 8,500 h demonstrating a performance degradation rate of <0.5%/1000 h. In a repeat test of Design 2 cell, thermal cycling capability was evaluated over 10 thermal cycles, showing a performance loss of only 0.8 mV/cycle. Design 2 was implemented in 16-cell stacks.

Single cell tests of coated cathode side hardware to evaluate Manganese–Cobalt Oxide (MCO) coatings developed by Nextech and PNNL showed promising results. Nextech coated hardware was tested for over 10,000 h, showing a low performance degradation rate of 0.45%/1000 h. PNNL coated hardware was tested for over 8,400 h. The cell performance degradation rate over the 7,390 h-period at 10% cathode gas humidity condition was estimated to be 0.45%/ 1000 h.

In Phase I, the stack building block was scaled up to a stack size of 64 cells (550 cm^2 cell active area). End-of-Phase I metric testing based on the 64-cell stack block was conducted successfully. The stack completed the required 5,000 h of steady state testing demonstrating a performance degradation rate of 2.7%/1000 h, much lower than DOE SECA requirement of <4%/1000 h.

In Phase II, the stack building block was further scaled up from a stack size of 64 cells to 92 cells. Operation at more aggressive system-representative conditions was also pursued. The block power output increased from 10 kW to 18 kW (peak). Thin TSC-3 (third generation TSC) cell technology was implemented in stacks. End-of-Phase II metric test was conducted by simultaneous testing of a stack tower containing two 92-cell building blocks and of a 120-cell thin TSC-3 cell stack. The stack tower generated 30.2 kW DC, whereas the 120-cell stack achieved a power density of 381 mW/cm^2. The stack demonstrated a performance degradation rate of 0.9%/1000 h in first 1500 h of testing. This was well within the Phase II target of ≤2%/1000 h. In Phase III, the stack building block was scaled up to a stack size of 96 cells, to serve as a representative of the manufactured building blocks for large-scale modules (>50 kW). One 96-cell stack block tested for performance stability at system-representative conditions exhibited a degradation rate of 1.4%/1000 h during ~3500 h of steady state testing.

A 10-cell stack containing 1000 cm^2 cell active area scaled-up cells was designed and tested successfully demonstrating a power output of 4 kW.

A 60 kW-class SOFC module design accommodating four stacks supported on a quad base was developed. The 60 kW quad-base module test was conducted using four 96-cell stack blocks. The 60 kW module achieved 1,645 hours of hot operational time including 1,130 hours on load and demonstrated a maximum power level of 60.6 kW. The test and data analysis validated the robustness of the module configuration as a platform for future proof-of-concept systems.

The design of a 2nd generation 50 kW Proof of Concept Module was completed. Integration of some hot balance-of-plant (BOP) components within the module was performed to increase performance and reduce plant footprint and cost. The BOP components located within the module enclosure included Catalytic Cathode Air Preheater and Fuel Pre-reformer (integrated with Fuel Pre-heater). The integrated module design offers system compactness, reduced piping (and related cost savings), reduced module enclosure penetrations (and heat losses) and better thermal integration.

The stack tower concept containing multiple stack building blocks was developed. A test of the first tower, assembled using three 64-cell building blocks, validated the concept successfully. Subsequently, a tower containing two 92-cell stack blocks generated 30.2 kW DC power. In Phase III, a stack tower assembled using two 96-cell blocks accumulated over 3,300 h of on-load operations. The test results and data analysis validated the feasibility and operability of the 30 kW tower configuration as an assembly of stack blocks in a vertical array arrangement.

Overall, during the three phases of the project, over 700 stacks were manufactured and tested, out of which, 128 stacks were fabricated using the baseline full-area cells (550 cm^2 active area).

Advanced Baseline Power Plant system configurations were developed to achieve higher efficiency. The Baseline System employed catalytic gasification and warm gas cleanup technology. The system further employed oxy-combustion of the anode exhaust for CO_2 capture. The system electrical efficiency of 58.7% (coal HHV) was achieved (significantly exceeding >50% efficiency target). The Baseline Power Plant system produced 414.6 MW net AC power while capturing >99% carbon (as CO_2) from coal syngas (significantly exceeding 90% minimum removal requirement). The coal-based SOFC system consumes 75% less water compared to pulverized coal boiler plants using scrubbing technology for carbon capture.

A conceptual layout of the Baseline Power Plant was developed. The footprint of the integrated gasification fuel cell plant was slightly smaller (5.5 acres or 22,407 m^2) than a comparable integrated gasification combined cycle plant (5.6 acres or 22,814 m^2).

Factory Cost Estimates were performed. The estimates were based on Year 2007 US dollars (Phase III) for easy comparison with DOE's cost targets. The stack block cost was $147/kW and the power island Factory Equipment Cost was $635/kW. The costs met the SECA requirements of $175/kW and $700/kW for stack cost and power island Factory Equipment Cost, respectively.

A 50 kW (60 kW peak) proof-of-concept module (PCM) system was developed. For full power operation case, the system electrical efficiency was estimated at 61.9% (LHV natural gas) with the potential for nearly 84% overall efficiency for combined heat and power applications.

The engineering package for the 50 kW PCM system design was prepared. The plant was designed as single-skid with removable façade for easy replacement of plant equipment or the SOFC module. The plant has a footprint similar to a standard 20 feet (6.1 meters) shipping container.

The design and fabrication of a catalytic heat exchanger to oxidize unused fuel from SOFC and recover waste heat for preheating of cathode air were carried out. The catalytic air preheater design was validated through testing in FCE's 400 kW facility.

Although significant progress related to performance, endurance and cost reduction of the SOFC cell and stack technologies was made during the course of the project, the following outstanding technical issues, listed below, remain to be addressed in the future.

- Finalize Cr-tolerant cell technology through development of interconnect coatings and cell materials.
- Incorporate and validate Cr-tolerant cell technology into large area (550 cm^2 active area) stack design.
- Implement large area stack design improvements to achieve optimal balance of electrical contact and gas sealing.
- Implement Quality Improvement Plan to enhance stack block repeatability, reliability and robustness.
- Demonstrate stable operation of a thermally self-sustained stack with ≤0.2%/1000 hours performance degradation rate.
- Design, build and fabricate subMW systems (50-500 kW) to demonstrate large area SOFC stack operation under real-world system conditions.

REFERENCES

[1]. H. Ghezel-Ayagh and J. Doyon, Coal Based Large SOFC/T Systems, 2006 Fuel Cell Seminar, Honolulu, Hawaii, November 13-17, 2006

[2] H. Ghezel-Ayagh, FuelCell Energy's SECA Coal-Based Solid Oxide Fuel Cell Power Plant Development Project, DOE Office of Fossil Energy Fuel Cell Program, FY 2008 Annual Report, II.A

[3] T. Zhang, W. G. Fahrenholtz, S. T. Reis and R. K. Brow, Borate Volatility from SOFC Sealing Glasses, Journal of the American Ceramic Society, 91: (2008) 2564–2569

[4] Hossein Ghezel-Ayagh, Stephen Jolly, Dilip Patel and David Stauffer, "Solid Oxide Fuel Cell System Utilizing Syngas from Coal Gasifiers", American Chemical Society Industrial & Engineering Chemistry Research Publication, Special Issue: Process Engineering of Energy Systems, 2013, 52, 3112-3120

[5] Hossein Ghezel-Ayagh, James Walzak, Stephen Jolly, Dilip Patel and David Stauffer, Design Optimization of Integrated Coal Gasification Solid Oxide Fuel Cell Systems, Proceedings of the ASME 2010 Eighth International Fuel Cell Science, Engineering and Technology Conference, FuelCell 2010-33191, June 14-16, 2010

[6] H. Ghezel-Ayagh, S. Jolly, D. Patel, J. Nagar, K. Davis, C. Willman, C. Howard, M. Lukas, E. Tang, M. Pastula and R. Petri, "SOFC Technology Development for Distributed and Centralized Power Generation", 2012 Fuel Cell Seminar and Exposition, November 5 – 8, 2012, Uncasville, CT

LIST OF ACRONYMS

A	Ampere
AC	Alternative Current
AFL	Anode Functional Layer
AI	Air In
AIC	Air In Center
AO	Air Out
AOC	Air Out Center
ASR	Area Specific (cell) Resistance
ASU	Air Separation Unit
Atm	Atmosphere
BFD	Block Flow Diagram
BOL	Beginning of Life
BOP	Balance of Plant
CAD	Computer Aided Drafting
CBPP	Coal-Based Power Plant
CC	Current Collection (DC)
CDR	Component Development Requirement
CFD	Computational Fluid Dynamics
CFL	Cathode Functional Layer
CGCU	Selexol Cold Gas Cleanup
COR	Contracting Officers Representative
CT	Cooling Tower
CTE	Coefficient of Thermal Expansion
CTF	Critical-To-Function
CTP	SECA Core Technology Program
CW	Cooling Water
CWP	Cooling Water Pump
DC	Direct Current
DFC	Direct Fuel Cell (FCE Molten Carbonate Fuel Cell)
DIR	Direct Internal Reforming, meaning in-stack reforming
DOE	United States Department of Energy
DSRP	Direct Sulfur Recovery Process
EOL	End of Life

FCE	FuelCell Energy, Inc.
FEA	Finite Element Analysis
FGD	Flue Gas Desulfurization
FI	Fuel In
FIC	Fuel In Center
FO	Fuel Out
FOC	Fuel Out Center
GA	General Arrangement (Plant Layout)
GT	Gas Turbine
HAZOP	HAZard and OPerability analysis
HDS	Hydrodesulfurization
HEX	Heat Exchanger
HHCs	Heavier Hydrocarbons (C2+)
HHV	Higher Heating Value
HMI	Human Machine Interface
H&MB	Heat and Mass Balance
HP	High Pressure
HPC	High Performance Cathode
HRSG	Heat Recovery Steam Generator
HTDS	High-Temperature Desulfurization
I	Electrical Current
IC	Interconnect or separator plate
ICM	In-Cell Manifolded
IGFC	Integrated Gasification Fuel Cell
IIR	Indirect Internal Reforming, meaning in-stack, between-cell, reforming
IR	Internal Resistance, of the cell or stack, ohm-cm2.
K	degrees Kelvin
kW	Kilo-Watt
LHV	Lower Heating Value
LTS	Low Temperature Supercell
MDU	Module Demonstration Unit
MF	Mineral Fiber (thermal insulation)
MT	Microporous (thermal insulation)
MW	Mega-Watt

NETL	National Energy Technology Laboratory
Ni/YSZ	Nickel – Yttria-Stabilized Zirconia
NOC	Normal Operation Condition
OCV	Open Circuit Voltage
OTM	Oxygen Transport Membrane
PCI	Pre-Commercial Integrated-Manifold
PFD	Process Flow Diagram
P&ID	Piping & Instrumentation Diagram
PNNL	Pacific Northwest National Laboratory
POC	Proof-of-Concept
PPC	Peak Power Condition
psi	Pound per square inch pressure
psid	pounds per square inch pressure differential (pressure drop)
Q	Quarter
Redox	Reduction - oxidation
S1 (2)	Stage 1 (2)
SECA	Solid State Energy Conversion Alliance
SG	Syngas
SLPM, Slpm	Standard liter per minute (at conditions of 1 atm and 70°F (21.1°C))
SOFC	Solid Oxide Fuel Cell
ST	Steam Turbine
TIPS	Thermally Integrated Power System
TSC	Tape casting Screen-printing Cofiring
UA	Total heat transfer coefficient times heat transfer surface area, a designation for heat exchanger design
Ua, U_o, UtO	Air (Oxygen) Utilization
Uf, UtF	Fuel Utilization
USA	United States of America
V	Volt
VFD	Variable Frequency Drive
VPS	Versa Power Systems Ltd.
W	Watts
WGCU	Warm Gas Cleanup